

Loop-induced lepton and quark dipole transitions in Randall-Sundrum models

Dissertation

vorgelegt von

Paul Christof Moch

Betreuer: Prof. Dr. Martin Beneke

Lehrstuhl für Theoretische Elementarteilchenphysik T31

Fakultät für Physik der Technischen Universität München



Technische Universität München

Lehrstuhl für Theoretische Elementarteilchenphysik T31

Loop-induced lepton and quark dipole transitions in Randall-Sundrum models

Paul Christof Moch

Vollständiger Abdruck der von der Fakultät für Physik
der Technischen Universität München zur Erlangung des akademischen Grades eines

Doktors der Naturwissenschaften

genehmigten Dissertation

Vorsitzender : Univ. – Prof. Dr. Peter Fierlinger
Prüfer der Dissertation : 1. Univ. – Prof. Dr. Martin Beneke
2. Univ. – Prof. Dr. Andreas Weiler

Die Dissertation wurde am 28.9.2015 bei der Technische Universität München
eingereicht und durch die Fakultät für Physik
am 10.11.2015 angenommen.

Abstract

The successful first and second run of the LHC experiment with the discovery of the Higgs boson elevates the importance of direct and indirect searches for physics beyond the standard model. One interesting possibility to find new physics is to concentrate on dipole transition mediated low energy observables. Such processes can not only potentially be detected at scales lower than the typical energy scale of the LHC, but they also provide the potential to scan new physics models beyond the reach of the latest LHC run. In this thesis, we perform a comprehensive study of dipole operator transitions for leptons as well as for quark fields in the Randall-Sundrum (RS) model. To this end we develop an effective field theory, which allows us to systematically examine the Randall-Sundrum contributions to the muon $g-2$ and the typical range for the branching fractions of $\mu \rightarrow e\gamma$, $\mu \rightarrow 3e$, $\mu N \rightarrow eN$ as well as $\tau \rightarrow \mu\gamma$, $\tau \rightarrow 3\mu$. Additionally we use this effective theory to analyse the contributions of the Kaluza-Klein gluons to the inclusive radiative decay $\bar{B} \rightarrow X_s\gamma$. The computation of the Wilson coefficients of the effective field theory is done for the RS model with minimal field content as well its custodial protected extension. In addition we consider three different Higgs field localisation schemes. Amongst other this thesis contains the consideration of bulk Higgs including Higgs Kaluza-Klein excitations as well as their non-decoupling effects. We conduct the matching computation using a fully 5D formalism.

Zusammenfassung

Der erste und zweite erfolgreiche Lauf des LHC Experiment zusammen mit der Entdeckung des Higgs Bosons, gibt der direkten und indirekten Suche für Physik jenseits des Standard Modells der Teilchenphysik eine höhere Bedeutung. Eine interessante Möglichkeit neue Physik zu finden ist es sich auf durch Dipol Übergänge vermittelte Niederenergie Observablen zu konzentrieren. Solche Prozesse können nicht nur potentiell auf einer gegenüber der typischen Energieskala des LHCs geringeren Skala gefunden werden, sie bieten ferner noch das Potential neue Physik Modelle auf Skalen weiter über die Reichweite des jetzigen Lauf des LHCs zu scannen. In dieser Doktorarbeit führen wir eine umfangreiche Analyse von Dipol-Operator Übergängen für Lepton Felder wie auch für Quark Felder im Randall-Sundrum (RS) Modell durch. Zu diesem Zweck entwickeln wir eine effektive Feldtheorie, welche es uns systematisch erlaubt die Beiträge des Randall-Sundrum Modells zu dem Muon $g-2$ and der typischen Größe der Zerfallsraten von $\mu \rightarrow e\gamma$, $\mu \rightarrow 3e$, $\mu N \rightarrow eN$ so wie auch $\tau \rightarrow \mu\gamma$, $\tau \rightarrow 3\mu$ zu untersuchen. Zusätzlich nutzen wir diese effektive Theorie um die Beiträge der Kaluza-Klein Gluonen zu dem inklusiven Strahlungszerfall $\bar{B} \rightarrow X_s\gamma$ zu analysieren. Die Berechnung der Wilson-Koeffizienten der effektiven Theorie wird im RS Model mit minimalen Feldinhalt so wie der Erweiterung mit dem custodialen Schutz durchgeführt. Zusätzlich betrachten wir drei verschiedene Arten das Higgs Feld zu lokalisieren. Unter anderem enthält diese Doktorarbeit die Betrachtung eines bulk Higgs zusammen mit Higgs Kaluza-Klein Anregungen sowie deren nicht-entkopplungs Effekte. Wir führen die Anpassungrechnung unter Verwendung eines kompletten 5D Formalismus durch.

Contents

1	Introduction	3
2	The Randall–Sundrum Model	7
2.1	Extra dimensions before the RS model	7
2.2	The original Randall–Sundrum model	8
2.3	Minimal RS model	11
2.3.1	5D Lagrangian	12
2.3.2	Kaluza-Klein decomposition	13
2.3.2.1	Bulk fermions	14
2.3.2.2	Bulk gauge-bosons	17
2.3.3	5D Picture	19
2.3.4	Higgs localisation	21
2.3.5	Minimal RS model constraints	23
2.4	The custodial protected RS model (RSc)	24
2.4.1	Gauge group	24
2.4.2	Gauge and Higgs sector	25
2.4.3	Fermion sector	26
2.4.4	Fundamental 5D action	28
2.4.5	RSc constraints	30
3	Effective Field Theory	33
3.1	Dimension six Lagrangian	33
3.2	Lepton low energy observables	36
3.3	Effective weak Hamiltonian	43
4	Tree-level dimension-six operators	47
4.1	Four-fermion operators	47
4.2	Higgs-Fermion operators	50
4.3	Yukawa-type operators	51
5	Loop-induced dipole operators	55
5.1	Internal gauge-boson exchange	55
5.1.1	Example Diagram	58
5.1.2	R_ξ Gauge invariance and scheme independence	62
5.1.3	KK Higgs contributions	65
5.1.4	Numerical evaluation	66
5.2	Internal Higgs exchange	70
5.2.1	On-shell zero-mode Higgs exchange	70

CONTENTS

5.2.1.1	Topologies HT1 and HT2	71
5.2.1.2	Topologies HT3 to HT5	74
5.2.1.3	Topology HT6	76
5.2.2	Off-shell zero-mode Higgs exchange contribution	77
5.2.3	Zero-mode Higgs exchange matching	82
5.2.4	Bulk Higgs with a beta profile	83
5.3	Dimension-eight operators	89
6	Phenomenology	93
6.1	Estimates	93
6.2	Numerical analysis	97
6.2.1	Muon g-2	99
6.2.2	LFV	102
6.2.2.1	Minimal model	102
6.2.2.2	Custodially protected model	104
6.2.2.3	EDM constraint	106
6.2.2.4	A note on LFV τ decays	107
6.2.3	Radiative b decays	107
6.3	Discussion	111
7	Summary	115
A	5D Feynman rules	117
A.1	Vertices	117
A.2	Propagators	119
A.2.1	Fermion propagators	119
A.2.2	Gauge boson propagator	124
B	The bulk Higgs	127
B.1	Zero mode and vacuum expectation value	127
B.2	Higgs Propagator	129
B.3	Yukawa matrix scaling	130
B.4	KK Higgs example: Four-fermion operators	131
B.5	KK Higgs contributions	132
C	Explicit diagram expressions	135
C.1	Gauge boson exchange diagrams	136
C.2	Higgs exchange diagrams	144
C.3	Wilson coefficients of the extended electroweak Hamiltonian at the scale μ_{KK}	149

Chapter 1

Introduction

The successful run of the LHC has led to the outstanding discovery of a new particle [1,2], that seems to resemble the Standard Model (SM) Higgs boson. This remarkable feat opens finally the era of direct tests of the electroweak symmetry breaking (EWSB) enabling us to check the predictions of the SM in the hope of finding possible signs of new physics beyond the SM.

Although the SM has been very successful in almost all its prediction up to now, there are still several puzzles it is not able to answer. One of them is the nature and composition of dark matter, whose existence is by now extremely well experimentally established on a range of different scales. The SM simply does not contain any kind of particle that could possibly explain the dark matter observation.

Ignoring the dark matter puzzle, the SM as a renormalisable theory could be in principle considered as a complete theory if gravity would not exist in nature. As the SM does not describe gravity one has to replace it with a quantum gravity theory somewhere around the Planck scale demoting the SM to an effective theory with an ultraviolet (UV) cut-off. At this point a new problem arises automatically as the possible UV cut-off could be assumed to be around the Planck scale $M_{\text{Pl}} \simeq 10^{18}$ GeV, while the electroweak scale is set around the Higgs vacuum expectation value (vev) $v \simeq 246$ GeV. This huge hierarchy induced by the large separation of scales introduces a problems at quantum level for a SM Higgs as it is as a scalar not protected by chiral or gauge symmetries. Thus its potential receives large radiative corrections, that are quadratical sensitive to the cut-off. Generically this require the EW scale to be set by the Planck scale unless one assumes a tremendous fine tuning leading to huge cancellations. This issue is known as the famous gauge-gravity hierarchy problem [3,4]. The discovery of the SM like Higgs elevates its severeness further.

A different kind of hierarchy problem of the SM can be encountered in the quark sector. There the masses of the quarks for different generation seem to span a range of about five orders of magnitude. Further, the very hierarchical Cabibbo-Kobayashi-Maskawa (CKM) [5] matrix is determined by quark mixing angles that are separated by at least three order of magnitude. The SM does not provide any kind of mechanism how these two hierarchies can be generated naturally. In particular the CKM matrix entries and fermion masses are just parameters of the model to be determined by appropriate experiments.

The standard model in its original version [6] does not include neutrino masses. The experimentally observed neutrino oscillations are not possible in the SM and demand either a simple addition of Neutrino mass terms or another more complex theory model. Furthermore, the CP violations of the SM are not sufficient to explain the baryogenesis, that is the processes that produced an asymmetry between matter and antimatter in the early universe.

CHAPTER 1. INTRODUCTION

Collecting these puzzles we consider it worthwhile to study a model beyond the SM, which can at least potentially solve some of the aforementioned problems. There are numerous attempts to perform such a feat. The stabilisation of the EW scale against quantum corrections can be easily achieved in supersymmetric models [7–9]. The flavour hierarchy problem can be solved for example by the introduction of flavour symmetries [10–12]. However a simultaneous attempt to solve both problems without running into the strong experimental bounds like the electroweak precision test, remains still difficult. Here supersymmetric models have been the most promising candidates, especially since these models also include possible candidates for dark matter particles [13].

Aside from supersymmetry there is also the intriguing framework created by Lisa Randall and Raman Sundrum [14, 15] of a quantum field theory in a non factorisable warped five dimensional spacetime. The original Randall Sundrum (RS) addressed the weakness of gravity [14] and therein the gauge-gravity problem [15]. In the original model only gravity is allowed to traverse all dimensions (bulk) of the spacetime, while all other fields are confined on one four dimensional boundary (brane) called IR brane. It was soon realised that the gauge-gravity solution can be preserved even after the promotion of all fields except the Higgs to bulk fields [16–20]. The delocalisation of the fermion fields opens interesting possibilities to explain via the geometry of the spacetime the quark flavour mass hierarchies and the CKM mixing matrices [19–22].

Electroweak precision tests give one of the most stringent constraints on the parameter space of the RS model [23]. These constraints can be decreased by extending the gauge group to incorporate explicitly the custodial gauge symmetry [24–27], however even with such an extended gauge group direct searches at the LHC for RS like signals are not very promising any more. That is precisely the situation where low-energy observables can be used to obtain further constraints on the model. In this thesis we therefore focus on the calculation of low energy observables in the context of the Randall Sundrum model. The main part of the calculations of this thesis is dedicated to the lepton sector. Here we compute the muon ($g-2$) as well as the lepton flavour number violating (LFV) processes $\mu \rightarrow e\gamma$, $\mu \rightarrow 3e$ and $\mu N \rightarrow eN$.

The anomalous magnetic moment of the muon is one of the most precisely predicted and measured observables in particle physics. Over the last 65 years tremendous effort has been invested in determining the deviation of the g -factor from two, see [124] for a review. The extraordinary precision naturally imposes constraints on extensions of the Standard Model (SM), whose contribution Δa_μ to the anomalous magnetic moment

$$a_\mu = \frac{g_\mu - 2}{2} = a_\mu^{\text{SM}} + \Delta a_\mu \quad (1.1)$$

should not increase the observed slight tension between SM and experimental value for a_μ . The anomalous magnetic moment in the minimal RS model has been studied in a 5D formalism in [28]. In this thesis we will extend the results of [28] to the custodially protected RS model.

Rare lepton decays are among the most promising probes for physics beyond the SM. This is even more true for decays that involve lepton flavour number violation (LFV). As the neutrino mass has to be below 1 eV and the SM model contribution does not exist the possible experimental signals are clean. Due to the absence of the SM background we will especially focus in this thesis on the processes $\mu \rightarrow e\gamma$ and $\mu \rightarrow 3e$ as well as muon-to-electron conversion in nuclei. Lepton-flavour violating processes have been studied in the context of the RS model in the past, beginning with [22, 29, 30]. Particularly relevant is [31], which gives the first comprehensive analysis of charged LFV, and [32] with the first fully five-dimensional treatment of loop effects, which dominate the $\mu \rightarrow e\gamma$ decay. However,

neither of the two can be said to provide a complete description of the loop-induced dipole operator coefficient.

Once the loop effects in the lepton sector have been determined in the RS model they can be transferred easily to electromagnetic radiative penguin decays in the quark sector. Hence we also calculate the inclusive $\bar{B} \rightarrow X_s \gamma$ decay. Compared to the LFV sector the $\bar{B} \rightarrow X_s \gamma$ includes a large SM contribution and is therefore a stringent test for the SM as well as any new physics model. In fact there has been tremendous effort (see e.g. [33–36] and references therein) to understand the intricacies of the $b \rightarrow s \gamma$ transition in the SM. The most recent result [37] is given by

$$\text{Br}(B \rightarrow X_s \gamma)_{E_\gamma > 1.6 \text{ GeV}}^{th} = (336 \pm 23) \times 10^{-6}. \quad (1.2)$$

It is in very good agreement with the experimental HFAG average [38], which is calculated out of the ever increasing data of numerous experiments [39–46]

$$\text{Br}(B \rightarrow X_s \gamma)_{E_\gamma > 1.6 \text{ GeV}}^{exp} = (342 \pm 21 \pm 7) \times 10^{-6}, \quad (1.3)$$

where the all contributing experimental results were converted as to correspond to a lower photon energy cut of 1.6 GeV. The Belle II experiment is expected to be able to measure the branching fraction with an uncertainty of about 6% [47]. This will lead to further improvements to the experimental world average.

The decay $\bar{B} \rightarrow X_s \gamma$ has already been studied previously in the context of RS models in [48]. The work kept its focus on the effect of 5D penguin diagrams and neglects the so-called wrong-chirality Higgs couplings terms [31, 49]. Quiet recently there was another study of the transition $\bar{B} \rightarrow X_s \gamma$ [50], which has its focus on a RS model with an exactly localised Higgs field on the IR brane. It includes all important contributions treats the Yukawa interactions exactly.

This work is organised as follows. In chapter 2 we introduce the RS setup after a short overview other the history of the idea of spacetimes with additional spacial dimensions. Following the introductions of the original RS setup we allow the standard model fields to propagate freely through the bulk and give a short overview over the formalism that is necessary to treat bulk fields in RS models. This includes the introduction of the important 5D formalism, which we will use throughout this thesis, as well as the careful treatment of the Higgs localisation together with its physical implications. After the introduction of the necessary formalism we study some constraints on the parameter space of the minimal RS model that is the SM promoted to a RS setup. Due to the strong constraints induced by the electroweak weak precision sector [23] we then shift our focus to a RS model with custodial symmetry (RSc) for the remainder of the chapter.

As the typical scale of the RS model lies in the $\mathcal{O}(\text{TeV})$ region we integrate the heavy degrees of freedom out and match the RS model on the SM extended by gauge-invariant dimension-six operators [51, 52] in chapter 3. The resulting Lagrangian is then first used to calculate all processes of interest in the lepton sector and also in the quark sector. This approach has the advantage to organise the computation in a fully transparent and complete way. We adapt throughout this thesis the notation of [28], which introduced this formalism for the first time in this complete fashion in the context of the muon g-2 calculation in the minimal RS model. We restrict ourselves only to the loop-induced dipole operators and operators that can be generated be generated at tree-level in the RS model. In the quark sector we match the Wilson coefficients to a effective weak Hamiltonian, whose operators are then evolved from the RS scale down to the typical scale of the process $b \rightarrow s \gamma$, μ_b , via renormalisation group equations (RGE).

After setting up the strategy of the calculation in chapter 3 using effective field theories,

CHAPTER 1. INTRODUCTION

we continue by giving explicit expressions for the Wilson coefficients in chapter 4 and 5. Here we distinguish between the Wilson coefficients that are generated at tree-level and the loop induced dipole coefficients. For the tree-level Wilson coefficient we give analytic expression in chapter 4. The chapter 5 is dedicated to the loop induced dipole coefficients. Here we differentiate between the contributions generated via gauge-boson exchange and contributions via the exchange of the Higgs boson. The first contributing can only be evaluated fully numerically while the latter contains partially computations, which can still be done fully analytically, despite the non factorisable curved spacetime.

The sixth chapter chapter is dedicated to the numerical analysis of the processes of interest. First we compute semi analytic approximations of the different RS contributions to the processes of interest in the lepton sector. This is followed with the muon $g-2$ contributions of the custodial protected Randall-Sundrum model as a first example for our numerical scan. Afterwards we perform the complete numerical analysis of all in this thesis considered LFV processes. The last part of this chapter then contains the phenomenology of the radiate decay $B \rightarrow X_s \gamma$.

We conclude in chapter last chapter. This thesis is based on the publications [53–56].

Chapter 2

The Randall–Sundrum Model

The aim of this chapter is to introduce the reader to the setup of RS models. For this purpose we will first review briefly the history of the idea of spacetimes with additional spacial extra dimensions as well as the original RS model. Following this we introduce the SM on the bulk, which is called the minimal RS model. In this context we discuss the Kaluza-Klein decomposition, the 5D formalism and the treatment of the Higgs. With the basic formalism at hand we then give a short view other the major constraints on the minimal RS model, which then leads to the introduction of the custodial protected RS model.

2.1 Extra dimensions before the RS model

The idea that our world might include more than four space time dimensions is over one hundred years old. The first proposal for a theory with extra dimensions was done by Nordstroem [57] in 1914, who showed that there is a possible unified description of electrodynamics and Newton's gravity in a five-dimensional world. After the formulation of general relativity Kaluza [58] realised, that it was indeed possible to completely integrate classical electrodynamics into a five-dimensional metric, which also yields via the five-dimensional Einstein equation the correct Maxwell-equations. This was done by simply identifying the vector potential with the (5μ) -components of the metric. Kaluza's theory contained the so called "cylinder condition", which stated that none of the components of the five-dimensional metric does depend on the fifth coordinate. This needed but at this time unexplained feature was later motivated by Klein [59] in 1929. He proposed the hypothesis that the fifth dimension is in fact curled up as a circle of the size comparable to the Planck length.

It turned out however that Kaluza's and Klein's theory could not be quantised without serious problems. Moreover the discovery of the strong and the weak force and formulation of the standard model of particle physics let this theory to become obsolete. This lead to the situation that the notion of extra dimensions was almost forgotten until the upcoming development of the super string theories in 70's and 80's [60, 61], which need several extra dimensions to be consistent. For the theoretical particle physics community these developments were not of large interest as the proposed extra-dimensions were believed to be still of the size of the Planck scale and therefore too small to be detected in any future experiment. Only in the beginning of the 90's of the last century it was realised that the existence of extra dimensions with sizes within the sub-millimetre regime could not be excluded by gravity short distance experiment [62, 63]. This lead to the intriguing idea, that quantum field theories with large compact extra-dimension could possible solve the hierarchy problem

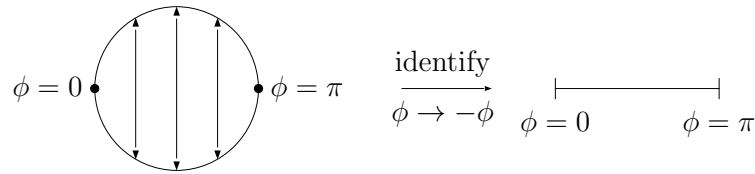


Figure 2.1: Visualisation of the orbifold transformation acting on S^1 .

of the standard model. The Arkani-Hamed-Dimopoulos-Dvali (ADD) [64] model was one prominent example of this era. It suggested one or two additional large extra-dimensions, which could be only traversed by the graviton, while all other standard model fields are confined to a four dimensional boundary (brane). Therefore a four dimensional observer on the brane automatically sees a weaker gravitational force compared to the other known fundamental forces. Thus the fundamental scale of gravity does not have to be of the order of the Planck scale as perceived through an observer on the 4d brane. To be more precise the ADD model contains the following relation

$$M_{\text{Pl}}^2 \sim M^{2+n} V_n, \quad (2.1)$$

where M_{Pl} is the observed four-dimensional Planck mass, M the fundamental scale of gravity in all spacetime dimensions (the bulk), n the number of extra dimensions and V_n the volume of the compact extra dimensions. For the choice $n=2$ and a compactification size close to the sub-millimetre regime this relation connects a fundamental gravity scale of the size of the electroweak scale with the Planck scale.

However this solution of the EW-gravity hierarchy introduces a new hierarchy into the theory: To suppress gravity sufficiently without too many extra dimension, the compactification scale r_c has to be chosen of the order of $1/r_c \sim \mathcal{O}(10^{-3} \mu\text{eV})$. Thus the compactification scale generates a new hierarchy problem as it is much smaller than the EW scale. Therefore the ADD model does not give a satisfactory solution to the hierarchy problem, it just moves this problem to a different energy scale.

2.2 The original Randall–Sundrum model

Inspired by the shortcomings of the ADD model Randall and Sundrum developed their original extra dimension model with the following assumptions [14, 15]: Their model contains only one extra dimension, which has the geometry of a S^1/\mathbb{Z}^1 , i.e. a circle with orbifold symmetry. They assume 4d Lorentz invariance and also demand that all dimensional parameters are of the order of the Planck mass M_{Pl} . Like the ADD model it is assumed that only gravity is allowed to propagate through all spacetime dimensions, i.e. the bulk. All other fields are confined to four-dimensional branes.

The choice along the fifth direction, where the non-gravity fields are localised can be obtained by the orbifold symmetry of the compact fifth dimension. Let $z = r_c \phi$ an arbitrary point on the circle of the fifth dimension, where r_c is the compactification radius. Then the orbifold symmetry identifies this point with its mirrored point on the circle $z = -r_c \phi$ see figure 2.1. Under this transformation the points $\phi = 0$ and $\phi = \pi$ are fixed points. Thus the fixed points are the natural choice for the localisation of all gauge and matter fields. The convention is to call the 4d subspace at $\phi = 0$ as the UV brane and the subspace at $\phi = \pi$

2.2. THE ORIGINAL RANDALL–SUNDRUM MODEL

as the IR brane.

With all of these assumptions the 5D action can be written as

$$S = S_{\text{Bulk}} + S_{\text{IR}} + S_{\text{UV}}, \quad (2.2)$$

$$S_{\text{Bulk}} = \int d^4x \int_{-\pi}^{\pi} d\phi \sqrt{-G} (-\Lambda + 2M^3 R), \quad (2.3)$$

$$S_{\text{UV}} = \int d^4x \sqrt{-G}|_{\phi=0} (-V_{\text{UV}} + \mathcal{L}_{\text{UV}}), \quad (2.4)$$

$$S_{\text{IR}} = \int d^4x \sqrt{-G}|_{\phi=\pi} (-V_{\text{IR}} + \mathcal{L}_{\text{IR}}), \quad (2.5)$$

where M is the five dimensional Planck mass and G_{MN} the metric of the spacetime. Our convention is to use Latin (Greek) indices for 5D (4d) Lorentz indices. We use the $(+, -, -, -, -)$ signature for the five dimensional metric. $V_{\text{UV/IR}}$ denotes the vacuum energies on the branes. \mathcal{L}_{IR} describes our visible four dimensional world, i.e. to a good approximation $\mathcal{L}_{\text{IR}} = \mathcal{L}_{\text{SM}}$. \mathcal{L}_{UV} is only written here for completeness. It could describe some hidden world at $\phi = \pi$, but at this point we set it for simplicity to zero.

The determination of the form of the five dimensional metric is done by using the assumption of 4d Poincare invariance. This can be incorporated into the ansatz

$$ds^2 = e^{-2\sigma(\phi)} \eta_{\mu\nu} dx^\nu dx^\mu + r_c^2 d\phi^2. \quad (2.6)$$

Here the unknown function $\sigma(\phi)$ of the metric (2.6) can then be computed by solving the five dimensional Einstein equation. We use the standard semi-classical approach of quantum field theory in curved spacetime, i.e. we neglect the back-reactions of gauge and matter fields as, they are expected to be small. Thus we set $\mathcal{L}_{\text{IR}} = 0$ in the equation of motion. As the vacuum energies $V_{\text{UV/IR}}$ on the branes can be potentially large they are kept here. Under these assumptions the 5D Einstein equations yield the differential equations [14]

$$\sigma'(\phi)^2 = -\frac{\Lambda r_c^2}{24M^3}, \quad (2.7)$$

$$\sigma'' = \frac{r_c}{12M^3} (\delta(\phi - \pi)V_{\text{IR}} + \delta(\phi)V_{\text{UV}}). \quad (2.8)$$

Equation (2.7) yields the non-trivial solution

$$\sigma(\phi) = \sqrt{\frac{-\Lambda}{24M}} r_c |\phi| \equiv k r_c |\phi|. \quad (2.9)$$

Here the absolute value of ϕ is needed to ensure the orbifold symmetry $\phi \rightarrow -\phi$ of the solution and therefore the correct kinks in equation (2.8). Finally after inserting the solution into equation 2.8 we find the relation

$$V_{\text{UV}} = -V_{\text{IR}} = 24M^3 k. \quad (2.10)$$

Physically this solution implies a non-zero negative bulk cosmological constant. To generate the 4d Lorentz invariance this cosmological constant is directly coupled to the 4d brane vacuum energies. As the vacuum energy V_{IR} can be interpreted as the four dimensional cosmological constant relation (2.10) just reflects the fine-tuning of the ordinary cosmological

CHAPTER 2. THE RANDALL–SUNDRUM MODEL

constant problem. The RS setup does not give any solution for this issue. Inserting the solution (2.9) into the metric we find the form

$$ds^2 = e^{-2kr_c|\phi|} \eta_{\mu\nu} dx^\nu dx^\mu + r_c^2 d\phi^2. \quad (2.11)$$

This metric actually represents the metric of a slice of a 5D Anti–De-Sitter spacetime, i.e. the maximally symmetric five dimensional spacetime with negative cosmological constant. To make this more explicit we transform the metric into the conformal version via the coordinate transformation

$$z = \frac{e^{-kr_c\phi}}{k}. \quad (2.12)$$

This yields

$$ds^2 = \frac{1}{(kz)^2} (\eta_{\mu\nu} dx^\nu dx^\mu - dz^2). \quad (2.13)$$

For the rest of the thesis we will exclusively use the conformal metric (2.13). Note that the UV brane has the coordinate $z = \frac{1}{k}$ in direction of the fifth dimension in this coordinate system. The IR brane has the fifth coordinate $z = \frac{e^{-kr_c\pi}}{k} \equiv \frac{1}{T}$. Thus the RS metric induces via the geometry of the spacetime two physical scales k and T . k is of the size of the Planck mass. T is a priori not specified by the initial assumptions of the model. But it is exponentially suppressed by the compactification radius r_c of the fifth dimension. To specify the value of T we investigate the gauge–hierarchy problem for this setup.

As a SM field the Higgs is localised on the IR-Brane in the original RS model formulation. Because the spacetime on the IR-brane can be obtained by the conformal transformation $\eta_{\mu\nu} \rightarrow (T/k)^2 \eta_{\mu\nu}$ we have to rescale the Higgs field by $\Phi \rightarrow \Phi k/T$ in order to directly generate an action with canonical kinetic terms.

$$\begin{aligned} S_{\text{Higgs}} &= \int d^4x \underbrace{\sqrt{-G_{\text{IR}}}}_{(T/k)^4} \left(\underbrace{G_{\text{IR}}^{\mu\nu}}_{(k/T)^2 \eta^{\mu\nu}} \left(\frac{k}{T} \right)^2 \partial_\mu \Phi^\dagger \partial_\nu \Phi - \frac{\lambda_5}{2} \left(\Phi^\dagger \Phi - \frac{v_5^2}{2} \right)^2 \right) \\ &= \int d^4x \left(\eta^{\mu\nu} \partial_\mu \Phi^\dagger \partial_\nu \Phi - \frac{\lambda_5}{2} \left(\Phi^\dagger \Phi - \left(\frac{T}{k} \right)^2 \frac{v_5^2}{2} \right)^2 \right). \end{aligned} \quad (2.14)$$

Comparison with the 4d Minkowski spacetime Higgs sector of the SM yields

$$\lambda = \lambda_5, \quad v = \frac{T}{k} v_5 = e^{-kr_c\pi} v_5. \quad (2.15)$$

Because the spacetime is conformal the rescaling of the mass dimension one parameter v_5 by the inverse of the conformal factor (T/k) is natural. The scalar selfcoupling remains untouched, because it has mass dimension zero. Due to the initial assumptions of the model the vacuum expectation value (vev) v_5 should be of the order of the Planck mass. Therefore, to ensure a four–dimensional vev to be around $\mathcal{O}(\text{TeV})$ one has to impose

$$\frac{T}{k} \sim \frac{\mathcal{O}(\text{TeV})}{M_{\text{Pl}}} \sim 10^{-16}, \quad (2.16)$$

which is equivalent to $kr_c \sim 12$.

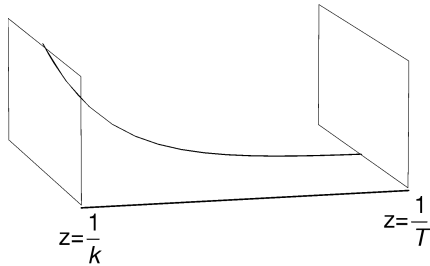


Figure 2.2: Picture of the slice of AdS_5 in the fifth coordinate direction with z being the 5th coordinate.

Thus, the large hierarchy $v \ll M_{\text{Pl}}$ is just created by the geometry of the spacetime. There is no large hierarchy for the fundamental parameters of the Lagrangian in this model. That protects the theory also from problematic correction to the Higgs potential. That is due to a bare Higgs mass, which by assumptions of this model is of the order of the Planck scale. The quantum corrections are on the same footing. However the physical Higgs mass as dimension one parameter will always be scaled down to the EW regime by the exponential $e^{-kr_c\pi}$ with $kr_c \sim 12$.

It is also interesting to calculate the proper length of the extra dimension

$$l = \int_{\frac{1}{k}}^{\frac{1}{T}} dz \frac{1}{kz} = \frac{1}{k} \ln\left(\frac{k}{T}\right) = \pi r_c \sim \frac{1}{M_{\text{Pl}}}. \quad (2.17)$$

Thus, the size of the extra dimension remains to be of the order of one over the Planck mass for a large variation of the parameter T .

There are still two issues remaining for the original RS setup. The first one is the question how this spacetime with the two four dimensional branes around a slice of a five dimensional Anti-De-Sitter spacetime remains stable against perturbations of the compactification radius. This can be answered by the Goldberg-Wise mechanism [66], which uses an additional scalar field to stabilize the metric. We will not discuss it detail in this thesis. The second and more fundamental question is how the original RS setup can be generated by a more fundamental model of physics, which also includes a quantum description of gravity. While such a theory is still far away from completion it is interesting to note, that there are certain string theory setups [67, 68], which include compactification procedures for the extra dimensions that yield a warp factor.

2.3 Minimal RS model

The original RS setup assumes all of the SM fields to be restricted to the IR brane. However the solution of the hierarchy problem is not lost after allowing all gauge fields [16–19] and all fermions [19, 20] to propagate in the bulk. In fact by allowing all fields except the Higgs to travel through the extra dimension one generates a model with several advantages compared to the original ansatz. First of all bulk fermions lower the constraints coming from higher dimensional operators, that generate proton decay and FCNCs like meson mixing [19]. Another advantage of bulk fermions is the possibility to generate naturally the flavour mass

hierarchy. This can be achieved by employing anarchical fundamental Yukawas and appropriate localisation positions of the bulk fermions in the fifth dimension without building the flavour hierarchies explicitly into the the fundamental parameters [19–22]. This mechanism of generating the flavour mass hierarchies also automatically generates the correct entries of the CKM matrix [69] and also mediates potentially model constraining FCNCs with light quarks [19], which is also sometimes denoted as the RS–GIM mechanism [69, 70]. Furthermore bulk fermions lower the constraints coming from the corrections to the Peskin–Takeuchi S parameter, that are caused by bulk weak gauge-bosons [19, 71, 72]. The setup of the SM in the bulk is called the minimal RS model. For this thesis we will use this model exclusively together with the custodial protected RS model.

2.3.1 5D Lagrangian

To begin the discussion of the minimal RS model it is useful to consider first the generalisation of the SM to the non-trivial five dimensional RS metric. The initial steps are straightforward. All four dimensional gauge fields have to be replaced by five dimensional fields. For example for the SU(2) fields we have to use

$$W^\mu \rightarrow W^N. \quad (2.18)$$

where $W^N = (W^\mu, W^5)$.

To incorporate all fermion fields we need to find a five dimensional Clifford algebra

$$\{\Gamma^N, \Gamma^M\} = 2\eta^{NM} \times \mathbb{1}_{5 \times 5}. \quad (2.19)$$

This implies the determination of a suitable Γ^4 matrix. For this thesis we use the representation

$$\Gamma^N = (\gamma^\mu, -i\gamma^5). \quad (2.20)$$

Additionally one has also to incorporate the fermion field spinors into the curved spacetime. This is done usually by introducing a coordinate transformation into a local Minkowski coordinate system via the vielbein formalism, see for example [20]. Note that there is no equivalent to γ_5 for a five-dimensional Clifford algebra as the Dirac-spinor representation is irreducible in five dimensions. Thus a priori all 5D fermion fields are vector fermions in the RS model.

Using the conformal metric as defined in (2.13) we can write down the SM Lagrangian for the minimal RS model in the flavour basis

$$\begin{aligned} S_{(5D)} = & \int d^4x \int_{1/k}^{1/T} dz \sqrt{G} \left\{ -\frac{1}{4} F^{MN} F_{MN} - \frac{1}{4} W^{a,MN} W_{MN}^a - \frac{1}{4} G^{a,MN} G_{MN}^a \right. \\ & \left. + \sum_{\psi=E,L,Q,d,u} \left(e_m^M \left[\frac{i}{2} \bar{\psi}_i \Gamma^m (D_M - \overleftarrow{D}_M) \psi_i \right] - M_{\psi_i} \bar{\psi}_i \psi_i \right) \right\} + S_{GF+ghost} + S_{Higgs}, \end{aligned} \quad (2.21)$$

where $e_m^M = (1, 1, 1, 1, 1)kz$ is the five dimensional inverse vielbein. The five dimensional metrical tensor G is given in conformal coordinates as $G = 1/(kz)^{10}$. We use the following definition for the covariant derivative for quark fields

$$D_N = \partial_N - ig_5' \frac{Y}{2} B_N - ig_5 \frac{\tau^a}{2} W_N^a - ig_{s5} T^a G_N^a. \quad (2.22)$$

2.3. MINIMAL RS MODEL

Y is the hypercharge, τ^a the Pauli matrices and T^A the generators of $SU(3)_c$. Note that for an arbitrary curved spacetime the covariant derivative of a fermion field also needs to contain the spin-connection $[\omega_A]_{NM} = G_{CD}e_N^C (\partial_A e_M^B + \Gamma_{AE}^D e_N^E)$. However for the conformal coordinate system of the AdS_5 the spin connection drops out, because the metric is diagonal [20]. The field strength tensors are written in the standard way

$$F_{NM} = \partial_M A_N - \partial_N A_M \quad W_{NM} = \partial_M W_N^a - \partial_N W_M^a + g_5 \epsilon^{abc} W_N^b W_M^c \quad (2.23)$$

$$G_{NM} = \partial_M G_N^a - \partial_N G_M^a + g_5 f_{abc} G_N^b G_M^c. \quad (2.24)$$

The action of the Higgs strongly depends on the localisation prescription, therefore we only write the Higgs action down for an exactly IR brane localised Higgs field. The subtleties concerning the localisation scheme will be discussed in subsection 2.3.4.

$$S_{\text{Higgs}} = \int d^4x [(D^\mu \Phi)^\dagger D_\mu \Phi - V(\Phi)] + S_{\text{Yukawa}}$$

$$S_{\text{Yukawa}} = \int d^4x \left[- \left(\frac{T}{k} \right)^3 \left[y_{ij}^{(5D)} (\bar{L}_i \Phi) E_j + y_{dij}^{(5D)} (\bar{Q}_i \Phi) d_j + y_{u ij}^{(5D)} (\bar{u}_i \Phi) Q_j \right] + \text{h.c.} \right]. \quad (2.25)$$

The potential is written as

$$V(\phi) = -\mu_{5D} \left(\frac{T}{k} \right)^2 \Phi^\dagger \Phi + \frac{\lambda}{4} (\Phi^\dagger \Phi)^4. \quad (2.26)$$

All fields in (2.25) are evaluated at the fifth coordinate $z = \frac{1}{T}$. Here the indices of the fermion fields denote the fermion flavour. As already noted in section (2.2) the powers of (T/k) are generated after applying a normalisation to generate a canonical kinetic term for the Higgs Lagrangian.

In correspondence to the initial assumptions of the original RS model all dimensionful parameters of the 5D Lagrangian $g_5, g'_5, g_{s5}, M_{\psi_i}, y_{ij}^{(5D)}, y_{dij}^{(5D)}, y_{u ij}^{(5D)}$ are of the order of M_{Pl} . As 5D fermion fields are automatically vector fermions, there is no argument not to include the bulk 5D fermion masses M_{ψ_i} . The standard convention is to consider dimensionless quantities for these masses $c_i = M_{\psi_i}/k$. Additionally we define the dimensionless Yukawa matrices $Y_{ij} = y_{ij}^{(5D)}/k, Y_{d/uj} = y_{d/uj}^{(5D)}/k$. Note that although the action (2.21) is written in the flavour basis, the Yukawa matrices do not have to be simultaneously be diagonal in the RS model. This means in particular a violation of the lepton number conservation and the CP invariance in the lepton sector for the RS model.

The Lagrangian for a brane Higgs minimal RS model contains in total $3 \cdot 9 + 5 \cdot 3 = 42$ free parameters. The question of their determination will be discussed in the next section.

2.3.2 Kaluza-Klein decomposition

Inspired by other 5D field theories with compact extra dimensions like for example the universal extra dimension models [73] one expects the fifth component of the momentum of all bulk fields to be quantised in a discrete manner. Such a behaviour of all bulk fields can then be used for a Kaluza-Klein decomposition of the 5D theory into a four dimensional field theory. Thus, we expect all bulk fields to gain a huge tower of heavy partner particles, which are often called Kaluza-Klein particles or excitations. In this section, we will briefly derive the Kaluza-Klein decomposition for fermions and then for gauge fields in the unbroken phase. In doing so we will shed some light on how the SM Lagrangian can be obtained as the low energy limit of the 5D Lagrangian (2.21). Furthermore, the Kaluza-Klein decomposition is also important for the determination of the free parameters of (2.21).

CHAPTER 2. THE RANDALL–SUNDRUM MODEL

2.3.2.1 Bulk fermions

We start by evaluating the bilinear terms for a general fermion field of the action (2.21). After inserting the definition of the vielbein and the covariant derivatives one finds

$$S_F = \int d^4x \int_{\frac{1}{k}}^{\frac{1}{\tilde{k}}} dz \left(\frac{1}{kz} \right)^4 \bar{\psi} \left(i\cancel{\partial} + i\Gamma^4 \left(\partial_z + \frac{2}{z} \right) - \frac{c}{z} \right) \psi + \dots \quad (2.27)$$

As defined above c is the dimensionless bulk mass $c = M/k$. To find the appropriate factorization ansatz for the fermion field ψ , we insert into equation (2.27) the explicit form of the fifth gamma matrix Γ^4 using the Weyl representation for the Dirac matrices.

$$\Gamma^4 = -\gamma_5 = i \text{Diag}(\mathbb{1}_{2 \times 2}, -\mathbb{1}_{2 \times 2}) \quad (2.28)$$

This enables us to rewrite the action (2.27) in terms of the chiral components of ψ [20]

$$S_F = \int d^4x \int_{\frac{1}{k}}^{\frac{1}{\tilde{k}}} dz \left(\frac{1}{kz} \right)^4 \left(\bar{\psi}_L i\cancel{\partial} \psi_L + \bar{\psi}_R i\cancel{\partial} \psi_R \right) \quad (2.29)$$

$$+ \bar{\psi}_L \left(\partial_z - \frac{2}{z} - \frac{c}{z} \right) \psi_R - \bar{\psi}_R \left(\partial_z - \frac{2}{z} + \frac{c}{z} \right) \psi_L \Big). \quad (2.30)$$

We use the standard definition $\psi_{L/R} = P_{L/R} \psi$ together with

$$P_{L/R} = \frac{1 \pm \gamma_5}{2}. \quad (2.31)$$

Because the four-vector partial derivatives and the derivative with respect to the fifth coordinate z do not mix in the action 2.30, it is convenient to introduce a factorisation ansatz for the 5D fields $\psi_{L/R}$ of the form

$$\psi_L(x, z) = \sum_n f^{(n)}(z) \psi_L^{(n)}(x) \quad \psi_R(x, z) = \sum_n g^{(n)}(z) \psi_R^{(n)}(x), \quad (2.32)$$

where $\psi_{L/R}^{(n)}$ are the chiral components of a massive four dimensional Dirac field satisfying the Dirac equation.

$$(i\cancel{\partial} - m_n) \psi^{(n)} = 0 \quad (2.33)$$

The usage of this ansatz automatically leads to the mode equations [20]

$$\left(\partial_z - \frac{2}{z} - \frac{c}{z} \right) f^{(n)}(z) = -m_n g^{(n)}(z) \quad (2.34)$$

$$\left(-\partial_z + \frac{2}{z} - \frac{c}{z} \right) g^{(n)}(z) = -m_n f^{(n)}(z), \quad (2.35)$$

together with the orthonormality conditions

$$\int_{\frac{1}{k}}^{\frac{1}{\tilde{k}}} dz \left(\frac{1}{kz} \right)^4 f^{(n)}(z) f^{(m)}(z) = \int_{\frac{1}{k}}^{\frac{1}{\tilde{k}}} dz \left(\frac{1}{kz} \right)^4 g^{(n)}(z) g^{(m)}(z) = \delta_{n,m}. \quad (2.36)$$

Before discussing the solution of the mode equations let us first insert naively the factorization ansatz into the action (2.27). Doing so we can perform the integration of the fifth coordinate integral in (2.27) trivially via the orthonormality conditions for the mode functions. The Kaluza-Klein decomposition then leads to a in principle infinite series of 4d fermion actions

$$S_{\text{F}} = \sum_n \int d^4x \bar{\psi}^{(n)} (i\cancel{\partial} - m_n) \psi^{(n)}, \quad (2.37)$$

i.e. each fermion field obtains a large tower of massive fermions, after integrating out the fifth dimension. It is customary to identify the zero mode term of the Kaluza-Klein decomposition with the four dimensional SM field. However SM fermions are chiral and massless in the unbroken phase. Therefore one needs to demand additional conditions on the mode functions in order to generate the correct low energy limit. For this we note that there is still the freedom to choose the boundary conditions on the branes of the chiral components of the fermion field. Note that the boundary conditions of each chiral component are in fact not independent of each other, but coupled via the mode equations (2.34) and (2.35). For fermion fields it turns out, that Dirichlet conditions on the mode functions eliminate a massless zero-mode function of the wrong chirality [20]. Therefore, the requirement to recover the SM in the low energy limit leads to the boundary conditions

$$f_X^{(n)}(z)|_{z=\frac{1}{k}} = f_X^{(n)}(z)|_{z=\frac{1}{T}} = 0 \quad (2.38)$$

$$g_Y^{(n)}(z)|_{z=\frac{1}{k}} = g_Y^{(n)}(z)|_{z=\frac{1}{T}} = 0, \quad (2.39)$$

where $X = E, d, u$ and $Y = L, Q$. This condition automatically eliminates the zero-mode wrong chirality modes $g_X^{(0)}$ and $f_Y^{(0)}$.

In the standard literature the notation $E_L(-, -)$ is used to denote, that the left handed component of the lepton singlet field satisfies Dirichlet boundary conditions on the UV (IR) brane. Here the first (second) entry indicates the boundary conditions on the UV (IR) brane. The other chiral component is then written with flipped signs $E_R(+, +)$ in this notation, where the $+$ represents Neumann boundary conditions under the operator $d^- = (-\partial_z + \frac{2}{z} - \frac{c}{z})$. Note that $(+, +)$ for a left handed fermion field implies Neumann boundary conditions on both branes under the operator $d^+ = (\partial_z - \frac{2}{z} - \frac{c}{z})$.

With the correct boundary conditions the left handed zero mode function of a SM doublet fermion field $f_X^{(0)}$ and the right handed zero mode function for a SM singlet field $g_Y^{(0)}$ can be obtained as [20]

$$f_X^{(0)}(z) = \sqrt{\frac{1-2c}{1-\epsilon^{1-2c}}} \sqrt{T}(kz)^2 (Tz)^{-c} = g_Y^{(0)}(z)|_{c \rightarrow -c}, \quad (2.40)$$

where $\epsilon = T/k$. The n th Kaluza-Klein mode function for SM doublet fermion takes the form [20]

$$f_X^{(n)}(z) = Nz^{\frac{5}{2}} \left(Y_{c+1/2}(m_n z) - \frac{Y_{c+1/2}(m_n/T) J_{c+1/2}(m_n/z)}{J_{c-1/2}(m_n/T)} \right) \quad (2.41)$$

$$f_X^{(n)}(z) = Nz^{\frac{5}{2}} \left(Y_{c-1/2}(m_n z) - \frac{Y_{c-1/2}(m_n/T) J_{c-1/2}(m_n/z)}{J_{c-1/2}(m_n/T)} \right), \quad (2.42)$$

where m_n denotes the Kaluza-Klein mass and N a normalisation to ensure the normalisation of the modes (2.36). The mass eigenvalues can be computed as the zeros of the equation [20]

$$Y_{c-1/2}(m_n/k) J_{c-1/2}(m_n/T) - J_{c-1/2}(m_n/k) Y_{c+1/2}(m_n/T) = 0. \quad (2.43)$$

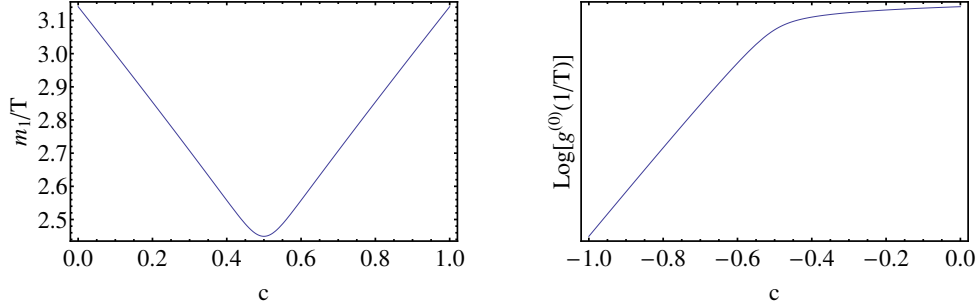


Figure 2.3: *Left panel:* Mass of the first Kaluza-Klein for a SM doublet as a function of the bulk mass parameter c . *Right panel:* $g_{E_j}^{(0)}\left(\frac{1}{T}\right)$ as a function of the bulk mass.

The solution for the singlet KK mode functions and their mass eigenvalues have a similar form and can be also found in [28].

The left panel of Figure 2.3 shows the general dependence of the first KK mass of a SM doublet field on the bulk mass parameter c . This does not yield an answer how to determine the bulk mass parameters. However, one can clearly observe that the masses are of the order of T . Thus the inverse conformal coordinate of the IR brane can be interpreted as the typical mass scale of the minimal RS model. We will see down below that this holds true for bulk gauge-bosons.

In order to understand the selection of the parameters c we consider the determination of the 4d mass eigenvalues of the zero-mode fermions after breaking the electroweak symmetry. For simplicity we keep here to a brane localised Higgs. The implications done here still hold for different localisation schemes, see section 2.3.4. After inserting the vacuum expectation value into the Higgs doublet the zero mode leptonic part of the Yukawa sector ((2.25)) yields

$$S_{\text{Yukawa}} \supseteq \int d^4x \frac{v}{\sqrt{2}} \frac{T^3}{k^4} Y_{ij} f_{L_i}^{(0)} \left(\frac{1}{T} \right) g_{E_j}^{(0)} \left(\frac{1}{T} \right) (\bar{l}_i) E_j, \quad (2.44)$$

where l_i is the spinor field for the charged left handed leptons. Using expression (2.44) we can immediately identify the 4d Yukawa matrix before rotation as

$$y_{ij} = \frac{v}{\sqrt{2}} \frac{T^3}{k^4} Y_{ij} f_{L_i}^{(0)} \left(\frac{1}{T} \right) g_{E_j}^{(0)} \left(\frac{1}{T} \right). \quad (2.45)$$

Equation (2.45) contains together with the 5D Yukawa matrix 15 a priori unknown 5D parameters of the order $\mathcal{O}(1)$. After rotation to the mass basis (2.45) equals to the lepton mass spectrum. Thus, this allows us to fix three of the 15 5D parameters. Our strategy here is to use the low-energy mass spectrum to fix the bulk masses of the doublet field. For the remaining parameters we adopt the so called anarchical scenario:

- We randomly generate the Yukawa matrix Y_{ij} with a certain range of possible absolute values. The complex phases are also randomly generated.
- The remaining three bulk masses of the singlet lepton field are randomly chosen. We use for the different generations the bulk mass intervals $(-0.70, -0.5)$ for the electron, $(-0.68, -0.48)$ for the muon and $(-0.57, -0.45)$ for the the tau. Note that we work in

the unbroken phase. Thus the name electron just denotes the bulk mass of the first generation in the flavour basis.

- As a last step we solve the equation (2.45) after rotation to the mass basis for the correct 4d lepton mass spectrum. This solution can only be obtained numerically. Furthermore there are situations, where the random number parameters are such that the 4d spectrum solution cannot be found. Hence we repeat the first steps until a valid set has been found.

The different intervals for the random number generation of the singlet bulk masses is motivated by the behaviour of $g_{E_j}^{(0)}\left(\frac{1}{T}\right)$ as function of the bulk masses. $g_{E_j}^{(0)}\left(\frac{1}{T}\right)$ is growing monotonic with increasing bulk masses. However this growth is exponential up to the point $c = -0.5$, see right panel of Figure 2.3. Afterwards the function $g_{E_j}^{(0)}\left(\frac{1}{T}\right)$ only grows as \sqrt{c} . Therefore, the point $c = -0.5$ can be considered as the turning point of the localisation of the bulk fermion fields from the UV brane to the IR brane. Thus one has to assign for heavy fermion fields larger bulk masses in order to generate the correct 4d mass hierarchy.

The bulk masses of the quark fields can be determined in a similar fashion. The only difference is the necessary inclusion of the CKM matrix. However this can be achieved by an adoption of the Froggatt-Nielsen Mechanism, see [74] for the original idea and [23] for the adoption in the context of RS model. We will not discuss this in detail in this thesis.

2.3.2.2 Bulk gauge-bosons

5D gauge fields contain an additional fifth component, which is not present in the SM. To complicate the situation it also mixes with the other components of the gauge fields due to the structure of the kinetic terms in (2.21). It is therefore customary to introduce a 5D R_ξ gauge fixing in order to eliminate this mixing in the bilinear terms of the gauge Lagrangian. As the procedure can be transferred to any type of bulk gauge field, we will only consider gluon fields here. The 5D R_ξ gauge can be introduced by the following gauge fixing action [75]

$$S_{\text{Gf}} = \int d^4x \int_{\frac{1}{k}}^{\frac{1}{T}} -\frac{1}{2\xi k z} \left[\partial_\nu G^\nu - \xi z \partial_z \left(\frac{1}{z} G_5 \right) \right]^2. \quad (2.46)$$

Note that this 5D covariant gauge introduces ghost fields. However ghost fields are not needed for this work, because we do not consider one loop corrections to the the gauge propagator. Using the gauge fixing as defined above in (2.46) the bilinear part of the gluon action takes the form

$$S_{\text{G+Gf}} = \int d^4x \int_{\frac{1}{k}}^{\frac{1}{T}} \frac{1}{2kz} \left[G_\nu \left(\partial^2 \eta^{\nu\mu} - \left(1 - \frac{1}{\xi} \right) \partial^\nu \partial^\mu - z \partial_z \left(\frac{1}{z} \partial_z \right) \eta^{\nu\mu} \right) G_\mu \right. \\ \left. - G_5 \partial^2 G_5 + \xi G_5 \partial_z \left(z \partial_z \left(\frac{1}{z} G_5 \right) \right) \right] + \dots \quad (2.47)$$

Note that for the formulation of (2.47) one needs to perform an integration by parts of (2.21), in order to ensure that no boundary terms after this integration survive [75]. This can be done by assigning the fifth component of the gauge field Dirichlet boundary conditions on the brane [75]. As in the fermion sector one can separate the fifth coordinate in all gauge

CHAPTER 2. THE RANDALL–SUNDRUM MODEL

fields using the factorisation ansatz $G^\nu(x, z) = \sum_n f_G^{(n)}(z) G^\nu(x)$. Following the paradigm of massive 4d Kaluza-Klein fields we can automatically write the equation of motion for the mode functions as

$$z \partial_z \left(\frac{1}{z} \partial_z \right) f_G^{(n)}(z) = -m_n^2 f_G^{(n)}(z), \quad (2.48)$$

together with the orthonormality conditions

$$\int_{\frac{1}{k}}^{\frac{1}{T}} \frac{1}{2kz} f_G^{(n)}(z) f_G^{(m)}(z) = \delta_{n,m}. \quad (2.49)$$

To ensure an massless zero mode profile one has to demand Neumann boundary condition for the mode functions [75]

$$\partial_z f_G^{(n)}(z)|_{\frac{1}{k}} = \partial_z f_G^{(n)}(z)|_{\frac{1}{T}} = 0. \quad (2.50)$$

Using this construction the zero mode profile can be determined as [75]

$$f_G^{(0)}(z) = \sqrt{\frac{k}{\ln \frac{k}{T}}}. \quad (2.51)$$

It is noteworthy that the zero mode function of the four vector part of the bulk gauge bosons is a constant function. This represents an important feature for penguin diagrams that involve the emission of a real SM gauge-boson. For completeness we give the solution for the n th Kaluza-Klein mode profile [75]

$$f_G^{(n)}(z) = Nz \left(J_1(m_n z) - \frac{J_0(m_n/k)}{Y_0(m_n/k)} Y_1(m_n z) \right), \quad (2.52)$$

where the mass eigenvalues m_n are the zeros of the equation [75]

$$\left(J_0(m_n/T) - \frac{J_0(m_n/k)}{Y_0(m_n/k)} Y_0(m_n/T) \right) = 0, \quad (2.53)$$

which follows directly out of the boundary condition (2.50) on the IR brane. Solving (2.53) numerically we find for the first three Kaluza-Klein masses of the gauge-bosons $m_1 \sim 2.45T$, $m_2 \sim 5.57T$ and $m_3 \sim 8.7T$. Thus, the first KK excitations of the four vector gauge-bosons have mass of the order $\mathcal{O}(T)$, which validates the previous statement of T being the natural scale of the RS model. Note that the spacing between the KK masses is not equidistant. That can be compared to other extra dimension models like for example universal extra dimensions, where at tree-level the KK masses have an equidistant spacing.

To conclude this section we still have to deal with the scalar component of 5D bulk gauge-bosons. To this end we also apply a KK decomposition to the field G_5 . Using the bilinear action (2.47) we can directly write the equation of motion for the mode profiles

$$\xi \partial_z \left(z \partial_z \left(\frac{1}{z} f_{G_5}^{(n)}(z) \right) \right) = -\xi m_n^2 f_{G_5}^{(n)}(z), \quad (2.54)$$

where the mass eigenvalues m_n of the pseudo Goldstone boson G_5 have to be the same as for the vector part. That is because equation (2.54) is solved directly after the trivial identification

$$f_{G_5}^{(n)}(z) = \partial_z f_G^{(n)}(z), \quad (2.55)$$

which also guaranties the correct Dirichlet boundary conditions

$$f_{G_5}^{(n)}(z)|_{\frac{1}{k}} = f_{G_5}^{(n)}(z)|_{\frac{1}{\bar{k}}} = 0 \quad (2.56)$$

Note that (2.55) implies, that there is no massless zero mode for G_5 .

2.3.3 5D Picture

As shown in the last section the dynamics of the 5D theory without interactions can be fully absorbed into an extended 4d Lagrangian, where each fermion and gauge field includes a large tower of heavy Kaluza-Klein partners with masses of the order of $\mathcal{O}(T)$. Unfortunately the situation does not look so bright after turning on the interaction terms of the 5D Lagrangian. Consider for example the coupling of the B field to an arbitrary fermion field. After insertion of the Kaluza-Klein decomposition one remains with coordinate integrals over three mode functions, which cannot be done easily by orthonormality relations, unless the gauge-boson profile function is a zero mode. Furthermore, the inevitable presence of 5D propagators in perturbation theory induces even more problems as each propagator automatically generates an infinite series in the KK picture. To see this, let us investigate the solution of the vector part of the 5D propagator. Naturally such propagator will depend on the four momentum after performing a standard 4d Fourier transformation into 4d momentum space and the starting and end point 5th coordinate. We can write this propagator as [28]

$$\Delta_G^{\mu\nu}(p, x, y) = \Delta_G(p, x, y) \eta^{\mu\nu} + \frac{p^\mu p^\nu}{p^2} \left(\Delta_G\left(\frac{p}{\sqrt{\xi}}, x, y\right) - \Delta_G(p, x, y) \right), \quad (2.57)$$

using the general R_ξ gauge. In such a coordinate representation the partial differential equation for to the transverse part of the gauge boson propagator can be written as [28]

$$\left(p^2 + x \partial_x \frac{1}{x} \partial_x \right) \Delta_G(p, x, y) = -ikx \delta(x - y), \quad (2.58)$$

with the additional boundary conditions

$$\partial_x \Delta_G(p, x, y)|_{x=\frac{1}{\bar{k}}} = 0 \quad \partial_x \Delta_G(p, x, y)|_{x=\frac{1}{k}} = 0. \quad (2.59)$$

Then it is clear that the partial differential equation can be solved directly with the mode equation for gluons (2.48). We find immediately

$$\Delta_G(p, x, y) = \sum_n f_G^{(n)}(x) \frac{i}{p^2 - m_n^2} f_G^{(n)}(y). \quad (2.60)$$

Thus after the application of the Kaluza-Klein decomposition a typical one-loop diagram in RS will include at least one infinite sum. Additionally for each vertex an integral over the 5th coordinate has to be taken. Naturally the evaluation of even one infinite sum over the difficult terms of the mode function cannot be done easily. Therefore we will not use the Kaluza-Klein decomposition for our following calculations. Still the knowledge of the existence of such decomposition allows us in some cases to simplify the computation.

One way out of possible issues concerning infinite Kaluza-Klein sums is to use the well established 5D formalism [32, 75]. We make use of this formalism almost entirely throughout this thesis. The 5D formalism implies the evaluation of the perturbation theory entirely at

CHAPTER 2. THE RANDALL–SUNDRUM MODEL

5D level. The price one pays for this is a complicated 5D propagator structure, for example the 5D gauge boson propagator of the gluon takes the form

$$\Delta_G(p, x, y) = kxy \frac{\theta(x-y) \left(K_0\left(\frac{p}{k}\right) I_1(py) + I_0\left(\frac{p}{k}\right) K_1(py) \right) \left(K_0\left(\frac{p}{T}\right) I_1(px) + I_0\left(\frac{p}{T}\right) K_1(px) \right)}{K_0\left(\frac{p}{k}\right) I_0\left(\frac{p}{T}\right) - I_0\left(\frac{p}{k}\right) K_0\left(\frac{p}{T}\right)} + (x \longleftrightarrow y). \quad (2.61)$$

It is noteworthy that all propagator in the 5d formalism have a similar form. This complicates the structure of all appearing diagrams on the first sight. However, on the second sight the disappearance of infinite sums simplifies significantly the computation of all tree-level diagrams. Loop diagrams do not gain much from this aside from a potentially clearer structure of the involved scales in the loop integrand.

A complete 5D calculation gives rise to the question, how to relate the 5D coupling constants to the usual 4d couplings constants. As usual for extra dimension theories this can be done by analysing the zero mode terms of the associated interaction. Let us for example consider the coupling of SM singlet leptons to a zero mode B boson. Here we have to use the constancy of the gauge-boson zero mode function in order to evaluate the coordinate vertex integral.

$$-i \frac{Y}{2} g'_5 \int_{\frac{1}{k}}^{\frac{1}{T}} \frac{dz}{(kz)^4} g^{(0)}(z) g^{(0)}(z) f_B^{(0)}(z) = -i \frac{Y}{2} g'_5 f_B^{(0)}(z). \quad (2.62)$$

Thus, we identify $g'_5 f_B^{(0)}(z) = g'$, because the zero mode interactions should resemble the SM vertices in the low energy limit. This procedure can be used for all other gauge-fermion 5D vertices.

$$g_X = g_{X5} f_X^{(0)}(z), \quad (2.63)$$

where X is an arbitrary SM gauge-boson. It is important to note that all 5D calculation done for this thesis are performed in the unbroken phase before EWSB, i.e. we treat the Yukawa interaction as a small perturbation. The error induced by this is at least of the order of v^2/T^2 , where v is the vacuum expectation value. Thus, even for a $T = 1$ TeV the possible induced error is small. However we will see in section 2.3.5 and 2.4.5 that the typical lower limit of the RS scale T lies in the range of 2 – 4 TeV, which drastically diminishes the error caused by performing all 5D computations in the unbroken phase. To conclude we summarise how the typical RS calculation has to be done in the 5D formalism.

- Draw all diagrams as in the SM model and include all necessary prefactors and 4d loop integrals as usual. All couplings are five dimensional coupling constants. Include also the fifth component of all gauge fields if necessary and also keep track of the fifth coordinates of the vertices and 5D propagators.
- Include an integration over the associated fifth coordinates of each vertex $\int_{\frac{1}{k}}^{\frac{1}{T}} \frac{dz}{(kz)^{5-i}}$, where i counts how many times the metric is involved for the associated vertex, i.e. how many four vector contractions are involved.

The relation between the 5D gauge couplings and 4d gauge couplings (2.63) together with the summation of the infinite KK sums for the 5D formalism emphasises a problem, which we have so far ignored in our discussion. As $f_X^{(0)}(z)$ has mass dimension 1/2 the 5D gauge

coupling g_{X_5} has to have mass dimension $-1/2$. Of course this could be also directly deduced out of the 5D action, because 5D fermion fields have mass dimension 2 and 5D gauge field mass dimension $3/2$. Therefore, due to the negative mass dimension of the coupling constants the minimal RS models is not a renormalisable theory. It can be only be considered as an effective theory valid up to a cut-Off Λ . To complicate the situation the general belief is that the cut-off in a mixed coordinate–momentum representation generally depends on the fifth coordinate $\Lambda(z)$ [28]. Thus even if the cut-off $\Lambda(1/k)$ has the value of a few times k at the Planck brane the exponential scaling due to the warp factor will turn $\Lambda(1/T)$ to be of the order of T . This would render the 5D formalism into a completely unreliable computation method in a naive computation, because the 5D formalism always includes the complete summation of all KK excitations instead of the summation of only a few KK modes up to the cut-off $\Lambda(1/T)$. Therefore, one should only use the 5D formalism for perturbative calculation, where all KK sums do converge. This the case for finite quantities like for example the calculation of the muon $g-2$ moment [28]. In such a case the error done by the inclusion of the whole KK tower is expected to be of the order of $T^2/\Lambda(1/T)^2$, that is the generic correction one expects for the UV completion of the RS model [28].

2.3.4 Higgs localisation

So far in this thesis we have only approached the Higgs sector with an exactly brane localised Higgs field on the IR brane. However, it is well known that the physics of the RS model with an IR-brane localised Higgs depends strongly on the way the localisation is implemented, see for example [28, 53, 76–78]. To be more precise we have to explicitly define, whether the possible 5D wave function of the Higgs can be resolved in loops. One way to discuss this is to introduce a regularised delta function for the Higgs localisation. The easiest choice for this is a localisation of the Higgs inside a box with a narrow width

$$\delta(z - 1/T) = \lim_{\delta \rightarrow 0} \frac{T}{\delta} \Theta \left(z - \frac{1 - \delta}{T} \right). \quad (2.64)$$

The RS model is then completely defined only after one specifies the order of the limit $\delta \rightarrow 0$ and the limits of possible 4d loop momentum regulators like the dimensional regularisation parameter ϵ or a four dimensional momentum cut-off Λ . If one first performs the loop momentum limits for finite δ and then the limit $\delta \rightarrow 0$, it is indeed possible to resolve the 5D structure of the Higgs. This is most intuitive for a momentum cut-off loop regularisation with a fixed δ . For the case where first the finite width δ goes to zero, before any other limits are taken to their appropriate limits, we return to a true IR brane localised Higgs, whose 5D width cannot be resolved. We will use both cases of limiting ordering throughout this thesis. The first limiting procedure is called “narrow bulk Higgs” (in the terminology of [78]).

Of course a RS model with a “narrow bulk Higgs” gives rise to the question, whether the inevitable arising KK states give any meaningful contributions in the limit $\delta \rightarrow 0$. A narrow bulk KK Higgs is expected to have a mass of the T/δ , therefore the naive expectation is that the Higgs KK tower decouple for small δ , i.e. becomes negligible. However, a recent work [79] has shown that the effects of the full Higgs KK sum can produce sizeable effects in certain one-loop processes even after performing the localisation limit. In order to have a consistent description of KK Higgs modes, we abandon the ad-hoc regularization (2.64) and implement the Higgs field as a full 5D scalar doublet. Since we require both a vacuum expectation value and a zero-mode profile that is strongly localised near the IR brane we need to introduce additional brane potentials on both the IR and UV brane. We will follow the construction of [80] (see also [81]) and thus use the same Higgs profile as in [79]. The

CHAPTER 2. THE RANDALL–SUNDRUM MODEL

details of this realisation together with useful formulae are collected in Appendix B. The 5D profile of the vacuum expectation value takes the form

$$v(z) = \sqrt{\frac{2(1+\beta)}{1-\epsilon^{2+2\beta}}} k^{3/2} T^{\beta+1} v_{\text{SM}} z^{\beta+2}, \quad (2.65)$$

where $v_{\text{SM}} \equiv v \simeq 246 \text{ GeV}$ denotes the SM Higgs vacuum expectation value (vev), and the zero mode profile is, up to small corrections of order v^2/T^2 , proportional to $v(z)$. The parameter β is related to the 5D mass of the Higgs field and determines the degree of IR localisation; the larger β the stronger the localisation. Since we start with a genuine bulk field it is always implied that β is finite until all other regulators have been removed.

In order to obtain the correct SM parameters in the low-energy limit the Yukawa matrices and the Higgs self-coupling must themselves depend on β . For the Yukawa matrices we indicate this dependence by a superscript β , while no superscript refers to the β -independent, dimensionless matrix. The relation is (see Appendix B.3)

$$Y^\beta = \frac{Y}{\sqrt{k}} \frac{2 - c_{L_i} + c_{E_j} + \beta}{\sqrt{2(1+\beta)}} \quad (2.66)$$

with c_{L_i}, c_{E_j} the 5D mass parameters of the lepton fields in the Higgs-Yukawa interaction.

Ultimately, we are interested in large values of β . Whenever we give a result for the bulk Higgs case that does not show an explicit dependence on β , we tacitly assume that the $\beta \rightarrow \infty$ limit has been taken, and the result should be valid up to corrections of $\mathcal{O}(1/\beta)$. We will consider the three different implementations of the Higgs field:

- an exactly brane localised Higgs, that is we use (2.64) (necessary to avoid ambiguities in the calculation), but take $\delta \rightarrow 0$ first.
- a delta-function localised narrow bulk Higgs, that is we use (2.64), but keep δ finite until all other regulators are removed, then $\delta \rightarrow 0$. No Higgs KK modes are considered.
- a true bulk Higgs with the β -profile (2.65) and KK modes.

The second scenario is somewhat inconsistent as a Higgs field with a resolvable width should be accompanied by resolvable KK excitations. We will still consider it, as it turns out that this precisely captures the effect of the bulk Higgs zero-mode in the IR-localised $\beta \rightarrow \infty$ limit of the third scenario. In this thesis We will discuss explicitly the different localisation prescriptions only if they lead to different results.

The inclusion of Higgs fields that can propagate throughout the bulk leads to interactions between the wrong chiralities components of the 5D vector fermion fields. To understand these so called wrong chirality Higgs couplings let us consider the Lagrangian of the leptonic Yukawa sector:

$$\begin{aligned} \mathcal{L}_{\text{Yukawa}} &\supseteq \left(\frac{T}{k}\right)^3 y_{ij}^{(5\text{D})} (\bar{L}_i \Phi) E_j \\ &= \left(\frac{T}{k}\right)^3 y_{ij}^{(5\text{D})} ((\bar{L}_{L_i} \Phi) E_{R_j} + (\bar{L}_{R_i} \Phi) E_{L_j}), \end{aligned} \quad (2.67)$$

where $L_{L/Ri} = P_{L/R} L_i$ and $E_{L/Rj} = P_{L/R} E_j$. For a brane Higgs the second term would automatically vanish due to the boundary conditions of the right handed doublet fermion profiles and the left handed singlet fermion wave function (2.39). However for a bulk and even a narrow bulk Higgs this term does not vanish. The concept of wrong and righthanded chirality Higgs couplings was first introduced in [31].

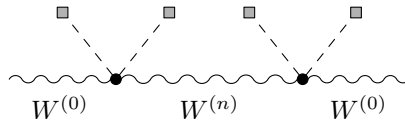


Figure 2.4: Tree level diagram contributing to gauge-boson vacuum polarisation. The boxes represent the Higgs vev.

2.3.5 Minimal RS model constraints

In the previous sections we have seen that the minimal RS model contains for each bulk field a possible large tower of heavy KK particles with masses of the order $\mathcal{O}(T)$. The solution of the gauge-gravity problem only demands [14, 15] the parameter T to be in the TeV region. However, for studies of the feasibility of possible experimental observations for instance at the LHC @ 14 TeV center of mass energy it would be important to find a lower bounds on the RS scale T .

The strongest constraint on the scale of the extra dimension comes from Kaluza-Klein (KK) gluon mediated $\Delta F = 2$ processes—notably in the kaon system [82], which would suggest $T > 13$ TeV, i.e. gauge-boson masses larger than 33 TeV far beyond the reach of the LHC. However this bound can be avoided by imposing some structure on the quark Yukawa matrices in the five-dimensional (5D) theory [83] or by extending the strong gauge group [84]. Notably the RS contributions to the Higgs production yields 2 TeV @ 95% CL for $Y_\star \approx 3$ in the minimal RS model [78]. However this bound depends on the size of the 5d Yukawas. Therefore, one can always avoid this bound by theory points, which include small Yukawas. Almost 5d parameter independent constraints on T are generated by the contributions of the RS model to the electroweak precision observables. In particular the minimal RS model contains tree-level contributions to the Peskin-Takeuchi parameters S and T [85]. In the flavour basis these can be defined as [24]

$$S = 16\pi^2 (\Pi'_{33}(0) - \Pi'_{3Q}(0)) \quad (2.68)$$

$$T = -\frac{16\pi^2}{e^2 v^2} (\Pi_{33}(0) - \Pi_{11}(0)), \quad (2.69)$$

where $\Pi_{ii}(q^2)$ is the vacuum polarisation amplitude for the gauge-boson W^i in SU(2) flavour basis. $\Pi_{3Q}(Q)$ is the vacuum polarisation between a W^3 gauge-boson and a photon. At three level there is no contribution to this amplitude [24]. The tree-level contributions to $\Pi_{ii}(q^2)$ are generated via a coupling of the zero mode gauge-boson field to their KK excitations through the Higgs vev, see figure 2.4. Using the 5D formalism one can directly express the tree-level contributions as [24]

$$\Pi'_{11}(q) = (f_\gamma^{(0)})^2 \left(\frac{v^2}{4}\right)^2 g^4 \Delta^{\text{ZMS}} \left(0, \frac{1}{T}, \frac{1}{T}\right) \quad (2.70)$$

$$\Pi'_{33}(q) = (f_\gamma^{(0)})^2 \left(\frac{v^2}{4}\right)^2 (g^4 + g'^4) \Delta^{\text{ZMS}} \left(0, \frac{1}{T}, \frac{1}{T}\right), \quad (2.71)$$

where Δ^{ZMS} is the zero mode subtracted gauge-boson propagator. In the 5D formalism it can be directly obtained by Taylor expanding equation (2.61) with respect to the loop

momentum.

$$\begin{aligned} \Delta^{\text{ZMS}}(q \rightarrow 0, x, y) = \Theta(x - y) \frac{ik}{\ln \frac{k}{T}} \left(\frac{1}{4} \left\{ \frac{1/T^2 - 1/k^2}{\ln \frac{k}{T}} - x^2 - y^2 + 2x^2 \ln(xT) \right. \right. \\ \left. \left. + 2y^2 \ln(yT) + 2y^2 \ln \frac{k}{T} \right\} + \mathcal{O}(q^2) \right) + (x \leftrightarrow y) \end{aligned} \quad (2.72)$$

After a short calculation one can find for the oblique parameter T in the minimal model [23]

$$\Delta T = \frac{\pi\nu^2}{2 \cos^2 \theta_W T^2} \left(\ln \left(\frac{k}{T} \right) - \frac{1}{2 \ln \left(\frac{k}{T} \right)} \right) \quad (2.73)$$

$$\Delta S = \frac{2\pi\nu^2}{T^2} \left(1 - \frac{1}{\ln \left(\frac{k}{T} \right)} \right). \quad (2.74)$$

Note that the contribution to the T parameter is logarithmic enhanced by a factor proportional to the fifth dimension volume $1/k \ln \left(\frac{k}{T} \right)$. If we insist on the solution of the gauge gravity problem of the original RS setup, then the logarithmic enhancement yields a factor of $\ln \left(\frac{k}{T} \right) \sim 36$. There is no such enhancement for the contribution to the S parameter. Hence the S parameter yields a weaker lower bound on the minimal possible Kaluza-Klein mass than the T parameter. The oblique parameter ΔT leads to a constraint on the RS scale T of $T > 4$ TeV or a first Kaluza-Klein mass of a standard model gauge-boson of around 10 TeV [23]. Such masses for the lowest KK mass are beyond the reach of the LHC.

The most obvious way to remedy this situation would be to consider RS models with a smaller fifth dimension volume, i.e. models where the logarithmic enhancement factor $\ln \left(\frac{k}{T} \right)$ becomes negligible. However, by doing so we would also lose the solution of the gauge-gravity hierarchy problem. We will therefore not consider such a possibility in this thesis. There is also the possibility, to introduce brane localised kinetic gauge-bosons terms [86,87]. Nonetheless, kinetic gauge-bosons terms correspond to unknown UV physics beyond the UV cut-off. Hence the introduction of such terms would further reduce the predictability of the RS model. Another more exotic solution would be to deform the geometry of AdS_5 close to the IR brane [88–90]. Albeit such models could potentially be considered for this thesis we want to stick to the original RS geometry. The last possibility to circumvent this constraint, is to extend the bulk group with an explicit custodial symmetry [24–27,91]. That is the ansatz we will be following in the next section.

2.4 The custodial protected RS model (RSc)

The discussion in the last subsection 2.3.5 led to the conclusion that the minimal RS model exhibits large 5D parameter independent tree-level contributions to the electroweak precision parameters. This leads to RS scales beyond the reach of the LHC. To mitigate these constraints one can extend the gauge group of the RS model in the bulk. This brings us to the custodial protected RS model, which we will introduce in the next subsections.

2.4.1 Gauge group

The construction of the custodial protected RS model starts at the consideration of the gauge group. We choose the gauge group for this model is in the bulk

$$SU(3)_c \times SU(2)_L \times SU(2)_R \times U(1)_X \times P_{L,R}. \quad (2.75)$$

2.4. THE CUSTODIAL PROTECTED RS MODEL (RSC)

The factor $SU(2)_L \times SU(2)_R$ explicitly includes the custodial symmetry into the model. This protects the Peskin-Takeuchi parameter from large contribution at three level [24], see also section 2.4.5. The gauge group also includes the discrete \mathbb{Z}_2 symmetry $P_{L,R}$, which is defined by

$$P_{L,R} : SU(2)_L \leftrightarrow SU(2)_R. \quad (2.76)$$

To satisfy this symmetry the coupling constants of $SU(2)_L$ and $SU(2)_R$ gauge field need to be equal, i.e the following condition must be true the 5D coupling constants

$$g_{5L} = g_{5R} = g_5. \quad (2.77)$$

Also this symmetry can only be achieved by demanding that all fermion multiplets are symmetric under the $P_{L,R}$ transformation in this model. The inclusion of $P_{L,R}$ protects the coupling $Z\bar{b}b$ to all orders [26]. The addition of the abelian $U(1)_X$ symmetry is necessary to fix the hypercharges on the correct values in this model.

In order to achieve the standard model gauge group and particle content the gauge group has to be broken on both branes. On the UV brane one breaks the gauge group by postulating boundary conditions to the standard model gauge group

$$SU(3)_c \times SU(2)_L \times SU(2)_R \times U(1)_X \times P_{L,R} \rightarrow SU(3)_c \times SU(2)_L \times U(1)_B. \quad (2.78)$$

On the IR-Brane the bulk symmetry is broken by a Higgs vacuum expectation value

$$SU(2)_L \times SU(2)_R \xrightarrow{\langle H \rangle} SU(2)_V$$

preserving the custodial symmetry on the IR-brane. By breaking the custodial symmetry only on the UV-brane the effects of the explicit breaking of the custodial symmetry are minimal for physical observables depending on the physics closely to the IR-brane.

2.4.2 Gauge and Higgs sector

The gauge sector consists out two $SU(2)$ gauge-bosons fields $W_{L,R}^a$ and one $U(1)_X$ gauge-boson X . Here the W_L^a gauge field correspond to the known $SU(2)_L$ gauge fields. The symmetry breaking on the UV-brane

$$SU(2)_R \times U(1)_X \rightarrow U(1)_Y \quad (2.79)$$

yields directly the necessary boundary conditions for the different gauge-bosons.

To this end one identifies the Z_X and B gauge fields by performing the following rotation of the original fields

$$\begin{aligned} W_R^3 &= \cos \phi Z_X + \sin \phi B \\ X &= -\sin \phi Z_X + \cos \phi B. \end{aligned} \quad (2.80)$$

The mixing angles are defined similar to the mixing of the B and W_L^3 field

$$\cos \phi = \frac{g_5}{\sqrt{g_5^2 + g_{5X}^2}}, \quad \sin \phi = \frac{g_{5X}}{\sqrt{g_5^2 + g_{5X}^2}}, \quad (2.81)$$

where g_5 is the 5D coupling of the $SU(2)_{L,R}$ gauge fields and g_{5X} equals to the coupling of the $U(1)_X$ gauge field. Thus, in the custodial protected Randall-Sundrum model

CHAPTER 2. THE RANDALL–SUNDRUM MODEL

the B gauge-boson field is generated by a mixing of a W_R^3 and X field. Using this mixing one can identify the $U(1)_Y$ hypercharge coupling constant by

$$g'_5 = \frac{g_5 g_{5X}}{\sqrt{g_5^2 + g_{5X}^2}}. \quad (2.82)$$

To ensure the existence of the standard model gauge group on the UV brane and the custodial symmetry on the IR brane, the boundary conditions of the different gauge fields must be chosen the following way [26]

$$W_{L\mu}^a(+,+) \quad , \quad W_{R\mu}^b(-,+) \quad (2.83)$$

$$B_\mu(+,+) \quad , \quad Z_{X\mu}(-,+). \quad (2.84)$$

Note that index b goes only from 1 to 2. Further, for gauge fields the + sign indicates Neumann boundary conditions under the standard partial derivative ∂_z .

Due the choice of the boundary conditions the $W_{L\mu}$ and the B_μ fields have a massless zero mode, while the new gauge bosons fields $W_{R\mu}^b$ and Z_x only consist of a massive tower of KK excitations. The 5D propagators for these fields can be found in Appendix A.2.2

The Higgs sector includes only small changes in the custodial protected Randall-Sundrum model. The Higgs field is now written explicitly in the bi-doublet $SU(2)_L \times SU(2)_R$ form raising the $SU(2)_L \times SU(2)_R$ invariance of the unbroken SM Higgs-action as a feature of the model. In order to achieve the correct phenomenology the Higgs field has to be chosen neutral under the $U(1)_X$ field. Hence we can write the Higgs field as

$$H = \begin{pmatrix} \pi^+/\sqrt{2} & -(h^0 - i\pi^0)/\sqrt{2} \\ (h^0 + i\pi^0)/\sqrt{2} & \pi^-/\sqrt{2} \end{pmatrix}, \quad (2.85)$$

which can be also expressed by the known $SU(2)$ Higgs doublet h as

$$H = \begin{pmatrix} h & \epsilon h^* \end{pmatrix}. \quad (2.86)$$

The field h^0 gets a vacuum expectation value such that

$$\langle H \rangle = \begin{pmatrix} 0 & -\nu_5/\sqrt{2} \\ \nu_5/\sqrt{2} & 0 \end{pmatrix} \quad (2.87)$$

close to IR brane.

2.4.3 Fermion sector

To extended the gauge group of the custodial protected Randall-Sundrum model gives rise to a more complicated set of fermion multiplets. We begin the discussion of the construction of the fermion multiplets with the quarks, where the protection of the coupling $Z\bar{b}b$ to all orders of perturbation theory gives the decisive constraints on the choice of the multiplets. From now on we assume that all quark fields are triplets under the $SU(2)_C$ symmetry. The choice of the third component of the isospins of $SU(2)_L$ and $SU(2)_R$ and of the charge of the X field are restricted by the fundamental electrical charge of each quark field. The charge can be found by tracking the the mixing of the fields that lead the generation of the B field

$$Q = T_L^3 + T_R^3 + Q_X, \quad (2.88)$$

2.4. THE CUSTODIAL PROTECTED RS MODEL (RSC)

where $T_{L,R}^3$ is the third component of the $SU(2)_{L,R}$ hypercharge and Q_X the charge of the $U(1)_X$ field.

Then the protection of the coupling $Z\bar{b}b$ yields the constraint $T_R^3 = T_L^3 = -\frac{1}{2}$ for the left-handed bottom quark [26]. This implies that the (t_L, b_L) quark doublet transforms as a $(2, 2)$ bi-doublet under the $SU(2)_L \times SU(2)_R$ gauge group. In order to ensure flavour symmetry one applies this also to the (u_l, d_l) and (s_L, c_L) doublets. To generate the correct charge for the left-handed bottom quark field the $(2, 2)$ bi-doublet has to have the charge $Q_X = 2/3$. This fixes all quantum numbers of the bi-doublet for all flavours leading to new fermion fields with charge $5/3$.

To implement the right handed up and down type quarks one starts first to consider the constraints coming from the construction of a standard model compatible Yukawa interaction yields. To construct such Yukawa interaction we need terms, which couple left-handed chirality quark fields with right-handed chirality quark fields. Since the Higgs doublet does not carry any charge under the $U(1)_X$ field this fixes the charge Q_X of the right-handed quark fields to be $2/3$.

Thus the right-handed up-type quarks needs to satisfy $T_R^3 = 0$ to get the correct electrical charge in this model. The $P_{L,R}$ symmetry then yields that the right-handed up quarks are $SU(2)_L \times SU(2)_R$ singlets.

For the right-handed down type quarks we find $T_R^3 = -1$. This means that these quark fields are at least contained as the components of a $SU(2)_R$ triplet, which would mean after taking the $P_{L,R}$ symmetry into account a $(3, 1) \otimes (1, 3)$ triplet of $SU(2)_L \times SU(2)_R$. This is only the most economic choice of parametrisation. In principle, the d_R^i quarks could be contained as components of a $(2j+1, 1) \otimes (1, 2j+1)$ representation of $SU(2)_L \times SU(2)_R$. For $j > 1$ there might be problems to write down the Yukawa interactions of the quark fields, because in this case the $(2j+1, 1) \otimes (1, 2j+1)$ contains quarks with electric charge larger than $q = 5/3$, which is the largest charge one can obtain with bi-doublet for the left-handed quark fields.

For now on we will restrict us to the case $j = 1$. We find for the quark fields the representations per generation i ($i=1,2,3$) [26]

$$\begin{aligned}
 \xi_{1L}^i &= \begin{pmatrix} \chi_L^{u_i}(-, +)_{5/3} & q_L^{u_i}(+, +)_{2/3} \\ \chi_L^{d_i}(-, +)_{2/3} & q_L^{d_i}(+, +)_{-1/3} \end{pmatrix} \\
 \xi_{2R}^i &= u_R^i(+, +)_{2/3} \\
 \xi_{3R}^i &= T_{3R}^i \otimes T_{4R}^i = \begin{pmatrix} \tilde{\Psi}_R^i(-, +)_{5/3} \\ \tilde{U}_R^i(-, +)_{2/3} \\ \tilde{D}_R^i(-, +)_{-1/3} \end{pmatrix} \otimes \begin{pmatrix} \Psi_R^i(-, +)_{5/3} \\ U_R^i(-, +)_{2/3} \\ D_R^i(+, +)_{-1/3} \end{pmatrix}, \quad (2.89)
 \end{aligned}$$

where the subscript of the different quark fields gives the electrical charge the signs in parentheses are the boundary conditions on the UV and IR brane. These boundary conditions were chosen such way, that each standard model quark field has $(+, +)$ boundary conditions ensuring the existence of a zero-mode field. For the new field one cannot choose Dirichlet boundary conditions on both frames, since the fields of opposite chirality would then have $(-, -)$ boundary conditions due to the coupling of the mode equations and therefore a massless zero-mode field. Hence these quark fields have to have mixed boundary conditions.

The embedding the leptons into $SU(2)_L \times SU(2)_R$ multiplets is achieved by using the same arguments as in the quark case. To achieve the correct electrical charges for the SM lepton fields, all leptons have to be neutral under the $U(1)_X$ gauge field. Thus there is a global lepton charge $2/3$ difference for all components of the lepton multiplets compared to the

CHAPTER 2. THE RANDALL–SUNDRUM MODEL

quark case. We write the lepton multiplets for every generation i as

$$\begin{aligned}
\xi_{1L}^{il} &= \begin{pmatrix} \chi_L^{\nu_i}(-, +)_1 & l_L^{\nu_i}(+, +)_0 \\ \chi_L^i(-, +)_0 & l_L^i(+, +)_{-1} \end{pmatrix} \\
\xi_{2R}^{il} &= \nu_R(+, +)_0 \\
\xi_{3R}^{il} &= T_{3R}^i \otimes T_{4R}^i = \begin{pmatrix} \tilde{\lambda}_R^i(-, +)_1 \\ \tilde{N}_R^i(-, +)_0 \\ \tilde{L}_R^i(-, +)_{-1} \end{pmatrix} \otimes \begin{pmatrix} \lambda_R^i(-, +)_1 \\ N_R^i(-, +)_0 \\ E_R^i(+, +)_{-1} \end{pmatrix}. \quad (2.90)
\end{aligned}$$

As for the quark case all standard model like leptons satisfy $(+, +)$ boundary conditions. It is noteworthy that this model includes a right-handed neutrino.

Note that this choice of multiplets is not the minimal possible incorporation of the extended gauge group in the lepton sector. That because the protection of the $ZU\bar{1}$ is not necessary for leptons. Instead of the complicated triplet structure we could embed the right handed neutrino together with the SM singlet fermion and the SM doublet into a $SU(2)_L \times SU(2)_R$ $(1, 2)$ multiplet. However such an extension does not differ much from the minimal setup. Therefore we use the next to minimal version of the custodial protected RS model (RSc) in the lepton sector.

2.4.4 Fundamental 5D action

We decompose the action of the custodial protected Randall-Sundrum model in four parts

$$S = \int d^4x \int_{\frac{1}{k}}^{\frac{1}{\bar{k}}} dy (\mathcal{L}_{gauge} + \mathcal{L}_{fermion} + \mathcal{L}_{Higgs} + \mathcal{L}_{Yuk}). \quad (2.91)$$

The enhanced gauge group of the custodial protected Randall-Sundrum model leads to additional term in gauge Lagrangian

$$\mathcal{L}_{gauge} = \sqrt{g} \left[-\frac{1}{4} G_{MN}^A G^{AMN} - \frac{1}{4} L_{MN}^a L^{aMN} - \frac{1}{4} R_{MN}^\alpha R^{\alpha MN} - \frac{1}{4} X_{MN} X^{MN} \right] + \mathcal{L}_{GF}. \quad (2.92)$$

Here G_{MN}^A corresponds to the $SU(3)_C$ field strength tensor

$$G_{NM}^A = \partial_N G_M^A - \partial_M G_N^A - g_{5s} f^{ABC} G_N^B G_M^C \quad (2.93)$$

where g_{5s} is the strong 5D coupling.

The tensor L_{MN}^a and R_{NM}^α are the field strength tensor of the $SU(2)_L$ and $SU(2)_R$ gauge fields

$$L_{NM}^a = \partial_N W_{LM}^a - \partial_M W_{LN}^a + g_5 \epsilon^{abc} W_{LN}^b W_{LM}^c \quad (2.94)$$

$$R_{NM}^\alpha = \partial_N W_{RM}^\alpha - \partial_M W_{RN}^\alpha + g_5 \epsilon^{\alpha\beta\gamma} W_{RN}^\beta W_{RM}^\gamma. \quad (2.95)$$

We only write down the fundamental 5D Lagrangian for the quarks, because due to the organisation of the leptons in similar multiplets the lepton sector does not differ much aside

2.4. THE CUSTODIAL PROTECTED RS MODEL (RSC)

from missing gluon interaction terms. The Lagrangian for all quark fields is given by [26]

$$\begin{aligned}
\mathcal{L}_{fermion} = & \frac{1}{2}\sqrt{g}\sum_{i=1}^3 e_m^M \left[(\bar{\xi}_1^i)_{a\alpha} i\Gamma^m (D_M^1)_{ab\alpha\beta} (\xi_1^i)_{b\beta} + (\bar{\xi}_1^i)_{a\alpha} (i\Gamma^m \omega_M - M_1^i) (\xi_1^i)_{a\alpha} \right. \\
& + (\bar{\xi}_2^i) i\Gamma^m (D_M^2) (\xi_2^i) + (\bar{\xi}_2^i) (i\Gamma^m \omega_M - M_2^i) (\xi_2^i) \\
& + \left(\tilde{T}_3^i \right)_a i\Gamma^m (D_M^3)_{ab} \left(\tilde{T}_3^i \right)_b + \left(\tilde{T}_3^i \right)_a (i\Gamma^m \omega_M - M_3^i) \left(\tilde{T}_3^i \right)_a \\
& \left. + \left(\tilde{T}_4^i \right)_\alpha i\Gamma^m (D_M^4)_{\alpha\beta} \left(\tilde{T}_4^i \right)_{b\beta} + \left(\tilde{T}_4^i \right)_\alpha (i\Gamma^m \omega_M - M_3^i) \left(\tilde{T}_4^i \right)_\alpha \right] + h.c. \quad (2.96)
\end{aligned}$$

where e_m^M is the vielbein and ω_M the spin-connection for spin 1/2 fields.

With this definition the covariant derivatives for the quark fields can be found to be [26]

$$\begin{aligned}
(D_M^1)_{ab\alpha\beta} = & (\partial_M - ig_5 t^A G_M^A - ig_X Q_X X_M) \delta_{ab} \delta_{\alpha\beta} \\
& - ig_5 \frac{(\tau^c)_{ab}}{2} W_{LM}^c \delta_{\alpha\beta} - ig_5 \delta_{ab} \frac{(\tau^c)_{\alpha\beta}}{2} W_{RM}^c \quad (2.97)
\end{aligned}$$

$$(D_M^2) = \partial_M - ig_5 t^A G_M^A - ig_X Q_X X_M \quad (2.98)$$

$$(D_M^3)_{ab} = (\partial_M - ig_5 t^A G_M^A - ig_X Q_X X_M) \delta_{ab} - g_5 \epsilon^{abc} W_{L,M}^c \quad (2.99)$$

$$(D_M^3)_{\alpha\beta} = (\partial_M - ig_5 t^A G_M^A - ig_X Q_X X_M) \delta_{\alpha\beta} - g_5 \epsilon^{\alpha\beta\gamma} W_{R,M}^\gamma. \quad (2.100)$$

As usual $t^A = \lambda^A/2$ are the fundamental generators of $SU(3)_C$ where λ^A are the known Gell-Mann matrices. The generators of the $SU(2)_L$ ($SU(2)_R$) fundamental representation are the usual Pauli matrices τ^a (τ^α). Note that the generators of $SU(2)_{L,R}$ do have the same matrices, but due to the different indices they work on different internal spaces.

One should be aware of that inside the Lagrangian the triplets \tilde{T}_3^i and \tilde{T}_4^i are not written in the form of (2.89). Instead one writes them here as

$$\left(\tilde{T}_3^i \right) = \begin{pmatrix} \frac{1}{\sqrt{2}} (\tilde{\Psi}^i + \tilde{D}^i) \\ \frac{i}{\sqrt{2}} (\tilde{\Psi}^i - \tilde{D}^i) \\ \tilde{U}^i \end{pmatrix} \quad \left(\tilde{T}_4^i \right) = \begin{pmatrix} \frac{1}{\sqrt{2}} (\Psi^i + D^i) \\ \frac{i}{\sqrt{2}} (\Psi^i - D^i) \\ U^i \end{pmatrix}, \quad (2.101)$$

to reproduce all gauge-fermion interactions, which appear in the standard model. This notation is used to shorten the form of the Lagrangian.

The application of this Lagrangian to the lepton sector is straightforward since the lepton multiplets have the same form as the quark fields. To perform the adaptation of the Lagrangian one just has to remove the coupling to the strong gauge field G_M^A and set the charges Q_X to zero, since lepton multiplets are not charged under the $U(1)_X$ field. Note that for the leptons the components of the \tilde{T}_3^i and \tilde{T}_4^i are given as

$$\left(\tilde{T}_3^i \right) = \begin{pmatrix} \frac{1}{\sqrt{2}} (\tilde{\lambda}^i + \tilde{L}^i) \\ \frac{i}{\sqrt{2}} (\tilde{\lambda}^i - \tilde{L}^i) \\ \tilde{N}^i \end{pmatrix} \quad \left(\tilde{T}_4^i \right) = \begin{pmatrix} \frac{1}{\sqrt{2}} (\lambda^i + E^i) \\ \frac{i}{\sqrt{2}} (\lambda^i - E^i) \\ N^i \end{pmatrix}. \quad (2.102)$$

In the RSc model the Lagrangian for the Higgs bi-doublet field can be written as

$$\mathcal{L}_{Higgs} = \delta \left(y - \frac{1}{T} \right) \left(\frac{1}{2} (D_\nu H)^\dagger_{a\alpha} (D^\nu H)_{a\alpha} - V(H) \right), \quad (2.103)$$

CHAPTER 2. THE RANDALL–SUNDRUM MODEL

where we only write down case for an exactly brane localised Higgs. $V(H)$ is the potential of the Higgs field leading to the correct electro-weak-symmetry breaking. Note that for our choice for the form of the Higgs vev one has to put an additional factor $1/2$ before the kinetic term to generate the correct gauge-Higgs vertices. The covariant derivative of the Higgs bi-doublet has the form

$$(D_\nu H)_{a\alpha} = \partial_\nu H_{a\alpha} + ig \frac{(\tau^c)_{ab}}{2} W_{L\nu}^c H_{b\alpha} + ig \frac{(\tau^\gamma)_{\alpha\beta}}{2} W_{R\nu}^\gamma H_{a\beta}. \quad (2.104)$$

Remember that H does not have a charge Q_x , which is the reason why there is no coupling to the X field. Thus the coupling of the Higgs bi-doublet to the B gauge field is only generated by the W_R^3 field. The kinetic term of the Higgs action contains the operators, which lead to the tree-level contributions to the Peskin-Takeuchi S and T after EWSB.

The Lagrangian of the Yukawa is constrained fundamentally by the Yukawa SM Lagrangian, which should be obtainable through a Kaluza-Klein decomposition of all fields. This requirement yields a term of the form $\bar{\xi}_1^i H \xi_2^j$ and a term of the form of $\bar{\xi}_1^i \tau H T_3^j$. That is because the first term contains the zero-mode term $\bar{u}_L h u_R$ and the second term contains a zero-mode term $\bar{d}_L h d_R$. Then due to the $P_{L,R}$ symmetry the Yukawa Lagrangian should also contain a term of the form $\bar{\xi}_1^i \tau H T_4^j$.

Hence the most general Yukawa Lagrangian one can write down is as follows in the custodial protected Randall-Sundrum model [26]

$$\begin{aligned} \mathcal{L}_{Yuk} = & -\delta \left(y - \frac{1}{T} \right) \left(\frac{T}{k} \right)^3 \sum_{i,j=1}^3 \left[-\lambda_{5D}^u{}_{ij} (\bar{\xi}_1^i)_{a\alpha} H_{a\alpha} \xi_2^j \right. \\ & \left. + \sqrt{2} \lambda_{5D}^d{}_{ij} \left[(\bar{\xi}_1^i)_{a\alpha} \frac{(\tau^c)_{ab}}{2} (\tilde{T}_3^j)_c H_{b\alpha} + (\bar{\xi}_1^i)_{a\alpha} \frac{(\tau^\gamma)_{\alpha\beta}}{2} (\tilde{T}_4^j)_\gamma H_{a\beta} \right] \right] + h.c.. \end{aligned} \quad (2.105)$$

The additional $\sqrt{2}$ in the second term appears to cancel the $1\sqrt{2}$ factor coming from components of the $SU(2)_{L,R} T_{3,4}^j$ triplets.

2.4.5 RSc constraints

With the formulation of the RS model with custodial protection at hand we can now go back to the computation of the electroweak precision parameter S and T . The RSc model contains the minimal RS contributions to the $\Pi_{ii}(q^2)$ amplitudes. However, $\Pi_{33}(q^2)$ obtains also the contribution of a Z_X exchange. That is because the B boson is generated via a mixing of the X and W_R^3 boson on the UV brane in the RSc model. Thus, we can directly translate any diagram, that includes a B boson exchange, into an RSc diagram with Z_X exchange. The new contribution to $\Pi_{33}(q^2)$ has the form

$$\Pi'_{33}(q) = \left(f_\gamma^{(0)} \right)^2 \left(\frac{v^2}{4} \right)^2 g_{5X}^4 \Delta_{pm} \left(0, \frac{1}{T}, \frac{1}{T} \right). \quad (2.106)$$

The propagator Δ_{pm} is calculated in Appendix A.2.2 explicitly. The zero momentum Taylor expansion can be found as

$$\Delta_{mp}(q \rightarrow 0, x, y) = \frac{i}{2k} \left[k^2 \min\{x^2, y^2\} - 1 \right]. \quad (2.107)$$

2.4. THE CUSTODIAL PROTECTED RS MODEL (RSC)

Then together with the relation of the new coupling g_X with respect to $SU(2)_L \times U(1)_B$ coupling constants

$$g_X^2 = g^2 - g'^2. \quad (2.108)$$

we find for the RSc model [23]

$$\Delta T = -\frac{\pi v^2}{4 \cos^2 \theta_W T^2} \frac{1}{\ln\left(\frac{k}{T}\right)} \quad (2.109)$$

$$\Delta S = \frac{2\pi v^2}{T^2} \left(1 - \frac{1}{\ln\left(\frac{k}{T}\right)}\right). \quad (2.110)$$

We observe that the log enhancement drops for the in the RSc model contribution to the T parameter (2.109). In fact, this lowers significantly the lower on T generated by the T parameter, such that the main constrain on the RS scale T comes from the S parameter. For the RSc model the electroweak precision parameters yield a lower bound of $T > 2.3$ TeV [23]. This corresponds to lowest gauge boson Kaluza Klein mass of about 5.6 TeV. Thus even with the custodial symmetry the chance of a discovery of the RS model by direct production at the LHC is not large.

Additionally due to the larger set of heavy fermion field the RSc yields larger contributions to loop-induced processes, which are sensitive to the amount of heavy particles inside the loops. One such process is the Higgs production, where the KK scale T can be constrained up to (4) TeV @ 95% CL for $Y_\star \approx 3$ for a the RSc model with narrow bulk Higgs [78]. That is almost double the size of the Higgs production bounds to the minimal RS model. For large Yukawas this bound alone would destroy all gains by the introduction of the extended gauge group.

CHAPTER 2. THE RANDALL-SUNDRUM MODEL

Chapter 3

Effective Field Theory

As seen in the last chapter the typical scale of the RS model is determined by the parameter T , which lies in the $\mathcal{O}(\text{TeV})$ range. Thus, due to the clear separation of the electroweak scale and the KK scale it is perfectly valid to organise the calculation of all low energy observables in an effective theory by integrating the heavy 5D degrees out. In this chapter we first introduce this effective theory EFT in the lepton as well as in the quark sector in the first section. We then focus first on the determination of the lepton observables $\mu \rightarrow e\gamma$, $\mu \rightarrow 3e$, $\mu N \rightarrow eN$ in terms of the EFT. That is being achieved by matching to appropriate low energy Lagrangians, which allow an easy evaluation of all considered lepton processes. In the end of this chapter we then match the dimension six EFT on an effective weak Hamiltonian. That is then used for the computation of $\bar{B} \rightarrow X_s \gamma$.

3.1 Dimension six Lagrangian

In this thesis, we follow the ansatz of [28], i.e. the heavy degrees of freedom get incorporated into an effective SM Lagrangian, which includes the SM and $SU(3) \times SU(2) \times U(1)$ invariant higher-dimension operators

$$\mathcal{L}_{RS} \rightarrow \mathcal{L}_{SM} + \frac{1}{T^2} \sum_i \mathcal{O}_i = \mathcal{L}_{SM} + \mathcal{L}^{\text{dim6}}, \quad (3.1)$$

where we use T as the dimensional expansion parameter for our effective theory. We capture the dominant effects with the dimension six operators of the Buchmüller-Wyler Lagrangian [51]. For this thesis we use the minimal basis provided by [52].

As the muon g-2 calculation is just a mere extension of the similar computation [28] for the minimal RS setup, we follow for the selection of dimension six operators the strategy of [28]. That means, that we turn special attention to the matrix element $f_i \rightarrow f_j \gamma$, where f can be either a lepton field or a parton. Under this process we select operators that either contribute at tree-level to this matrix element, but are generated at one-loop level in the RS model, or contribute at one-loop level for the matrix element of the EFT, but are generated at tree-level in the 5D theory. Furthermore we take all four fermion operators into account, which contribute at three level via neutral currents like to processes like for instance $\mu \rightarrow 3e$. All operators considered for this thesis are of dimension six. The only dimension five operator in the lepton sector of [52] does not contribute either to flavour conserving or flavour violating processes.

CHAPTER 3. EFFECTIVE FIELD THEORY

In the lepton sector, our complete dimension six Lagrangian before electroweak symmetry breaking is given by

$$\begin{aligned}
\mathcal{L}_{\text{Lepton}}^{\text{dim6}} = & a_{ij}^B (\bar{L}_i \sigma^{\mu\nu} E_j) \Phi B_{\mu\nu} + a_{ij}^W (\bar{L}_i \tau^A \sigma^{\mu\nu} E_j) \Phi W_{\mu\nu}^A + \text{h.c.} \\
& + b_{ijkl}^{LL} (\bar{L}_i \gamma^\mu L_j) (\bar{L}_k \gamma_\mu L_l) + b_{ij}^{LE} (\bar{L}_i \gamma^\mu L_i) (\bar{E}_j \gamma_\mu E_j) + b_{ij}^{EE} (\bar{E}_i \gamma^\mu E_i) (\bar{E}_j \gamma_\mu E_j) \\
& + c_{ij}^1 \Phi^\dagger i \overleftrightarrow{D}_\mu \Phi (\bar{E}_i \gamma_\mu E_j) + c_{ij}^2 \Phi^\dagger i \overleftrightarrow{D}_\mu \Phi (\bar{L}_i \gamma_\mu L_j) + c_{ij}^3 \Phi^\dagger i \overleftrightarrow{T^A} D_\mu \Phi (\bar{L}_i \tau^A \gamma_\mu L_j) \\
& + h_{ij} (\Phi^\dagger \Phi) \bar{L}_i \Phi E_j + \text{h.c.} \\
& + \sum_{\ell=E,L} \sum_{q=Q,U,D} b_{ij}^{\ell q} (\bar{\ell}_i \gamma^\mu \ell_i) (\bar{q}_j \gamma_\mu q_j) + b_{ij}^{L\tau Q} (\bar{L}_i \tau^A \gamma_\mu L_i) (\bar{Q}_j \tau^A \gamma_\mu Q_j), \quad (3.2)
\end{aligned}$$

where T^A are the $SU(2)$ generators in the appropriate representation (e.g. $T^A = \tau^A/2$ with τ^A the Pauli matrices for the doublet), and Y the hypercharge. The hermitian conjugate in (3.2) only applies to terms in the same line. Of all the operators given in (3.2) only the dipole operators in the first line cannot be generated at tree-level in the RS model. These operators are also the only ones, which contribute to the process $f_i \rightarrow f_j \gamma$ at tree-level. The flavour structure of the four fermion operators in (3.2) is not the most general one as it is already adapted to the form of the Wilson coefficients, which can be generated in the RS model. Even though Lagrangian (3.2) aims at the study of low energy processes in the lepton sector it also includes four fermion operators with an mixing of quark and lepton fields. These operator are necessary for the muon conversion in nuclei.

In the quark sector we focus on the KK contribution of the gluon exchange to $\bar{B} \rightarrow X_s \gamma$. Therefore we consider here only on dimension six operators that can be generated by the exchange of Kaluza-Klein gluons in the RS model. Furthermore we can forego all operators that do not contribute at leading logarithmic (ll) accuracy to $b \rightarrow s \gamma$. This yields the dimension six Lagrangian

$$\begin{aligned}
\mathcal{L}_{\text{quark}} = & a_{ij}^g \bar{Q}_i \Phi \sigma^{\mu\nu} T^A D_j G_{\mu\nu}^A + a_{ij}^B (\bar{Q}_i \sigma^{\mu\nu} D_j) \Phi B_{\mu\nu} + a_{ij}^W (\bar{Q}_i \tau^A \sigma^{\mu\nu} D_j) \Phi W_{\mu\nu}^A + \text{h.c.} \\
& + b_{ij}^{QQ} \bar{Q}_i \gamma^\mu T^A Q_i \bar{Q}_j \gamma_\mu T^A Q_j + b_{ij}^{QU} \bar{Q}_i \gamma^\mu T^A Q_i \bar{U}_j \gamma_\mu T^A U_j \\
& + b_{ij}^{QD} \bar{Q}_i \gamma^\mu T^A U_i \bar{D}_j \gamma_\mu T^A D_j + b_{ij}^{DD} \bar{D}_i \gamma^\mu T^A D_i \bar{D}_j \gamma_\mu T^A D_j \\
& + b_{ij}^{DU} \bar{D}_i \gamma^\mu T^A D_i \bar{U}_j \gamma_\mu T^A U_j \\
& + \dots, \quad (3.3)
\end{aligned}$$

where Q_i corresponds to a quark doublet of with generation index i ; D and U are down- and up-type singlets. G and F are gluonic and electromagnetic field strength tensor, respectively. T^A is a generator of $SU(3)$ in the fundamental representation. The ellipses indicate a sizeable set of omitted operators. These are either operator like $\Phi^\dagger i \overleftrightarrow{D}_\mu \Phi (\bar{d}_i \gamma_\mu d_j)$, which cannot be generated by QCD, or operators like $(\Phi^\dagger \Phi) \bar{Q}_i \Phi D_j$, which do not contribute at ll accuracy. Obviously, exchange of hypercharge bosons and $SU(2)$ bosons will also generate four-fermion operators, contribute to both dipoles and give rise to operators of the schematic form $\Phi^\dagger D_\mu \Phi \bar{q} \gamma^\mu q$. The latter class of operators will contribute to e.g. flavour-changing Z couplings.

The $U(1)$ gauge coupling at a scale of 1 TeV is roughly $\alpha_{U(1)} \sim 0.01$. The $SU(2)_L$ coupling is significantly larger with $\alpha_{SU(2)}(\mu = 1 \text{ TeV}) \sim 0.032$, but still smaller than $\alpha_s(\mu = 1 \text{ TeV}) = 0.09$. The fact that the weak coupling is only about a factor of three smaller than the strong coupling may warrant including weak effects in the matching calculation. Including the

3.1. DIMENSION SIX LAGRANGIAN

effect of the other gauge bosons is not a principle problem; their contribution to the four-fermion coefficients as well as the dipole coefficients can directly be obtained from results for leptonic dipoles.

A further effect that would have been taken into account when considering weak corrections is the modification of SM parameters and relations that have been utilised in the SM computation. In particular the relation of G_F and the W mass, that is frequently used when rewriting the SM expressions is affected by higher-dimensional operators (see [92] for the general case and [93] for a discussion within the RS model).

Note that the Lagrangians (3.2) and (3.3) are initially written in the unbroken flavour basis. We introduce the transition to the broken theory with a broken electroweak gauge symmetry via the standard substitution rules,

$$\Phi \rightarrow \begin{pmatrix} \phi^+ \\ \frac{1}{\sqrt{2}}(v + h + iG) \end{pmatrix} \quad L_i \rightarrow U_{ij} P_L \begin{pmatrix} \nu_j \\ \ell_j \end{pmatrix} \quad E_i \rightarrow V_{ij} P_R \ell_j \quad (3.4)$$

$$Q_i \rightarrow P_L \begin{pmatrix} U_{ij}^u u_j \\ U_{ij}^d d_j \end{pmatrix} \quad U_i \rightarrow V_{ij}^u P_R u_j \quad D_i \rightarrow V_{ij}^d P_R d_j \quad (3.5)$$

and

$$D_\mu \rightarrow \partial_\mu - ieQA_\mu - \frac{ig}{c_W}(T^3 - s_W^2 Q)Z_\mu - \frac{ig}{\sqrt{2}}(T^1 + iT^2)W_\mu^+ - \frac{ig}{\sqrt{2}}(T^1 - iT^2)W_\mu^-, \quad (3.6)$$

with $Z_\mu = c_W W_\mu^3 - s_W B_\mu$, and $A_\mu = c_W B_\mu + s_W W_\mu^3$. Inserting (3.4) and (3.6) into (3.2) generates many operators, most of which cannot contribute to the processes we are interested in, see [28] for details. Collecting all operators that contribute according to the strategy above the lepton sector Lagrangian sector dimension six Lagrangian becomes

$$\begin{aligned} \mathcal{L}_{\text{Lepton}}^L \rightarrow \mathcal{L}_{\text{Lepton}}^{\text{broken}} &= \frac{\alpha_{ij}^A + \alpha_{ji}^{A*}}{2} \frac{v}{\sqrt{2}} (\bar{\ell}_i \sigma^{\mu\nu} \ell_j) F_{\mu\nu} + \frac{\alpha_{ij}^A - \alpha_{ji}^{A*}}{2} \frac{v}{\sqrt{2}} (\bar{\ell}_i \sigma^{\mu\nu} \gamma_5 \ell_j) F_{\mu\nu} \\ &+ \beta_{ijkl}^{EE} (\bar{\ell}_i \gamma^\mu P_R \ell_j) (\bar{\ell}_k \gamma_\mu P_R \ell_l) + \beta_{ijkl}^{LE} (\bar{\ell}_i \gamma^\mu P_L \ell_j) (\bar{\ell}_k \gamma_\mu P_R \ell_l) \\ &+ \beta_{ijkl}^{LL} (\bar{\ell}_i \gamma^\mu P_L \ell_j) (\bar{\ell}_k \gamma_\mu P_L \ell_l) \\ &- \gamma_{ij}^1 \frac{gv^2}{4c_W} Z^\mu (\bar{\ell}_i \gamma_\mu P_R \ell_j) - [\gamma_{ij}^2 + \gamma_{ij}^3] \frac{gv^2}{4c_W} Z^\mu (\bar{\ell}_i \gamma_\mu P_L \ell_j) \\ &+ \gamma_{ij}^3 \frac{gv^2}{2\sqrt{2}} W^{+\mu} (\bar{\nu}_i \gamma_\mu P_L \ell_j) + \text{h.c.} \\ &+ \eta_{ij} \frac{3v^2}{2} \frac{h}{\sqrt{2}} (\bar{\ell}_i P_R \ell_j) + \eta_{ij} \frac{v^3}{2\sqrt{2}} (\bar{\ell}_i P_R \ell_j) + \text{h.c.} \\ &+ \beta_{ijkl}^{Eu} (\bar{\ell}_i \gamma^\mu P_R \ell_j) (\bar{u}_k \gamma^\mu P_R u_l) + \beta_{ijkl}^{Ed} (\bar{\ell}_i \gamma^\mu P_R \ell_j) (\bar{d}_k \gamma^\mu P_R d_l) \\ &+ \beta_{ijkl}^{EQ} (\bar{\ell}_i \gamma^\mu P_R \ell_j) (\bar{u}_k \gamma^\mu P_L u_l) + \beta_{ijkl}^{EQ} (\bar{\ell}_i \gamma^\mu P_R \ell_j) (\bar{d}_k \gamma^\mu P_L d_l) \\ &+ \beta_{ijkl}^{Lu} (\bar{\ell}_i \gamma^\mu P_L \ell_j) (\bar{u}_k \gamma^\mu P_R u_l) + \beta_{ijkl}^{Ld} (\bar{\ell}_i \gamma^\mu P_L \ell_j) (\bar{d}_k \gamma^\mu P_R d_l) \\ &+ (\beta_{ijkl}^{LQ} - \beta_{ijkl}^{L\tau Q}) (\bar{\ell}_i \gamma^\mu P_L \ell_j) (\bar{u}_k \gamma^\mu P_L u_l) \\ &+ (\beta_{ijkl}^{LQ} + \beta_{ijkl}^{L\tau Q}) (\bar{\ell}_i \gamma^\mu P_L \ell_j) (\bar{d}_k \gamma^\mu P_L d_l), \end{aligned} \quad (3.7)$$

CHAPTER 3. EFFECTIVE FIELD THEORY

with $P_{L/R} = \frac{1}{2}(1 \mp \gamma_5)$, and

$$\begin{aligned}\alpha_{ij}^A &= [U^\dagger a^A V]_{ij}, & \gamma_{ij}^1 &= \sum_{m,n} [V^\dagger]_{im} V_{nj} c_{mn}^1, \\ \eta_{ij} &= \sum_{n,m} [U^\dagger]_{im} h_{mn} V_{nj}, & \gamma_{ij}^x &= \sum_{m,n} [U^\dagger]_{im} U_{nj} c_{mn}^x \quad (x = 2, 3), \\ \beta_{ijkl}^{LL} &= \sum_{m,n,o,p} [U^\dagger]_{im} U_{nj} [U^\dagger]_{ko} U_{pl} b_{mnop}^{LL}, & \beta_{ijkl}^{FF'} &= \sum_{m,n} [M^\dagger]_{in} M_{nj} [M'^\dagger]_{km} M'_{ml} b_{mnl}^{FF'}. \quad (3.8)\end{aligned}$$

Here $a_{ij}^A = c_W a_{ij}^B - s_W a_{ij}^W$, $M^{(\prime)} \in \{U, V, U^u, V^u, U^d, V^d\}$ are the appropriate flavour rotation matrices for the fermion $F^{(\prime)}$, and a similar definition applies to $\beta_{ijkl}^{L\tau Q}$. In the the quark sector, we apply the identical definitions. We find for the effective Lagrangian in the quark sector

$$\begin{aligned}\mathcal{L}_{\text{Quark}}^{\text{dim6}} \rightarrow \mathcal{L}_{\text{Quark}}^{\text{broken}} &= \frac{\alpha_{ij}^{Aq} + \alpha_{ji}^{Aq^*}}{2} \frac{v}{\sqrt{2}} (\bar{d}_i \sigma^{\mu\nu} d_j) F_{\mu\nu} + \frac{\alpha_{ij}^{Aq} - \alpha_{ji}^{Aq^*}}{2} \frac{v}{\sqrt{2}} (\bar{d}_i \sigma^{\mu\nu} \gamma_5 D_j) F_{\mu\nu} \\ &+ \alpha_{ij}^g \frac{v}{\sqrt{2}} (\bar{d}_i \sigma^{\mu\nu} T^A d_j) G_{\mu\nu}^A + \beta_{ijkl}^{DD} (\bar{d}_i \gamma^\mu T^A P_R d_j) (\bar{d}_k \gamma_\mu T^A P_R d_l) \\ &+ \beta_{ijkl}^{UU} (\bar{u}_i \gamma^\mu T^A P_R u_j) (\bar{u}_k \gamma_\mu T^A P_R u_l) \\ &+ \sum_{q_1=u,d} \beta_{ijkl}^{Q_{q_1} D} (\bar{q}_1 \gamma^\mu T^A P_L q_{1j}) (\bar{d}_k \gamma_\mu T^A P_R d_l) \\ &+ \sum_{q_1=u,d} \beta_{ijkl}^{Q_{q_1} U} (\bar{q}_1 \gamma^\mu T^A P_L q_{1j}) (\bar{u}_k \gamma_\mu T^A P_R u_l) \\ &+ \beta_{ijkl}^{Q_{q_1} Q_{q_2}} \sum_{q_1, q_2=u,d} (\bar{q}_1 \gamma^\mu T^A P_L q_{1j}) (\bar{q}_2 \gamma_\mu T^A P_R q_{2l}), \quad (3.9)\end{aligned}$$

where we use the abbreviation

$$\beta_{ABCD}^{FF'} = [R^F]_{Ai}^\dagger [R^{F'}]_{Cj}^\dagger b_{ij}^{F'F} R_{iB}^F R_{jD}^{F'} \quad (3.10)$$

with the appropriate flavour rotation matrices $R^{F^{(\prime)}}$ for all quark four fermio operators.

3.2 Lepton low energy observables

The main observables considered for this thesis are the radiative transitions of the type $\ell_1 \rightarrow \ell_2 \gamma$, the lepton conversion close to nuclei, and tri-lepton decays $\ell_1 \rightarrow 3 \ell_2$. These processes are usually studied in high intensity, low energy set-ups. The typical energy release of the process is the mass of the initial (charged) lepton, a muon or a tau. Our strategy is to construct an effective low energy langrangian out of the at the electroweak scale defined dimension six Lagrangian of the last section. The constuction is done by integrating out the heavy gauge-bosons and quarks and the fluctuations associated with scales above the charged lepton mass. For $\mu \rightarrow e \gamma$, muon conversion and $\mu \rightarrow 3e$ such low-energy theories have been discussed in great detail in the literature, see e.g. [94, 95], and especially [96]. We follow [96] and consider first the determination of the muon g-2 and the radiative decay $\mu \rightarrow e \gamma$. We use the Lagrangian

$$\mathcal{L}_{\ell_i \rightarrow \ell_j \gamma} = A_{Rij} m_i \bar{\ell}_j \sigma^{\sigma\rho} F_{\sigma\rho} P_R \ell_i + A_{Lij} m_i \bar{\ell}_j \sigma^{\sigma\rho} F_{\sigma\rho} P_L \ell_i + \text{h.c.}, \quad (3.11)$$

3.2. LEPTON LOW ENERGY OBSERVABLES

where our convention for $A_{L,R}$ and g_i below differs from [96], Eq. (54) by the factor $-4G_F/\sqrt{2}$ and complex conjugation. In order to incorporate directly at this step lepton conserving transitions we generalised the Lagrangian [96] to arbitrary initial and final lepton states. The label i and j denote the lepton flavour ($i, j = e, \mu, \tau$), i.e. for the process $\mu \rightarrow e\gamma$ one has to consider calculate the coefficients $A_{L,R\mu e}$. This Lagrangian is supposed to be valid at scales below the mass of the lepton of the generation j —all quantum fluctuations involving leptons have been integrated out and have been absorbed into the two coefficients of the dipole operators. In fact instead of this Lagrangian we might just as well consider the general $U(1)_{em}$ invariant vertex function for on-shell fermions (the photon momentum q is ingoing)

$$\begin{aligned} \Gamma_{ij}^\mu(p, p') &= ieQ_\ell \bar{u}_i(p', s') \left[\gamma^\mu F_{1ij}(q^2) + \frac{i\sigma^{\mu\nu} q_\nu}{2m_i} F_{2ij}(q^2) + \frac{\sigma^{\mu\nu} q_\nu}{2m_i} \gamma_5 F_{3ij}(q^2) \right. \\ &\quad \left. + (q^2 \gamma^\mu - \not{q} q^\mu) \gamma_5 F_{4ij}(q^2) \right] u_j(p, s). \end{aligned} \quad (3.12)$$

The on-shell dipole form factors of the electromagnetic muon-electron vertex are related to the coefficients A_L and A_R by

$$A_{Rij} = \frac{Q_\ell e (F_{2ij}(0) - iF_{3ij}(0))}{4m_i^2} \quad A_{Lij} = \frac{Q_\ell e (F_{2ij}(0) + iF_{3ij}(0))}{4m_i^2}, \quad (3.13)$$

where $Q_\ell = -1$ is the electron charge in units of the positron charge e .

Using these results we can directly express the $g-2$ and the electric dipole moment of an arbitrary lepton as

$$a_i = -4 \frac{m_i^2}{e} \text{Re}(A_{Rii}) \quad (3.14)$$

$$d_i = m_i \text{Im}(A_{Rii}) \quad (3.15)$$

Up to terms suppressed by powers of the ℓ_j mass the branching fraction $\ell_i \rightarrow \ell_j \gamma$ can be written as [96]

$$\text{Br}(\ell_i \rightarrow \ell_j \gamma) = \frac{m_i^5}{4\pi\Gamma_i} (|A_{Lij}|^2 + |A_{Rij}|^2). \quad (3.16)$$

Here Γ_i is the total decay width of ℓ_i , where $i = \mu, \tau$

The process $\mu \rightarrow 3e$ is described by the extended Lagrangian [96]

$$\begin{aligned} \mathcal{L}_{\mu \rightarrow e/3e} &= A_R m_\mu \bar{\ell}_e \sigma^{\sigma\rho} F_{\sigma\rho} P_R \ell_\mu + A_L m_\mu \bar{\ell}_e \sigma^{\sigma\rho} F_{\sigma\rho} P_L \ell_\mu \\ &\quad + g_1 \bar{\ell}_e P_R \ell_\mu \bar{\ell}_e P_R \ell_e + g_2 \bar{\ell}_e P_L \ell_\mu \bar{\ell}_e P_L \ell_e \\ &\quad + g_3 \bar{\ell}_e \gamma^\nu P_R \ell_\mu \bar{\ell}_e \gamma_\nu P_R \ell_e + g_4 \bar{\ell}_e \gamma^\nu P_L \ell_\mu \bar{\ell}_e \gamma_\nu P_L \ell_e \\ &\quad + g_5 \bar{\ell}_e \gamma^\nu P_R \ell_\mu \bar{\ell}_e \gamma_\nu P_L \ell_e + g_6 \bar{\ell}_e \gamma^\nu P_L \ell_\mu \bar{\ell}_e \gamma_\nu P_R \ell_e + \text{h.c.} \end{aligned} \quad (3.17)$$

For convenience we dropped the general flavour notation at this part, i.e. the Wilson coefficients A_{LR} satisfy the trivial relation $A_{LR} = A_{LR\mu e}$. The generalisation to arbitrary flavours is straightforward. Note that the coefficients $A_{L,R}$ and g_i have mass dimension -2 . The appearance of the same coefficients $A_{L,R}$ as in (3.11) indicates that all quantum fluctuations are again integrated out. In practice, absorbing e.g. electron loop diagrams involving a four-fermion operator into $A_{L,R}$ and into a loop correction to the g_i is convenient as we do not have to treat the different lepton flavours separately. In particular, in writing (3.17) the effect of the off-shell ($q^2 \neq 0$) form factors in (3.12) is absorbed into the g_i coefficients

CHAPTER 3. EFFECTIVE FIELD THEORY

(see the [96] for details). In any case, since this represents a loop correction to the Wilson coefficients, which are already generated at the tree-level, we neglect these effects in our calculation.

The branching fraction of $\mu \rightarrow 3e$ can easily be expressed through the coefficients g_i and $A_{L,R}$ [96]:¹

$$\begin{aligned} \text{Br}(\mu \rightarrow 3e) &= \frac{m_\mu^5}{1536\pi^3\Gamma_\mu} \left[\frac{|g_1|^2 + |g_2|^2}{8} + 2(|g_3|^2 + |g_4|^2) + |g_5|^2 + |g_6|^2 \right. \\ &\quad \left. - 8e \text{Re} [A_R(2g_4^* + g_6^*) + A_L(2g_3^* + g_5^*)] \right. \\ &\quad \left. + 64e^2 \left(\ln \frac{m_\mu}{m_e} - \frac{11}{8} \right) (|A_L|^2 + |A_R|^2) \right] \end{aligned} \quad (3.18)$$

with Γ_μ the muon decay width. The first line arises from tree-level KK exchange in the RS model, while the second and third involve the loop-induced dipole operator coefficients. One reason to keep the contribution of the loop-induced dipole operator here is the significant enhancement factor $(\ln \frac{m_\mu}{m_e} - \frac{11}{8})$. This argument might be misleading at first glance as one-loop corrections to the g_i may have a similar logarithmic enhancement. However one-loop contribution to the g_i induce only small shifts to the coefficients without altering the general expression. The loop suppressed contributions of the dipole operator on the other hand induce a sensitivity of the processes to other aspects of the underlying theory. In RS models $A_{L,R}$ have a specific dependence on the Yukawa couplings, which can provide an important contribution to the branching fraction in sizeable parts of the model parameter space. In these regions the effect of $A_{L,R}$ should not be neglected, as it will significantly alter the signatures of the RS model in flavour observables.

Muon conversion in nuclei is mediated by both, operators containing quark fields and electromagnetic dipole operators. The effective Lagrangian is [96, 97]

$$\begin{aligned} \mathcal{L}_{\mu N \rightarrow e N} &= A_R m_\mu \bar{\ell}_e \sigma^{\sigma\rho} F_{\sigma\rho} P_R \ell_\mu + A_L m_\mu \bar{\ell}_e \sigma^{\sigma\rho} F_{\sigma\rho} P_L \ell_\mu \\ &\quad + \sum_{q=u,d} c_{VR}^q \bar{\ell}_e \gamma^\nu P_R \ell_\mu \bar{q} \gamma_\nu q + \sum_{q=u,d} c_{VL}^q \bar{\ell}_e \gamma^\nu P_L \ell_\mu \bar{q} \gamma_\nu q \\ &\quad + \sum_{q=u,d,s} \frac{m_q m_\mu}{M_H^2} c_{SL}^q \bar{\ell}_e P_R \ell_\mu \bar{q} q + \sum_{q=u,d,s} \frac{m_q m_\mu}{M_H^2} c_{SR}^q \bar{\ell}_e P_L \ell_\mu \bar{q} q \\ &\quad + \frac{\alpha_s m_\mu}{M_H^2} c_{gg}^L \bar{\ell}_e P_R \ell_\mu G^{A,\sigma\rho} G_{\sigma\rho}^A + \frac{\alpha_s m_\mu}{M_H^2} c_{gg}^R \bar{\ell}_e P_L \ell_\mu G^{A,\sigma\rho} G_{\sigma\rho}^A + \text{h.c.} \end{aligned} \quad (3.19)$$

Here M_H denotes the Higgs mass, and $G_{\mu\nu}^A$ is the gluon field strength tensor. We do not include operators with pseudo-scalar, axial vector or tensor quark currents. Their contributions are suppressed by the nucleon number conservation of the target nuclei and can be neglected. We also neglect the strange quark contribution in the vector operators, since the coefficient is not enhanced by the strange-quark mass. The conversion branching fraction depends on properties of the nucleus that participates in the reaction. The expression, taken from [95, 97] and adjusted to match our conventions, is

$$\begin{aligned} \text{Br}(\mu N \rightarrow e N) &= \frac{m_\mu^5}{4\Gamma_{\text{capture}}} \left| A_R \mathcal{D} + 4 \left[\frac{m_\mu m_p}{M_H^2} (\tilde{C}_{SL}^p - 12\pi \tilde{C}_{L,gg}^p) \mathcal{S}^p + \tilde{C}_{VL}^p \mathcal{V}^p \right. \right. \\ &\quad \left. \left. + \{p \rightarrow n\} \right] \right|^2 + \{L \leftrightarrow R\}, \end{aligned} \quad (3.20)$$

¹The sign of the interference term (second line in (3.18)) depends on the convention for the covariant derivative. In the convention of [96] the sign is '+'. This is compensated by the Wilson coefficients $A_{L,R}$, the sign of which is also convention dependent.

3.2. LEPTON LOW ENERGY OBSERVABLES



Figure 3.1: *Left*: Matching of LFV couplings of the Z -boson onto four-fermion operators in the low-energy theory. *Right*: Higgs exchange diagram that contributes to $g_{1,2}$ and $c_{SR/L}^q$.

where Γ_{capture} is the total muon capture rate for nucleus N . The coefficients \mathcal{D} , $\mathcal{V}^{p/n}$, $\mathcal{S}^{p/n}$ (the superscript refers to the proton and neutron) encode properties of the target nucleus, see [95]. The tilded coefficients are defined as

$$\tilde{C}_{SL}^p = \sum_{q=u,d,s} c_{SL}^q f_q^p, \quad (3.21)$$

$$\tilde{C}_{L,gg}^p = c_{gg}^L f_Q^p, \quad (3.22)$$

$$\tilde{C}_{VL}^p = \sum_{q=u,d} c_{VL}^q f_{V_q}^p, \quad (3.23)$$

and analogously for the $p \rightarrow n$ and $L \rightarrow R$ cases. The form factors $f_q^{p,n}$ and $f_{V_q}^{p,n}$ parametrise the coupling strengths of the quark scalar and vector currents of flavour q to nucleons, respectively. $f_Q^{p,n}$ represent the scalar couplings of heavy quarks (c, b or t).

Following the expression of all in this thesis considered lepton observables in terms of the effective low energy Lagrangians we now focus on the matching of the dimension six Lagrangian to the Wilson coefficients of the low energy Lagrangians. We start with the tree-level matching of the four-fermion operators, which is straightforward. However the four-fermion operators in (3.17), (3.19) also can be generated by lepton flavour Z -Boson exchange $\ell_i \gamma_\mu P_{L,R} \ell_j Z^\mu$ once the Z boson is integrated out, see Figure 3.1. For example, in case of $\mu \rightarrow 3e$, the insertion of $\ell_e \gamma^\mu P_R \ell_\mu Z_\mu$ evaluates to

$$i\mathcal{M} = i\gamma_{12}^1 \left[\frac{2s_W^2 - 1}{2} \bar{u}_e(p_2) \gamma^\mu P_R u_\mu(p_1) \bar{u}_e(p_4) \gamma^\mu P_L v_e(p_3) + s_W^2 \bar{u}_e(p_2) \gamma^\mu P_R u_\mu(p_1) \bar{u}_e(p_4) \gamma^\mu P_R v_e(p_3) + \text{Fierz diagram} \right], \quad (3.24)$$

which gives a contribution to g_3 and $g_5 \cdot \gamma^{2,3}$ will lead to contributions to g_4 and g_6 . Contributions to c_{VR}^q follow analogously. Thus we find the relations:

$$g_1 = g_2 = 0 \quad (3.25)$$

$$g_3 = \frac{1}{T^2} (s_W^2 \gamma_{12}^1 + \beta_{1211}^{EE} + \beta_{1112}^{EE}) \quad (3.26)$$

$$g_4 = \frac{1}{T^2} \left(\frac{2s_W^2 - 1}{2} (\gamma_{12}^2 + \gamma_{12}^3) + \beta_{1211}^{LL} + \beta_{1112}^{LL} \right) \quad (3.27)$$

$$g_5 = \frac{1}{T^2} \left(\frac{2s_W^2 - 1}{2} \gamma_{12}^1 + \beta_{1112}^{LE} \right) \quad (3.28)$$

$$g_6 = \frac{1}{T^2} (s_W^2 (\gamma_{12}^2 + \gamma_{12}^3) + \beta_{1211}^{LE}), \quad (3.29)$$

CHAPTER 3. EFFECTIVE FIELD THEORY

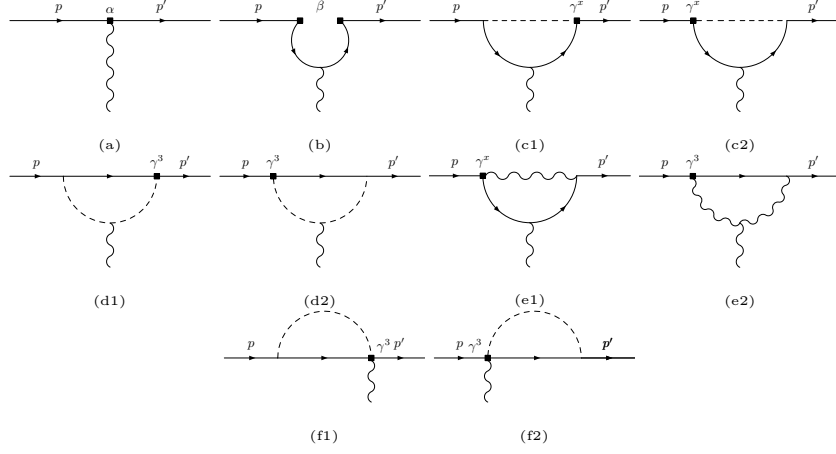


Figure 3.2: All tree and one-loop diagrams contributing to $A_{L/R}$.

$$c_{VR}^u = \frac{1}{2T^2} \left[\beta_{1211}^{Eu} + \beta_{1211}^{EQ} + \frac{1}{2} \gamma_{12}^1 \left(1 - \frac{8}{3} s_W^2 \right) \right] \quad (3.30)$$

$$c_{VL}^u = \frac{1}{2T^2} \left[\beta_{1211}^{LQ} - \beta_{1211}^{L\tau Q} + \beta_{1211}^{Lu} + \frac{1}{2} (\gamma_{12}^2 + \gamma_{12}^3) \left(1 - \frac{8}{3} s_W^2 \right) \right] \quad (3.31)$$

$$c_{VR}^d = \frac{1}{2T^2} \left[\beta_{1211}^{Ed} + \beta_{1211}^{EQ} + \frac{1}{2} \gamma_{12}^1 \left(-1 + \frac{4}{3} s_W^2 \right) \right] \quad (3.32)$$

$$c_{VL}^d = \frac{1}{2T^2} \left[\beta_{1211}^{LQ} + \beta_{1211}^{L\tau Q} + \beta_{1211}^{Ld} + \frac{1}{2} (\gamma_{12}^2 + \gamma_{12}^3) \left(-1 + \frac{4}{3} s_W^2 \right) \right] \quad (3.33)$$

$$c_{SL}^q = -\frac{v}{\sqrt{2}m_\mu T^2} \eta_{12} \quad (3.34)$$

$$c_{SR}^q = -\frac{v}{\sqrt{2}m_\mu T^2} [\eta^\dagger]_{12}, \quad (3.35)$$

as well as [98, 99]

$$c_{gg}^L = -\frac{1}{12\pi} \sum_{q=c,b,t} c_{SL}^q, \quad c_{gg}^R = -\frac{1}{12\pi} \sum_{q=c,b,t} c_{SR}^q. \quad (3.36)$$

Note that the expressions (3.36) result from the nucleus nucleus matrix element of $\langle n | \bar{q}q | n \rangle$, where $q = s, b, t$ are heavy quarks. These matrix elements can be put in relation to the gluon condensate matrix element via a triangle anomaly diagram, where the heavy quark condensate decays to two gluons in the presence of the nucleus. With a heavy quark theory expansion one can find [98]

$$m_q \langle n | \bar{q}q | n \rangle = -\frac{2}{3} \frac{\alpha_s}{8\pi} \langle n | G^{\mu\nu} G_{\mu\nu} | n \rangle + \mathcal{O} \left(\frac{\alpha_s^2}{m_q^2} \right) \quad (3.37)$$

It should be noted that g_1 and g_2 receive contributions from the tree-level Higgs exchange diagram, Figure 3.1 (right diagram), with an insertion of one flavour-changing Higgs operator $h \bar{\ell}_i P_R \ell_j + \text{h.c.}$, but these are suppressed by powers of the electron mass (light lepton mass in the general case) and we neglect them. The same diagram (with the two fermion lines on the

3.2. LEPTON LOW ENERGY OBSERVABLES

right being quarks) also generates c_{SL}^q . Here we should comment on a (well-known) subtlety. Naively, the operator $\bar{L}_i \Phi E_j \Phi^\dagger \Phi$ in (3.2) modifies the Yukawa interaction according to

$$\frac{y_{ij}}{\sqrt{2}} h \bar{\ell}_i P_R \ell_j \rightarrow \frac{y_{ij}}{\sqrt{2}} h \bar{\ell}_i P_R \ell_j - h_{ij} \frac{3v^2}{2\sqrt{2}T^2} h \bar{\ell}_i P_R \ell_j \quad (3.38)$$

after electroweak symmetry breaking but before flavour rotations. Here y_{ij} is not the SM Yukawa coupling but the coefficient of the operator $\bar{L}_i \Phi E_j$ in the dimension-four Lagrangian. However, the fermion mass matrix is also modified by dimension-six operator,

$$\frac{y_{ij}v}{\sqrt{2}} \rightarrow m_{ij} = \frac{y_{ij}v}{\sqrt{2}} - h_{ij} \frac{v^3}{2\sqrt{2}T^2}. \quad (3.39)$$

Since the flavour rotation matrices U and V by construction diagonalise the modified mass term m_{ij} , we have to rewrite the shift of the Yukawa couplings as (see also [49])

$$\left(\frac{1}{\sqrt{2}} y_{ij} - h_{ij} \frac{3v^2}{2\sqrt{2}T^2} \right) h \bar{\ell}_i P_R \ell_j \rightarrow \left(\frac{m_{ij}}{v} - h_{ij} \frac{v^2}{\sqrt{2}T^2} \right) h \bar{\ell}_i P_R \ell_j. \quad (3.40)$$

As a consequence the factor 3/2 in the flavour-violating Higgs interaction $h \bar{\ell}_i P_R \ell_j + \text{h.c.}$ of (3.7) must be replaced by 1 for the computation of c_{SL}^q , c_{SR}^q above.

The determination of the coefficients $A_{L,R}$ is more complicated. One can identify three contributions: (1) from tree or one-loop diagrams involving the operators in the dimension-six Lagrangian [28, 54]. All relevant diagrams are drawn in figure 3.2. Their contribution has been already calculated in the naive dimensional regularisation scheme in [28], which involves anti-commuting γ_5 matrices. The only contributions missing in [28] are the diagrams e1 and e2. We will not repeat this part of the calculation of [28] at this point. The diagrams e1 and e2 are standard electroweak one-loop diagrams. The second contribution to $A_{L,R}$ is coming from dimension-eight operators, which may become relevant if the dimension-six contributions are suppressed. We will discuss them later specifically in the context of the RS model. (This contribution can effectively be included via a modification of the $a_{B,W}^{ij}$ Wilson coefficients.) (3) from enhanced two-loop ‘‘Barr-Zee type diagrams’’ with a flavour-changing Higgs coupling [100], see [101] for a discussion in the context of $\mu \rightarrow e\gamma$. An example diagram, which avoids the coupling of the Higgs boson to a light lepton through the coupling to a top or gauge-boson loop, is shown in Figure 3.3. These terms are known to give sizeable contributions in models where the Higgs interactions are the dominant sources of new flavour violation. In the RS model this is generally not the case. Nonetheless we

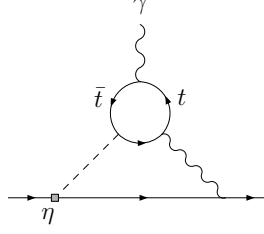


Figure 3.3: Example of a Barr-Zee type diagram. The box denotes the insertion of the lepton-flavour violating Higgs interaction. The internal gauge-boson can be a Z or a photon.

include these terms as they may become relevant in specific scenarios. We obtain²

$$\begin{aligned}
 m_i A_{Rij} &= \alpha_{ji}^A \frac{v}{\sqrt{2}T^2} - \sum_{k=1,2,3} \frac{Q_{\ell e}}{16\pi^2 T^2} m_{\ell_k} \beta_{jkk}^{EL} \\
 &\quad - \frac{Q_{\ell e}}{3(4\pi)^2 T^2} \left(s_W^2 [m_i(\gamma_{ji}^2 + \gamma_{ji}^3) + m_i \gamma_{ji}^1] + m_i \gamma_{ji}^2 - \frac{3}{2} m_i \gamma_{ji}^3 - \frac{3}{2} m_i \gamma_{ji}^1 \right) \\
 &\quad + A_{BZ} \left[\eta_{ji} \frac{v^2}{\sqrt{2}T^2} \right] \tag{3.41}
 \end{aligned}$$

$$\begin{aligned}
 m_i A_{Lij} &= [\alpha^{A\dagger}]_{ji} \frac{v}{\sqrt{2}T^2} - \sum_{k=1,2,3} \frac{Q_{\ell e}}{16\pi^2 T^2} m_{\ell_k} \beta_{kij}^{EL} \\
 &\quad - \frac{Q_{\ell e}}{3(4\pi)^2 T^2} \left(s_W^2 [m_j(\gamma_{ji}^2 + \gamma_{ji}^3) + m_i \gamma_{ji}^1] + m_j \gamma_{ji}^2 - \frac{3}{2} m_j \gamma_{ji}^3 - \frac{3}{2} m_i \gamma_{ji}^1 \right) \\
 &\quad + A_{BZ} \left[\eta_{ji}^\dagger \frac{v^2}{\sqrt{2}T^2} \right], \tag{3.42}
 \end{aligned}$$

where [101]

$$\begin{aligned}
 A_{BZ} &= \frac{Q_{\ell e} \alpha_{em} \sqrt{2} G_F v}{32\pi^3} \left[2N_c Q_t^2 f(r_t) - 3f(r_W) - \frac{23}{4}g(r_W) - \frac{3}{4}h(r_W) \right. \\
 &\quad - \frac{f(r_W) - g(r_W)}{2r_W} + \frac{1 - 4s_W^2}{4s_W^2} \left\{ \frac{1 - 4Q_t s_W^2}{4c_W^2} 2N_c Q_t \tilde{f}(r_t, r_{tZ}) \right. \\
 &\quad - \frac{1}{2} (5 - s_W^2/c_W^2) \tilde{f}(r_W, r_{WZ}) - \frac{1}{2} (7 - 3s_W^2/c_W^2) \tilde{g}(r_W, r_{WZ}) - \frac{3}{4}g(r_W) \\
 &\quad \left. \left. - \frac{3}{4}h(r_W) - \frac{1 - s_W^2/c_W^2}{4r_W} (\tilde{f}(r_W, r_{WZ}) - \tilde{g}(r_W, r_{WZ})) \right\} \right. \\
 &\quad - \frac{1}{4s_W^2} \left(D_e^{(3a)}(r_W) + D_e^{(3b)}(r_W) + D_e^{(3c)}(r_W) + D_e^{(3d)}(r_W) + D_e^{(3e)}(r_W) \right. \\
 &\quad \left. \left. + D_e^{(4a)}(r_Z) + D_e^{(4b)}(r_Z) + D_e^{(4c)}(r_Z) \right) \right] \tag{3.43}
 \end{aligned}$$

with $r_t = m_{\text{top}}^2/M_{\text{Higgs}}^2$, $r_{tZ} = m_{\text{top}}^2/m_Z^2$, $r_{WZ} = m_W^2/m_Z^2$, $r_W = m_W^2/M_{\text{Higgs}}^2$, $r_Z = m_Z^2/M_{\text{Higgs}}^2$, and $N_c = 3$, $Q_t = 2/3$. The functions f, g, h and \tilde{f}, \tilde{g} can be found in [101] and

²In practice, we can drop the terms proportional to the lighter lepton mass, here m_e .

the functions D_a^X in [102]. Note again that relative signs in (3.41), (3.42) depend on the convention for the covariant derivative.

All expressions for $\mu \rightarrow 3e$ and $\mu \rightarrow e\gamma$ in this section can be trivially extended to $\tau \rightarrow e\gamma$ or $\tau \rightarrow 3\mu$ by exchanging the appropriate flavour indices, masses and widths. We note that we do not take into account the running of the Wilson coefficients between the high and the low scale in the lepton sector, see e.g. [92, 103, 104] for the anomalous dimensions of the dimension-six operator basis.

3.3 Effective weak Hamiltonian

The typical energy release in a decay of the type $\bar{B} \rightarrow X_s \gamma$ is of the order of the b quark mass and a typical scale choice is thus $\mu_b = M_B/2 \approx 2.6$ GeV. From the Standard Model calculation of $b \rightarrow s\gamma$ in the framework of the weak effective Hamiltonian, see [105] for an overview, it is known that the RGE evolution from the weak scale $\mu_W \sim M_W$ down to μ_b introduces sizeable operator mixing [106, 107].

Our matching of the dimension six Lagrangian was done at the high scale T , which means that QCD corrections are bound to be important. To evolve all operators to the low scale we have two choices. The first choice is to pursue a two step matching calculation, where we first evolve down from the unbroken dimension six Lagrangian at the high scale down to a unbroken SM at the electroweak scale. At this point we have reached the standard initial conditions for calculations within the SM, i.e. the next evolution to scale m_b can be done like for similar computations in the SM. The anomalous dimension matrix for the first step can be found in [92, 103, 104]. Although this matching procedure seem to be more in the spirit of a dimension six Lagrangian we will not pursue it here for this thesis. Instead we transition to the "broken" operator basis at the high scale and then perform the evolution down to the low scale in one step (taking into account the top-mass threshold). This one step has the advantage of having a simpler "logistics" as we only need consider a single RGE. Both strategies are valid and ultimately must be equivalent in a situation where no additional dynamics between μ_{KK} and μ_W need to be taken into account.

However, for the specific process at hand the second option has the additional advantage that the structure of the required evolution equations has been studied in some detail in [108]. While [108] ultimately focusses on scenarios with e.g. a flavour-changing Z' , their operator basis contains the full set of normal and colour-flipped four-quark operators. We therefore choose to follow this approach.

Let us for clarity introduce the effective Hamiltonian at the high scale μ_{KK} , that is used in [108]

$$\begin{aligned}
 \mathcal{H}^{(b \rightarrow s)} = & -\frac{4G_F}{\sqrt{2}} V_{ts}^* V_{tb} \left[\Delta C_{7\gamma}(\mu_{KK}) Q_{7\gamma} + \Delta C_{8g}(\mu_{KK}) Q_{8g} + \Delta C'_{7\gamma}(\mu_{KK}) Q'_{7\gamma} + \Delta C'_{8g}(\mu_{KK}) Q'_{8g} \right. \\
 & + \sum_{A,B=L,R} \sum_{q=u,c,t,d,s,b} \Delta C_1^q[A,B](\mu_{KK}) Q_1^q[A,B] + \Delta C_2^q[A,B](\mu_{KK}) Q_2^q[A,B] \\
 & \left. + \sum_{A,B=L,R} \Delta \widehat{C}_1^d[A,B](\mu_{KK}) \widehat{Q}_1^d[A,B] + \Delta \widehat{C}_2^d[A,B](\mu_{KK}) \widehat{Q}_2^d[A,B] \right]
 \end{aligned} \tag{3.44}$$

CHAPTER 3. EFFECTIVE FIELD THEORY

where the operators are given by

$$\begin{aligned}
Q_{7\gamma} &= \frac{e m_b}{16\pi^2} \bar{s}_\alpha \sigma^{\mu\nu} P_R b_\alpha F_{\mu\nu} & Q_{8g} &= \frac{g_s m_b}{16\pi^2} \bar{s}_\alpha \sigma^{\mu\nu} P_R T_{\alpha\beta}^A b_\beta G_{\mu\nu}^A \\
Q'_{7\gamma} &= \frac{e m_b}{16\pi^2} \bar{s}_\alpha \sigma^{\mu\nu} P_L b_\alpha F_{\mu\nu} & Q'_{8g} &= \frac{g_s m_b}{16\pi^2} \bar{s}_\alpha \sigma^{\mu\nu} P_L T_{\alpha\beta}^A b_\beta G_{\mu\nu}^A \\
Q_1^q[A, B] &= (\bar{s}_\alpha \gamma^\mu P_A b_\beta) (\bar{q}_\beta \gamma_\mu P_B q_\alpha) & Q_2^q[A, B] &= (\bar{s}_\alpha \gamma^\mu P_A b_\alpha) (\bar{q}_\alpha \gamma_\mu P_B q_\alpha) \\
\widehat{Q}_1^d[A, B] &= (\bar{s}_\alpha \gamma^\mu P_A d_\beta) (\bar{d}_\beta \gamma_\mu P_B b_\alpha) & \widehat{Q}_2^d[A, B] &= (\bar{s}_\alpha \gamma^\mu P_A d_\alpha) (\bar{d}_\alpha \gamma_\mu P_B b_\alpha)
\end{aligned} \tag{3.45}$$

with $P_{L/R} = \frac{1}{2}(1 \mp \gamma_5)$ as usual and α, β are colour indices. Note that while the usual current-current and penguin operators

$$\begin{aligned}
Q_1 &= (\bar{s}_\alpha \gamma^\mu P_L c_\beta) (\bar{c}_\beta \gamma_\mu P_L b_\alpha) & Q_2 &= (\bar{s}_\alpha \gamma^\mu P_L c_\alpha) (\bar{c}_\beta \gamma_\mu P_L b_\beta) \\
Q_3 &= (\bar{s}_\alpha \gamma^\mu P_L c_\alpha) \sum_{q=u,c,d,s,b} (\bar{q}_\beta \gamma_\mu P_L q_\beta) & Q_4 &= (\bar{s}_\alpha \gamma^\mu P_L c_\beta) \sum_{q=u,c,d,s,b} (\bar{q}_\beta \gamma_\mu P_L q_\alpha) \\
Q_5 &= (\bar{s}_\alpha \gamma^\mu P_L c_\alpha) \sum_{q=u,c,d,s,b} (\bar{q}_\beta \gamma_\mu P_R q_\beta) & Q_6 &= (\bar{s}_\alpha \gamma^\mu P_L c_\beta) \sum_{q=u,c,d,s,b} (\bar{q}_\beta \gamma_\mu P_R q_\alpha)
\end{aligned} \tag{3.46}$$

are not included in (3.44), they do enter the renormalisation group equations. This operator basis is obviously non-minimal as e.g. Q_1 and $Q_2^c[L, L]$ are related via Fierz identities. As we only consider the LO corrections due to new physics, this does not invalidate the RG analysis [105]. In total we have to consider 70 operators. Fortunately, there are only a few independent entries in the leading order (LO) anomalous dimension matrix. Most of which can be taken from [109, 110] once the different operator normalisation has been taken into account³. The remaining entries (computed in the HV scheme) can be taken directly from [108]. The anomalous dimensions matrix has the form

$$\begin{pmatrix}
X_1 & X_2 & X_3 & 0 & 0 & 0 & 0 \\
0 & X_4 & X_5 & 0 & 0 & 0 & 0 \\
0 & 0 & X_6 & 0 & 0 & 0 & 0 \\
0 & Y_1 & Y_2 & Y_3 & 0 & 0 & 0 \\
0 & 0 & 0 & 0 & X_4 & X_5 & 0 \\
0 & 0 & 0 & 0 & 0 & X_6 & 0 \\
0 & 0 & 0 & 0 & Y_1 & Y_2 & Y_3
\end{pmatrix}, \tag{3.47}$$

for the operator vector

$$\vec{O} = (Q^{cc}, Q_P, Q_D, Q^{nn}, Q'_P, Q'_D, Q'_{nn}), \tag{3.48}$$

where Q^{cc} are the operators $Q_{1,2}$, Q_P the penguin operators $Q_{3,4,5,6}$, Q_D the dipole operators and Q_{nn} all remaining operators of (3.45). Note that we use the scheme independent dipole operators $C_{7\gamma}^{eff}$ and $C_{8\gamma}^{eff}$ in this basis. That is important because our C_7 and C_8 are calculated in the NDR scheme, while the anomalous dimension is computed in the HV scheme. Only after introducing the effective dipole operators after the inclusion of one-loop four fermion corrections the whole computation becomes scheme independent [105]. Non vanishing entries of the matrices X can be directly taken from [105] as they belong to the

³In [105] the corresponding operators Q_{1-8} are only rescaled by a factor of 1/4 compared to their definition in (3.45),(3.46). The anomalous dimensions remain therefore the same.

3.3. EFFECTIVE WEAK HAMILTONIAN

SM analysis. The matrices Y have been taken from [108]. With the anomalous dimensions at hand, the renormalisation group evolution equation (RGE)

$$\mu \frac{d}{d\mu} C_i(\mu) = \frac{\alpha_s(\mu)}{4\pi} [\gamma^T]_{ij} C_j(\mu) \quad (3.49)$$

can be solved in the standard way, provided the initial conditions at the high scale μ_{KK} are known. As the anomalous dimension matrix γ is sparse, a basis where the evolution is diagonal can be determined very efficiently. For the strong coupling constant we use $\alpha_s(M_Z) = 0.1185$ with decoupling of the top quark at $m_t = 170$ GeV.

Once the evolution down to μ_b has been performed the result for the branching fraction of $\bar{B} \rightarrow X_s \gamma$ can be obtained using the formula [108, 111]

$$\frac{\text{Br}(B \rightarrow X_s \gamma)|_{E_\gamma > 1.6 \text{ GeV}}}{\text{Br}(B \rightarrow X_s \gamma)|_{E_\gamma > 1.6 \text{ GeV}}^{SM}} = \frac{1}{|C_{7\gamma}(\mu_b)_{SM}|^2 + N} \left(|C_{7\gamma}(\mu_b)|^2 + |C'_{7\gamma}(\mu_b)|^2 + N \right). \quad (3.50)$$

Here we use a minimum photon energy of $E_\gamma^{min} = 1.6$ GeV; the same as was used for the HFAG world average. Here the constant N is a non-perturbative correction [112–115] and we use $N(E_\gamma = 1.6 \text{ GeV}) = 3.6 \times 10^{-3}$.

Since we work in leading order in the new physics contribution, BSM effects only induce a shift in the Wilson coefficients

$$C_{7\gamma}^{(\prime)}(\mu_b) \rightarrow \left[C_{7\gamma}^{(\prime)}(\mu_b) \right]_{SM} + \Delta C_{7\gamma}^{(\prime)}(\mu_b). \quad (3.51)$$

The SM value of the dipole coefficients

$$C_{7\gamma}(\mu_b) = -0.368 \quad (3.52)$$

can be taken from [37]. The primed coefficient $C'_{7\gamma}$ is tiny as it is suppressed by m_s/m_b and can be neglected.

The last part for the determination of the $\bar{B} \rightarrow X_s \gamma$ is to find the initial conditions for the RGE flow. They can be found by matching the dimension six Lagrangian at the high scale T (3.9) to the weak Hamiltonian at the KK scale. Here we only explicitly give the matching of the operator $\bar{d}_i \gamma^\mu T^A d_i \bar{u}_j \gamma_\mu T^A u_j$. After applying the Fierz algebra for the fundamental $SU(3)_C$ generators

$$(T^A)_{ij} (T^A)_{kl} = \frac{1}{2} \left(\delta_{il} \delta_{jk} - \frac{1}{N_c} \delta_{ij} \delta_{kl} \right) \quad (3.53)$$

we find

$$\begin{aligned} \beta_{sbq_u q_u}^{DU} \bar{s} \gamma^\mu T^A P_R b \bar{q}_u \gamma_\mu T^A P_R q_u &= -\frac{1}{2N_c} \beta_{sbq_u q_u} \bar{s} \gamma^\mu P_R b \bar{q}_u \gamma_\mu P_R q_u \\ &+ \frac{1}{2} \beta_{sbq_u q_u}^{DU} \bar{s} \alpha \gamma^\mu P_R b \beta (\bar{q}_u)_\beta \gamma_\mu P_R (q_u)_\alpha \\ &= -\frac{1}{2N_c} \beta_{sbq_u q_u}^{DU} O_2^{q_u}[R, R] + \frac{1}{2} \beta_{sbq_u q_u}^{DU} O_1^{q_u}[R, R] \end{aligned} \quad (3.54)$$

where a simple single sum over $q_u = u, c, t$ is implied.

Comparing (3.54) with (3.44), we obtain

$$\frac{4G_F V_{ts}^* V_{tb}}{\sqrt{2}} \Delta C_1^{q_u}[R, R](\mu_{KK}) = \frac{1}{2T^2} \beta_{sbq_u q_u}^{DU}, \quad \frac{4G_F V_{ts}^* V_{tb}}{\sqrt{2}} \Delta C_2^{q_u}[R, R](\mu_{KK}) = -\frac{1}{2N_c T^2} \beta_{sbq_u q_u}^{DU}. \quad (3.55)$$

CHAPTER 3. EFFECTIVE FIELD THEORY

The remaining four-quark operators can be related to operators in the weak Hamiltonian in the same fashion. For clarity, we have relayed the expressions for the Wilson coefficient of (3.44) to the Appendix, see C.3.

To conclude this chapter we need to write down the matching of the dipole terms between the dimension six Lagrangian (3.9) and (3.44). We find

$$\begin{aligned}
\frac{4G_F V_{ts}^* V_{tb}}{\sqrt{2}} C_{7\gamma}^{eff}(\mu_{KK}) &= -\frac{16\pi^2}{e m_b T^2} \alpha_{sb}^\gamma \frac{v}{\sqrt{2}} - \sum_q \frac{Q_q m_q C_F}{m_b T^2} \beta_{qbsq}^{QD} \\
\frac{4G_F V_{ts}^* V_{tb}}{\sqrt{2}} C_{7\gamma}^{eff,'}(\mu_{KK}) &= -\frac{16\pi^2}{e m_b T^2} [\alpha^\gamma]_{sb}^\dagger \frac{v}{\sqrt{2}} - \sum_q \frac{Q_q m_q C_F}{m_b T^2} \beta_{sqqb}^{QD} \\
\frac{4G_F V_{ts}^* V_{tb}}{\sqrt{2}} C_{8g}^{eff}(\mu_{KK}) &= -\frac{16\pi^2}{g_s m_b T^2} \alpha_{sb}^g \frac{v}{\sqrt{2}} + \sum_q \frac{m_q}{2N_c m_b T^2} \beta_{qbsq}^{QD} \\
\frac{4G_F V_{ts}^* V_{tb}}{\sqrt{2}} C_{8g}^{eff,'}(\mu_{KK}) &= -\frac{16\pi^2}{g_s m_b T^2} [\alpha^g]_{sb}^\dagger \frac{v}{\sqrt{2}} + \sum_q \frac{m_q}{2N_c m_b T^2} \beta_{sqqb}^{QD}. \tag{3.56}
\end{aligned}$$

Note that equation (3.56) includes a global minus sign. We had to include it to compensate for the different the different covariant derivative definition of [105, 108]. All quantities on the right-hand side of (3.56) are implied to be evaluated at the scale μ_{KK} .

Chapter 4

Tree-level dimension-six operators

After setting up the computation of all low energy observables in terms of an effective theory the next step is to match all Wilson coefficients to the 5d theory. In this chapter we compute the explicit expressions for all tree-level induced Wilson coefficients of interest. Here we distinguish between the four-fermion, Higgs-fermion and Yukawa type operators. Throughout this chapter we use the 5D formalism as defined in section 2.3.3.

4.1 Four-fermion operators

The tree-level diagram contributing to the matching of the Wilson coefficients of four-fermion operators is shown in generic form in Figure 4.1. The exchanged particle could be an off-shell KK gauge-boson or a KK Higgs excitation. The latter vanishes for $\beta \rightarrow \infty$ and can safely be ignored. This can be verified by explicit analytic calculation, see Appendix B.4. The gauge contributions in the minimal model were discussed at length in [28]. Most of these results carry over to the custodially protected model. We only need to account for effects that originate from the additional particles in the spectrum. The additional four fermion operators like for example b_{LL}^{ijkl} can then be directly inferred from [28] and the effects from the additional particles of the RSc spectrum by adjusting hypercharge and weak isospin factors. Note that for example b_{LL}^{ijkl} also exhibits two contractions during the computation of the associated matrix element, which give rise to an additional “t-channel” diagram. In the custodial protected RS model, there is only one new possible diagram, that can contribute to the four fermion operators. The reason for this is that an interaction with

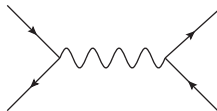


Figure 4.1: Generic topology of 5D diagrams that give rise to the four-fermion operators upon integrating out the exchanged particle. External states can be doublets or singlets. Consequently the intermediate boson can be a G, B or Z_X or the $SU(2)$ W gauge-boson, if all external states are doublets. Due to the chirality of the external states the fifth component of the boson cannot propagate.

CHAPTER 4. TREE-LEVEL DIMENSION-SIX OPERATORS

the new non-abelian gauge-bosons $W_R^{1,2}$ always changes the $SU(2)_R$ quantum number of leptons and quarks in such a way that at least one of the external fermion fields cannot be a zero-mode. Only the Z_X boson can modify the Wilson coefficients of tree-level operators relative to their value in the minimal model. That is because the Z_X is generated as a linear combination of the W_R^3 and the X like the B boson and shares therefore similar couplings to the fermions. Note, that the fifth component of the Z_X or any 5D gauge-boson cannot appear as the external modes at each vertex have the same handedness. Since the external momenta are always much smaller than the KK scale T we only need the expression for the Z_X^μ propagator in the limit of vanishing 4D momentum q :

$$\Delta_{pm}(q \rightarrow 0, x, y) = \frac{i}{2k} [k^2 \min\{x^2, y^2\} - 1] . \quad (4.1)$$

This expression can be directly computed via a simple Taylor series of the explicit expression of the Δ_{pm} propagator (A.48). Using this expansion the Z_X contribution to the four-fermion operator $b_{ij}^{LE} (\bar{L}_i \gamma^\mu L_i) (\bar{E}_j \gamma_\mu E_j)$ can be computed in the 5D formalism as

$$b_{ij}^{LE Z_X} = i (i g_5 X)^2 \frac{Y_L Y_E}{4} T^2 \int_{\frac{1}{k}}^{\frac{1}{T}} \int_{\frac{1}{k}}^{\frac{1}{T}} \frac{dx}{(kx)^4} \frac{dy}{(ky)^4} \left(f_{L_i}^{(0)}(x) g_{E_j}^{(0)}(y) \right)^2 \Delta_{pm}(q \rightarrow 0, x, y), \quad (4.2)$$

which can be integrated analytically. Using this result as well the results for the KK B boson exchange [28] we find for $b_{ij}^{LE} (\bar{L}_i \gamma^\mu L_i) (\bar{E}_j \gamma_\mu E_j)$ the form

$$b_{ij}^{LE} = \frac{Y_L Y_E}{4} \left[g'^2 (b_0 + b_1(c_{L_i}) + b_1(-c_{E_j}) + b_2(c_{L_i}, c_{E_j})) + (g^2 - g'^2) b_2(c_{L_i}, c_{E_j}) \right] \quad (4.3)$$

with

$$b_0 = -\frac{1}{4} \frac{1}{\ln(1/\epsilon)}, \quad (4.4)$$

$$b_1(c) = -\frac{1}{4} \frac{(5-2c)(1-2c)}{(3-2c)^2} \frac{\epsilon^{2c-1}}{1-\epsilon^{2c-1}}, \quad (4.5)$$

$$b_2(c_L, c_E) = -\frac{1}{2} \frac{(1-2c_L)(1+2c_E)(3-c_L+c_E)}{(3-2c_L)(3+2c_E)(2-c_L+c_E)} \ln \frac{1}{\epsilon} \frac{\epsilon^{2c_L-1}}{1-\epsilon^{2c_L-1}} \frac{\epsilon^{-2c_E-1}}{1-\epsilon^{-2c_E-1}}. \quad (4.6)$$

As in [28] we drop terms suppressed by the tiny ratio $\epsilon = T/k$. Note that the coupling constant g_X of the Z_X can be replaced by solving equation (2.82)

$$g_X^2 = (g^2 - g'^2). \quad (4.7)$$

Hence to determine the result for the minimal RS model we just have to set the coupling g_X to zero, i.e. drop the $(g^2 - g'^2)$ term in (4.3). Using these expressions the Wilson coefficient of the operator $(\bar{E}_i \gamma_\mu E_i) (\bar{E}_j \gamma^\mu E_j)$ takes the form

$$b_{ij}^{EE} = \frac{Y_E}{2Y_L} b_{ij}^{LE}(c_{L_i} \rightarrow -c_{E_i}). \quad (4.8)$$

Here and above Y_E and Y_L are the hypercharges of singlet and doublet lepton field, respectively. Note that the additional factor of $\frac{1}{2}$ is consequence of all external fermion legs being the same leptons. This can be seen as follows: After applying the necessary contractions using the effective field theory the exchange symmetry automatically generates a factor of

4.1. FOUR-FERMION OPERATORS

two. However, the KK-Klein gauge-boson exchange between the fermion legs appears in the second order of the standard time dependent perturbation theory. There the factor two of the exchange symmetry is directly cancelled by the $\frac{1}{2!}$ factor coming from the second order term in perturbation theory. Dividing the factor of two from the effective field theory side then yields the additional $\frac{1}{2}$ factor.

For the operator $(\bar{L}_i \gamma^\mu L_j)(\bar{L}_k \gamma_\mu L_l)$ there are contributions from abelian Z_X or B bosons as above, and additionally from the exchange of a W boson. The abelian contribution due to Z_X , B exchange is given by

$$b_{ijkl, B+Z}^{LL} = \frac{Y_L}{2Y_E} \delta_{ij} \delta_{kl} b_{ik}^{LE} (c_{E_k} \rightarrow -c_{L_k}) \quad (\text{no sum over } i, k) \quad (4.9)$$

The non-abelian bosons generate the operator $(\bar{L}_i \tau^A \gamma^\mu L_i)(\bar{L}_j \tau^A \gamma_\mu L_j)$, which is not part of our basis, and has to be rewritten using the SU(2) Fierz identity

$$(\bar{L}_i \tau^A \gamma^\mu L_i)(\bar{L}_j \tau^A \gamma_\mu L_j) = 2(\bar{L}_i \gamma^\mu L_j)(\bar{L}_j \gamma_\mu L_i) - (\bar{L}_i \gamma^\mu L_i)(\bar{L}_j \gamma_\mu L_j). \quad (4.10)$$

We then find the Wilson coefficient of $(\bar{L}_i \gamma^\mu L_j)(\bar{L}_k \gamma_\mu L_l)$ to be

$$\begin{aligned} b_{ijkl}^{LL} &= b_{ijkl, B+Z}^{LL} + \frac{g^2}{4} (b_0 + b_1(c_{L_i}) + b_1(c_{L_j}) + b_2(c_{L_i}, -c_{L_j})) \delta^{il} \delta^{kj} \\ &\quad - \frac{g^2}{8} (b_0 + b_1(c_{L_i}) + b_1(c_{L_k}) + b_2(c_{L_i}, -c_{L_k})) \delta^{ij} \delta^{kl}. \end{aligned} \quad (4.11)$$

The Wilson coefficients of the seven quark-lepton four-fermion operators are even simpler to compute as there are never two identical fields and all operators but one, $(\bar{L}_i \gamma^\mu \tau^A L_j)(\bar{Q}_k \tau^A \gamma_\mu Q_l)$, are generated via the exchange of an abelian gauge-boson. The result is

$$\begin{aligned} b_{ij}^{\ell q} &= \frac{Y_\ell Y_q}{4} g'^2 \left[b_0 + b_1(s_\ell c_{\ell_i}) + b_1(s_q c_{q_j}) + b_2(s_\ell c_{\ell_i}, -s_q c_{q_j}) \right] \\ &\quad + \frac{Y_\ell Y_q^X}{4} (g^2 - g'^2) b_2(s_\ell c_{\ell_i}, -s_q c_{q_j}) \end{aligned} \quad (4.12)$$

$$b_{ij}^{L\tau Q} = \frac{g^2}{4} (b_0 + b_1(c_{Q_j}) + b_1(c_{L_i}) + b_2(c_{L_i}, -c_{Q_j})) \quad (4.13)$$

with $\ell \in (L, E)$ and $q \in (Q, U, D)$. s_f is -1 for a singlet fermion f and $+1$ for a doublet, Y_f is the hypercharge of fermion f , and $Y_q^X = T_R^3 - 4 \tan^2 \Theta_W / (3(1 - \tan^2 \Theta_W))$ with $T_R^3 = \{-1, -2, 0\}$ for $q = Q, D, U$. The second line in (4.12) is only present in the custodially protected model. The dependence on the 5D mass parameters of the quarks shows that muon conversion depends not only on the model parameters of the lepton sector. However, ultimately we only need operators which are built of light quarks fields after EWSB, and of these only the quark-flavour diagonal part. Since both the up- and the down-quark sector masses are hierarchical, the RS Froggatt-Nielsen mechanism generates hierarchical flavour rotation matrices in the quark sector (see e.g. [23]). Consequently, the $b_2(c_x, c_y)$ terms—the only terms that are simultaneously sensitive to 5D quark parameters and contribute to the flavour-non-diagonal lepton couplings—are suppressed for light quarks, and we neglect them. The only unsuppressed sources of LFV are then the terms $b_1(c_{L_i})$ or $b_1(-c_{E_i})$. For the pure quark four fermion operators needed for the matching to the Lagrangian (3.3) we only need to reuse the results above with adjusted prefactors to incorporate KK gluon exchange. Because we only consider gluon KK exchange in the quark sector in this thesis the Wilson coefficients look the same for both minimal as well as custodial RS model. We find

$$b_{ij}^{QD} = b_0 + b_1(c_{Q_i}) + b_1(-c_{D_j}) + b_2(c_{Q_i}, c_{D_j}), \quad (4.14)$$

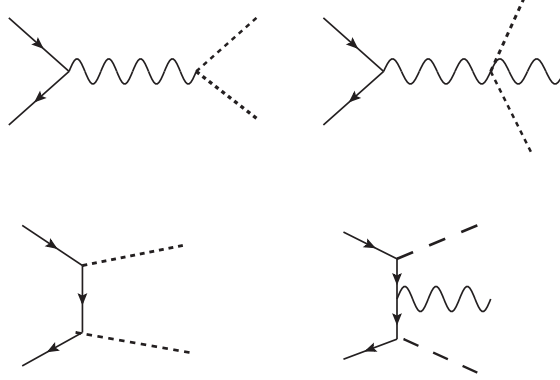


Figure 4.2: Generic topologies that contribute to operators of the type $\Phi^\dagger i \overleftrightarrow{D}_\mu \Phi (\bar{\psi}_i \gamma_\mu \psi_j)$. External fermion states can be either E or L . Intermediate and external gauge-bosons can be abelian or non-abelian, the external Higgses are indicated by dashed lines.

The Wilson coefficients of all other operators are related to b_{ij}^{QD} . They only differ by symmetry factors that take into account the exchange of identical quarks and the potentially different external wave functions $f^{(0)}$ and $g^{(0)}$. In particular, one finds

$$b_{ij}^{QU} = b_{ij}^{QD} \{c_{D_j} \rightarrow c_{U_j}\} \quad b_{ij}^{QQ} = \frac{1}{2} b_{ij}^{QD} \{c_{D_j} \rightarrow -c_{Q_j}\} \quad (4.15)$$

$$b_{ij}^{DD} = \frac{1}{2} b_{ij}^{QD} \{c_{Q_i} \rightarrow -c_{D_i}\} \quad b_{ij}^{UD} = b_{ij}^{QD} \{c_{Q_i} \rightarrow -c_{U_i}\}. \quad (4.16)$$

4.2 Higgs-Fermion operators

The tree-level matching coefficients of the Higgs-fermion operators $\Phi^\dagger i \overleftrightarrow{D}_\mu \Phi (\bar{\psi}_i \gamma_\mu \psi_j)$ follow from the diagrams in Figure 4.2, where the ones with an external gauge field are related to those without by gauge invariance.

The diagrams in the first row of Figure 4.2 have already been computed in [28] in the minimal RS model. In the custodial protected model there are additional contributions to the coefficients c^a ($a = 1, 2$) via an exchange of a Z_X boson. An exchange of W_R^a ($a = 1, 2$) gauge-bosons would change one of the fermion final states to a non SM lepton field. Therefore these gauge-bosons are also irrelevant just like for the four-fermion operators. The additional contribution to c^1 due the Z_X exchange can be calculated via the integral

$$c_{Z_X}^1 = -i(i g_{5X})^2 \frac{Y_E}{2} T^2 \int_{\frac{1}{k}}^{\frac{1}{T}} \frac{dy}{(ky)^4} \left(g_{E_j}^{(0)}(y) \right)^2 \Delta_{pm}(q \rightarrow 0, 1/T, y), \quad (4.17)$$

Together with [28] we then determine the contribution to the c^i from the first line of Figure

4.2 to be $c_{ij}^a = c_i^a \delta_{ij}$, $a = 1, 2, 3$ is given by

$$c_i^1 = \frac{g'^2 Y_E}{8} \left(1 - \frac{1}{\ln 1/\epsilon} - \left[\frac{(1+2c_{E_i})(5+2c_{E_i})}{(3+2c_{E_i})^2} - \frac{2(1+2c_{E_i}) \ln 1/\epsilon}{(3+2c_{E_i})} \right] \frac{\epsilon^{-2c_{E_i}-1}}{1-\epsilon^{-2c_{E_i}-1}} \right) + \frac{(g^2 - g'^2) Y_E}{4} \left[\frac{(1+2c_{E_i}) \ln 1/\epsilon}{(3+2c_{E_i})} \right] \frac{\epsilon^{-2c_{E_i}-1}}{1-\epsilon^{-2c_{E_i}-1}}, \quad (4.18)$$

$$c_i^2 = \frac{g'^2 Y_L}{8} \left(1 - \frac{1}{\ln 1/\epsilon} - \left[\frac{(1-2c_{L_i})(5-2c_{L_i})}{(3-2c_{L_i})^2} - \frac{2(1-2c_{L_i}) \ln 1/\epsilon}{(3-2c_{L_i})} \right] \frac{\epsilon^{2c_{L_i}-1}}{1-\epsilon^{2c_{L_i}-1}} \right) + \frac{(g^2 - g'^2) Y_L}{4} \left[\frac{(1-2c_{L_i}) \ln 1/\epsilon}{3-2c_{L_i}} \right] \frac{\epsilon^{2c_{L_i}-1}}{1-\epsilon^{2c_{L_i}-1}}, \quad (4.19)$$

$$c_i^3 = \frac{g^2}{8} \left(1 - \frac{1}{\ln 1/\epsilon} - \left[\frac{(1-2c_{L_i})(5-2c_{L_i})}{(3-2c_{L_i})^2} - \frac{2(1-2c_{L_i}) \ln 1/\epsilon}{3-2c_{L_i}} \right] \frac{\epsilon^{2c_{L_i}-1}}{1-\epsilon^{2c_{L_i}-1}} \right). \quad (4.20)$$

As in the case of the four-fermion operators the minimal RS model results can be obtained by removing the terms proportional $(g^2 - g'^2)$. The Wilson coefficients are independent of the Higgs localisation provided the limit $\beta \rightarrow \infty$ is taken in the bulk Higgs case.

The diagrams in the second row of Figure 4.2 also exist, but it turns out that they are numerically small compared to the previous contribution. Hence, we only give the explicit expression for the minimal RS model:

$$\delta c_{ij}^1 = -\frac{T^8}{k^8} g_{E_i}(1/T) g_{E_j}(1/T) F(c_{L_k}) Y_{ik}^\dagger Y_{kj} \quad (4.21)$$

$$\delta c_{ij}^2 = \delta c_{ij}^3 = \frac{1}{2} \frac{T^8}{k^8} f_{L_i}(1/T) f_{L_j}(1/T) F(-c_{E_k}) Y_{ik} Y_{kj}^\dagger \quad (4.22)$$

with

$$F(c) = -\frac{k^4}{T^5} \frac{(1+2c) + (3-2c)\epsilon^{2-4c} - (1+2c)(3-2c)\epsilon^{1-2c}}{(1+2c)(3-2c)(1-\epsilon^{1-2c})^2}. \quad (4.23)$$

A similar expression is found in the custodially protected model. The smallness of this contribution arises from the zero-mode profiles of the light external leptons. We ignore the Yukawa contributions δc_{ij}^a in the subsequent analysis. These contributions might be important for heavy quarks. However due to our restriction to the Kaluza-Klein gluons in the quark sector, we dropped the associated Higgs operators directly at the beginning of the formulation of the EFT.

4.3 Yukawa-type operators

The dominant contribution to the Wilson coefficient of the dimension-six Yukawa-like operators $(\Phi^\dagger \Phi) \bar{L}_i \Phi E_j$ is generated by diagrams of the type shown in Figure 4.3. In the minimal RS model there is only one diagram as the two intermediate fermions must be a doublet and a singlet lepton. In the custodially protected model both triplet fermions, T_3 and T_4 , can substitute the singlet.

The diagram in Figure 4.3 contains three Yukawas. Because such structures also appear for Higgs exchange dipole transitions we consider this diagram in greater detail for the minimal RS model. The contribution of the RSc, can be covered identical. The diagram expression is

CHAPTER 4. TREE-LEVEL DIMENSION-SIX OPERATORS

not well defined for an exactly brane localised Higgs. Therefore we adapt the box regularisation of the Higgs width (2.64). Then the diagram can 4.3 can be written as

$$\begin{aligned} & \left(-i \frac{T^3}{k^4}\right)^3 Y_{ia} Y_{ab}^\dagger Y_{bj} \int_{\frac{1-\delta}{T}}^{\frac{1}{T}} dx \int_{\frac{1-\delta}{T}}^{\frac{1}{T}} dy \int_{\frac{1-\delta}{T}}^{\frac{1}{T}} dz \left(\frac{T}{\delta}\right)^3 f_{L_i}^{(0)}(x) g_{E_j}^{(0)}(z) (\bar{L}^i(p) \Phi) P_R \\ & \times \Delta_{E_a}(q', x, y) \Phi^\dagger \Phi \Delta_{L_b}(q, y, z) P_R E^j(p'). \end{aligned} \quad (4.24)$$

Next we decompose the 5D propagators into their chiral components using (A.9) for both fermion propagators. Then the leading contribution to the $(\Phi^\dagger \Phi) \bar{L}_i \Phi E_j$ operator is generated by the term

$$\begin{aligned} & \left(-i \frac{T^3}{k^4}\right)^3 Y_{ia} Y_{ab}^\dagger Y_{bj} \int_{\frac{1-\delta}{T}}^{\frac{1}{T}} dx \int_{\frac{1-\delta}{T}}^{\frac{1}{T}} dy \int_{\frac{1-\delta}{T}}^{\frac{1}{T}} dz \left(\frac{T}{\delta}\right)^3 f_{L_i}^{(0)}(x) g_{E_j}^{(0)}(z) (\bar{L}^i(p) \Phi) \\ & \times (\Phi^\dagger \Phi) d^+ F_{E_a}^-(0, x, y) d^+ F_{L_b}^-(0, y, z) P_R E^j(p'). \end{aligned} \quad (4.25)$$

We perform here an expansion around zero external momenta. That is because we do not want to keep terms with momentum scale below the KK scala. In the brane localisation limit we let $\delta \rightarrow 0$. Therefore we can expand for small δ , the $d^- F^+$ functions around the IR-brane. To be more precise we expand $d^- F_E^+(0, x, y)$ $d^- F_L^+(p, y, z)$ around $x \approx \frac{1}{T}$, $y \approx \frac{1}{T}$ and $z \approx \frac{1}{T}$. The expansion around the the IR-Brane yields

$$d^- F_E^+(0, x, y) = d^- F_{pm}^+(0, x, y) = \frac{ik^4}{T^4} \theta(x - y) + \mathcal{O}(\delta) \quad (4.26)$$

$$d^- F_D^+(0, y, z) = d^- F_{mp}^+(0, y, z) = -\frac{ik^4}{T^4} \theta(y - z) + \mathcal{O}(\delta). \quad (4.27)$$

Then setting the fermion zero mode functions for the limit $\delta \rightarrow 0$ we can directly perform the vertex integrals

$$\int_{\frac{1-\delta}{T}}^{\frac{1}{T}} dx \int_{\frac{1-\delta}{T}}^{\frac{1}{T}} dz \int_{\frac{1-\delta}{T}}^{\frac{1}{T}} dw \left(\frac{T}{\delta}\right)^3 \theta(z - x) \theta(w - x) = \frac{1}{3}. \quad (4.28)$$

Collecting the results we find then for the leading contribution to the Wilson coefficient h_{ij}

$$h_{ij} = \frac{N_{cs}}{3} \times \frac{T^3}{k^4} f_{L_i}^{(0)}(1/T) [Y Y^\dagger Y]_{ij} g_{E_j}^{(0)}(1/T) \quad (4.29)$$

where N_{cs} equals one in the minimal and two in the custodially protected model. Note that this contribution is valid for bulk Higgs in the limit $\beta \rightarrow \infty$ as well for an exactly brane localised Higgs.

For completeness we remark that the diagrams in the second line of figure 4.2 also contribute to the Wilson coefficient of $(\Phi^\dagger \Phi) \bar{L}_i \Phi E_j$ through derivative terms that can be eliminated by the fermion equation of motion, such as $\not{D} L_i = y_{ij} \Phi E_j$. In the minimal model we find

$$\begin{aligned} \delta h_{ij} = & -\frac{1}{2} \frac{T^8}{k^8} g_{E_l}(1/T) g_{E_j}(1/T) F(c_{L_k}) y_{il} Y_{lk}^\dagger Y_{kj} \\ & -\frac{1}{2} \frac{T^8}{k^8} f_{L_i}(1/T) f_{L_i}(1/T) F(-c_{E_k}) Y_{ik} Y_{kl}^\dagger y_{lj}. \end{aligned} \quad (4.30)$$

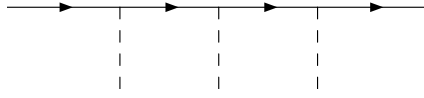


Figure 4.3: Diagram topology that gives the dominant contribution to the operator $(\Phi^\dagger \Phi) \bar{L}_i \Phi E_j$.

Due to the appearance of the small SM lepton Yukawa matrix y this contribution is tiny. This also holds true in the custodially protected model, and hence in the numerical analysis we neglect this term. However, in studies of flavour violation involving third generation quarks (notably top quarks) the contribution can be sizeable and must be included. However we did not include the associated quark operator for our analysis in the quark sector, because of our focus on the exchange of KK gluons in this thesis.

Chapter 5

Loop-induced dipole operators

The dipole operators are generated by genuine 5D one-loop diagrams. We distinguish between two classes of diagrams—those with an internal gauge-boson exchange proportional to one Yukawa coupling Y and those with Higgs exchange, which involve three Yukawa couplings. Diagrams such as shown in Figure 5.1 below count as gauge-boson exchange, since it involves only a single Y . Because we only need the electromagnetic dipole operator for the lepton low energy transitions in this thesis, we reduce the number diagrams needed for the one-loop coefficient a_{ij} by imposing that the external gauge-boson is a photon. In addition, we set the Higgs doublet in the operators $\bar{L}_i \Phi \sigma^{\mu\nu} E_j B_{\mu\nu}$, $\bar{L}_i \tau^A \Phi \sigma^{\mu\nu} E_j W_{\mu\nu}^A$ to its vacuum expectation value. The complete set of non-vanishing diagrams can be found in [28] for the minimal RS model. However part of this thesis was to repeat the dipole calculation for the minimal RS model in order to test the numerical codes used for the more demanding custodial RS model.

5.1 Internal gauge-boson exchange

We start the discussion with the gauge-boson contribution. In Figure 5.1 we have drawn all possible diagram topologies contributing to the dipole operators at one-loop level in the minimal and the custodial RS model. Note that each diagram topology contains at least one Yukawa interaction in order to ensure the correct chirality of both external fermion fields. In the lepton sector the possible particle content is displayed in the tables below. The explicit expressions for all new non-abelian RSc diagrams, can be found in appendix C.1. All other diagrams are either minimal RS diagrams, see [28] for explicit expressions, or abelian diagrams with an Z_X exchange. In this case they only differ by the different internal gauge-boson propagator and the coupling constant g_X from the minimal RS case

The one-loop dipole diagrams needed for $\bar{B} \rightarrow X_s \gamma$ can be derived directly from the leptonic case. Because we consider only gluon exchange all topologies, which include a Higgs-gluon coupling vanish. Because gluon exchange cannot change any $SU(2)$ quantum number all fields of the remaining diagrams are minimal RS model fields. Hence to adapt the leptonic diagrams to the associated QCD diagrams we only have to adapt the appropriate colour factors and for the topology $W2$ the internal fermion propagators. Since we focus on gluon exchanges, the electromagnetic dipole operator gets only contributions from the abelian topologies $A1, A2, A3, A4$, while the gluonic dipole operator additionally contains diagrams generated with the topologies $W1, W2$. Note that the inclusion of B, Z_X, W_L, W_R exchange can be done also easily using the leptonic results.

CHAPTER 5. LOOP-INDUCED DIPOLE OPERATORS

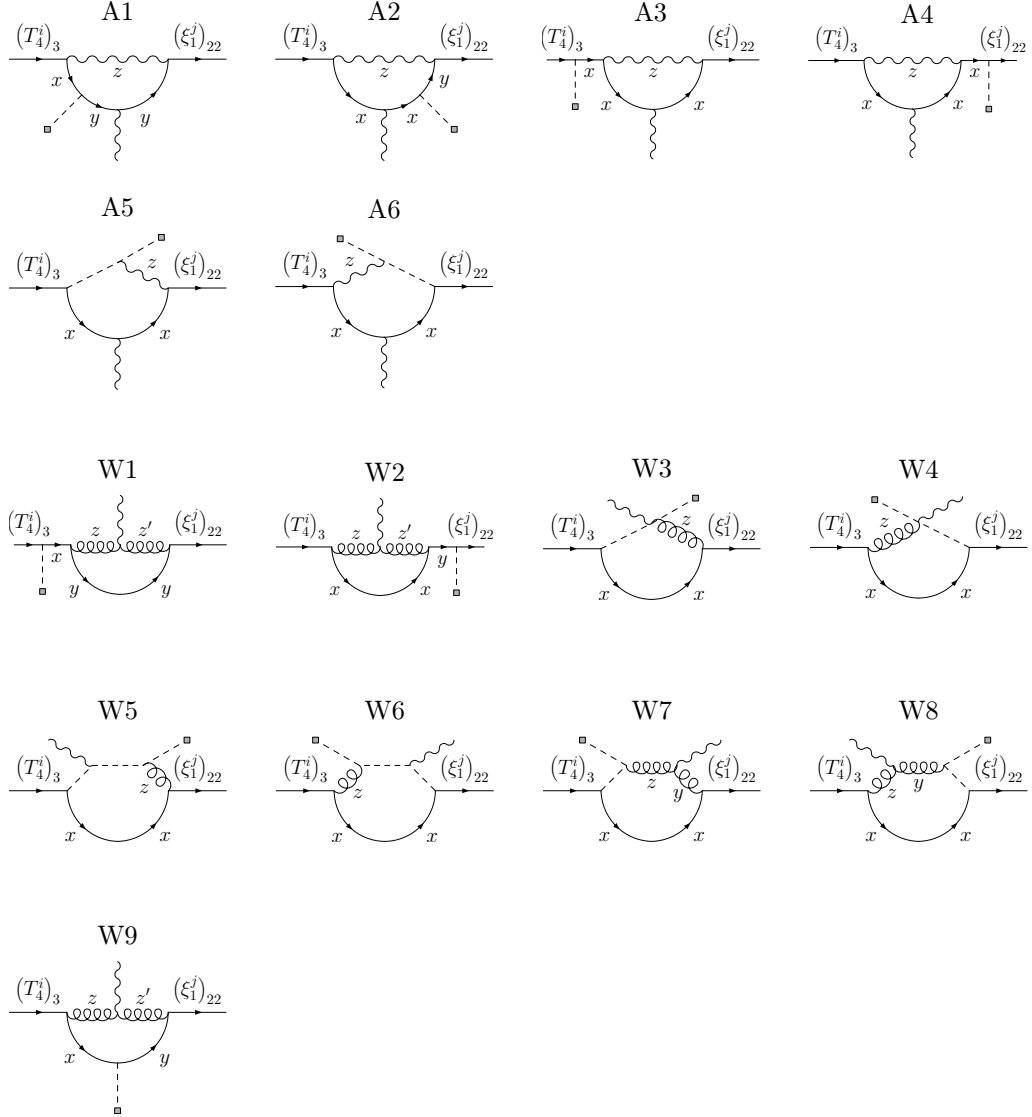


Figure 5.1: All topologies with internal gauge-bosons that contribute to the matching of the dipole operator Wilson coefficient at one-loop. Abelian topologies are labelled by A1-6, non-abelian topologies by W1-10. Fermions represented by straight lines and Higgs bosons by dashed lines. The final and initial fermions are always assumed to be $(T_4)_3$ and $(\xi_1)_{22}$ —the fields corresponding to the SM singlet and doublet. x, y, z, z' label the species of the internal propagators, see tables 5.1 and 5.2 for the the allowed particles.

5.1. INTERNAL GAUGE-BOSON EXCHANGE

	x	y	z		x	y	z
A1	$(T_4^i)_3$	$(\xi_1^j)_{22}$	B^N	A2	$(T_4^i)_3$	$(\xi_1^j)_{22}$	B^N
	$(T_4^i)_3$	$(\xi_1^j)_{22}$	Z_X^N		$(T_4^i)_3$	$(\xi_1^j)_{22}$	Z_X^N
A3	$(\xi_1^j)_{22}$	/	B^N	A4	$(T_4^i)_3$	/	B^N
	$(\xi_1^j)_{22}$	/	Z_X^N		$(T_4^i)_3$	/	Z_X^N
	$(\xi_1^j)_{22}$	/	W_L^{3N}				
A5	$(\xi_1^j)_{22}$	/	B^μ	A6	$(T_4^i)_3$	/	B^μ
	$(\xi_1^j)_{22}$	/	Z_X^μ		$(T_4^i)_3$	/	Z_X^μ
	$(\xi_1^j)_{22}$	/	$W_L^{3\mu}$				

Table 5.1: Possible field configuration inside the loop of the abelian diagram topologies A1-A6 in the lepton sector. A capital roman index on a gauge field indicates that both the vector and the scalar fifth component are valid options, a small Greek index shows that only the vector components may propagate.

	x	y	z	z'		x	y	z	z'
W1	$(\xi_1^j)_{22}$	$(\xi_1^j)_{12}$	W_L^{-N}	$W_L^{+N'}$	W2	$(T_4^i)_2$	$(T_4^i)_3$	W_R^{-N}	$W_R^{+N'}$
	$(\xi_1^j)_{22}$	$(\xi_1^j)_{21}$	W_R^{-N}	$W_R^{+N'}$					
W3	$(\xi_1^j)_{12}$	/	$W_L^{+\mu}$	/	W4	$(T_4^i)_2$	/	$W_R^{+\mu}$	/
W5	$(\xi_1^j)_{12}$	/	$W_L^{+\mu}$	/	W6	$(T_4^i)_2$	/	$W_R^{+\mu}$	/
W7	$(\xi_1^j)_{12}$	W_L^{+N}	$W_L^{-\mu}$	/	W8	$(T_4^i)_2$	$W_R^{+\mu}$	W_R^{-N}	/
W9	$(T_4^i)_2$	$(\xi_1^j)_{21}$	W_R^{-N}	$W_R^{+N'}$					

Table 5.2: Possible field configuration inside the loop of the non-abelian diagram topologies W1-W8 in the lepton sector. A capital roman index on a gauge field indicates that both the vector and the scalar component are valid options, a small Greek index shows that only the vector components may propagate.

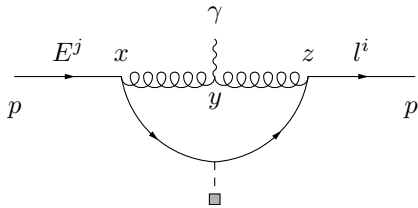


Figure 5.2: Example diagram W1c. The label on each vertex denote the fifth coordinates, which have to be integrated.

Compared to the tree-level Wilson coefficient matching the dipole coefficients contain possible SM contributions, which have to be removed as we are only interested in the effects generated by heavy degrees of freedom of the 5D theory and we want to avoid double counting. The double counting issue also appears in the low 4D momentum region, where the propagators of KK modes can be shrunk to an effective vertices resulting a one-loop insertion of an dimension six operator [28]. However, such contributions have already been added in the effective theory, thus we have to select for the momentum integration only the region around $l \sim T$ in order to avoid further double counting. We therefore follow closely the strategy already formulated in [28]:

- Subtract all possible zero-mode gauge boson propagators of the diagram. If a 5D one-loop diagram with gauge-boson exchange inside the loop contains a zero-mode gauge-boson propagator, than the gauge-fermion vertices contain two fermion mode functions and one zero-mode gauge-boson wave function in the Kaluza-Klein picture. Remember that the zero-mode function of the gauge-boson is constant. Thus there are only two fermion mode functions remaining, which contain a non-trivial coordinate dependence. Thus all vertex coordinate integrals can be done directly via the completeness relations of the fermions. Due to the initial and final states being SM zero mode states this automatically fixes all fermion fields inside the loop to be also zero-mode fields. Thus we can subtract any SM contribution to a given one-loop process by only working with zero-mode subtracted gauge-boson propagators.
- Expand all propagators in the external fermion momenta p, p' . By doing so we only keep the momentum regions that are of the order $l \sim T$. This is important because some gauge-boson diagrams contain contributions from tree-level operators [28] for low four dimensional momentum. These contributions however have already been taken into account by the one-loop diagrams with insertions of an operator that is generated at tree-level.

5.1.1 Example Diagram

For illustration of the standard approach of the calculation let us compute a sample diagram. For this purpose we selected the non-abelian RSc diagram W1c, which is generated via the topology W9. For simplicity we work with an exactly brane-localised Higgs. In section 5.1.3 we will consider the case of a bulk Higgs. The diagram leads to the expression

5.1. INTERNAL GAUGE-BOSON EXCHANGE

$$\begin{aligned}
\text{W1c} &= ig_5^2 (-e_5) \left(-i \frac{\sqrt{2} T^3}{k^3} y_{ij}^{5D} \right) \frac{\nu}{\sqrt{2}} \frac{(\tau^a)_{2c}}{2} \frac{(\tau^b)_{c1}}{2} \epsilon^{dek} C^e \epsilon^{ak3} \int_{\frac{1}{k}}^{\frac{1}{T}} \frac{dx}{(kx)^4} \\
&\int_{\frac{1}{k}}^{\frac{1}{T}} \frac{dy}{(ky)} \int_{\frac{1}{k}}^{\frac{1}{T}} \frac{dz}{(kz)^4} \int \frac{d^4 l}{(2\pi)^4} f_{l_i}^{(0)}(z) f_{\gamma}^{(0)} g_{E_j}(x) \epsilon^{*\mu} \Delta_{mp}^{\lambda\kappa}(\hat{p}, x, y) \Delta_{mp}^{\nu\theta}(\hat{p}', y, z) \\
&\times \left[(p' - 2p + l)_\nu \eta_{\mu\lambda} + (p' + p - 2l)_\mu \eta_{\nu\lambda} + (p - 2p' + l)_\lambda \eta_{\mu\nu} \right] \\
&\times \bar{L}^i(p') P_R \gamma_\theta \Delta_c^{\xi_i^1}(l, z, 1/T) \Delta_{bd}^{T^4_j}(l, 1/T, x) \gamma_\kappa P_R E^j(p) \\
&= -\frac{g_5^2 e_5 T^3 y_{ij}^{5D}}{2k^3} \frac{\nu}{\sqrt{2}} \int_{\frac{1}{k}}^{\frac{1}{T}} \frac{dx}{(kx)^4} \int_{\frac{1}{k}}^{\frac{1}{T}} \frac{dy}{(ky)} \int_{\frac{1}{k}}^{\frac{1}{T}} \frac{dz}{(kz)^4} \int \frac{d^4 l}{(2\pi)^4} \\
&f_{l_i}^{(0)}(z) f_{\gamma}^{(0)} g_{E_j}(x) \epsilon^{*\mu} \Delta_{mp}^{\lambda\kappa}(\hat{p}, x, y) \Delta_{mp}^{\nu\theta}(\hat{p}', y, z) \\
&\times \left[(p' - 2p + l)_\nu \eta_{\mu\lambda} + (p' + p - 2l)_\mu \eta_{\nu\lambda} + (p - 2p' + l)_\lambda \eta_{\mu\nu} \right] \\
&\times \bar{L}^i(p') l^2 F_{mp_i}^+(l, z, 1/T) F_{pm_j}^-(l, 1/T, x) [\gamma_\theta \gamma_\kappa] P_R E^j(p) \tag{5.1}
\end{aligned}$$

where $\hat{p}' = p' - l$ and $\hat{p} = p - l$. In the second step of (5.1) we have simplified the SU(2) algebras and decomposed the fermion propagators into their chiral components, see for example (A.6). Note that the fermion propagators explicitly depend on the SU(2)_L × SU(2)_R indices in the custodial RS model. For the next step we explicitly insert the 5D gauge propagator in its components in the R_ξ gauge

$$\Delta_{mp}^{\mu\nu}(p, x, y) = \Delta_{mp}(p, x, y) \eta^{\mu\nu} + \frac{p^\mu p^\nu}{p^2} \left(\Delta_{mp} \left(\frac{p}{\sqrt{\xi}}, x, y \right) - \Delta_{mp}(p, x, y) \right), \tag{5.2}$$

where the expression for Δ_{mp} can be found in (A.48). We expand all gauge propagators around the external momenta $p = p' = 0$

$$\Delta_{mp}(\hat{p}, x, y) = \Delta_{mp}(l, x, y) - 2p \cdot l \partial_{l^2} \Delta_{mp}(l, x, y) + \dots \tag{5.3}$$

$$\Delta_{mp}(\hat{p}', x, y) = \Delta_{mp}(l, x, y) - 2p' \cdot l \partial_{l^2} \Delta_{mp}(l, x, y) + \dots \tag{5.4}$$

CHAPTER 5. LOOP-INDUCED DIPOLE OPERATORS

To match this diagram into the structure of the resulting amplitude for the dipole operator, we only keep terms, that are proportional to p^μ and p' . We find

$$\begin{aligned}
\text{W1c} = & -\frac{g_5^2 e_5 T^3 y_{ij}^{5D}}{2k^3} \frac{\nu}{\sqrt{2}} \int_{\frac{1}{k}}^{\frac{1}{T}} \frac{dx}{(kx)^4} \int_{\frac{1}{k}}^{\frac{1}{T}} \frac{dy}{(ky)} \int_{\frac{1}{k}}^{\frac{1}{T}} \frac{dz}{(kz)^4} \int \frac{d^4l}{(2\pi)^4} \\
& f_{l_i}^{(0)}(z) f_\gamma^{(0)} g_{E_j}(x) \epsilon_\mu^* \left[p^\mu \left(3l^2 \partial_{l^2} \Delta_{mp}(l, x, y) \Delta_{mp}(l, y, z) \right. \right. \\
& + \partial_{l^2} \Delta_{mp}(l, x, y) \left(\Delta_{mp}\left(\frac{l}{\xi}, y, z\right) - \Delta_{mp}(l, y, z) \right) \frac{l^2}{2} \\
& + \left(\Delta_{mp}\left(\frac{l}{\xi}, x, y\right) - \Delta_{mp}(l, x, y) \right) \Delta_{mp}(l, y, z) \frac{1}{2} \left. \right) \\
& + p'^\mu \left(3l^2 \Delta_{mp}(l, x, y) \Delta_{mp}(l, y, z) \right. \\
& + \Delta_{mp}(l, x, y) \left(\partial_{l^2} \Delta_{mp}\left(\frac{l}{\xi}, y, z\right) - \partial_{l^2} \Delta_{mp}(l, y, z) \right) \frac{l^2}{2} \\
& + \left(\Delta_{mp}\left(\frac{l}{\xi}, x, y\right) - \Delta_{mp}(l, x, y) \right) \Delta_{mp}(l, y, z) \frac{1}{2} \\
& \left. \left(+ \left(\Delta_{mp}\left(\frac{l}{\xi}, x, y\right) - \Delta_{mp}(l, x, y) \right) \partial_l^2 \Delta_{mp}(l, y, z) \frac{l^2}{2} \right) \right. \\
& \left. \times \bar{L}^i(p') l^2 F_{mp_i}^+(l, z, 1/T) F_{pm_j}^-(l, 1/T, x) P_R E^j(p) \right.
\end{aligned} \tag{5.5}$$

The RSc diagram W1c also appears for the gluonic dipole operator with an exchange of KK gluon instead of the right-handed W bosons. The corresponding diagram expression can be found by replacing the fermion and gauge-boson propagators.

$$\begin{aligned}
\Delta_{mp} & \rightarrow \Delta^{\text{ZMS}} \\
F_{pm_j}^- & \rightarrow F_{d_j}^-, F_{mp_i}^+ \rightarrow F_{Q_i}^+,
\end{aligned} \tag{5.6}$$

where Δ^{ZMS} is the zero-mode subtracted gauge boson propagator. It only remains to exchange the coupling constants and the correct colour factors. In this case, the whole expression has to be multiplied with $-3 \frac{g_s^3}{e g_5^3}$, where the factor three is generated by the colour algebra $f^{abc} T^a T^b = i \frac{3}{2} T^c$. Following a similar procedure every gluon exchange diagram can be directly generated out of the expressions of diagrams contributing to the leptonic dipole operator.

Expression (5.5) is still not in its final version. To continue we recall, that the photon zero-mode wavefunction is constant. Thus in the Kaluza-Klein picture only the two mode functions coming from the W_R gauge propagators contain a non trivial dependence on the fifth coordinate y . To see this recall that the gauge propagator can be written as an infinite sum off massive 4d gauge propagators dressed with two Kaluza-Klein mode functions in the KK picture. In this picture the dependence on the starting and end points fifth coordinates of the vertices are contained in the gauge wave functions. Then the integration of the y coordinate integral can be performed using the orthonormality relations (2.49). This leads

5.1. INTERNAL GAUGE-BOSON EXCHANGE

for example to

$$\begin{aligned}
\int_{\frac{1}{k}}^{\frac{1}{l}} \frac{dy}{(ky)} \Delta_{mp}(l, x, y) \Delta_{mp}(l, y, z) &= - \int_{\frac{1}{k}}^{\frac{1}{l}} \frac{dy}{(ky)} \sum_{a,b} f_{mp}^{(a)}(x) \frac{1}{(l^2 - m_a^2)^2} f_{mp}^{(a)}(y) f_{mp}^{(b)}(y) \\
&\times \frac{1}{(l^2 - m_b^2)^2} f_{mp}^{(b)}(z) = - \sum_n f_{mp}^{(n)}(x) \frac{1}{(l^2 - m_n^2)^2} f_{mp}^{(n)}(z) \\
&= \partial_{l^2} i \Delta_{mp}(l, x, z). \tag{5.7}
\end{aligned}$$

Although the resulting expression looks more complicated than before, it turns out that for the numerical integration, that the reduction of one coordinate integral increases the speed of convergence as well as the the final numerical precision significantly. Therefore we perform the photon vertex integration using the completeness relations of the mode functions whenever possible. As a non-trivial example let us consider the term $\Delta_{mp}\left(\frac{l}{\xi}, x, y\right) \Delta_{mp}(l, y, z)$ of (5.5) for $\xi \neq 1$. Using the orthonormality conditions we compute

$$\int_{\frac{1}{k}}^{\frac{1}{l}} \frac{dy}{(ky)} \Delta_{mp}\left(\frac{l}{\xi}, x, y\right) \Delta_{mp}(l, y, z) = - \sum_n f_{mp}^{(n)}(x) \frac{1}{\left(\frac{l^2}{\xi} - m_n^2\right) (l^2 - m_n^2)} f_{mp}^{(n)}(z). \tag{5.8}$$

Here the way back to the 5D picture is not straightforward, but it can be done by using a partial fraction decomposition. The final result of this integral is

$$\int_{\frac{1}{k}}^{\frac{1}{l}} \frac{dy}{(ky)} \Delta_{mp}\left(\frac{l}{\xi}, x, y\right) \Delta_{mp}(l, y, z) = i \frac{\xi}{\xi - 1} \frac{1}{l^2} \left(\Delta_{mp}\left(\frac{l}{\xi}, x, z\right) - \Delta_{mp}(l, x, z) \right) \tag{5.9}$$

It is noteworthy that the limit $\xi \rightarrow 1$ of this expression converges to result (5.7). However, this limit cannot be taken continuously in a numerical program. As a consequence any implementation of diagrams with non-abelian photon vertices that are analytic integrable needs to separate the case $\xi = 1$ from general values of ξ .

Similar expressions can be found for all other combinations of propagators at a photon vertex.

Note that the analytic photon vertex integration is not possible for diagrams with a vertex that includes a photon, gauge-boson and Higgs boson field; examples for this case are any diagram of the topologies $W3$ or $W4$. However, these diagrams starts directly with only one coordinate integral as all other vertices are being evaluated at the IR brane due to the presence of the Higgs. Therefore it contains a relative simple integrand structure.

After integrating the photon vertex the terms proportional to p^μ and p'^μ are only equal to each other for the case $\xi = 1$, for the general case both terms differ. As the amplitude of the dipole operator has the form $\sigma^{\mu\nu} q_\nu$ we consider only the symmetric combination $(p^\mu + p'^\mu)/2$. The term proportional to $p'^\mu - p^\mu = q^\nu$, which corresponds to an anapole moment that cannot be measured experimentally [28], is discarded. The integrand proportional to $(p^\mu + p'^\mu)/2$ cannot be evaluated analytically. Here we have to perform a numerical integration, see subsection 5.1.4.

In this thesis we work in the unbroken phase neglecting all 4D masses, that means the on-shell condition $\not{p} X(p) = 0$ for all external spinors $X = L, E$. However diagrams. that include a mass insertion at an external line, have to considered carefully in this context.

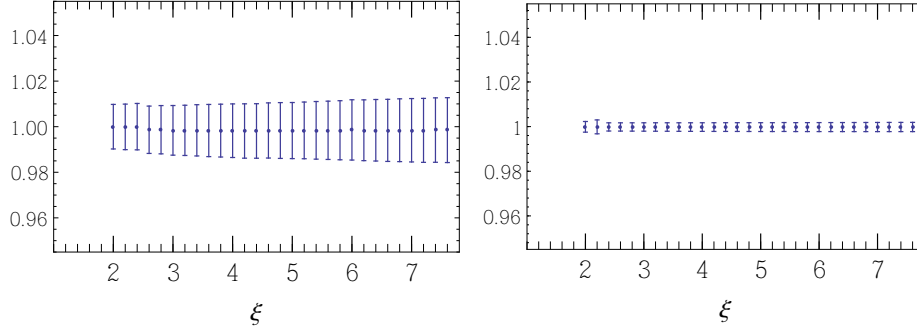


Figure 5.3: *Left panel:* Residual dependence of a_{ij} on the gauge parameter ξ normalised on the value of a_{ij} for $\xi = 2$ in the minimal RS model (the error bars indicate the numerical uncertainties as estimated by our integration routines). *Right panel:* Residual dependence of the RSc contribution to a_{ij} on the gauge parameter ξ normalised on the value of a_{ij} for $\xi = 2$

For such diagrams it is in principle possible for the external propagator to be an off-shell zero-mode propagator. As an example let us consider the external leg of the a diagram of the topology $A3$ for a brane Higgs

$$\dots \Delta^{L_i}(p, x, 1/T) P_R E(p) = \dots - F_{L_i}^+(p, x, 1/T) \not{p} P_R E(p) + \dots d^- F_{L_i}^+(p, x, 1/T) P_R E(p). \quad (5.10)$$

If one inserts into the first term the zero mode propagator

$$F_{L_i}^+(p, x, 1/T) = f_{L_i}^{(0)}(x) \frac{-i}{p^2} f_{L_i}^{(0)}(1/T) + \text{KKmodes}, \quad (5.11)$$

then we are not allowed to use directly $\not{p} P_R E(p) = 0$ to eliminate this term. That is because an expansion of the propagators inside the loop with respect to the external momenta could yield a factor of \not{p} , which could cancel the $\frac{i}{p^2}$ term. That means for an external fermion insertion that we always get additional terms. We denote these terms as off-shell terms, while the term generated by the second term in expression (5.10) are called on-shell terms. The external mass insertions are usually suppressed by a fermion mass and we therefore do not need them consider for the matching of the dipole coefficient as they are numerically small compared to the on-shell terms. However they are indeed import for the consideration of the gauge invariance of the next sections

5.1.2 R_ξ Gauge invariance and scheme independence

The dipole matching computation is done by using the naive dimensional regularisation scheme and a R_ξ gauge for the gauge-exchange contributions. Obviously at this point we have to answer the questions, whether the whole matching computation is scheme independent as well as gauge invariant. Let us first start the scheme independence. There we can use directly the scheme independence results proven in [28], as our set of gauge diagrams is only extended by the new particles introduced via the RSc model. To be more precise we note that the scheme dependence in the minimal RS gauge exchange dipole operator is introduced by the diagram $W8$ ($W7$) [28], where the name in the brackets is the name of the associated

5.1. INTERNAL GAUGE-BOSON EXCHANGE

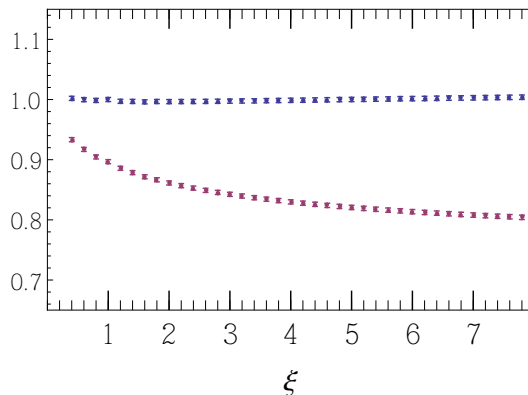


Figure 5.4: Residual dependence of a_{ij} on the gauge parameter ξ normalised on the value of a_{ij} for $\xi = 2$ in the minimal RS model (the error bars indicate the numerical uncertainties as estimated by our integration routines). The red points only contain the on shell contribution, while the blue points also the off shell contributions

topology of Figure 5.1. This diagram contains an $1/\epsilon$ IR-pole [28] inside an ϵ evanescent Dirac algebra in naive dimensional regularisation. In total the pole is of the form $1/\epsilon \times \epsilon$ and yields a finite scheme dependent term to a_{ij} . Note that the diagrams $B1a(A1)$ and $B1b(A1)$ also contain IR poles [28]. However the resulting finite scheme dependent terms vanish in the sum of both diagrams. This statement can be transferred directly to the RSc equivalent of those two diagrams, as these only have a Z_X propagator instead of a B boson propagator with the same fermion propagators. The RSc equivalent to the minimal diagram W8 is the diagram W8c see appendix C.1. Compared to the minimal diagram W8c only includes fermion and gauge-boson fields without zero-mode fields. Therefore this diagram cannot have $1/\epsilon$ poles, which would generate a scheme dependence. In total the new RSc diagrams contributing to the dipole operators do not introduce any new scheme dependence into the Wilson coefficient. Note that the scheme dependence of the Wilson coefficient of dipole operator in the minimal model is being cancelled by the one-loop four-fermion insertions in the NDR scheme, we refer the reader to [28] for the complete calculation.

All gauge-boson diagrams included for the matching inherently depend on the R_ξ gauge parameter, which was introduced to disentangle the mixing between the vector and scalar part of the gauge-boson fields in the bilinear terms of the 5D Lagrangian. Because this parameter is non-physical the complete sum of all diagrams with the same gauge-boson fields should be gauge independent. [28] gives a complete analytic proof of the gauge invariance for the abelian sector as well as for the sum of all minimal non-abelian diagrams. As the proofs for both sectors do not need the explicit form of the 5D propagators they can be both directly applied for the new abelian and non-abelian diagrams in the RSc sector. Especially the proof for the gauge invariance of the abelian sector can be transferred immediately, because the new abelian diagrams of the RSc model only differ by the gauge propagator, which does not play any role in the proof. In our topology notation all abelian gauge dependent terms cancel due to the relation of the hypercharges in the sum off all diagrams [28]

$$Y_L[A1] - Y_E[A3] - Y_\phi[A5] = -1 + 2 - 1 = 0. \quad (5.12)$$

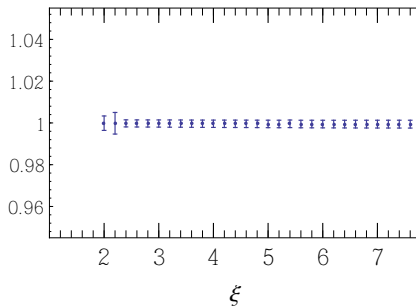


Figure 5.5: Residual dependence of a_{ij}^g on the gauge parameter ξ normalised on the value of a_{ij} for $\xi = 2$ in the minimal RS model (the error bars indicate the numerical uncertainties as estimated by our integration routines).

Thus in the abelian diagrams for the decay $\bar{B} \rightarrow X_s \gamma$ remain also gauge invariant. This conclusion can be seen via the gluon quark "hypercharges", which can be written as $Y_L^G[A1] = Y_E^G[A3] = 2$ and $Y_\phi^G[A5] = 0$ for a Kaluza-Klein gluon gauge boson exchange.

In order to test the correctness of the numerical implementation we show the gauge invariance of all sets of diagrams in the minimal as well as custodial RS model. This involves the numerical calculation of the sum for different bulk mass parameters and for different values of ξ . Note that after the expansion in the external momenta the sum off the integrals is only gauge invariant after taking the sum of the on-shell and off-shell terms. However, in general for a suitable choice of external bulk mass parameters the off-shell terms are smaller, than the numerical precision and can therefore be neglected. Therefore, we mostly used only the bulk mass parameters $c_L = -c_E = 0.5478$, for which the off-shell terms are negligible. In spite of this, to provide a benchmark for the precision of our numerical implementation we computed the abelian minimal and custodial RS diagrams with the non-physical bulk mass parameters $c_L = -0.1$ and $c_R = 1.1$, where the off-shell terms become sizeable.

The residual dependence on the bulk mass parameters is shown in Figure 5.8 for the parameters $c_L = -c_E = 0.5478$. Here the minimal RS contributions are calculated in the first implementation of the numerical code for this thesis, where the photon vertex is not analytically integrated. For the RSc result on the other hand we already integrated the photon vertex for arbitrary values of ξ . The comparison of the estimated errorbars shows the significant improvement due to the photon vertex integration.

In Figure 5.4 we illustrate the residual gauge dependence of the sum off all abelian diagrams for bulk mass parameters $c_L = -0.1$ and $c_R = 1.1$. In this region, the off-shell terms are not small and have to be included in order to achieve a gauge invariant result.

We observe that the complete set of non-abelian RSc diagrams contains actually two subsets of diagrams, whose sum is independent of the gauge parameter ξ . Using the names for all non-abelian diagrams as defined in the appendix C.1, the sum of the diagrams W1c-W3bc, W4c-W6bc times $\frac{1}{2}$ and W11c-W13bc is gauge invariant as well as the sum of W4c-W6bc times $\frac{1}{2}$ and W7c-W10c. Physically the occurrence of two gauge invariant sets is not surprising, because the first set of diagrams resembles the complete set of non-abelian diagrams contributing to the gluonic dipole operator. With the numerical indication that our set of diagrams is gauge invariant dipole matching calculation is done from this point on with

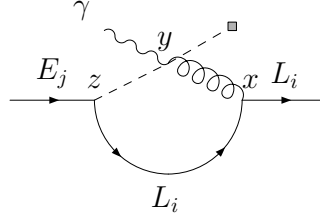


Figure 5.6: Example diagram with internal KK Higgs modes.

Feynmann gauge $\xi=1$. For this choice of gauge parameter all $\left(\Delta_X\left(\frac{l}{\xi}, x, y\right) - \Delta_X(l, x, y)\right)$ terms vanish for any kind of gauge-boson propagator $X = \text{ZMS, mp}$, simplifying the resulting integrands.

5.1.3 KK Higgs contributions

In the calculation of the gauge exchange contribution to the dipole operator we only considered a brane Higgs. However there still remains the question whether there are additional contributions for a bulk Higgs scenario with a β localisation scheme. The presence of a bulk Higgs introduces in principle the new scales T/δ and βT for gauge boson diagrams, which contain at least one Higgs propagator. In [53] it was shown that the effect of this additional momentum scale does not contribute to the gauge-boson exchange diagrams for $\delta \rightarrow 0$ (or, equivalently, $\beta \rightarrow \infty$) when only the Higgs zero-mode is considered. For the bulk Higgs case it still needs to be shown that the contribution of the infinite tower of Higgs KK modes also vanishes for $\beta \rightarrow \infty$. To this end let us examine the minimal RS diagram shown in Figure 5.6. Up to a constant prefactor it is given by

$$\mu^{4-d} \int \frac{d^d l l^2}{(2\pi)^d} \int_{\frac{1}{k}}^{\frac{1}{T}} \frac{dz dx dy}{k^{13} z^5 x^5 y^3} Y_{ij}^\beta f_{L_i}^{(0)}(z) f_{E_j}^{(0)}(x) \Phi^{(0)}(y) \Delta_\Phi^{\text{ZMS}}(l, z, y) F_{L_i}^+(l, x, z) \frac{\partial}{\partial l^2} \Delta_B^{\text{ZMS}}(l, y, x), \quad (5.13)$$

For the explicit expressions for the zero-mode subtracted gauge-boson propagator Δ_B^{ZMS} and the fermion propagator $F_{L_i}^+$ we refer to the appendix of [28]. The Higgs propagator $\Delta_\Phi(l, z, y)$, its zero-mode subtracted version $\Delta_\Phi^{\text{ZMS}}(l, z, y)$, the Higgs zero-mode $\Phi^{(0)}(y)$, and the Yukawa coupling Y^β are discussed in Appendix B.

We now show that the KK Higgs contribution is $\mathcal{O}(1/\beta)$ and therefore can be neglected for large β . The Yukawa matrix Y^β and zero-mode profile $\Phi^{(0)}(y)$ both scale as $\sqrt{\beta}$. Since the zero-mode profile is localised near the IR brane, the associated 5D coordinate integral over y is effectively restricted to the interval $[(1-1/\beta)1/T, 1/T]$ of length $1/(\beta T)$. Hence the y integration introduces a factor of $1/\beta$. The integration over y then compensates the factor β from the product $Y^\beta \Phi^{(0)}(y)$ independent of the magnitude of the 4D loop momentum l . For $l \ll T$ and $l \sim T$, the Higgs propagator scales as $1/\beta$ and, after a change of integration variables from $\{x, y, z\}$ to $\{y, y-z, z-x\}$, one finds that the integrand is dominated by the region where the distance $z-y$ is of the order $1/\beta$ (see also Appendix B.4). Putting all factors together, we conclude that the integrand scales as $1/\beta^2$ for small loop momenta, and hence the integral over these momentum regions also vanishes for $\beta \rightarrow \infty$. For loop-momenta l of order βT , we can expand the fermion and boson propagator for large momenta, in which case the expressions become simple and their dependence on the loop momentum can readily

CHAPTER 5. LOOP-INDUCED DIPOLE OPERATORS

be extracted. For example the chiral component F_L^+ of the fermion doublet propagator has the form

$$F_{L_i}^+(l, x, z) = \frac{1}{2} k^4 w^{5/2} x^{5/2} \sqrt{\frac{1}{lw}} \sqrt{\frac{1}{lx}} \theta(w-x) \left(e^{\frac{2l}{T}} + e^{2lw} \right) e^{l(-\frac{2}{T}-w+x)} \\ + \frac{1}{2} k^4 w^{5/2} x^{5/2} \sqrt{\frac{1}{lw}} \sqrt{\frac{1}{lx}} \theta(x-w) \left(e^{\frac{2l}{T}} + e^{2lx} \right) e^{l(-\frac{2}{T}+w-x)} + \mathcal{O}\left(\frac{1}{l^{\frac{3}{2}}}\right), \quad (5.14)$$

where l is the absolute value of the Euclidean 4D momentum of the propagator. The Higgs propagator is more complicated, but it can only depend on the scale βT and therefore scales as $1/(\beta T)$. We find that the product of all three propagators together with the derivative $\partial/\partial l^2$, which counts as $1/(\beta T)^2$, compensates the factor $l^5 \sim (\beta T)^5$ from $d^4 l l^2 \sim dl l^5$. We are then left with the two integrals over $y-z$ and $z-x$. For $l \sim \beta T$ the integrand is exponentially suppressed for $|z-x| > 1/l$ and $|y-z| > 1/l$, and hence each of the coordinate difference integration regions is effectively restricted to size $1/(\beta T)$. We then find that the total scaling of the integrand in this momentum region is $\propto 1/\beta^2$. The integral over dl can only compensate one inverse power of β and we conclude that the integral over the region $l \sim \beta T$ vanishes as well for $\beta \rightarrow \infty$. For very large loop momentum $l \gg \beta T$ we can expand all propagators. Now all bulk coordinate differences are constrained to be within about $1/l$ (l is now the largest scale) and the 5D Higgs propagator scales as $1/l$. This ensures the convergence of the integral as the integrand vanishes as $1/l^2$ for $l \rightarrow \infty$. The parameter β only enters through the integral over y , which is cancelled by Higgs profile and Yukawa coupling, hence the integrand is independent of β . This universal behaviour allows for a straightforward determination of the contribution of the region $l \gg \beta T$:

$$\int_{\beta T}^{\infty} \frac{dl}{l^2} = \frac{1}{\beta T}. \quad (5.15)$$

Hence the integral over this region vanishes in the large β limit. Since this holds in all regions, we conclude that KK Higgs contribution vanishes as $1/\beta$.

This can be verified numerically as shown in Figure 5.7. The three curves correspond to different values of β (10, 20 and 40, respectively). For better visibility all curves are normalized to the maximum of the $\beta = 10$ curve. The maximum of the integrand is close to $l \sim \beta T$ and exemplifies the $1/\beta^2$ scaling of the integrand in that region. For large modulus of the (euclidean) loop momentum the three curves lie on top of each other consistent with the β independent asymptotic expression. Consequently, the integral over l as well as the contribution to the dipole operator coefficient vanishes for $\beta \rightarrow \infty$.

We can apply a similar analysis to all gauge-boson diagrams with at least one Higgs propagator deriving the scaling to be $1/\beta$. Hence the KK excitations of the Higgs are not relevant for the gauge-boson contribution to the dipole operator.

5.1.4 Numerical evaluation

Even after integration of the photon vertex whenever possible, the remaining expressions are too complicated to be treated analytically. The integrand of the diagram W1c for example consists after the photon integration out of 267 lines of code of complicated rational functions of Bessel functions. Interestingly a recent paper on the matching of the quark dipole operators [50] achieved to solve at least the momentum integration for some diagrams, by rewriting the integrand as a derivative of the momentum, which then can be integrated directly. However, this approach does not eliminate the need of numerical calculations, as

5.1. INTERNAL GAUGE-BOSON EXCHANGE

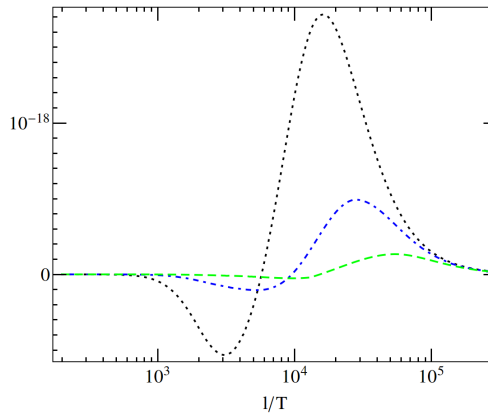


Figure 5.7: Integrand as a function of the loop-momentum l for $\beta = 10$ (black, dotted), $\beta = 20$ (blue, dashed) and $\beta = 40$ (green, solid). For clarity all curves have been rescaled relative to the maximum of the integrand for $\beta = 10$. For loop momenta in excess of βT the integrands show a universal $1/l^2$ behaviour.

the remaining vertex coordinate integrals still remain and even more as the boundary term $l \rightarrow \infty$ cannot be performed analytically.

The numerical implementation of the dipole operator coefficients consists of a two step procedure. In the first step all diagram integrands are written down in terms of all propagators in several Mathematica notebooks. Afterwards the explicit form of all propagators in terms of Bessel functions is being inserted and the resulting Mathematica function converted into a code with a C++ similar syntax using the method CForm. Note that for the numerical implementation we perform a Wick rotation in the four dimensional loop momentum.

In the second step this C++ code of the diagram integrand is then being inserted into a C++ function, which then has the possibility to evaluate the integrand for a sufficient large parameter space. For the evaluation of the Bessel functions of the propagators in C++ we employ the long double version of the BOOST C++ library ¹. To perform the numerical integration CUBA [116] is used. CUBA contains four different methods to perform numerical integrations. As the number of integrand dimension is at maximum only three for our purposes we choose the method Cuhre, which evaluates the integrands using Quadrature rules. The other integration routines CUBA provides use different Monte Carlo integration methods, however after several test we found Cuhre to be superior in terms of speed and accuracy for the integrands appearing in this thesis. To use Cuhre one just needs to provide the integrand in the correct C++ format, see [116], everything else is being done by the package itself. CUBA automatically detects the number of CPU cores available and distributes the needed integral calls to all cores.

The accuracy and duration of the integration can be set for each integration call in CUBA. The accuracy can be controlled to some degree by an internal calculated error estimate. CUBA offers the possibility to stop the integration after it finds a certain relative error estimation. For the purpose of dipole matching we tune CUBA to stop after an relative error of 10^{-3} is being found. However the numerical error estimation has to be taken with a grain of salt. Therefore, we additionally demand a computation of at least a minimum of one million integrand evaluation to ensure good convergence, before the relative error

¹<http://www.boost.org/>

CHAPTER 5. LOOP-INDUCED DIPOLE OPERATORS

integration truncation can be applied. It turned out for some diagrams with less than tree integration dimensions, that the error estimation of CUBA underestimated the numerical error leading to a premature termination of the integration.

The actual integration is performed in two different runs in the C++ program. In the first Cuhre integration run we integrate the momentum integral up to a value of $100T$ and over the whole range of all coordinate integrals. The value for the upper momentum cutoff of $100T$ is chosen as a compromise. At this point the integrand is already behaving asymptotic and the C++ routines are still able to compute the integrand reliably. A cut-off at higher momentum scales would be of course desirable, but at such higher scales one enters the domain where even long double precision is not good enough to handle the whole expression. At $100T$ all 5D propagators can be expanded into their asymptotic forms for large loop momentum, which take the form

$$\Delta(l, x, y) = f(x, y) \frac{1}{l} e^{l(x-y)}, \quad (5.16)$$

where $f(x, y)$ is a rational function of the fifth coordinates x and y . For almost all gauge-boson diagrams the number of propagator are such, that the $\frac{1}{l}$ are cancelled by the loop momentum factors in the numerator of the integrand. Then each vertex integral yields after integration a factor of $\frac{1}{l}$. Most minimal and RSc integrals have two vertex integrals, thus after integration of the fifth coordinates the remaining loop integrand scales as $\frac{1}{l^2}$ in the high loop momentum region. For diagrams with only one vertex integration the integral structure is such, that after bulk integration the integrand also scales as $\frac{1}{l^2}$. Hence in the second Cuhre run we just integrate the bulk integrations at a loop momentum of $100T$. Because the remaining integral scales asymptotic as described above, the value of the momentum integration from $100T$ to ∞ can be estimated to have the numerical value $100T \times R_2$, where R_2 is the result of the second Cuhre run.

For the gauge invariance check, see the Figure 5.4, the integration routine as prescribed above does not yield a sufficient accuracy to observe the cancellation of the gauge dependence of the on-shell term with the cancellation of the residual gauge dependence of the off-shell terms. To improve the accuracy we divided the first Cuhre run into a set of 2180 Cuhre integrations over fixed loop-momentum values. These are used to construct an interpolation grid for the l -integrand. The first 2000 points capture the structure of this integrand in the interval $l \in (0, 10T)$. Then the remaining 180 cover the remaining momentum range to $100T$. The grid together with the asymptotic result are then used to construct an interpolating function of the integrand for all values of l . As a final step, this interpolating function is integrated with Mathematica. Obviously this approach is nothing less than a simple increase of the minimum number of integrand evaluation. However this done in such way, that the different Cuhre runs can be parallelised on different computer machines.

The final result of each diagram depends on the scale T and the $SU(2)_L$ doublet and singlet bulk masses of the external fermion lines. For the numerical implementation we differentiate between diagrams, which have the chirality changing Yukawa coupling at an external fermion line, and diagrams, where the vev insertion via a Yukawa coupling is inside the loop and not connected to an external line. The first kind of diagrams only depends on one bulk mass, because one external wave function is evaluated on the brane and can therefore be factorised. The latter contains two zero mode fermion functions, over which the vertex integrals are performed. Thus these diagrams explicitly depend on a 2D grid of bulk masses. points. We compute the gauge-boson exchange diagrams numerically for $T = 0.5 \text{ TeV}, 1 \text{ TeV}, 2 \text{ TeV}, 4 \text{ TeV}, 8 \text{ TeV}$ for bulk mass ranges of $c_L \in [-1.5, 0.8]$ and $c_R \in [-0.8, 1.5]$ in the quark sector. In the lepton sector, we only need to compute a grid for bulk mass ranges $c_L \in [0.4, 0.8]$ and $c_R \in [-0.8, -0.4]$. The discrete spacing between

5.1. INTERNAL GAUGE-BOSON EXCHANGE

two bulk mass points has the size 0.004 for diagrams, which effectively depend only on one bulk mass parameter. For diagrams, which depend on both bulk mass parameters, we selected a distance of 0.016 between two point of the 2D grid. One C++ implementation of an arbitrary RS gauge exchange dipole diagram only calculates one specific bulk mass and T . Such a computation takes for a typical diagram with two vertex coordinate integrals usually about 7 minutes CPU time on a Pentium I7 950 CPU with the standard two step CUBA implementation. To parallelise the whole computation, the complete grids for all diagrams are distributed via the qsub system on the TU Munich theory group computer cluster, which contains 1425 CPU cores in total.

While we cannot give an analytic result for the gauge-boson exchange dipole Wilson coefficient we can understand the numerical size by factorising all terms that combine to the 4D Yukawa matrix before rotation to the mass basis:

$$a_{ij}^g = Y_{ij} \frac{T^3}{k^4} f_{L_i}^{(0)}(1/T) g_{E_j}^{(0)}(1/T) \mathcal{A}_{ij} = y_{ij} \mathcal{A}_{ij} . \quad (5.17)$$

Hence the function \mathcal{A}_{ij} depends only on the 5D bulk masses of the external fermion fields with flavours i, j and the RS scales k and T . \mathcal{A}_{ij} can be interpreted as a measure of the misalignment between the mass matrix of the lepton sector and the dipole coefficient a_{ij}^g before rotation to the mass basis. If \mathcal{A}_{ij} were proportional to the unit matrix, no LFV would be generated by the gauge-boson exchange diagrams. Figure 5.8 shows the result of the numerical computation of \mathcal{A}_{ij} for the custodially protected model at the KK scale $T = 1$ TeV. There is a small asymmetry in the dependence of \mathcal{A}_{ij} on the bulk mass parameters of the external lepton fields, which arises from 5D diagrams with non-abelian gauge-bosons as the W bosons do not couple equally to singlet and doublet fields. To reproduce the 4D lepton mass matrix the bulk mass parameter c_L of the doublet muon (electron) has to be around 0.57 (0.66) and the masses of the corresponding singlets around -0.57 (-0.66), if the SM mass hierarchy is carried by both singlet and doublets. As illustrated in the figure the variation of \mathcal{A}_{ij} in this region is around $\pm(2-3)\%$. In an extreme case where e.g. all singlets are “delocalised” with bulk mass parameter $c_E = -0.5$, the bulk mass of the doublet muon (electron) has to be around 0.64 (0.8), and the variation is less pronounced. For the minimal RS model the dependence of \mathcal{A}_{ij} on the bulk mass parameters is slightly smaller in the region of mass parameters relevant to muons and electrons than in the custodially protected model [28, 53]. It follows that the gauge-boson exchange contribution α_{ij}^g to the dipole coefficient has smaller off-diagonal elements by a factor 30 to 50 compared to the flavour-conserving diagonal entries the RS model has a built-in protection from large gauge-boson induced LFV transitions. It is interesting to note that the variation of \mathcal{A}_{ij} increases for decreasing absolute value of both bulk masses. Since typically the absolute values of the 5D bulk masses decrease with decreasing magnitude of the 5D Yukawa couplings, a smaller absolute value of the 5D Yukawa couplings leads to more pronounced LFV transitions from internal gauge-boson exchange in the Lepton sector.

Figure 5.8 also shows the the result of the numerical computation of \mathcal{A}_{ij}^G , that is the sum of all gluon exchange diagrams contributing to the gluonic dipole operator in the convention of (5.17). For quarks the potential range of the bulk masses is larger, than for the leptons. That is because the the quark bulk masses have to generate the large bottom and top quark masses. This can lead to bulk masses of the size of $c_3 = 0.1$ for a right-handed up quark field of the third generation. Thus we expect that the contribution of the gauge-boson exchange in the quark sector can be larger for than in the lepton sector.

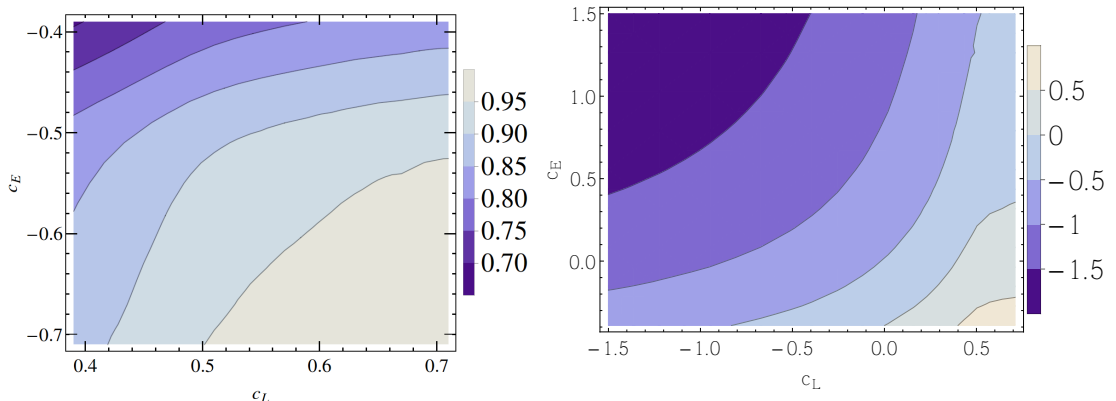


Figure 5.8: *Left panel:* Contour plot of \mathcal{A}_{ij} in the custodially protected RS model in the lepton sector normalized to its value for $c_L = |c_E| = 0.7$ as a function of the 5D mass parameters c_L and c_E for $T = 1 \text{ TeV}$, $k = 2.44 \cdot 10^{18} \text{ GeV}$. *Right panel:* Same as above but for the gluonic dipole operator \mathcal{A}_{ij}^G

5.2 Internal Higgs exchange

In contrast to the gauge-boson diagrams contributions contributing to the Wilson coefficients of the dipole operator the Higgs exchange diagrams depend strongly on the 5D parameters as well as the localisation scheme of the Higgs. In this section, we compute first the zero-mode Higgs contribution to the dipole operator, afterwards we turn on the computation of KK Higgs diagrams. In contrast to the gauge-boson diagrams the zero mode Higgs exchange diagrams can be computed analytically. We will present this computation in detail in the first two subsections. As described in section 2.3.4 we regulate the Higgs width using a narrow box for the IR brane delta function

$$\delta(z - 1/T) = \lim_{\delta \rightarrow 0} \frac{T}{\delta} \Theta \left(z - \frac{1 - \delta}{T} \right). \quad (5.18)$$

The final result of this computation can be found in the third subsection. In the fourth subsection we establish the direct relation between the naive narrow width localisation scheme and bulk Higgs zero mode exchanges in the limit $\beta \rightarrow \infty$. Finally, the last subsection is devoted to the KK Higgs exchange calculation

5.2.1 On-shell zero-mode Higgs exchange

The Higgs exchange diagrams can be divided into six different topologies see Figure 5.9. It is therefore most effective to work on topology level as long as possible. In this section we will calculate the on-shell zero mode Higgs exchange contributions to the dipole operator. For most of the time we use the narrow width Higgs, however the computation of the topology HT6 deserves a careful treatment of the Higgs localisation scheme, as it is the only topology, which contains terms with right-chirality Higgs couplings. The on-shell contribution off all other topologies is generated by wrong-chirality Higgs couplings only. Note that all diagrams with wrong-chirality Higgs couplings vanish in the case of an exactly brane-localised Higgs.

5.2. INTERNAL HIGGS EXCHANGE

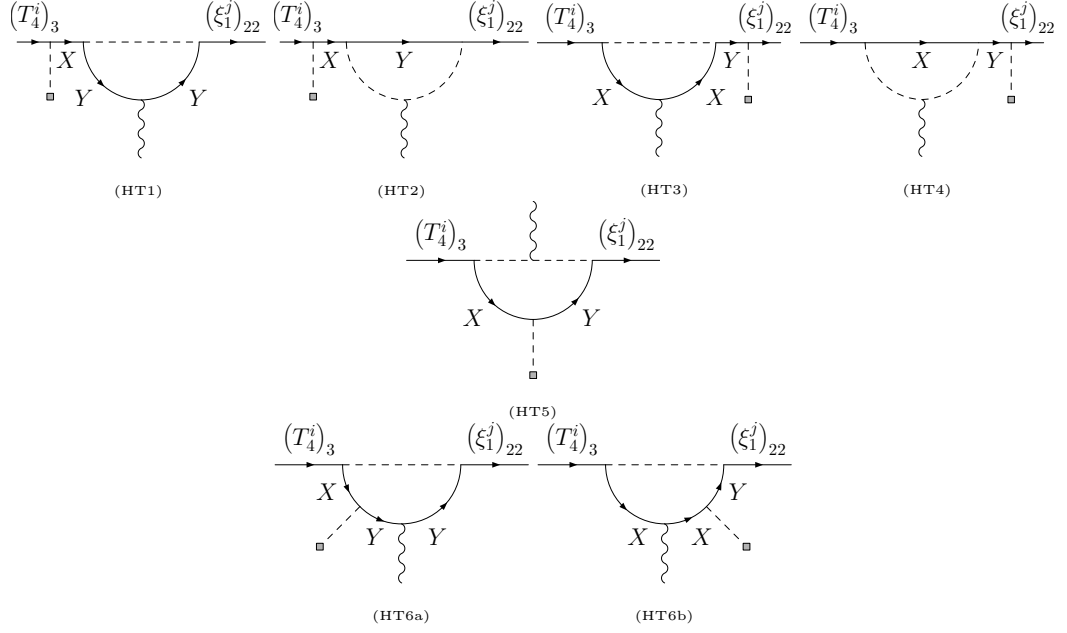
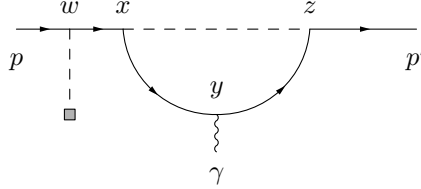


Figure 5.9: All Higgs exchange dipole topologies.

5.2.1.1 Topologies HT1 and HT2

We start the computation with the topology HT1 (C.21).



$$\begin{aligned}
&= -c_{Diag} \int_{\frac{1-\delta}{T}}^{\frac{1}{T}} dx \int_{\frac{1}{k}}^{\frac{1}{T}} \frac{dy}{(ky)^4} \int_{\frac{1-\delta}{T}}^{\frac{1}{T}} dz \int_{\frac{1-\delta}{T}}^{\frac{1}{T}} dw \left(\frac{T}{\delta}\right)^3 \mu^{d-4} \int \frac{d^d l}{(2\pi)^d} \epsilon^{*\mu} \frac{i}{l^2} \\
&\quad \times (Y)_{ia} (Y^\dagger)_{ab} (Y)_{bj} f_{li}^{(0)}(z) f_\gamma^{(0)}(z) g_{E_j}(w) \bar{L}^i(p') [d^- F_{Y_a}^+(\hat{p}', z, y) F_{Y_a}^+(\hat{p}, y, x) \gamma_\mu \not{p} \\
&\quad + F_{Y_a}^-(\hat{p}', z, y) d^- F_{Y_a}^+(\hat{p}, y, x) \not{p}' \gamma_\mu] d^- F_{X_b}^+(p, x, w) P_R E^j(p) \quad (5.19)
\end{aligned}$$

where c_{diag} represents the $SU(2)_L \times SU(2)_R$ factor, which has to be determined for each diagram generated by this class independently. Since this expression is almost the same for HT2 (C.22) we concentrate mainly on the topology HT1.

First we extract the coefficients of p^μ and p'^μ by expanding the F-functions, which depend on the momentum $\hat{p} = p - l$ and $\hat{p}' = p' - l$ around the loop momentum l . Then we perform the Dirac and Lorentz algebra keeping only p^μ and p'^μ terms. As an example the momentum expansion of $F_Y^-(\hat{p}', z, y)$ yields

$$F_{Y_a}^-(\hat{p}', z, y) = F_Y^-(l, z, y) - 2p' \cdot l \partial_{p^2} F_{Y_a}^-(p, z, y)|_{p=l} + \mathcal{O}(p'^2), \quad (5.20)$$

CHAPTER 5. LOOP-INDUCED DIPOLE OPERATORS

HT1	X	Y	HT3	X	Y
H1	ξ_1	T_4	H3	ξ_1	T_4
H5	ξ_1	T_3	H7	ξ_1	T_3
			H9	ξ_1	ξ_2
HT2	X	Y	HT4	X	Y
H2	ξ_1	T_4	H4	ξ_1	T_4
H6	ξ_1	T_3	H8	ξ_1	T_3
HT5	X	Y	HT6	X	Y
H10	ξ_1	T_4	H11	ξ_1	T_4
H12	ξ_1	T_3	H13	ξ_1	T_3
H14	ξ_1	ξ_2			

Table 5.3: All possible combination of leptonic Higgs exchange diagrams contributing to the dipole operators. The names H1-H14 denote the labels of one diagram.

Using this kind of expansion for all F functions in (5.19) one finds the p^μ and p'^μ terms

$$\begin{aligned}
 & -\bar{L}^i(p') \left[d^- F_{Y_a}^+(\hat{p}', z, y) F_{Y_a}^+(\hat{p}, y, x) \gamma_\mu \not{p} + F_{Y_a}^-(\hat{p}', z, y) d^- F_{Y_a}^+(\hat{p}, y, x) \not{p}' \gamma_\mu \right] \\
 & d^- F_{X_b}^+(p, x, w) P_R E^j(p) \doteq - \left[p'^\mu \frac{4}{d} l^2 \partial_{p^2} d^- F_{Y_a}^+(l, z, y) F_Y^+(l, y, x) \right. \\
 & \left. + p^\mu \frac{4}{d} l^2 F_{Y_a}^-(l, z, y) \partial_{p^2} d^- F_{Y_a}^+(l, y, x) \right] d^- F_{X_b}^+(p, x, w) \bar{L}^i(p') P_R E^j(p) \quad (5.21)
 \end{aligned}$$

where \doteq implies that we only keep terms in p^μ and p'^μ . To perform this step we used the rotational invariance of the loop momentum in d dimensions under the loop integral $l^\nu l^\mu = \frac{1}{d} \eta^{\nu\mu}$, together with the anticommutator relation for the Dirac matrices $\{\gamma^\mu, \gamma^\nu\} = 2 \eta^{\mu\nu} 1_{4 \times 4}$. Further we used the massless Dirac equations

$$\not{p} E^j(p) = 0 \quad (5.22)$$

$$\bar{L}^i(p') \not{p}' = 0 \quad (5.23)$$

to remove some terms.

To compute the integrals analytically it is essential to decompose the F functions in (5.21) into Kaluza-Klein mode functions using the mode expansions (A.9-A.12). We start the integration by evaluating the coordinate integral over the photon vertex, which can be done again by using the orthonormality conditions of the mode functions

$$\int_{\frac{1}{k}}^{\frac{1}{T}} \frac{dy}{(ky)^4} f_X^{(n)}(y) f_X^{(m)}(y) = \int_{\frac{1}{k}}^{\frac{1}{T}} \frac{dy}{(ky)^4} g_X^{(n)}(y) g_X^{(m)}(y) = \delta_{nm}. \quad (5.24)$$

Recall that we can use this relation here because the zero-mode function of the photon does not depend on the spacetime coordinate, which means that the only mode functions

5.2. INTERNAL HIGGS EXCHANGE

depending on the y-coordinate are inside the F-functions. Thus we get

$$\begin{aligned}
& - \int_{\frac{1}{k}}^{\frac{1}{T}} \frac{dy}{(ky)^4} \left(p'^\mu \frac{4}{d} l^2 \partial_{p^2} d^- F_{Y_a}^+ (l, z, y) F_{Y_a}^+ (l, y, x) + p^\mu \frac{4}{d} l^2 F_{Y_a}^- (l, z, y) \partial_{p^2} d^- F_{Y_a}^+ (l, y, x) \right) \\
& = \frac{4}{d} l^2 (p'^\mu + p^\mu) \sum_n g_{Y_a}^{(n)}(z) f_{Y_a}^{(n)}(x) \frac{m_n}{(l^2 - m_n^2)^3} l^2. \quad (5.25)
\end{aligned}$$

The next step is to evaluate the integral over the loop momentum. Note that the complete expression of the topology HT1 (5.19) includes a term $\frac{i}{l^2}$ coming from the Higgs propagator, which we have to include to get the correct result. We compute then in the Kaluza-Klein picture

$$\begin{aligned}
& \mu^{d-4} \int \frac{d^d l}{(2\pi)^d} \frac{4}{d} l^2 (p'^\mu + p^\mu) \sum_n g_{Y_a}^{(n)}(z) f_{Y_a}^{(n)}(x) \frac{m_n}{(l^2 - m_n^2)^3} \frac{i}{l^2} \\
& = -i \frac{4}{d} (p'^\mu + p^\mu) \mu^{d-4} \sum_n g_{Y_a}^{(n)}(z) f_{Y_a}^{(n)}(x) \frac{i m_n \Gamma(3 - \frac{d}{2})}{(4\pi)^{\frac{d}{2}} 2} \left(\frac{1}{m_n^2} \right)^{3 - \frac{d}{2}} \\
& \stackrel{d=4-2\epsilon}{=} -i \frac{(p'^\mu + p^\mu)}{32\pi^2} \sum_n g_{Y_a}^{(n)}(z) f_{Y_a}^{(n)}(x) \frac{i m_n}{m_n^2} + \mathcal{O}(\epsilon) \stackrel{\epsilon \rightarrow 0}{=} i \frac{(p'^\mu + p^\mu)}{32\pi^2} d^- F_{Y_a}^+ (0, z, x). \quad (5.26)
\end{aligned}$$

Note that we used [117] for the actual loop integration. The integral remains finite in the limit $d \rightarrow 4$.

After performing the y integral and the loop integral the terms in $(p'^\mu + p^\mu)$ of the topology HT1 take the form

$$\begin{aligned}
& c_{Diag} (Y)_{ia} (Y^\dagger)_{ab} (Y)_{bj} \int_{\frac{1-T}{T}}^{\frac{1}{T}} dx \int_{\frac{1-T}{T}}^{\frac{1}{T}} dz \int_{\frac{1-T}{T}}^{\frac{1}{T}} dw \left(\frac{T}{\delta} \right)^3 \epsilon_\mu^* f_{l_i}^{(0)}(z) f_\gamma^{(0)} g_{E_j}(w) \\
& \times i \frac{(p'^\mu + p^\mu)}{32\pi^2} d^- F_{Y_a}^+ (0, z, x) d^- F_{X_b}^+ (p, x, w) \bar{L}^i(p') P_R E^j(p). \quad (5.27)
\end{aligned}$$

For small δ , i.e. a almost localised Higgs bi-doublet, one can expand the $d^- F^+$ functions around the IR-brane. To be more precise we expand $d^- F_Y^+ (0, z, x)$ $d^- F_X^+ (p, x, w)$ around $x \approx \frac{1}{T}$, $w \approx \frac{1}{T}$, $z \approx \frac{1}{T}$ and $p \ll T$. Thus we employ the approximation

$$d^- F_{X_b}^+ (p, x, w) \approx d^- F_{X_b}^+ (0, x, w). \quad (5.28)$$

The expansion around the the IR-Brane yields

$$d^- F_E^+ (0, x, y) = d^- F_{pm}^+ (0, x, y) = \frac{ik^4}{T^4} \theta(x - y) + \mathcal{O}(\delta) \quad (5.29)$$

$$d^- F_D^+ (0, x, y) = d^- F_{mp}^+ (0, x, y) = -\frac{ik^4}{T^4} \theta(y - x) + \mathcal{O}(\delta). \quad (5.30)$$

We observe here that the leading terms in this expansion only differ in the sign, which depends only on the IR-brane boundary conditions. All diagrams generated by HT1 contain always a $d^- F^+$ coming from the ξ^1 bi-doublet and a $d^- F^+$ coming from the $T_3 \otimes T_4$ triplet. Thus we find

$$d^- F_{Y_a}^+ (0, z, x) d^- F_{X_b}^+ (0, x, w) = \frac{k^8}{T^8} \theta(z - x) \theta(w - x) + \mathcal{O}(\delta). \quad (5.31)$$

CHAPTER 5. LOOP-INDUCED DIPOLE OPERATORS

Note that the leading order term of this expansion loses completely the dependence on the generation indices.

Setting the zero mode functions of $f_{l_i}^{(0)}(z) g_{E_j}(w)$ to the brane we can evaluate the remaining coordinate integrals according to

$$\int_{\frac{1-\delta}{T}}^{\frac{1}{T}} dx \int_{\frac{1-\delta}{T}}^{\frac{1}{T}} dz \int_{\frac{1-\delta}{T}}^{\frac{1}{T}} dw \left(\frac{T}{\delta}\right)^3 \theta(z-x) \theta(w-x) = \frac{1}{3}. \quad (5.32)$$

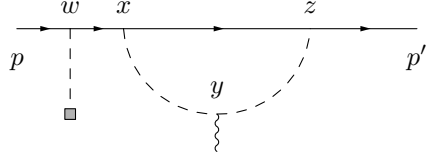
Thus we find the final result of the linear terms in $(p'^\mu + p^\mu)$ of the topology HT1

$$c_{Diag}^i \frac{(p'^\mu + p^\mu)}{96\pi^2} \epsilon_\mu^* f_{l_i}^{(0)} \left(\frac{1}{T}\right) f_\gamma^{(0)} g_{E_j} \left(\frac{1}{T}\right) \frac{k^8}{T^8} \bar{L}^i(p') P_R E^j(p) [YY^\dagger Y]_{ij}. \quad (5.33)$$

Note that this expression remains finite in the limit $\delta \rightarrow 0$, which means on the other side that the neglected $\mathcal{O}(\delta)$ of the expansion (5.31) vanish for an IR-localised Higgs bi-doublet. One can apply the same steps on the diagram topology HT2 to extract the analytic form of the $(p'^\mu + p^\mu)$ coefficient. This yields the same result as for the topology HT2 up to the different c_{diag} .

5.2.1.2 Topologies HT3 to HT5

Like in the case of HT1 and HT2 the topologies HT3 and HT4 have similar expressions. Hence we concentrate only on the expression for HT3 here.



$$\begin{aligned} &= c_{Diag} \int_{\frac{1-\delta}{T}}^{\frac{1}{T}} dx \int_{\frac{1-\delta}{T}}^{\frac{1}{T}} dy \int_{\frac{1-\delta}{T}}^{\frac{1}{T}} dz \int_{\frac{1-\delta}{T}}^{\frac{1}{T}} dw \left(\frac{T}{\delta}\right)^4 \mu^{d-4} \int \frac{d^d l}{(2\pi)^d} \epsilon^{*\mu} (p + p' - 2l)_\mu \\ &\quad \times (Y')_{ia} (Y'^\dagger)_{ab} (Y)_{bj} f_{l_i}^{(0)}(z) f_\gamma^{(0)} g_{E_j}(x) \frac{i}{(p' - l)^2} \frac{i}{(p - l)^2} \\ &\quad \times \bar{L}^i(p') d^- F_{Y_a}^+(l, z, x) d^- F_{X_b}^+(p, x, w) P_R E^j(p) \end{aligned} \quad (5.34)$$

The calculation of the topologies HT3 (5.34) and HT4 (C.24) follows the same strategy as for the topology HT1. First we expand both Higgs propagators around the loop momentum l in expression (5.34). This leads to

$$\begin{aligned} (p + p' - 2l)^\mu \frac{i}{\hat{p}^2} \frac{i}{\hat{p}'^2} &\doteq -\frac{d-4}{d} \frac{1}{l^4} (p'^\mu + p^\mu) \\ &\stackrel{d=4-2\epsilon}{=} \frac{1}{2} \epsilon \frac{1}{l^4} (p'^\mu + p^\mu) + \mathcal{O}(\epsilon^2) \end{aligned} \quad (5.35)$$

where we used the rotational invariance of the loop momentum in d dimensions to derive this result. Note that this expression depends linear in ϵ , which means that we need to get

5.2. INTERNAL HIGGS EXCHANGE

a $1/\epsilon$ IR-pole coming from the loop integral to obtain a non zero result. Obviously the same calculation done in $d=4$ dimensions would not yield the correct terms.

Since no F functions depend on the y coordinate in HT3 (5.34) and HT4 (C.24) the y integration is trivial and yields $\frac{\delta}{T}$. For the loop integral one has to calculate

$$\mu^{d-4} \int \frac{d^d l}{(2\pi)^d} \frac{1}{l^4} d^- F_{Y_a^+}^+(l, z, x) = \sum_{n=0} g_{Y_a^+}^{(n)}(z) f_{Y_a^+}^{(n)}(x) \underbrace{\mu^{d-4} \int \frac{d^d l}{(2\pi)^d} \frac{1}{l^4} \frac{i m_n}{l^2 - m_n^2}}_{\equiv A} \quad (5.36)$$

where we used the Kaluza-Klein decomposition (A.11). Introducing a Feynman parameter the integral becomes

$$\begin{aligned} A &= \int_0^1 dx 2x \mu^{d-4} \int \frac{d^d l}{(2\pi)^d} \frac{i m_n}{(l^2 - (1-x)m_n^2)^3} \\ &= \mu^{d-4} i \int_0^1 dx 2x \frac{(-i) m_n}{(4\pi)^{\frac{d}{2}}} \frac{\Gamma(3 - \frac{d}{2})}{\Gamma(3)} \left(\frac{1}{(1-x)m_n^2} \right)^{3 - \frac{d}{2}} \\ &= \mu^{d-4} i \frac{(-i)}{(4\pi)^{\frac{d}{2}}} \frac{\Gamma(3 - \frac{d}{2})}{m_n^2} \frac{4m_n}{(4-d)(2-d)} \\ &\stackrel{d=4-2\epsilon}{=} -i \frac{(-i)}{16\pi^2} \frac{m_n}{m_n^2 \epsilon} + \mathcal{O}(1). \end{aligned} \quad (5.37)$$

Observe that the Feynman parameter integral only exist, if d is larger than 4, i.e. $\epsilon < 0$. That means that we are extracting here the IR-pole of the loop integral as we wanted in the beginning of the calculation. Inserting this result into the original integral yields

$$\int \frac{d^d l}{(2\pi)^d} \frac{1}{l^4} d^- F_{Y_a^+}^+(l, z, x) = \frac{-i}{\epsilon} \frac{1}{16\pi^2} d^- F_{Y_a^+}^+(0, z, x) + \mathcal{O}(1). \quad (5.38)$$

Thus we find for the terms linear in $(p'^\mu + p^\mu)$ of HT3

$$\begin{aligned} &-c_{Diag} (Y')_{ia} (Y'^\dagger)_{ab} (Y)_{bj} \int_{\frac{1-\delta}{T}}^{\frac{1}{T}} dx \int_{\frac{1-\delta}{T}}^{\frac{1}{T}} dz \int_{\frac{1-\delta}{T}}^{\frac{1}{T}} dw \left(\frac{T}{\delta} \right)^3 \epsilon_\mu^* f_{l_i}^{(0)}(z) f_\gamma^{(0)} g_{E_j}(w) \\ &\times i \frac{(p'^\mu + p^\mu)}{32\pi^2} d^- F_{Y_a^+}^+(0, z, x) d^- F_{X_b^+}^+(p, x, w) \bar{L}^i(p') P_R E^j(p) + \mathcal{O}(\epsilon) \end{aligned}$$

where the ϵ independent terms have the same form as the topologies HT1 and HT2. Hence the further integration can be done the same way as for HT1. We derive the final answer for the topology HT1 in the limit $\epsilon \rightarrow 0$

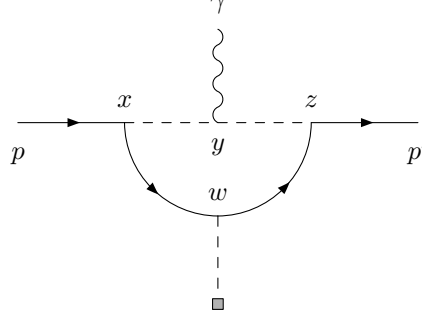
$$-c_{Diag} i \frac{(p'^\mu + p^\mu)}{96\pi^2} \epsilon_\mu^* f_{l_i}^{(0)} \left(\frac{1}{T} \right) f_\gamma^{(0)} g_{E_j} \left(\frac{1}{T} \right) \frac{k^8}{T^8} \bar{L}^i(p') P_R E^j(p) [Y' Y'^\dagger Y]_{ij}. \quad (5.39)$$

As for HT2 and HT1 we can apply the steps for the calculation of the terms linear in $(p'^\mu + p^\mu)$ of HT3 onto the same terms of HT4. Therefore we derive for HT4 the result.

$$-c_{Diag} i \frac{(p'^\mu + p^\mu)}{96\pi^2} \epsilon_\mu^* f_{l_i}^{(0)} \left(\frac{1}{T} \right) f_\gamma^{(0)} g_{E_j} \left(\frac{1}{T} \right) \frac{k^8}{T^8} \bar{L}^i(p') P_R E^j(p) [Y Y^\dagger Y]_{ij}. \quad (5.40)$$

CHAPTER 5. LOOP-INDUCED DIPOLE OPERATORS

The topology HT5 can be written as



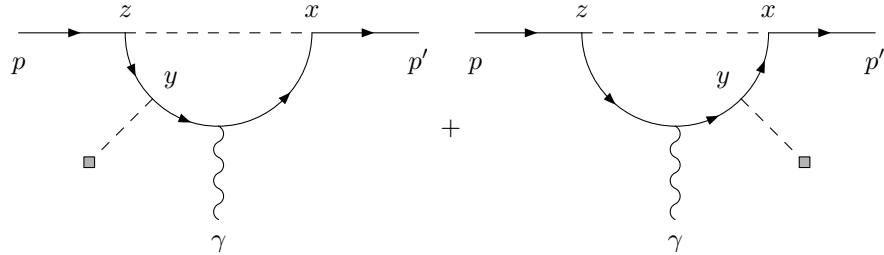
$$\begin{aligned}
 &= c_{Diag} \int_{\frac{1-\delta}{T}}^{\frac{1}{T}} dx \int_{\frac{1-\delta}{T}}^{\frac{1}{T}} dy \int_{\frac{1-\delta}{T}}^{\frac{1}{T}} dz \int_{\frac{1-\delta}{T}}^{\frac{1}{T}} dw \left(\frac{T}{\delta}\right)^4 \mu^{d-4} \int \frac{d^d l}{(2\pi)^d} \epsilon^{*\mu} (p + p' - 2l)_\mu \\
 &\quad \times (Y')_{ia} (Y'^\dagger)_{ab} (Y)_{bj} f_{l_i}^{(0)}(z) f_\gamma^{(0)} g_{E_j}(x) \frac{i}{(p' - l)^2} \frac{i}{(p - l)^2} \\
 &\quad \times \bar{L}^i(p') d^- F_{Y_a}^+(l, z, x) d^- F_{X_b}^+(l, x, w) P_R E^j(p). \quad (5.41)
 \end{aligned}$$

We note that the integrand structure is almost the same as for the topology HT3. Hence this diagram topology can be computed in the same way as described above. Therefore, we find for this diagram topology the result

$$-c_{Diag} i \frac{(p'^\mu + p^\mu)}{96\pi^2} \epsilon_\mu^* f_{l_i}^{(0)} \left(\frac{1}{T}\right) f_\gamma^{(0)} g_{E_j} \left(\frac{1}{T}\right) \frac{k^8}{T^8} \bar{L}^i(p') P_R E^j(p) [Y' Y'^\dagger Y]_{ij}. \quad (5.42)$$

5.2.1.3 Topology HT6

Compared to the aforementioned Higgs exchange topologies the topology HT6 exhibits right chirality Higgs couplings as well as wrong-chirality Higgs couplings. To write the expression in a particular easy form we use in this part of the Higgs exchange computation a cut-off regularisation.



$$\begin{aligned}
 &= c_{diag} \int_0^{\Lambda^2} \frac{dl^2}{16\pi^2} \int_{\frac{1-\delta}{T}}^{\frac{1}{T}} dx \int_{\frac{1-\delta}{T}}^{\frac{1}{T}} dy \int_{\frac{1-\delta}{T}}^{\frac{1}{T}} dz \left(\frac{T}{\delta}\right)^3 f_{L_i}^{(0)}(x) Y_{ik} Y_{kh}^\dagger Y_{hj} g_{E_j}^{(0)}(z) \\
 &\quad \times \frac{1}{2} \left[\partial_{l^2} \left(l^4 \partial_{l^2} (F_{X_k}^-(l, x, y) F_{Y_h}^+(l, y, z)) \right) + l^2 \partial_{l^2} \partial_{l^2} (d^- F_{X_k}^+(l, x, y) d^- F_{Y_h}^+(l, y, z)) \right]. \quad (5.43)
 \end{aligned}$$

5.2. INTERNAL HIGGS EXCHANGE

We already integrated the photon vertex in (5.43). In (5.43) the first term in the fermion contains the right chirality contribution. Due to it being a total derivative we can integrate the momentum integral directly to find

$$c_{diag} \int_{\frac{1-\delta}{T}}^{\frac{1}{T}} dx \int_{\frac{1-\delta}{T}}^{\frac{1}{T}} dy \int_{\frac{1-\delta}{T}}^{\frac{1}{T}} dz \frac{1}{16\pi^2} \frac{1}{2} \left(l^4 \partial_{l^2} (F_{X_k}^-(l, x, y) F_{Y_h}^+(l, y, z)) \right) \Big|_{l=0}^{l=\Lambda^2}, \quad (5.44)$$

where the boundary term for $l=0$ yields zero. To compute the boundary term $l = \Lambda^2$ we expand the remaining fermion propagators for large loop momenta $l \gg T$. The leading term of this expansion does not depend on the IR brane boundary conditions of the propagator, thus we do not have to specify the exact fermion fields and can still remain in the topology notation. After inserting the expansion

$$F_Y^+(l, x, z) = F_X^-(l, x, z) = \frac{i}{2} k^4 w^{5/2} x^{5/2} \sqrt{\frac{1}{lw}} \sqrt{\frac{1}{lx}} \theta(w-x) \left(e^{\frac{2l}{T}} + e^{2lw} \right) e^{l(-\frac{2}{T}-w+x)} \\ + \frac{i}{2} k^4 w^{5/2} x^{5/2} \sqrt{\frac{1}{lw}} \sqrt{\frac{1}{lx}} \theta(x-w) \left(e^{\frac{2l}{T}} + e^{2lx} \right) e^{l(-\frac{2}{T}+w-x)} + \mathcal{O}\left(\frac{1}{l^{\frac{3}{2}}}\right). \quad (5.45)$$

we find that the right-chirality term vanishes for the limit $\Lambda \rightarrow \infty$ in the narrow bulk Higgs localisation scheme, see section 2.3.4 for the exact definitions. This is due to the introduction of an additional $\frac{1}{l}$ factor through the exponential functions in (5.45) after the vertex integration. In the brane Higgs scenario, where we set $\delta \rightarrow 0$ before any other regulators, the exponential is cancelled. In this case the high momentum expansion of the $F^{+/-}$ functions simply yield

$$F_Y^+(l, 1/T, 1/T) = F_X^-(l, 1/T, 1/T) = \frac{i}{l} \frac{k^4}{T^4}. \quad (5.46)$$

Hence we find, that the l^4 term is cancelled in the brane Higgs scenario. As the wrong-chirality term vanishes the topology HT6 yields the value

$$-c_{Diag} i \frac{(p'^\mu + p^\mu)}{32\pi^2} \epsilon_\mu^* f_{l_i}^{(0)} \left(\frac{1}{T} \right) f_\gamma^{(0)} g_{E_j} \left(\frac{1}{T} \right) \frac{k^8}{T^8} \bar{L}^i(p') P_R E^j(p) [Y' Y'^\dagger Y]_{ij}, \quad (5.47)$$

for an exactly brane localised Higgs.

For the solution of wrong-chirality term in HT6 we perform twice a partial integration with respect to dl^2 in d dimensions. This yields a $\epsilon \int d^d l d^- F_{X_k}^+(l, x, y) d^- F_{Y_h}^+(l, y, z) \frac{1}{l^4}$ term, which can be treated the same way as for the topologies HT3-HT5. We therefore just give the final result of the topology HT6 without additional computations in the narrow bulk Higgs scenario

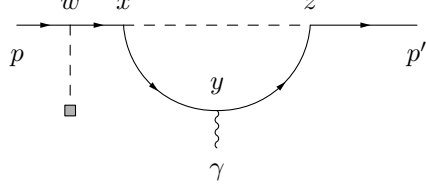
$$c_{Diag} i \frac{(p'^\mu + p^\mu)}{96\pi^2} \epsilon_\mu^* f_{l_i}^{(0)} \left(\frac{1}{T} \right) f_\gamma^{(0)} g_{E_j} \left(\frac{1}{T} \right) \frac{k^8}{T^8} \bar{L}^i(p') P_R E^j(p) [Y' Y'^\dagger Y]_{ij}. \quad (5.48)$$

5.2.2 Off-shell zero-mode Higgs exchange contribution

All Higgs exchange diagrams with a mass insertion on an external line, also contain contributions coming from off-shell zero-mode propagators adjacent to the Yukawa coupling. Thus the topologies HT1, HT2, HT3 and HT4 contain also off-shell contributions, which

CHAPTER 5. LOOP-INDUCED DIPOLE OPERATORS

have to be computed. We consider first the off-shell terms of the diagram topology HT1. These can be written as



$$\begin{aligned}
 &= -c_{Diag} \int_{\frac{1-\delta}{T}}^{\frac{1}{T}} dx \int_{\frac{1}{k}}^{\frac{1}{T}} \frac{dy}{(kz)^4} \int_{\frac{1-\delta}{T}}^{\frac{1}{T}} dz \int_{\frac{1-\delta}{T}}^{\frac{1}{T}} dw \left(\frac{T}{\delta}\right)^3 \mu^{d-4} \int \frac{d^d l}{(2\pi)^d} \epsilon^{*\mu} \frac{i}{l^2} \\
 &\times (Y)_{ia} (Y^\dagger)_{ab} (Y)_{bj} f_{li}^{(0)}(z) f_\gamma^{(0)} g_{Ej}(w) \bar{L}^i(p') [d^- F_{Y_a^+}(\hat{p}', z, y) d^+ F_{Y_a^-}(\hat{p}, y, x) \gamma_\mu \\
 &+ F_{Y_a^-}(\hat{p}', z, y) F_{Y_a^-}(\hat{p}, y, x) \not{p}' \gamma_\mu \not{p}] \frac{i \not{p}}{p^2} f_{lb}^{(0)}(x) f_{li}^{(0)}(w) P_R E^j(p). \quad (5.49)
 \end{aligned}$$

To compute it we follow the same strategy as for the on-shell contributions. The difference to the on-shell case is the factor $\frac{\not{p}}{p^2}$, which has to be removed by an additional \not{p} factor. To find all terms doing this it is necessary to expand the F functions to second order in the momentum, e.g. for $F_{Y_a^-}$ we would write

$$\begin{aligned}
 F_{Y_a^-}(\hat{p}, y, x) &= F_{Y_a^-}(l, y, x) + (p^2 - 2p \cdot l) \partial_{p^2} F_{Y_a^-}(p, y, x)|_{p=l} \\
 &+ \frac{1}{2} (p^2 - 2p \cdot l)^2 \partial_{p^2}^2 F_{Y_a^-}(l, y, x)|_{p=l} + O(p^5). \quad (5.50)
 \end{aligned}$$

The $d^- F_{Y_a^+}(\hat{p}', z, y) d^+ F_{Y_a^-}(\hat{p}, y, x) \gamma_\mu$ term cannot generate a \not{p} factor, thus it does not contribute to the dipole coefficient. For the $F_{Y_a^-}(\hat{p}', z, y) F_{Y_a^-}(\hat{p}, y, x)$ term we rewrite first the $\not{p}' \gamma_\mu \not{p}$ factor

$$\not{p}' \gamma_\mu \not{p} = \not{p}' \gamma_\mu p^2 - \not{p}' \gamma_\mu \not{l} p - \not{l} \gamma_\mu p^2 + \not{l} \gamma_\mu \not{p}. \quad (5.51)$$

Note that the terms $\not{p}' \gamma_\mu p^2 - \not{p}' \gamma_\mu \not{l} p$ are not relevant in the following calculation, because the term $\not{p}' \gamma_\mu p^2$ cannot remove the global \not{p} factor and one cannot remove the \not{p}' factor in $\not{p}' \gamma_\mu \not{l}$. The term $\not{l} \gamma_\mu p^2$ can only generate a term proportional to p_μ with a $\mathcal{O}(p \cdot l)$ term coming from the Taylor expansion from the F functions. The term $\not{l} \gamma_\mu \not{l} p$ needs terms of the order $\mathcal{O}((p \cdot l)^2)$ or $\mathcal{O}((p \cdot l)(p' \cdot l))$ to contribute to the coefficients of $(p + p')^\mu$. This yields for the $(p + p')^\mu$ coefficient of the off-shell part of HT1

$$\begin{aligned}
 &-\bar{L}^i(p') F_{Y_a^-}(\hat{p}', z, y) F_{Y_a^-}(\hat{p}, y, x) \not{p}' \gamma_\mu \not{p} \frac{\not{p}}{p^2} P_R E^j(p) \\
 &\doteq \bar{L}^i(p') [-2(p \cdot l) F_{Y_a^-}(l, z, y) \partial_{l^2} F_{Y_a^-}(l, y, x) \not{l} \gamma_\mu \\
 &-4(p' \cdot l)(p \cdot l) \partial_{l^2} F_{Y_a^-}(l, z, y) \partial_{l^2} F_{Y_a^-}(l, y, x) \not{l} \gamma_\mu \not{l} \frac{\not{p}}{l^2} \\
 &-2(p \cdot l)^2 F_{Y_a^-}(l, z, y) \partial_{l^2}^2 F_{Y_a^-}(l, y, x) \not{l} \gamma_\mu \not{l} p] P_R E^j(p) \\
 &\doteq \bar{L}^i(p') \left[\frac{-4p_\mu}{d} l^2 F_{Y_a^-}(l, z, y) \partial_{p^2} F_{Y_a^-}(l, y, x) - \frac{8p'_\mu}{d(d+2)} l^4 \partial_{l^2} F_{Y_a^-}(l, z, y) \partial_{l^2} F_{Y_a^-}(l, y, x) \right. \\
 &\quad \left. - \frac{8p_\mu l^4}{d(d+2)} F_{Y_a^-}(l, z, y) \partial_{l^2}^2 F_{Y_a^-}(l, y, x) \right] P_R E^j(p) \quad (5.52)
 \end{aligned}$$

5.2. INTERNAL HIGGS EXCHANGE

Because the propagator connecting the external Higgs emission to the loop was replaced by a zero mode propagator, zero mode fermion propagators inside the loop would make this diagram topology a standard model contribution. Thus we consider only zero-mode subtracted F_Y^- functions. This problem only appears in the diagram of the minimal RS model, because the fermions propagating in loops of pure RSc diagrams do not have a zero-mode due to their mixed boundary conditions.

As for on-shell contribution, we integrate first over the photon coordinate integral and then the loop momentum integral. Using the Kaluza-Klein decomposition (A.10) we find

$$\begin{aligned} & \int_{\frac{1}{k}}^{\frac{1}{\bar{k}}} \frac{dy}{(kz)^4} \left[\frac{-4p_\mu l^2}{d} F_{Y_a}^-(l, z, y) \partial_{l^2} F_{Y_a}^-(l, y, x) - \frac{8p'_\mu}{d(d+2)} l^4 \right. \\ & \times \partial_{l^2} F_{Y_a}^-(l, z, y) F_{Y_a}^-(l, y, x) - \left. \frac{8p_\mu}{d(d+2)} F_{Y_a}^-(l, z, y) \partial_{l^2}^2 F_{Y_a}^-(l, y, x) \right] = \sum_{n=1} g_{Y_a}^{(n)}(z) g_{Y_a}^{(n)}(x) \\ & \times \left[-\frac{4p_\mu}{d} \frac{l^2}{(l^2 - m_n^2)^3} + \frac{8p'_\mu}{d(d+2)} \frac{l^4}{(l^2 - m_n^2)^4} + \frac{16p_\mu}{d(d+2)} \frac{l^4}{(l^2 - m_n^2)^4} \right]. \end{aligned} \quad (5.53)$$

The factor $\frac{l^2}{(l^2 - m_n^2)^2}$ is the same as for the on-shell case, i.e. we can recycle most of the result (5.26). We find

$$\begin{aligned} & -\mu^{d-4} \int \frac{d^d l}{(2\pi)^d} \sum_{n=1} g_{Y_a}^{(n)}(z) g_{Y_a}^{(n)}(x) \frac{4p_\mu}{d} \frac{l^2}{(l^2 - m_n^2)^3} \frac{i}{l^2} \\ & \stackrel{d=4-2\epsilon}{=} i \frac{p_\mu}{32\pi^2} \sum_{n=1} g_{Y_a}^{(n)}(z) g_{Y_a}^{(n)}(x) \frac{i}{m_n^2} + \mathcal{O}(\epsilon) \stackrel{\epsilon \rightarrow 0}{=} i \frac{p_\mu}{32\pi^2} F_{ZMS Y_a}^-(0, z, x). \end{aligned} \quad (5.54)$$

For the the $\frac{l^4}{(l^2 - m_n^2)^4}$ terms we find

$$\begin{aligned} & \frac{8p'_\mu + 16p_\mu}{d(d+2)} \mu^{d-4} \int \frac{d^d l}{(2\pi)^d} \sum_{n=1} g_{Y_a}^{(n)}(z) g_{Y_a}^{(n)}(x) \frac{l^4}{(l^2 - m_n^2)^4} \frac{i}{l^2} \\ & = -i \frac{8p'_\mu + 16p_\mu}{d(d+2)} \mu^{d-4} \sum_{n=1} g_{Y_a}^{(n)}(z) g_{Y_a}^{(n)}(x) \frac{i d}{2(4\pi)^{\frac{d}{2}}} \frac{\Gamma(3 - \frac{d}{2})}{\Gamma(4)} \left(\frac{1}{m_n^2} \right)^{3 - \frac{d}{2}} \\ & \stackrel{d=4-2\epsilon}{=} -i \frac{2p'_\mu + 4p_\mu}{9} \sum_{n=1} g_{Y_a}^{(n)}(z) g_{Y_a}^{(n)}(x) \frac{1}{32\pi^2} \frac{i}{m_n^2} + \mathcal{O}(\epsilon) \\ & \stackrel{\epsilon \rightarrow 0}{=} -i \frac{2p'_\mu + 4p_\mu}{9 \cdot 32\pi^2} F_{ZMS Y_a}^-(0, z, x). \end{aligned} \quad (5.55)$$

Adding both integral results we compute

$$\begin{aligned} & -i \left(\frac{2p'_\mu + 4p_\mu}{9 \cdot 32\pi^2} - \frac{p_\mu}{32\pi^2} \right) F_{ZMS Y_a}^-(0, z, x) \\ & = \left[+i \frac{1}{192\pi^2} (p_\mu + p'_\mu) + i \frac{7}{576\pi^2} (p_\mu - p'_\mu) \right] F_{ZMS Y_a}^-(0, z, x). \end{aligned} \quad (5.56)$$

CHAPTER 5. LOOP-INDUCED DIPOLE OPERATORS

Thus after these steps the $(p_\mu + p'_\mu)$ coefficient of the off-shell terms of HT3 (5.49) becomes

$$-c_{Diag} (Y)_{ia} (Y^\dagger)_{ab} (Y)_{bj} \int_{\frac{1-\delta}{T}}^{\frac{1}{T}} dx \int_{\frac{1-\delta}{T}}^{\frac{1}{T}} dz \int_{\frac{1-\delta}{T}}^{\frac{1}{T}} dw \left(\frac{T}{\delta}\right)^3 \epsilon^{*\mu} f_{l_i}^{(0)}(z) f_\gamma^{(0)} g_{E_j}(w) \\ \frac{1}{192\pi^2} F_{ZMS Y_a}^-(0, z, x) f_{l_b}^{(0)}(x) f_{l_b}^{(0)}(w) \bar{L}^i(p') (p_\mu + p'_\mu) P_R E^j(p).$$

To perform the remaining integrals we expand $F_{ZMS Y_a}^-$ and all mode functions around $w \approx \frac{1}{T}$, $x \approx \frac{1}{T}$, and $z \approx \frac{1}{T}$

$$F_{ZMS Y_a}^-(0, z, x) = F_{ZMS Y_a}^-\left(0, \frac{1}{T}, \frac{1}{T}\right) + \mathcal{O}(\delta),$$

where $F_{ZMS Y_a}^-(0, \frac{1}{T}, \frac{1}{T})$ needs to be determined independently for all types of fermion fields. Using this expansions the final result for $(p_\mu + p'_\mu)$ coefficient of the off-shell terms of HT3 can be written as

$$-c_{Diag} (Y)_{ia} (Y^\dagger)_{ab} (Y)_{bj} \epsilon^{*\mu} f_{l_i}^{(0)}\left(\frac{1}{T}\right) f_\gamma^{(0)} g_{E_j}\left(\frac{1}{T}\right) f_{l_b}^{(0)}\left(\frac{1}{T}\right) f_{l_b}^{(0)}\left(\frac{1}{T}\right) \\ \bar{L}^i(p') \frac{1}{192\pi^2} F_{ZMS Y_a}^-\left(0, \frac{1}{T}, \frac{1}{T}\right) (p_\mu + p'_\mu) P_R E^j(p). \quad (5.57)$$

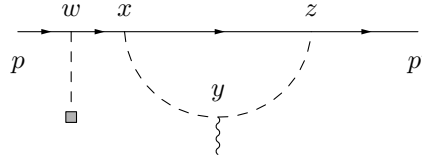
For the off-shell contribution of the topology HT2 we can use the same steps as above by applying the rules

$$p'_\mu \rightarrow p_\mu \quad p_\mu \rightarrow p'_\mu \\ F_{ZMS Y}^- \rightarrow F_{ZMS X}^+ \quad f_{l_i}^{(0)}(x) f_{l_i}^{(0)}(w) \rightarrow g_{E_j}^{(0)}(z) g_{E_i}^{(0)}(w). \quad (5.58)$$

This leads to the following expression for the off-shell terms of $(p_\mu + p'_\mu)$ for HT2

$$-c_{Diag} (Y)_{ia} (Y^\dagger)_{ab} (Y)_{bj} \epsilon^{*\mu} f_{l_i}^{(0)}\left(\frac{1}{T}\right) f_\gamma^{(0)} g_{E_j}\left(\frac{1}{T}\right) g_{l_a}^{(0)}\left(\frac{1}{T}\right) g_{l_a}^{(0)}\left(\frac{1}{T}\right) \\ \bar{L}^i(p') \frac{1}{192\pi^2} F_{ZMS X_b}^+\left(0, \frac{1}{T}, \frac{1}{T}\right) (p_\mu + p'_\mu) P_R E^j(p). \quad (5.59)$$

We deal with the off-shell terms of HT3 and HT4 using the same strategy as for the diagram topology HT1. The off-shell contribution of the diagram topology HT3 is again



$$c_{Diag} \int_{\frac{1-\delta}{T}}^{\frac{1}{T}} dx \int_{\frac{1-\delta}{T}}^{\frac{1}{T}} dy \int_{\frac{1-\delta}{T}}^{\frac{1}{T}} dz \int_{\frac{1-\delta}{T}}^{\frac{1}{T}} dw \left(\frac{T}{\delta}\right)^4 \mu^{d-4} \int \frac{d^d l}{(2\pi)^d} \epsilon^{*\mu} (p + p' - 2l)_\mu \\ \times (Y')_{ia} (Y'^\dagger)_{ab} (Y)_{bj} f_{l_i}^{(0)}(z) f_\gamma^{(0)} g_{E_j}(w) \frac{i}{(p' - l)^2} \frac{i}{(p - l)^2} \\ \times \bar{L}^i(p') F_{Y_a}^-(l, z, x) \frac{l \not{y}}{p^2} f_{l_b}^{(0)}(x) f_{l_b}^{(0)}(w) P_R E^j(p). \quad (5.60)$$

5.2. INTERNAL HIGGS EXCHANGE

To eliminate the \not{p} term we expand both Higgs propagators to second order and then only collect only terms, which will be proportional to p_μ or p'_μ in the end of the calculation. The relevant terms are

$$\begin{aligned} & \bar{L}^i(p') \frac{i}{(p' - l)^2} \frac{i}{(p - l)^2} \frac{\not{p}}{p^2} (p + p' - 2l)^\mu P_R E^j(p) \\ & \doteq (2l - p - p')^\mu \left[4 \frac{(p \cdot l)^2}{l^8} + 4 \frac{(p \cdot l)(p' \cdot l)}{l^8} + 2 \frac{(p \cdot l)}{l^6} \right] \\ & \bar{L}^i(p') \frac{\not{p}}{p^2} P_R E^j(p) \doteq \frac{16}{d(d+2)l^4} p^\mu + \frac{8}{d(d+2)l^4} p'^\mu - \frac{2}{dl^4} (p + p')^\mu \\ & \bar{L}^i(p') P_R E^j(p) = \frac{1}{l^4 d(d+2)} \left(-(2d-8)(p+p')^\mu + 4(p-p')^\mu \right) \bar{L}^i(p') P_R E^j(p). \end{aligned} \quad (5.61)$$

As usual we used rotational invariance of the loop momenta in d-dimensions to derive this result. Inserting $d = 4 - 2\epsilon$ we find then for the relevant $(p + p')^\mu$ coefficient

$$\frac{-(2d-8)}{l^4 d(d+2)} (p+p')^\mu \stackrel{d=4-2\epsilon}{=} \frac{1}{l^4} \frac{\epsilon}{6} + \mathcal{O}(\epsilon^2). \quad (5.62)$$

Note that this $\mathcal{O}(\epsilon)$ term has the same for as for the on-shell case of this topology (5.35). Thus we can reuse the loop integral off the on-shell contribution here. As in the case of the topology HT1 we have to remove the possible zero modes. The loop integral gives

$$\mu^{d-4} \int \frac{d^d l}{(2\pi)^d} \frac{1}{l^4} F_{Y_a}^- ZMS(l, z, x) = -\frac{1}{\epsilon} \frac{i}{16\pi^2} F_{Y_a}^- ZMS(0, z, x) + \mathcal{O}(1). \quad (5.63)$$

Putting everything together the off-shell term of HT3 proportional to $(p + p')^\mu$ yields

$$\begin{aligned} & c_{Diag}(Y')_{ia} (Y'^\dagger)_{ab} (Y)_{bj} \int_{\frac{1-\delta}{T}}^{\frac{1}{T}} dx \int_{\frac{1-\delta}{T}}^{\frac{1}{T}} dz \int_{\frac{1-\delta}{T}}^{\frac{1}{T}} dw \left(\frac{T}{\delta} \right)^3 (p+p')_\mu \epsilon^{*\mu} \\ & \times f_{l_i}^{(0)}(z) f_\gamma^{(0)} g_{E_j}(w) \frac{1}{96\pi^2} F_{Y_a}^- ZMS(0, z, x) f_{l_b}^{(0)}(x) f_{l_b}^{(0)}(w) \bar{L}^i(p') P_R E^j(p) \end{aligned} \quad (5.64)$$

To perform the remaining integrals we expand $F_{ZMS Y}^-$ and all mode functions around around $w \approx \frac{1}{T}$, $x \approx \frac{1}{T}$, and $z \approx \frac{1}{T}$. We find as the final result

$$\begin{aligned} & c_{Diag}(Y')_{ia} (Y'^\dagger)_{ab} (Y)_{bj} f_{l_i}^{(0)} \left(\frac{1}{T} \right) f_\gamma^{(0)} g_{E_j} \left(\frac{1}{T} \right) f_{l_b}^{(0)} \left(\frac{1}{T} \right) f_{l_b}^{(0)} \left(\frac{1}{T} \right) \\ & \times \epsilon^{*\mu} (p+p')_\mu \frac{1}{96\pi^2} F_{Y_a}^- ZMS \left(0, \frac{1}{T}, \frac{1}{T} \right) \bar{L}^i(p') P_R E^j(p). \end{aligned} \quad (5.65)$$

Again this result can at once be adapted to the topology HT4 by applying the rules

$$\begin{aligned} & p_{l\mu} \rightarrow p_\mu \quad p_\mu \rightarrow p'_\mu \\ & F_{ZMS Y}^- \rightarrow F_{ZMS X}^+ \quad f_{l_i}^{(0)}(x) f_{l_i}^{(0)}(w) \rightarrow g_{E_j}^{(0)}(z) g_{E_i}^{(0)}(w). \end{aligned} \quad (5.66)$$

We find

$$\begin{aligned} & -c_{Diag}(\lambda_{5D})_{ia} (Y^\dagger)_{ab} (Y)_{bj} f_{l_i}^{(0)} \left(\frac{1}{T} \right) f_\gamma^{(0)} g_{E_j} \left(\frac{1}{T} \right) g_{E_a}^{(0)} \left(\frac{1}{T} \right) g_{E_a}^{(0)} \left(\frac{1}{T} \right) \\ & \times \epsilon^{*\mu} (p+p')_\mu \frac{1}{96\pi^2} F_{X_b}^- ZMS \left(0, \frac{1}{T}, \frac{1}{T} \right) \bar{L}^i(p') P_R E^j(p). \end{aligned} \quad (5.67)$$

5.2.3 Zero-mode Higgs exchange matching

With the complete computation of all Higgs exchange diagrams at hand we can now perform the matching of the Higgs exchange diagrams to the dipole coefficients. To do this one has simply to compute all $SU(2)_L \times SU(2)_R$ group factors for each diagram and insert the correct factor c_{diag} . Note that the propagators of the RSc T^4 triplet fermions have a non-trivial dependence on the $SU(2)_R$ quantum number, which complicates the group factor computation slightly. All group factors can be found for all leptonic diagrams Appendix C.2.

Let us now collect the Higgs exchange results for a narrow bulk Higgs in the leptonic sector of the minimal RS model

$$a_{ij}^\gamma|_{Higgs} = \frac{e}{192\pi^2} \frac{T^3}{k^4} \frac{T^8}{2k^8} Q_e (F_L - F_E) + \frac{e}{192\pi^2} \frac{T^3}{k^4} Q_e f_{L_i}^{(0)}(1/T) [YY^\dagger Y]_{ij} g_{E_j}^{(0)}(1/T), \quad (5.68)$$

where the F_X ($X = E, L$) are abbreviations for

$$F_E = f_{L_i}^{(0)}(1/T) [Y]_{ik} F(-c_{E_k}) [Y^\dagger]_{kh} f_{L_h}^{(0)}(1/T)^2 [Y]_{hj} g_{E_j}^{(0)}(1/T) \\ F_L = f_{L_i}^{(0)}(1/T) [Y]_{ik} g_{E_k}^{(0)}(1/T)^2 [Y^\dagger]_{kh} F(c_{L_h}) [Y]_{hj} g_{E_j}^{(0)}(1/T). \quad (5.69)$$

The function $F(c_{L_k})$ is up to terms linear in $\frac{T}{k}$ equal to $F_{ZMS L_k}^- (0, \frac{1}{T}, \frac{1}{T})$. It can be found in equation (4.23).

In the custodially protected model the Higgs contribution to the leptonic dipole is given by

$$a_{ij}^\gamma|_{Higgs} = \frac{e}{192\pi^2} \frac{T^3}{k^4} \frac{T^8}{2k^8} Q_e (F_L + F_{T_3} - F_d + 2F_u) + \frac{e}{192\pi^2} \frac{T^3}{k^4} 2Q_e f_{L_i}^{(0)}(1/T) [YY^\dagger Y - Y_\nu Y_\nu^\dagger Y]_{ij} g_{E_j}^{(0)}(1/T), \quad (5.70)$$

where we introduce the additional abbreviations

$$F_{T_3} = f_{L_i}^{(0)}(1/T) [Y]_{ik} F_{T_3}(c_{E_k}) [Y^\dagger]_{kh} f_{L_h}^{(0)}(1/T)^2 [Y]_{hj} g_{E_j}^{(0)}(1/T) \\ F_u = f_{L_i}^{(0)}(1/T) [Y_\nu]_{ik} F(-c_{E_k}) [Y^\dagger]_{kh} f_{L_h}^{(0)}(1/T)^2 [Y]_{hj} g_{E_j}^{(0)}(1/T). \quad (5.71)$$

Here $[Y_\nu]$ is the u type Yukawa matrix, which generates the tiny masses of the zero-mode neutrino fields. F_{T_3} equals the function $F_{pm L_k}^+ (0, \frac{1}{T}, \frac{1}{T})$. A simple Taylor expansion yields

$$F_{T_3}(c) = -\frac{k^4}{T^5} \frac{1 - \epsilon^{1-2c}}{1 - 2c}, \quad (5.72)$$

with $\epsilon = T/k$. The associated dipole elements for the the Higgs exchange for an exactly brane localised Higgs are generated simply by dropping the wrong-chirality contributions proportional to $[YY^\dagger Y]$ in (5.68) for the minimal RS model. In the custodial RS model this approach only partially leads to the correct result. In the case of a brane Higgs we also need to add the right-chirality contribution from the diagrams generated by the topology HT6. We find for a brane Higgs in the custodial protected RS model

$$a_{ij}^\gamma|_{Higgs} = \frac{e}{192\pi^2} \frac{T^3}{k^4} \frac{T^8}{2k^8} Q_e (F_L + F_{T_3} - F_d + 2F_u) - \frac{e}{192\pi^2} \frac{T^3}{k^4} 3Q_e f_{L_i}^{(0)}(1/T) [YY^\dagger Y - Y_\nu Y_\nu^\dagger Y]_{ij} g_{E_j}^{(0)}(1/T). \quad (5.73)$$

5.2. INTERNAL HIGGS EXCHANGE

Note that the brane Higgs result contains a different sign in front of the $YY^\dagger Y$ compared to the narrow bulk Higgs case.

The appearance of a term of the $YY^\dagger Y$ in the brane Higgs case lowers the phenomenological difference of both localisation scheme in the custodial protected RS. Therefore we drop this localisation scheme in the quark sector. Note that the brane Higgs case was already considered in great details in [50]. Concentrating on the narrow bulk Higgs case we find for the minimal RS mode for the Higgs exchange contribution to quark dipole operators

$$a_{ij}^{\gamma}|_{Higgs} = -\frac{e}{192\pi^2} \frac{T^3}{k^4} \frac{T^8}{2k^8} ((2Q_e - Q_d - Q_u)F_Q - Q_d F_d + (2Q_e - Q_u)F_u) - \frac{e}{192\pi^2} \frac{T^3}{k^4} (2Q_d + Q_u - Q_e) f_{Q_i}^{(0)}(1/T) [Y_d Y_d^\dagger Y_d]_{ij} g_{d_j}^{(0)}(1/T) \quad (5.74)$$

$$a_{ij}^g|_{Higgs} = \frac{g_s}{192\pi^2} \frac{T^3}{k^4} \frac{T^8}{2k^8} (2F_Q + F_d + F_u) - \frac{g_s}{192\pi^2} \frac{T^3}{k^4} 3 f_{Q_i}^{(0)}(1/T) [Y_d Y_d^\dagger Y_d]_{ij} g_{d_j}^{(0)}(1/T), \quad (5.75)$$

where the F_q ($q = d, Q, u$) are simple adaptations of (5.69) and (5.71) to the quark sector, for example $F_Q = (F_L)|_{c_L=c_Q}$.

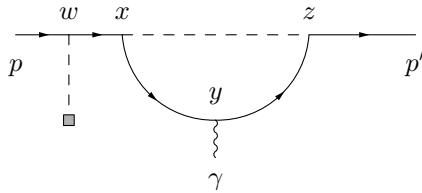
In the custodially protected model the Higgs contribution to the quark dipole is given by

$$a_{ij}^{\gamma}|_{Higgs} = -\frac{e}{192\pi^2} \frac{T^3}{k^4} \frac{T^8}{2k^8} ((2Q_e - Q_d - Q_u)(F_Q + F_{T_3}) - Q_d F_d + (2Q_e - Q_u)F_u) - \frac{e}{192\pi^2} \frac{T^3}{k^4} (4Q_d + 2Q_u - 2Q_e) f_{Q_i}^{(0)}(1/T) [Y_d Y_d^\dagger Y_d]_{ij} g_{d_j}^{(0)}(1/T) \quad (5.76)$$

$$a_{ij}^g|_{Higgs} = \frac{g_s}{192\pi^2} \frac{T^3}{k^4} \frac{T^8}{2k^8} (2F_Q + 2F_{T_3} + F_d + F_u) - \frac{g_s}{192\pi^2} \frac{T^3}{k^4} 6 f_{Q_i}^{(0)}(1/T) [Y_d Y_d^\dagger Y_d]_{ij} g_{d_j}^{(0)}(1/T). \quad (5.77)$$

5.2.4 Bulk Higgs with a beta profile

Next we consider the case of a bulk Higgs with the β profile (2.65). The dominant contributions were studied in some detail in [79] and numerical estimates were obtained by summing a large number of KK modes. Using 5D propagators the effect of the Higgs zero mode can be computed analytically for large β . To see this let us focus on a diagram generated by the topology HT1. The methods used here can be applied to all other Higgs exchange topologies analogously, but may require appropriate expansions of the fermion propagators for a fully analytic result. For light external fermions the dominant contribution can be written as



CHAPTER 5. LOOP-INDUCED DIPOLE OPERATORS

$$\begin{aligned}
&= Q_\mu e Y_{ih}^\beta [Y^\beta]_{hk}^\dagger Y_{kj}^\beta \int \frac{d^4 l}{(2\pi)^4} \int_{\frac{1}{k}}^{\frac{1}{T}} \frac{dz dy dx dw}{k^{19} x^5 y^4 z^5 w^5} f_{L_i}^{(0)}(z) g_{E_j}^{(0)}(w) d^- F_{L_k}^+(p, x, w) \\
&\times \Delta_\Phi(l, x, z) \Phi^{(0)}(w) [d^- F_{E_h}^+(p' - l, z, y) F_{E_h}^+(p - l, y, x) \gamma^\mu (\not{p} - \not{l}) \\
&+ F_{E_h}^-(p' - l, z, y) d^- F_{E_h}^+(p - l, y, x) (\not{p}' - \not{l}) \gamma^\mu]
\end{aligned} \tag{5.78}$$

where we chose p, p' for the incoming and outgoing fermion momentum, respectively. The integral over the w coordinate can be taken right away as we can set p to zero in the external fermion propagator:

$$\begin{aligned}
\mathcal{E}(x, \beta, c_L, c_E) &\equiv \int_{\frac{1}{k}}^{\frac{1}{T}} \frac{dw}{k^5 w^5} g_E^{(0)}(w) d^- F_L^+(p = 0, x, w) \Phi^{(0)}(w) \\
&= i \sqrt{\frac{1 + 2c_E}{1 - \epsilon^{1+2c_E}}} \sqrt{\frac{2(1 + \beta)}{1 - \epsilon^{2+2\beta}}} \frac{1}{2 - c_L + c_E + \beta} \frac{(Tx)^{2+c_L} \epsilon^{-5/2}}{1 - \epsilon^{2c_L-1}} \\
&\times \left[(Tx)^{2-c_L+c_E+\beta} (1 - \epsilon^{2c_L-1}) + (Tx)^{1-2c_L} (\epsilon^{2c_L-1} - \epsilon^{1+c_L+c_E+\beta}) - (1 - \epsilon^{1+c_L+c_E+\beta}) \right].
\end{aligned} \tag{5.79}$$

After expanding the remaining integrand for small p, p' we perform the integral over the photon vertex bulk position y using the completeness and orthogonality relations. We then find for the diagram

$$\begin{aligned}
&Q_\mu e Y_{ih}^\beta [Y^\beta]_{hk}^\dagger Y_{kj}^\beta \int \frac{d^4 l}{(2\pi)^4} \int_{\frac{1}{k}}^{\frac{1}{T}} \frac{dz dx}{k^{10} x^5 z^5} f_{L_i}^{(0)}(z) \mathcal{E}(x, \beta, c_{L_k}, c_{E_j}) \Delta_\Phi(l, x, z) \\
&\times \left[\frac{i}{2} l^2 \partial_{l^2}^2 d^- F_{E_h}^+(l, z, x) \right] (p^\mu + p'^\mu).
\end{aligned} \tag{5.80}$$

This leaves us with only three integrals over x, z and the loop momentum.

Let us first consider the Higgs zero-mode contribution by substituting $\Delta_\Phi(l, x, z) \rightarrow i/l^2 \times \Phi^{(0)}(x) \Phi^{(0)}(z)$. Since β is large but finite until all integrals have been carried out and all regulators removed, we can perform the momentum integral directly in $d = 4$ dimensions. To this end, we switch temporarily to the mode picture for the fermion propagator, evaluate the integral

$$\int \frac{d^4 l}{(2\pi)^4} \frac{1}{(l^2 - m_n^2)^3} = -\frac{i}{2(4\pi)^2} \frac{1}{m_n^2}, \tag{5.81}$$

and resum the mode expansion back into 5D propagators, which results in

$$\begin{aligned}
&-i Q_\mu e Y_{ih}^\beta [Y^\beta]_{hk}^\dagger Y_{kj}^\beta \int_{\frac{1}{k}}^{\frac{1}{T}} \frac{dz dx}{k^{10} x^5 z^5} f_{L_i}^{(0)}(z) \mathcal{E}(x, \beta, c_{L_k}, c_{E_j}) \Phi^{(0)}(x) \Phi^{(0)}(z) \\
&\times \frac{1}{2(4\pi)^2} d^- F_{E_h}^+(0, z, x) (p^\mu + p'^\mu).
\end{aligned} \tag{5.82}$$

Since the zero-momentum limit of the fermion propagator has a simple form, the two remaining integrals are elementary. The final analytic expression is lengthy and valid for any

5.2. INTERNAL HIGGS EXCHANGE

positive value of β . We refrain from giving the explicit expression. However, the limit $\beta \rightarrow \infty$ is straightforward. After using (B.37) to relate the Yukawa matrices for the bulk Higgs to the couplings for the delta-regularized Higgs we recover the same answer as already found in the section for the computation of the topology HT1,

$$-\frac{iQ_\mu e}{96\pi^2 T^2} \frac{T^3}{k^4} f_{L_i}^{(0)}(1/T) Y_{ih} Y_{hk}^\dagger Y_{kj} g_{E_j}^{(0)}(1/T) (p^\mu + p'^\mu). \quad (5.83)$$

This observation is general: the Higgs zero-mode contribution of the bulk Higgs in the $\beta \rightarrow \infty$ limit is always equal to the one of the theta-function regularized brane Higgs. In other words, the localisation limit of the bulk Higgs is independent of the bulk profile at finite Higgs localisation width.

We still have to determine the contribution from the tower of KK Higgs excitations in the loop. To illustrate the computation in the 5D framework, we consider again the diagram H1 in the topology class HT1. The KK contribution is obtained by the replacement $\Delta_\Phi(l, x, z) \rightarrow \Delta_\Phi^{\text{ZMS}}(l, x, z)$ in (5.80). An analytical evaluation seems difficult even for $\beta \gg 1$. Before turning to the numerical calculation we shall first show that the KK contribution does not go to zero for large β despite the fact that the lowest KK masses are of order βT . This confirms the non-decoupling effect found in [79], now in the 5D framework. To this end we look at the different loop-momentum regions separately. There are two relevant scales, the KK scale T and the Higgs localisation scale βT . This leads to several momentum regions that allow for various expansions of the propagators. The expanded forms can then either be integrated directly or at least their β scaling can be determined.

- For small loop momenta $l \ll T$ we can expand both the fermion and the Higgs propagator around $l = 0$. We can then analytically integrate the x and z coordinates as in (5.82). In this region the scaling with β must be the same as the scaling of the Wilson coefficient of the four-fermion operator discussed in section 4.1 and in appendix B.4. That is, for large β the integrand scales as $1/\beta$. Hence, the total contribution from this region vanishes for $\beta \rightarrow \infty$.
- The second region is $l \sim T$. For the Higgs propagator we can use the same expansion for small euclidean momenta as for $l \ll T$ but the fermion propagator can no longer be expanded. Nonetheless, $d^- F_E^+(l, x, z)$ does not introduce an additional β dependence in this momentum region. We recover the overall scaling $\propto 1/\beta$ for fixed values of l just as for $l \ll T$. The only difference to the region with $l \ll T$ is the scaling of the integrand with the loop momentum l , which no longer is a simple power law. However, for $l \sim T$, the scaling of the integral with β is the same as the integrand, that is $1/\beta$, and hence the contribution from this region also vanishes for $\beta \rightarrow \infty$.
- For loop momentum l of the order βT we can make use of an expansion of modified Bessel functions of the form $\mathcal{I}_\beta(\beta x)$ and $\mathcal{K}_\beta(\beta x)$ for large β , given by

$$\mathcal{I}_\beta(\beta x) \sim \sqrt{\frac{1}{2\pi\beta}} \frac{e^{\beta f(x)}}{(1+x^2)^{1/4}} g(x), \quad \mathcal{K}_\beta(\beta x) \sim \sqrt{\frac{\pi}{2\beta}} \frac{e^{-\beta f(x)}}{(1+x^2)^{1/4}} \tilde{g}(x). \quad (5.84)$$

The exact expressions for the functions f , g and \tilde{g} can be found in [118, 119]. Here we only need that f , g and \tilde{g} depend on β only via terms that vanish at least as fast as $1/\beta$ for $\beta \rightarrow \infty$ and that $f(x)$ is a strictly monotonically increasing function of x . Using these expansions one can show that the Higgs propagator retains the same $1/\beta$ scaling as in first two regions. Taking into account the behaviour of the fermion propagator for $l \gg T$ we find that $d^4 l l^2 \partial_{l^2}^2 d^- F^+(l, z, x)$ counts as a factor

CHAPTER 5. LOOP-INDUCED DIPOLE OPERATORS

of dl or equivalently $dl \cdot (\beta T)$. This cancels the $1/\beta$ from the Higgs propagator and leaves us with the coordinate integrals. Their counting is easier to determine when the integral over w has not yet been carried out. The integral over w then cancels the $\sqrt{\beta}$ factors from the Higgs zero-mode profile and one Yukawa coupling. Every integral over a coordinate difference counts as $1/\beta$ (compare the discussion of KK effects in the gauge contribution). Including the two remaining Yukawa couplings, we find that the integrand scales as $1/\beta$ in the region $l \sim \beta T$. Hence the integral over the domain $l \sim \beta T$ takes a constant value for $\beta \rightarrow \infty$.

- Finally, for $l \gg \beta T$ we expand the Higgs propagator for large momenta, since it is now dominated by the scale l and no longer by βT . Consequently, the Higgs propagator scales as $1/l$, and the distance $|x - z|$ is limited to be of order $1/l$. This effectively trades two powers of $1/(\beta T)$ for two powers of $1/l$ compared to result in the $l \sim \beta T$ region, resulting in the scaling $\propto \beta/l^2$ of the integrand. The final integral over the modulus of l is therefore convergent and since

$$\int_{\beta T}^{\infty} dl \frac{\beta}{l^2} = \frac{1}{T}, \quad (5.85)$$

the high-momentum region also gives a finite β -independent contribution to the dipole operator coefficient.

Since in every region the integral over l either vanishes ($l \ll T$, $l \sim T$) or converges ($l \gg \beta T$ and $l \sim \beta T$) to a constant, the contribution to the dipole Wilson coefficient due to the Feynman diagram H1 tends to a constant for large β as announced. For large values of β the integral is further dominated by the high-momentum regions and therefore the 5D masses of the fermions enter predominantly via the external zero-modes.

The left panel of Figure 5.10 shows the numerical result for the integrand as a function of the loop momentum l and demonstrates the expected inversion of the order of the curves for different β values from the intermediate to the high-momentum regions.² The right panel shows the KK Higgs contribution as a function of β normalized to the zero-mode contribution in the $\beta \rightarrow \infty$ limit. The plot illustrates the approach of the KK contribution to a constant. The relatively fast convergence with increasing β is a feature of the simple diagram topology under consideration. The plot shows that the KK Higgs contribution while somewhat smaller than the corresponding zero-mode contribution is of the same order of magnitude [79].

A similar scaling analysis can be applied to all other diagrams involving KK Higgs modes. We will not discuss them in detail, as we anyway have to resort to a numerical evaluation in the end. In appendix B.5 we give the numerical ratio of the KK tower to the zero-mode contribution for each diagram topology. The final result for the leptonic dipole operator contribution due to the exchange of the KK Higgses is

$$a_{ij}^{H, \text{KK}} = \frac{Q_{\mu} e}{192\pi^2} \frac{T^3}{k^4} \cdot \mathcal{A}_{\text{KK}} \cdot f_{L_i}^{(0)}(1/T) [YY^{\dagger}Y]_{ij} g_{E_j}^{(0)}(1/T) \quad (5.86)$$

in the minimal model and

$$a_{ij}^{H, \text{KK}} = \frac{Q_{\mu} e}{192\pi^2} \frac{T^3}{k^4} \cdot f_{L_i}^{(0)}(1/T) [\mathcal{A}_{\text{KK}}^{cs} YY^{\dagger}Y + \mathcal{B}_{\text{KK}}^{cs} Y_u Y_u^{\dagger} Y]_{ij} g_{E_j}^{(0)}(1/T) \quad (5.87)$$

²Note that the solid curve for $\beta = 160$ does not reach the asymptotic region of very large loop momentum $l \gg \beta T$, while $\beta = 10$ is on the small side for the $\beta \gg 1$ scaling to hold. When taking the coordinate integrals analytically (possible in some of the momentum regions) we encounter ratios of Γ functions such as $\Gamma(6 + \beta)/\Gamma(7 + \beta)$, which scale as $1/\beta$ for large β , but $\beta \sim 10$ is not quite large enough to make this manifest.

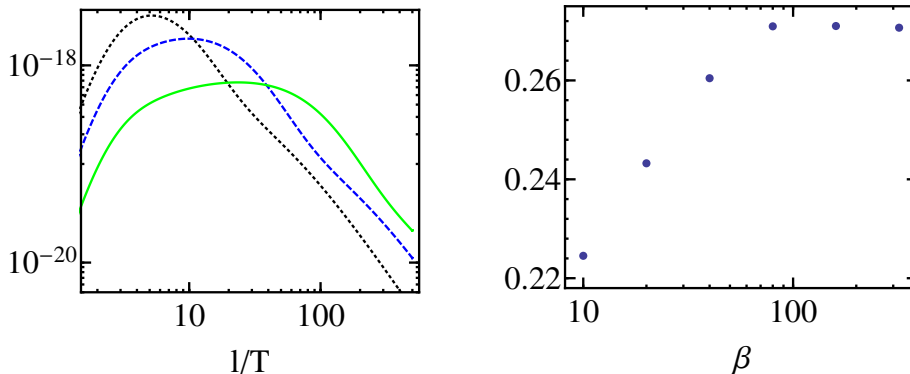


Figure 5.10: *Left:* Absolute value of the integrand for the diagram H1 with zero-mode subtracted Higgs propagator as a function of the loop momentum l . The curves correspond to $\beta = 10$ black (dotted), 40 blue (dashed) and 160 green (solid). The KK scale was set to $T = 1$ TeV. *Right:* KK Higgs contribution to the dipole operator as a function of β normalised to the $\beta \rightarrow \infty$ limit of the Higgs zero-mode contribution.

in the custodially protected model. Here we again dropped the suppressed off-shell terms similar. The numerical values of the coefficients are

$$\mathcal{A}_{\text{KK}} = 0.46(0.04) \quad \mathcal{A}_{\text{KK}}^{cs} = 1.4(0.2) \quad \mathcal{B}_{\text{KK}}^{cs} = 0.1(0.05), \quad (5.88)$$

where the number in parenthesis shows the estimated error due to the extrapolation to $\beta = \infty$. The sizeable relative uncertainty in $\mathcal{B}_{\text{KK}}^{cs}$ comes from large cancellations among the various contributions to the coefficient. In the minimal (custodial) mode the KK contribution is about 50% (75%) of the zero-mode contribution.

Note that by writing (5.86) and (5.87) we tacitly assumed that Higgs Kaluza-Klein contribution is roughly independent of the 5D mass parameters and therefore allowed for compact analytic expressions. Nevertheless there is a nontrivial dependence of the KK contribution on the 5D mass parameters; in particular for diagrams with a Higgs emission from an external line. In the lepton sector this effect is quite small especially when compared to the sizeable numerical uncertainties; we therefore neglected it in [55]. In the quark sector the wide range of 5D masses leads to more noticeable effects; since we can only determine these numerically we do not give an explicit expression. To give an idea of the potential size: the figure 5.11 shows the additional effect of the mass dependence (without numerical uncertainties) for the diagram. One can see that the effect is indeed of the order a few percent for leptons, but can potentially be of $\mathcal{O}(1)$ for quarks. It is therefore not feasible to use a simple analytic approximation as was done in the lepton sector.

Furthermore, we need to include KK Higgs corrections to the off-shell contributions to the Wilson coefficients. Again these terms are not necessarily suppressed in the quark sector, as the third generation Yukawa couplings are sizeable. However, we can only determine this contribution analytically for the Higgs zero-mode and not for the Higgs KK modes; it is only accessible numerically, but is quite small, only about 25% of the corresponding zero-mode effect.

We therefore treat the whole effect of Higgs KK modes similarly to how the gauge-contribution is handled. Here we only remark that the total effect of the KK modes is smaller than the

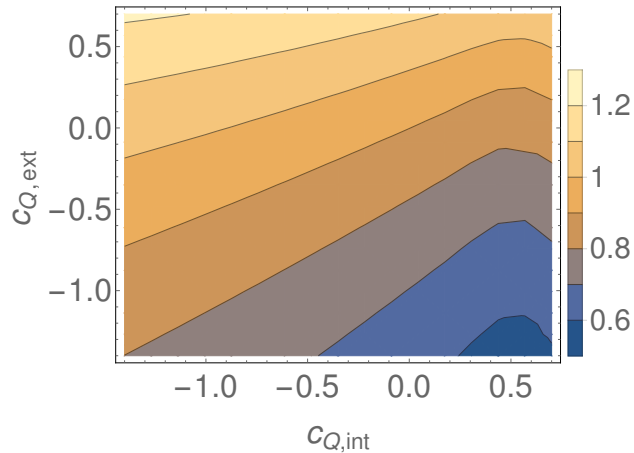


Figure 5.11: Illustration the additional dependence of the 5D mass parameter dependence of the KK Higgs contribution for the diagram on the right. $c_{Q_{int}}, c_{Q_{ext}}$ are the 5D masses of the internal doublet propagator and the external doublet zero-mode. For leptons generally only a small region in the upper right corner ($c_Q \sim 0.4 - 0.7$) would be required.

effect of the Higgs zero-mode but not parametrically so, see also [55, 79].

Note that the relative high uncertainties are generated mainly due to the implementation of the numerical integrals inside Mathematica, as the C++ code used for the gauge exchange has severe problems to evaluate even one integrand point. The main problem of the numerical evaluation of the Higgs KK diagrams is caused by the zero mode subtracted Higgs propagator, which contains Bessel functions of the type \mathcal{I}_β and \mathcal{K}_β . These Bessel functions can evaluate to extremely large numbers even for moderate values of β . The right chirality term of the topology class HT6 only could not be computed in Mathematica, because the integration did not terminate within a reasonable period of time to useful numerical precision. To tackle this diagram we had to dissect the Higgs propagator into potentially large terms and then add them up in a controlled way. This allowed us to evaluate the integrand up to loop momenta of $600 T$ in C++, which enabled us to perform the integration via the CUBA package. To this end we employed a integration routine inspired by the gauge invariance programs, which are able to compute the on-and-off shell terms.

To conclude this chapter we remark that irrespective of the Higgs localisation, the dipole coefficients a_{ij}^H generated by Higgs exchange is in general misaligned relative to the mass matrix in the lepton as well as the quark sector. For the bulk Higgs case the numerically dominant terms scale as $YY^\dagger Y$ in both the minimal and custodially protected RS model. After rotation to the mass basis this potentially generates large flavour violating transitions. For the same reason, even after the rotation to the mass basis, unlike the gauge-boson contribution, the Higgs contribution depends strongly on the values of the 5D bulk mass parameters and the 5D Yukawa matrices. It usually increases with the magnitude of the Yukawa matrix entries.

5.3 Dimension-eight operators

The effects of dimension-eight operators are suppressed relative to the dimension-six ones by a factor of $\mathcal{O}(v^2/T^2)$ and therefore negligible. However, for LFV observables this counting can be numerically upset, as noted in [32], since the leading dimension-6 contribution to the dipole operator from gauge-boson exchange is suppressed by a factor of 30-50 due to the near-alignment discussed above and in [28, 54]. Relevant dimension-eight effects can arise directly from dimension-eight operators and indirectly from v^2/T^2 corrections to the field rotation to the mass basis.

The first class corresponds to the descendant $(\bar{L}_i \sigma^{\mu\nu} E_i) \Phi X_{\mu\nu} \Phi^\dagger \Phi$ ($X = B, W$) of the dimension-six dipole operator $(\bar{L}_i \sigma^{\mu\nu} E_i) \Phi X_{\mu\nu}$, which after EWSB give rise to the same dipole vertex structure. However, the dimension-eight operator has a coefficient function proportional to $YY^\dagger Y$ even for the internal gauge-boson exchange contribution, and does not suffer from the alignment suppression of terms proportional to Y . Depending on the value of T , the dimension-eight contribution may then be the dominant source of flavour violation. This is relevant only for the case of an exactly brane localised Higgs in the minimal RS model, where the contributions to the dimension-six dipole Wilson coefficient cubic in the Yukawa coupling due to Higgs exchange are also suppressed (see previous subsection).

The second class of dimension-eight effects arises from the fact that the tree-level relation

$$\frac{v}{\sqrt{2}} U_{ij}^\dagger \sqrt{\frac{1-2c_{L_j}}{1-\epsilon^{1-2c_{L_j}}}} Y_{jk} \sqrt{\frac{1+2c_{E_k}}{1-\epsilon^{1+2c_{E_k}}}} V_{kn} = \text{diag}\{m_e, m_\mu, m_\tau\} \quad (5.89)$$

that defines the rotations U, V to the mass basis [20] receives corrections due to multiple Higgs vev insertions.³ The diagonalisation condition has the form

$$\frac{v}{\sqrt{2}} U_{ij}^\dagger \sqrt{\frac{1-2c_{L_j}}{1-\epsilon^{1-2c_{L_j}}}} \left[Y - \frac{v^2}{6T^2} YY^\dagger Y \right]_{jk} \sqrt{\frac{1+2c_{E_k}}{1-\epsilon^{1+2c_{E_k}}}} V_{kn} = \text{diag}\{m_e, m_\mu, m_\tau\}, \quad (5.90)$$

cf. (3.39). The modified U and V field rotation matrices applied to the Lagrangian (3.2) generate an additional source of LFV which formally enters at the same level in the v/T counting as dimension-eight operators, which can be taken into account by the substitution

$$a_{ij}^g \rightarrow a_{ij}^g + \frac{v^2}{6T^2} a_{ij}^g \Big|_{Y \rightarrow YY^\dagger Y} \quad (5.91)$$

The direct effect of the dimension-eight operators is more difficult to estimate. We have to evaluate the contributions to the dipole-like operators that appear at the dimension eight level, i.e.,

$$\mathcal{L}^{\text{dim-8}} \supset \frac{1}{T^4} a_{ij}^{B, \text{dim-8}} (\bar{L}_i \Phi \sigma^{\mu\nu} E_i) B_{\mu\nu} \Phi^\dagger \Phi + \frac{1}{T^4} a_{ij}^{W, \text{dim-8}} (\bar{L}_i \tau^A \Phi \sigma^{\mu\nu} E_i) W_{\mu\nu}^A \Phi^\dagger \Phi. \quad (5.92)$$

The computation of the electromagnetic dipole coefficient $a_{ij}^{\text{dim-8}} = \cos \Theta_W a_{ij}^{B, \text{dim-8}} - \sin \Theta_W a_{ij}^{W, \text{dim-8}}$ would require the computation of roughly 150 different diagrams in the 5D theory for the minimal RS model alone.

Fortunately, only some of these diagrams actually contribute. For the following we consider only the *minimal* RS model with an exactly brane-localised Higgs. For the other Higgs localisations the dimension-six dipole is always dominant and dimension-eight terms

³The square root factors arise from the explicit expressions for the lepton zero-mode profiles.

CHAPTER 5. LOOP-INDUCED DIPOLE OPERATORS

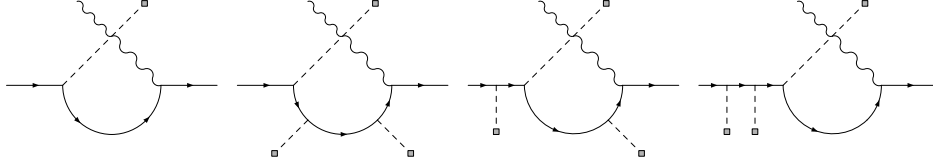


Figure 5.12: Example of a diagram contributing to the matching onto the dimension-six dipole operator and several related diagrams that contribute to the dimension-eight operator.

are negligible as discussed above. We then have two fundamentally different contributions: from the so-called wrong-chirality Higgs couplings (WCHC) and from the ordinary Higgs couplings to lepton modes with the same chirality as the SM zero modes. It turns out that for the exactly brane-localised Higgs the WCHC contribution can be computed analytically and is simply given by

$$a_{ij}^{\text{dim-8, WCHC}} = -\frac{1}{3} a_{ij}^g \Big|_{Y \rightarrow Y Y^\dagger Y} \quad (5.93)$$

in terms of the dimension-six gauge-boson exchange contribution.

To illustrate how this result arises let us consider the left-most diagram in Figure 5.12 (W8 in the notation of [28]), which contributes to the matching of the a_{ij}^W coefficient. There are 10 ways to add two additional external Higgs lines to the fermion line. However, since δ/T (δ being the Higgs localisation regulator) is much smaller than the dimensional regulator or, equivalently, than the inverse loop momentum cut-off, we find that only the three diagrams shown to the right in Figure 5.12 give a non-vanishing WCHC contribution for $\delta \rightarrow 0$. In each case the integrals over the Higgs vertices can be taken analytically. In the above example the WCHC contributions of the two right-most diagrams cancel, and the remaining diagram can be expressed in terms of the associated dimension-six diagram as shown in (5.93). Similarly the descendants of all other dimension-six diagrams can be shown to satisfy (5.93).

Hence the effect of the WCHC can be included via the redefinition

$$a_{ij}^g \rightarrow a_{ij}^g - \frac{v^2}{6T^2} a_{ij}^g \Big|_{Y \rightarrow Y Y^\dagger Y} \quad (5.94)$$

where we used that the Higgs fields will assume their vacuum expectation value ($\Phi^\dagger \Phi \rightarrow v^2/2$). Combining this with (5.91), we find that the direct and indirect contribution cancel. That is, at the dimension-eight level the WCHCs do not generate sizeable flavour-changing transitions by lifting the misalignment suppression and can be ignored.

This leaves us with the dimension-eight contributions that have no WCHCs. In the minimal model as defined in [28] there are no such contributions from the diagrams with non-abelian vertices. Then there are only seven non-vanishing diagrams that involve an internal W boson, but about 50 diagrams with a hypercharge boson. Fortunately, the limited particle content of the minimal model allows us to recast the expressions of all diagrams in the form of the original dimension-six diagram with modified fermion lines. For instance, the second diagram in Figure 5.12 has terms without WCHCs, but differs from the original diagram only by the two additional (zero-momentum) Higgs insertions that modify one fermion propagator. This can easily be calculated as the Higgs vertices can be treated analytically. Since the flavour-dependence of the fermion propagators (excluding zero-modes) is relatively mild, one can use the single-flavour approximation, where the Yukawa matrices are the only flavour-dependent quantities. It is then straightforward to

5.3. DIMENSION-EIGHT OPERATORS

compute the contribution to the dimension-eight coefficients. We find

$$a_{ij}^{\text{dim-8}} \approx -0.4 a_{ij}^g \Big|_{Y \rightarrow YY^\dagger Y} . \quad (5.95)$$

This size is in agreement with the estimate given on the basis of a subset of diagrams in [32], where the non-abelian contribution was found to be $a_{ij}^{W, \text{dim-8}} \approx -0.31 a_{ij}^W \Big|_{Y \rightarrow YY^\dagger Y}$. The minimal model requires a KK scale $T > 4$ TeV in order to pass the constraints set by electroweak precision observables [23]. Hence the dimension eight contribution to α_{ij} is suppressed by an additional factor v^2/T^2 of at least $1/500$. We therefore neglect the contribution of the dimension-eight terms to the off-diagonal elements of α_{ij} , since it is smaller than the effect of the Barr-Zee diagrams which also feature three Yukawa couplings without the need to take the dimension-eight term into account.

For the custodially protected model the dimension-eight coefficient would be much harder to compute. Not only does the number of non-trivial Feynman diagram topologies increase significantly, but the larger particle content leads to numerous non-vanishing possibilities to assign the various fermion species to each topology. However, independent of the Higgs localisation there always exists an unsuppressed dimension-six contribution proportional to $YY^\dagger Y$, hence the dimension-eight terms are never relevant.

Chapter 6

Phenomenology

In chapter 3 the main observables of interest a_μ , $\mu \rightarrow e\gamma$, $\mu \rightarrow 3e$, $\mu N \rightarrow \mu N$ and $\bar{B} \rightarrow X_s\gamma$, were all expressed in terms of Wilson coefficients of the dimension six SM effective theory. That was followed by the matching of the Wilson coefficients in chapter four and five. We are now equipped to calculate a_μ and all branching fractions of the observables for a specific set of 5d parameters.

In the first section we begin our analysis by computing some rough estimates of different Wilson coefficient contributions to the considered branching fractions processes. Afterwards we perform a numerical scan over a set of 5d parameters. To this end we first concentrate on the RSc contribution to the muon g-2 moment, which was the first for this thesis computed low energy loop-induced process. Following this we focus next on the scan over the lepton flavour violation (LFV) sector. Here we concentrate mainly on the decays $\mu \rightarrow e\gamma$, $\mu \rightarrow 3e$ and the muon conversion in the presence of nuclei. Here we ignore at first the strong bound generated by the measurements of the electron dipole moment [120]. However we consider later on the effects of an applied EDM bound on the LFV observables. In the last part of the numerical analysis we then focus on the the inclusive quark decay $\bar{B} \rightarrow X_s\gamma$, before concluding this chapter with a summary of all findings.

6.1 Estimates

We first consider the effect of the dimension-six dipole operators, where we distinguish two different contributions: from the Higgs-exchange diagrams, which involve three Yukawa matrices, and from gauge-boson exchange, which involves only one. We concentrate completely on the leptonic sector as the main conclusions extracted for $\mu \rightarrow e\gamma$ can be transferred to the $\bar{B} \rightarrow X_s\gamma$ branching fraction, because both processes are mediated by dimension six dipole operators.

The gauge contribution leads to naturally suppressed flavour-violating couplings, whereas the Higgs contribution does not have a built-in flavour protection. For not too small Yukawa couplings the Higgs contribution is dominant. We mainly focus on $\mu \rightarrow e$ transitions and the muon g-2, for which the dipole coefficients α_{12} , α_{21} and α_{22} are relevant.

To obtain an estimate of the Higgs-exchange contribution let us start with Wilson coefficient [see (5.70) and (5.87)]

$$a_{ij}^H = \frac{Q_\mu e}{192\pi^2} \frac{T^3}{k^4} \cdot f_{L_i}^{(0)}(1/T) [(2 + \mathcal{A}_{\text{KK}}^{cs}) Y Y^\dagger Y + \mathcal{B}_{\text{KK}}^{cs} Y_\nu Y_\nu^\dagger Y]_{ij} g_{E_j}^{(0)}(1/T) \quad (6.1)$$

CHAPTER 6. PHENOMENOLOGY

in the custodially protected model with a bulk Higgs. An analogous expression holds in the minimal model [(5.68) and (5.86)]. For an exactly brane-localised Higgs, a_{ij}^H is of similar size as above for the custodially protected model, cf. (5.70), but suppressed in the minimal model due to the absence of the numerical dominant wrong chirality terms. Now we recall that the relation of fermion zero-mode profiles, the 5D Yukawa matrix and SM Yukawa matrix (before rotation into the flavour basis) is given by

$$y_{ij} = \frac{T^3}{k^4} f_{L_i}^{(0)}(1/T) Y_{ij} g_{E_j}^{(0)}(1/T). \quad (6.2)$$

If the fermion mass hierarchy of the diagonalised SM Yukawa matrix is carried democratically by left- and right-handed fermion modes, i.e.

$$y_{ij} \sim \frac{\sqrt{m_i m_j}}{v/\sqrt{2}}, \quad (6.3)$$

we arrive at the estimate

$$a_{ij}^H \sim \frac{Q_\mu e \sqrt{2m_i m_j}}{192\pi^2 v} [(2 + \mathcal{A}_{KK}^{cs}) Y_\star^2 + \mathcal{B}_{KK}^{cs} Y_{\nu,\star}^2], \quad (6.4)$$

where we assume that

$$Y_\star^2 \equiv \frac{[Y Y^\dagger Y]_{ij}}{Y_{ij}} \quad Y_{\nu,\star}^2 \equiv \frac{[Y_\nu Y_\nu^\dagger Y]_{ij}}{Y_{ij}} \quad (6.5)$$

are approximately independent of ij ("anarchy"). For anarchic Yukawa matrices we also expect that the rotation matrices U and V follow the same hierarchy and hence, barring accidental cancellations, that $\alpha_{12} \sim a_{21}$. Further using that $\mathcal{A}_{KK}^{cs} \approx 1.4 \gg \mathcal{B}_{KK}$ we obtain¹

$$\begin{aligned} \alpha_{12}^H &\sim \frac{5Q_\mu e \sqrt{m_e m_\mu}}{192\pi^2 v} Y_\star^2 \\ \alpha_{22}^H &\sim \frac{5Q_\mu e m_\mu}{192\pi^2 v} Y_\star^2 \end{aligned} \quad (6.6)$$

which yields

$$\Delta a_{\mu|\text{Higgs dipole}} \sim 8.33 \cdot 10^{11} \times \frac{1 \text{ TeV}^2}{T^2} Y_\star^2 \quad (6.7)$$

$$\text{Br}(\mu \rightarrow e\gamma)_{|\text{Higgs dipole}} \sim 5 \cdot 10^{-9} \times \frac{1 \text{ TeV}^4}{T^4} Y_\star^4. \quad (6.8)$$

If the dipole also dominates $\mu \rightarrow 3e$ one can combine (3.16) and (3.18) to obtain the relation

$$\frac{\text{Br}(\mu \rightarrow 3e)}{\text{Br}(\mu \rightarrow e\gamma)} = \frac{2\alpha_{\text{em}}}{3\pi} \left[\log \frac{m_\mu}{m_e} - \frac{11}{8} \right] \approx 0.006, \quad (6.9)$$

which translates into an estimate of

$$\text{Br}(\mu \rightarrow 3e)_{|\text{Higgs dipole}} \sim 3 \cdot 10^{-11} \times \frac{1 \text{ TeV}^4}{T^4} Y_\star^4. \quad (6.10)$$

¹Our estimates always yield $\alpha_{21} \sim \alpha_{12}$, hence we only give α_{12} explicitly.

For muon conversion one finds

$$\text{Br}^{\text{Au}}(\mu N \rightarrow eN)_{|\text{Higgs dipole}} \sim 1.5 \times 10^{-11} \times \frac{1 \text{ TeV}^4}{T^4} Y_\star^4. \quad (6.11)$$

We emphasise that these are crude estimates. Even in the anarchic case the random phases of the different elements can lead to cancellations or add coherently. However, they provide useful guidance to the results of the numerical scan discussed below.

The Barr-Zee contribution is similar to the Higgs contribution, since the dominant contribution to the η_{ij} Wilson coefficient is also proportional to a product of three Yukawa factors. Comparing the prefactors in (3.41) we find that the Barr-Zee contribution to the dipole coefficient is smaller by a factor of about 170 than the contribution from the 5D Higgs loops. Thus we expect a $\mu \rightarrow e\gamma$ branching fraction of about

$$\text{Br}(\mu \rightarrow e\gamma)_{|\text{BZ}} \sim 2 \cdot 10^{-13} \times \frac{1 \text{ TeV}^4}{T^4} Y_\star^4, \quad (6.12)$$

if only the BZ contribution existed. The BZ contribution to the other processes is also smaller by a factor of about 170^2 .

Due to the Y_\star^4 dependence the Higgs-exchange induced dipole operator is less important for small Yukawa coupling. In this case, and also for the special case of the brane-localised Higgs in the minimal RS model, the dipole operator generated by gauge-boson exchange becomes crucial. We do not have an analytical expression for the gauge-boson contribution, but we know that there would be no flavour violation from it, if the function \mathcal{A}_{ij} in (5.17) was independent of ij . The 5D mass parameters must decrease with the absolute values of the Yukawa couplings in order to guarantee the correct values for the SM masses fermion masses. \mathcal{A}_{ij} varies more strongly for smaller absolute values of the 5D mass parameters, see Figure 5.8, and therefore the flavour-changing gauge-boson contribution should increase with decreasing Yukawa coupling. To verify this we fix the Yukawa matrix structure, that is the ratios of all matrix elements, and scale the maximal entry Y_{max} from 2 to 0.3. For simplicity we assumed symmetric 5D mass parameters $c_{L_i} = -c_{E_i}$. The resulting $\mu \rightarrow e\gamma$ branching fraction from a_{ij}^g alone in the minimal model is shown in Figure 6.1 (left). The precise value of $\text{Br}(\mu \rightarrow e\gamma)$ obviously depends on the arbitrarily chosen Yukawa matrix structure, but the variation with the size Y_\star of the Yukawa couplings is not very large compared to the fourth-power law of the Higgs-exchange contribution. For the Yukawa matrix used in Figure 6.1 we find a $\mu \rightarrow e\gamma$ branching fraction of a few $\times 10^{-12}$.

This agrees with the estimate based on the functional form of the gauge-boson induced dipole coefficient a_{ij}^g . The numerical value of the Wilson coefficient is [28, 54]

$$a_{ij}^{\text{gauge}} \approx -6(19) \cdot 10^{-4} y_{ij}. \quad (6.13)$$

The value without (in) parenthesis is valid for the minimal (custodial) model and is independent of the details of the Higgs localisation. y_{ij} is the 4D Yukawa matrix in the flavour eigenbasis. The matrix relation $a^{\text{gauge}} \propto y$ is only violated by corrections of about (2-3)% as discussed in Section 5. This violation is the source of charged LFV as it introduces small off-diagonal elements in the dipole coefficients α_{ij} in the mass eigenbasis after EWSB. Using (6.3) and applying a factor 2/100 for the 2% of misalignment between y_{ij} and a_{ij}^g , we estimate

$$\alpha_{A,12} \sim 2.6(8.1) \cdot 10^{-8} \times \frac{2}{100} \quad (6.14)$$

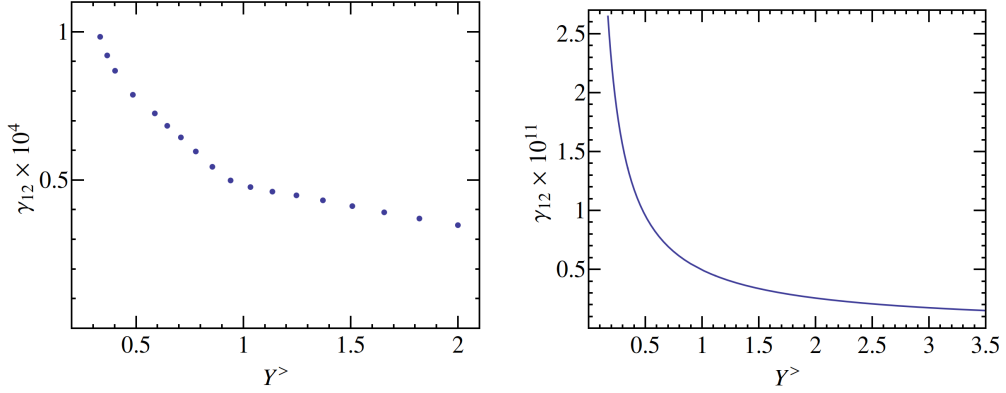


Figure 6.1: *Left*: Gauge contribution to $\text{Br}(\mu \rightarrow e\gamma)$ ($T = 1$ TeV) for fixed Yukawa structure as a function of the absolute Yukawa coupling size. *Right*: The Wilson coefficient γ_{12}^1 following the approximation (6.18) as a function of Yukawa coupling size for $T = 1$ TeV. The $\mathcal{O}(m_\mu/m_\tau)$ term is not included.

for the coefficient relevant to $\mu \rightarrow e$ transitions. Again, we regard this as a rough estimate, since there may be cancellations when the rotation into the mass basis is performed. We then find:

$$\text{Br}(\mu \rightarrow \bar{e}\gamma)|_{\text{gauge dipole}} \sim 0.5(5) \cdot 10^{-11} \times \frac{1\text{TeV}^4}{T^4} \quad (6.15)$$

$$\text{Br}(\mu \rightarrow \bar{e}ee)|_{\text{gauge dipole}} \sim 0.3(3) \cdot 10^{-13} \times \frac{1\text{TeV}^4}{T^4} \quad (6.16)$$

$$\text{Br}^{\text{Au}}(\mu N \rightarrow eN)|_{\text{gauge dipole}} \sim 0.2(2.2) \cdot 10^{-13} \times \frac{1\text{TeV}^4}{T^4} \quad (6.17)$$

Note that this contribution is independent of the typical size of anarchic Yukawa coupling up to the $\mathcal{O}(1)$ variation shown in Figure 6.1. It is typically smaller than the Higgs contribution, but provides the “gauge-boson floor” to the dipole coefficient, since it is less sensitive to 5D model parameters than the Higgs contribution and always present. In the custodially protected model the rate is a factor of 10 larger than in the minimal model.

The previous estimates were based on the assumption that the dipole operator dominates the LFV amplitudes. This is not always the case, especially for the $\mu \rightarrow 3e$ and muon conversion process. Next, we therefore consider the impact of the four-fermion and fermion-Higgs operators, which are generated at tree-level. In both cases the dimension-six Wilson coefficients are independent of the 5D Yukawa matrices. However, a dependence on the Yukawa matrices enters through the rotation to the mass basis after EWSB. For illustration we consider the operator $(\bar{E}_i \gamma^\mu E_j) \Phi^\dagger i \overleftrightarrow{D}_\mu \Phi$ with Wilson coefficient $c_{ij}^1 = c_i^1 \delta_{ij}$ and restrict ourselves to the minimal model. For all three muon flavour-violating processes the relevant matrix elements are $V_{1j}^\dagger c_{jk}^1 V_{k2}$. Flavour violation arises, because c_i^1 depends on the bulk mass parameter c_{E_i} , hence c_{ij}^1 while diagonal is not proportional to the unit matrix in flavour space. We can estimate $V_{1j}^\dagger c_{jk}^1 V_{k2}$ by making use of hierarchical fermion zero-mode functions. Assuming $f_{E_1}(1/T) \ll f_{E_2}(1/T) \ll f_{E_3}(1/T)$ and symmetric mass parameters we can employ the rough estimate $|V_{ij}| \sim \min(\sqrt{m_i/m_j}, \sqrt{m_j/m_i})$ with m_i being the SM

lepton masses to obtain

$$\gamma_{12} = V_{1j}^\dagger c_{jk}^1 V_{k2} \sim \sqrt{\frac{m_e}{m_\mu}} (c_2^1 - c_1^1 + \mathcal{O}(m_\mu/m_\tau)). \quad (6.18)$$

We can use this formula to study the dependence of γ_{ij}^a on the size of the 5D Yukawa couplings. Since the product of Yukawa matrix and 5D fermion zero-mode profiles must reproduce the SM mass matrix to leading order in v/T , the 5D profiles and therefore the 5D mass parameters are correlated with the Yukawa matrix. The simplest estimate (assuming symmetric mass parameters) yields the correlation $1/\sqrt{Y_\star} \sim f_{E_i}^{(0)}(1/T)$. Since the c_i^a Wilson coefficients arise from a coordinate integral over a single fermion-gauge-boson vertex they will roughly scale as $[f_{E_i}^{(0)}(1/T)]^2$, that is $1/Y_\star$. This behaviour was already observed and explained in [31]. The right panel of Figure 6.1 shows γ_{12}^1 as a function of Y_\star (keeping the lepton masses fixed). The curve can be fitted by $Y_\star^{-0.94}$ confirming the above scaling. This scaling is quite general, although if the mass hierarchy is mainly driven by the right-handed modes, the mass factors in the estimate (6.18) must change to account for the change in the relation (6.3).

Similar estimates can be obtained for the four-fermion operator coefficients. Here we have terms with different dependencies on flavour. The Wilson coefficient b_{ij}^{LE} of $(\bar{L}_i \gamma_\mu L_i) (\bar{E}_j \gamma^\mu E_j)$ has three contributions denoted by b_0 , b_1 and b_2 , see (4.3). b_0 does not depend on the 5D masses and hence does not contribute to flavour-changing processes. b_1 depends on a single bulk mass parameter and has the same scaling $\propto 1/Y_\star$ as the c^a Wilson coefficients. The b_2 function depends on two bulk mass parameters and scales roughly as $1/Y_\star^2$. However, as discussed below (4.13), for light leptons this term is suppressed and not relevant. This would be different for processes involving fermions with zero-modes that are IR brane localised such as the (right-handed) top quark, in which case the ratio of exponentials in b_2 no longer compensates the logarithmic enhancement factor and b_2 becomes the dominant term in (4.3).

From (3.41), (3.25ff) and (3.30ff) we see that the four-fermion coefficients usually appear in combination with the coefficients of the Higgs-lepton operators. For a typical RS model parameter point, which reproduces the lepton masses, the Higgs-lepton operator coefficients are larger by a factor $\log \epsilon$ relative to the four-fermion operator coefficients. This allows us to use (6.18) to estimate the effect of the tree-level operators on the generically tree-dominated LFV observables. We find

$$\text{Br}(\mu \rightarrow \bar{e}ee) \sim \text{few} \cdot 10^{-12} \times \frac{1\text{TeV}^4}{T^4} \frac{1}{Y_\star^2} \quad (6.19)$$

$$\text{Br}^{\text{Au}}(\mu N \rightarrow eN) \sim \text{few} \cdot 10^{-9} \times \frac{1\text{TeV}^4}{T^4} \frac{1}{Y_\star^2}, \quad (6.20)$$

where we used the parameters given in Table 6.1. We stress again that these numbers are rough estimates, which depend strongly on the precise structure of the flavour rotation matrices V and U . Thus we have three separate contributions to $\mu \rightarrow \bar{e}ee$ and muon conversion with different dependence on the size of the 5D anarchic Yukawa coupling (Y_\star^4 , Y_\star^0 , Y_\star^{-2}).

6.2 Numerical analysis

In the previous section we attempted to give an idea about the size and the relative importance of the various contributions to our three main LFV observables and the Higgs

CHAPTER 6. PHENOMENOLOGY

m_μ	0.105658 GeV	[121]	m_e	$5.10998 \cdot 10^{-4}$ GeV	[121]
s_W^2	0.231	[121]	M_H	125.7 GeV	[121]
M_Z	91.187 GeV	[121]	M_W	80.385 GeV	[121]
m_t	173 GeV	[121]	Γ_μ	$2.99598 \cdot 10^{-19}$ GeV	[121]
$\mathcal{D}[\text{Au}]$	0.189	[95]	$\mathcal{S}^p[\text{Au}]$	0.0614	[95]
$\mathcal{S}^n[\text{Au}]$	0.0918	[95]	$\mathcal{V}^p[\text{Au}]$	0.0974	[95]
$\mathcal{V}^n[\text{Au}]$	0.146	[95]	$\Gamma_{\text{capture}}^{\text{Au}}$	$8.71 \cdot 10^{-18}$ GeV *	[122, 123]
$\mathcal{D}[\text{Al}]$	0.0362	[95]	$\mathcal{S}^p[\text{Al}]$	0.0155	[95]
$\mathcal{S}^n[\text{Al}]$	0.0167	[95]	$\mathcal{V}^p[\text{Al}]$	0.0187	[95]
$\mathcal{V}^n[\text{Al}]$	0.0173	[95]	$\Gamma_{\text{capture}}^{\text{Al}}$	$4.64 \cdot 10^{-19}$ GeV	[123]
$f_{V_p}^u$	2		$f_{V_p}^d$	1	
$f_{V_n}^u$	1		$f_{V_n}^d$	2	
f_p^u	0.018		f_p^d	0.034	
f_n^u	0.016		f_n^d	0.038	
f_n^s	0.043		f_n^s	0.043	

Table 6.1: Input parameters for the numerical analysis. For the couplings of scalar quark currents to the nucleons we use the results of [97] and fix the value of the nucleon-pion σ -term to 50 MeV. The * indicates that we use the average of the values given in the references.

contribution to the muon g-2. While such estimates are useful to understand the rough dependence of our results on the input parameters, especially the Yukawa coupling size, they cannot replace a study of the full parameter dependence. To this end we next perform a numerical scan over the “generic” parameter space. We analyse four RS models: the minimal RS model (as defined in [28]) as well as a custodially protected model (as defined in chapter two), each with either an exactly brane-localised or a bulk Higgs include in chapter two) its KK excitations in the $\beta \rightarrow \infty$ limit. We refer to these models as $\mathcal{M}I$ (minimal, bulk), $\mathcal{M}II$ (minimal, exactly brane-localised), $\mathcal{C}I$ (custodial, bulk) and $\mathcal{C}II$ (custodial, exactly brane-localised).

The 5D input parameters needed for the numerical evaluation of the dimension-six Wilson coefficients are the 5D Yukawa matrices Y, Y_d, Y_u (and Y_ν in the custodially protected model), the 5D bulk mass parameters $c_\psi = M_\psi/k$ of the leptons and quark fields and the KK scale T . In case of the exactly brane-localised Higgs the wrong-chirality Yukawa couplings can in principle differ from the “standard” correct-chirality Yukawa couplings, but for simplicity we assume them to be equal. Since we do not want to give up the idea of “natural” Yukawa matrices, we further assume that the Yukawa entries are $\mathcal{O}(1)$ and anarchic. To illustrate how the size of the 5D Yukawa matrix entries affects the different observables, we adopt two scan strategies for the flavour violating sector. In both the modulus of the matrix elements is larger than 0.1, but in the first (second) scan the maximal modulus Y_{max} is bounded by 0.5 (3 for the second). Further, we require that the derived fundamental low-energy parameters, such as the measured values of lepton masses and quark masses, are reproduced by chosen sets of 5D parameters. In practice, we randomly generate 5D Yukawa matrices within the above mentioned constraints, and then fix the 5D mass parameters c_{ψ_i} such that the correct lepton and quark masses are obtained. Note that for the analysis of the Higgs contribution to the muon g-2 we followed a different scan strategy. Here we generated

5d parameter sets with Yukawa moduli in the range (0.1, 1/3), (1/3,3) and (3, 10) with T fixed on the value $T=1$ TeV.

Note that we only require that all (Dirac) neutrino masses are below 0.1 eV and that their mass splitting does not violate the bounds from neutrino oscillation; we do not require that the PMNS matrix is reproduced. Recall that the dependence on the neutrino Y_ν , which only enters in terms with at least three Yukawa factors, is quite small as the numerical dominant wrong-chirality Y_ν terms drop for zero-mode contributions. In the bulk Higgs model the Y_ν is mediated purely by the KK excitations of the bulk Higgs field. For fixed value of the KK scale T and given scan strategy, we generate about $2 \cdot 10^5$ Yukawa matrices. In the quark sector we additionally generate a set of $\sim 1 \cdot 10^5$ Yukawa matrices, where also KK scale T is chosen randomly between 1 TeV and 8 TeV. The generation of the Yukawa matrix data sets is done using Mathematica .m files which are distributed on the T30 theory computer cluster via the Sun Grid Engine. The packages, which create the Lepton Yukawa sets, are organised in such way, that they create two hundred sets of Yukawas, which are saved in a single file. Hence the generation of $2 \cdot 10^5$ for a specific size of T and Y_{\max} needs exactly 1000 jobs, which can be done in less than 10 minutes due to the Cluster being able to handle more than 1000 mathematica kernels at once. The generation of the quark Yukawa matrices on the other hand is at least a factor 100 slower. That is due to algorithm, which tries not only to generate the correct 4D mass spectrum but also the CKM matrix to a good approximation. The slowness of the generation of the quark Yukawa matrices is independent whether the scale T has been set to definite value or is being generated randomly.

For each of the saved Yukawa sets we calculate the Wilson coefficients. This yields then the custodial protected RS model contribution to the muon $g-2$ and the branching fractions of $\mu \rightarrow e\gamma$, $\mu \rightarrow e$ conversion, $\mu \rightarrow 3e$, $\tau \rightarrow \mu\gamma$, and $\tau \rightarrow 3\mu$ in the lepton sector. In the quark sector we evolve the Wilson coefficients by solving the RGE equation exactly and then extract the branching fraction $\bar{B} \rightarrow X_s\gamma$. The practical implementation of this process was also done by Mathematica .m files. Each Mathematica package reads exactly one Yukawa data set file and then evaluates all observables for each Yukawa and saves the result in a new file. Using the T30 theory computer cluster this process can be massively parallelised via the Sun Grid Engine. Here the programs, which compute the quark Wilson coefficients, are also slower than the leptonic versions, but only due to the loading process of the larger gauge boson numerical grids.

The required low-energy parameters are shown in Table 6.1. We also added the material constants of aluminium, which serves as the target for the next generation of muon conversion experiments.

6.2.1 Muon $g-2$

The gauge contributions are expected to be virtually independent of our parameter choice, as \mathcal{A}_{ij} , cf. (5.17), is approximately mass-parameter independent. The left panel of figure 6.2 shows the result for Δa_μ^g for a fixed value of $T = 1$ TeV. The result for $T = 4$ TeV is shown in the right panel. The histograms are generated from each $2 \cdot 10^5$ parameter sets. The distribution is centred around $2.72 \cdot 10^{-10}$ for $T = 1$ TeV while $T = 4$ TeV lead to a central value of $1.63 \cdot 10^{-11}$. This is in line with the typical scaling $\Delta a_\mu^{\text{gauge}} \propto \frac{1}{T^2} \times \ln k/T$. The model-independent gauge contribution to $g_\mu - 2$ in the custodially protected RS model can thus be reliably estimated via

$$\Delta a_\mu^g \approx 2.72 \times 10^{-10} \left(\frac{1 \text{ TeV}}{T} \right)^2 \quad (6.21)$$

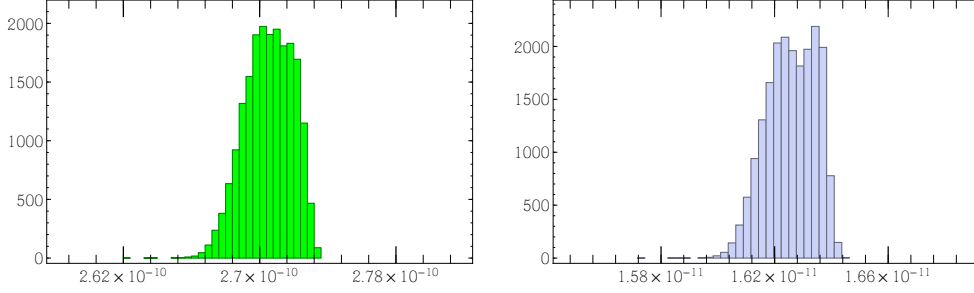


Figure 6.2: *left panel*: Histogram of the contribution of the gauge diagrams Δa_μ^g to the anomalous magnetic moment a_μ for fixed $T = 1$ TeV. *right panel*: Same for $T = 4$ TeV.

for any phenomenologically relevant value of T .

Comparing to the result in the minimal model [28], $\Delta a_\mu^{\min} \approx 0.88 \cdot 10^{-10} (1 \text{ TeV})^2 / T^2$ we see the minimal model gives a correction to the anomalous magnetic moment that is roughly a factor of 3 smaller, while the T dependence is, as expected, the same. Despite the significant enhancement compared to the minimal model, more realistic choices of $T > 2000$ GeV (which corresponds to KK masses larger than 4.7 TeV) only gives an enhancement to a_μ of at best $6.8 \cdot 10^{-11}$. The difference between the current experimental value and the SM prediction for the anomalous magnetic moment of the muon is given by [124]

$$a_\mu^{\text{exp}} - a_\mu^{\text{SM}} = 287(63)(49) \times 10^{-11} \quad (6.22)$$

where theory and experimental uncertainties are given separately. Thus, the gauge contribution Δa_μ^g to a_μ alone is too small to be noticed in experiments.

The effect of the modified W/Z coupling Δa_μ^{ZW} is not included in the above numbers. For mass parameters $|c_{L/E}| > 0.55$ it is given by

$$\Delta a_\mu^{ZW} \approx -0.46 \cdot 10^{-11} \left(\frac{1 \text{ TeV}}{T} \right)^2 \quad (6.23)$$

and is, for general 5D masses of the order of $\text{few} \times 10^{-12} \frac{1 \text{ TeV}^2}{T^2}$ in both the minimal and custodially protected model. This is negligible for the custodially protected and a $\sim 5\%$ correction in the minimal model.

The Higgs contributions are strongly dependent on the model parameters, especially the Yukawa matrices. So general statements as in the case of the gauge contribution are not feasible. However, it is worthwhile to study the effect of the Higgs exchange in several illustrative scenarios. Let us first go back to the minimal RS model which was already discussed in [28]. Obviously, the contribution to $g_\mu - 2$ will increase with the magnitude of the Yukawa matrix (in the minimal case there is only one lepton Yukawa). To quantify this statement we study the shift of $(g - 2)_\mu$ due to the dipole Wilson coefficient a^H for three hypothetical cases: the Yukawa entries are each in the range $(1/10, 1/3)$, $(1/3, 3)$ or $(3, 10)$, T is fixed to 1 TeV and we generate 10^4 random data sets for each scenario. Figure 6.3 (left panel) shows the result for the different Yukawa ranges using a logarithmic scale for the abscissa. One can see that the central values of the histograms scale with the square of the corresponding average Yukawa size. This was to be expected from (5.68) as the product of zero-mode profiles compensates for one Yukawa factor provided the Yukawa matrices themselves do not carry a strong hierarchy. As each of the distributions is spread

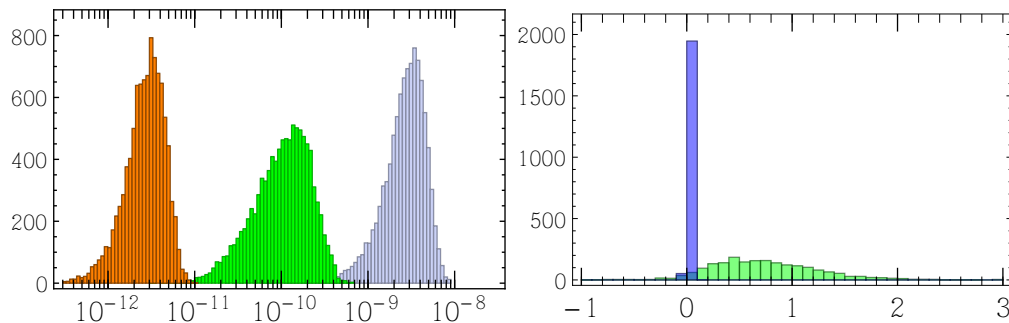


Figure 6.3: *left panel:* Higgs contribution to $g_\mu - 2$ for different average Yukawa sizes in the minimal model (see text for details). The red (light grey) histogram corresponds to $|Y| \in (1/10, 1/3)$, the green(grey) one to $|Y| \in (1/3, 3)$ and blue (dark grey) to $|Y| \in (3, 10)$. We use $T = 1$ TeV everywhere. *right panel:* Higgs contribution to $g_\mu - 2$ for the custodially protected model without the histogram for small Yukawa matrices. The x-axis uses a linear scale in units of 10^{-9} .

out over more than an order of magnitude it is not possible to make quantitative statements without a detailed knowledge of the Yukawa matrices. We also find that a^H favours a positive contribution to $(g - 2)_\mu$ if one constrains the Yukawas as described. Here the logarithmic scale on the x-axis is slightly misleading: it illustrates the scaling with the Yukawa size but misses a short tail in the negative region. Nonetheless, the contributions are predominantly positive. This is interesting as the Higgs contribution is then aligned with the gauge contribution: both reduce the difference between theory and experiment (6.22). We can use the current limits on $g_\mu - 2$ to give a rough bound on the ratio $\frac{Y_\star^2}{T^2}$. The bound is, in a sense, maximally weak, as the preference for a positive sign forces us to consider $\Delta a_\mu^{RS} < 6 \cdot 10^{-9}$ as an upper bound. Thus the constraining power of $g_\mu - 2$ for the lepton Yukawa sector is weaker than Higgs production [78] is for the quark sector. Note that both are sensitive to the ratio $\frac{Y_\star^2}{T^2}$ however there is no reason why the Y_\star^2 of the quark sector should be identical to the equivalent product in the lepton sector.

Only average Yukawa entries of at least 3 would allow for a correction that is sizeable enough to remove the current tension. However, such large values would, assuming Yukawa anarchy, also affect other observables. We also find that the general T -dependence is in agreement with the expected $1/T^2$ behaviour from power-counting.

Next, we turn to the custodially protected model. We now need to include the term with the novel Yukawa Y^ν in (5.70). The right panel of figure 6.3 shows the Higgs contribution to the anomalous moment in the RSc model. We only show the two cases of large and intermediate Yukawa entries; on a linear scale the histogram for small Yukawa entries is too narrowly centred around zero to be visible.

As in the minimal scenario we find potentially very large corrections to $g_\mu - 2$ for $T = 1$ TeV. The correction scales with an overall $1/T^2$ scaling factor. The preference for a positive contribution that is present in the minimal model is also observed. That is because the Y^ν term appears only due to the KK excitations of the Higgs. Therefore it is numerically suppressed compared to the standard Yukawa matrix term. It is noteworthy that this term also exists at zero mode, but it cancels after the summation of all possible Higgs exchange diagrams. In [54] we did not include the contribution coming from the diagram topology HT5 and HT6. Therefore this cancellation was missed leading to an custodial Higgs exchange

contribution, which centres almost uniformly around zero [54]. Some data sets with Yukawas in the interval $|Y| \in (3, 10)$ could potentially yield a sizeable $g-2$ contribution, however the energy scale of $T = 1$ TeV is below the bounds from the electroweak precision tests [23]. We conclude that the muon $g-2$ contribution does not provide any new constraints on the parameter space of the custodial protected RS model.

6.2.2 LFV

The muon $g-2$ computation generates almost no constraining power on the potential parameter space of the minimal and custodial RS model. Nonetheless this computation led to the computation of almost all in the LFV needed Wilson coefficients. The resulting numerical scans are shown in this section. We concentrate here mainly on the minimal model as the custodial protected RS model with its additional particle content only gives rise of larger branching fractions and no entirely new effects. In this section we will also investigate the electron dipole moment, which can be used to eliminate almost all theory points used for the initial scan.

6.2.2.1 Minimal model

The results of our numerical scan through the constrained parameter space are best illustrated in two-dimensional scatter plots, which visualize the typical range of values for the branching fractions and correlations between the observables. It is important to keep in mind that the point densities in these scatter plots should not be used as a measure for the likelihood of the corresponding value in a given model.

Figure 6.4 shows the values and correlation of the $\mu \rightarrow e\gamma$ and $\mu \rightarrow 3e$ branching fractions in the minimal RS model for two different values of T , $T = 4$ TeV (top) and $T = 8$ TeV (bottom). $T = 4$ TeV is also roughly the lower bound on the KK scale from electroweak precision observables [23]. The left panels correspond to the $\mathcal{M}I$ scenario, the right panels to the $\mathcal{M}II$ case. Each plot shows the results for $Y_{\max} = 3$ in blue (dark grey) and for $Y_{\max} = 1/2$ in orange (light grey). The current and expected future experimental upper bounds are shown by solid and dashed lines, respectively.

All four plots feature a sharp lower bound for $\mu \rightarrow 3e$ given the $\mu \rightarrow e\gamma$ rate, which is precisely given by the relation (6.9). $\mu \rightarrow 3e$ branching fraction values in the vicinity of this bound are dominated by the contributions from the dipole operator. For very large dipole coefficients or equivalently very large $\mu \rightarrow e\gamma$ branching fraction, the tri-lepton decay is always dominated by the dipole, and the two observables are strongly correlated. This generates the prominent thin line directed to the upper-right in the $\mathcal{M}I$ model with large Yukawa couplings.

In the bulk Higgs case $\mu \rightarrow e\gamma$ is, as expected, quite sensitive to the upper bound Y_{\max} . This is a consequence of the $YY^\dagger Y$ terms in the dipole coefficient. They are naturally flavour-violating and scale with Y_{\max}^2 . Consequently, the scan with larger Yukawa entries includes points with substantially larger $\mu \rightarrow e\gamma$ branching fraction than the small Yukawa coupling scan. However, the dipole coefficient has two components. While the Higgs and the small Barr-Zee contributions scale as Y_{\max}^2 and vanish when the 5D Yukawa couplings go to zero, the gauge-boson exchange contribution is not very sensitive to the Yukawa coupling size. In fact, for a generic anarchic Yukawa it grows mildly with decreasing Yukawa size, see Figure 6.1. Thus there has to be a smooth transition from the "Higgs-dominated" to the "gauge-dominated" regime when the Yukawa coupling decreases.

To illustrate this point we included three curves in the plots for the bulk Higgs case defined as follows. We chose three (random) Yukawa matrices with $Y_{\max} = 3$ and scale the matrices

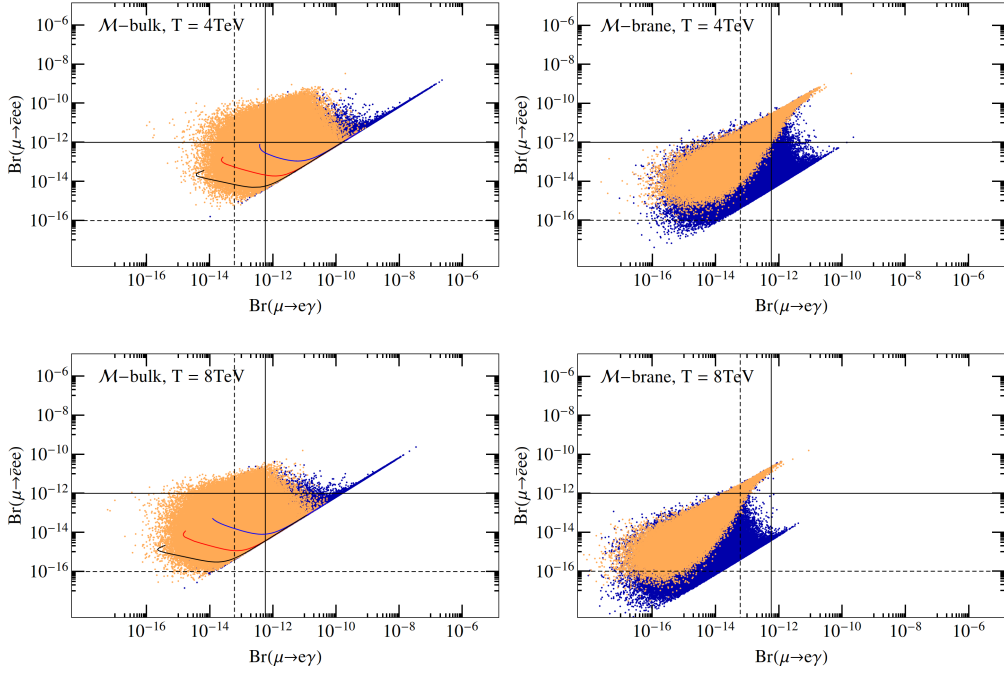


Figure 6.4: 2D scatter plots of the branching ratios $\mu \rightarrow e\gamma$ and $\mu \rightarrow 3e$ for fixed T (4 TeV upper row, 8 TeV lower row) with $Y_{\text{max}} = 0.5$ in orange (light grey) and $Y_{\text{max}} = 3$ in blue (dark grey), respectively. The *left panels* show the results for the \mathcal{M} I models, the *right panels* for the \mathcal{M} II ones. The current experimental bounds on the branching fractions are given by solid lines. The region above/to the left is excluded. The sensitivity of future experiments is shown by the dashed lines.

down to $Y_{\text{max}} = 0.25$, keeping the relative size of the matrix entries fixed. The curves show the resulting trajectories. For large Yukawa couplings the curves all run close to the dipole dominance bound. With decreasing Yukawa couplings $\text{Br}(\mu \rightarrow e\gamma)$ and $\text{Br}(\mu \rightarrow 3e)$ first also decrease following the change in the dipole coefficient. Then the growing effects of the tree-level operators begin to dominate $\mu \rightarrow 3e$ and the corresponding branching fraction begins to increase, while $\text{Br}(\mu \rightarrow e\gamma)$ continues to decrease. For even smaller Yukawa coupling the gauge-boson exchange contribution to $\text{Br}(\mu \rightarrow e\gamma)$ exceeds the rapidly decreasing Higgs contribution and $\text{Br}(\mu \rightarrow e\gamma)$ reaches a hard lower limit.

The exactly brane-localised Higgs case displayed in the right panels of Figure 6.4 behaves the same in this respect. However, since the leading Higgs contribution is suppressed for the exactly brane-localised Higgs, the range of values for $\text{Br}(\mu \rightarrow e\gamma)$ is almost independent of Y_{max} . A change in Y_{max} predominantly affects $\text{Br}(\mu \rightarrow 3e)$, which increases for smaller Y_{max} due to the larger coefficients of four-fermion and fermion-Higgs operators. This also explains the drop shape of the scatter plot for $Y_{\text{max}} = 1/2$. Points with large $\mu \rightarrow 3e$ branching fraction arise from large tree-level Wilson coefficients either due to the structure of the Yukawa matrix or due to accidentally small couplings. In both cases the process $\mu \rightarrow e\gamma$ also receives sizeable contributions from the tree operators leading to the roughly linear correlation in the upper-right corner of the scatter points.

Values and correlations of $\mu \rightarrow 3e$ and $\mu \rightarrow e\gamma$ with muon conversion in gold are shown in Figure 6.5 (colour coding as in the previous figure). The top row shows $\mu \rightarrow e\gamma$ against

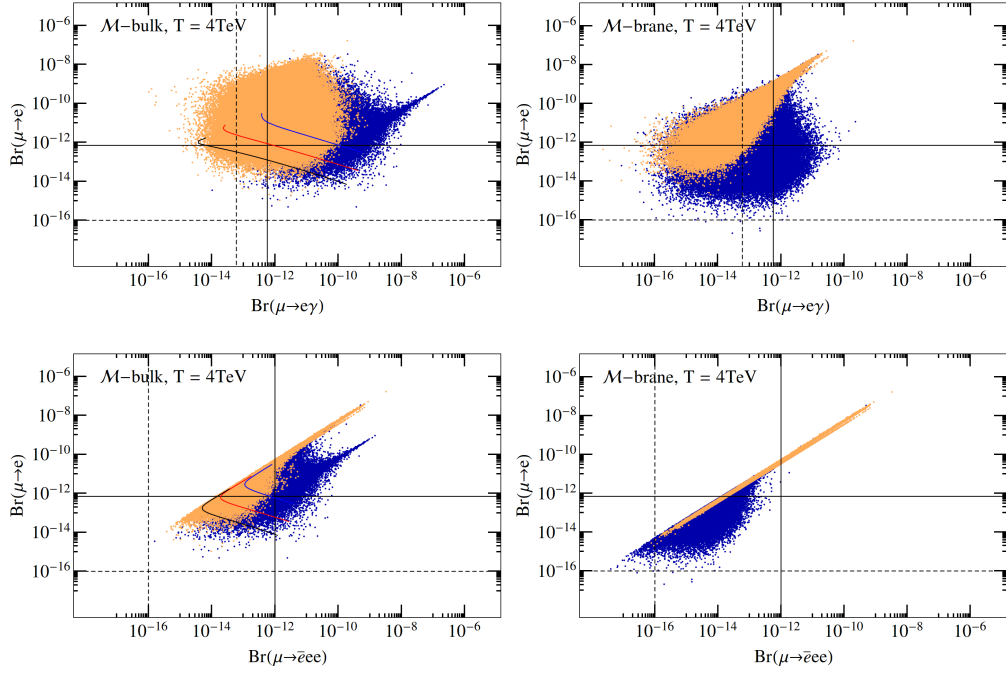


Figure 6.5: Correlation of the branching ratios for $\mu \rightarrow e\gamma$ and $\mu \rightarrow e$ (upper row) and for $\mu \rightarrow 3e$ and $\mu \rightarrow e$ (lower row), both for $T = 4\text{TeV}$. The *left panels* show the results for the *MI*, the *right panels* for the *MII* model.

$\mu \rightarrow e$ (*MI* left, *MII* right). The two observables are essentially uncorrelated in the bulk Higgs scenario. This agrees with our previous observation that muon conversion is mostly insensitive to the dipole coefficient a_{ij}^A which governs the $\mu \rightarrow e\gamma$ branching fraction. Only in rare cases is the dipole operator large enough to dominate also muon conversion leading to the noticeable spike towards the right in the upper-left plot. In the exactly brane-localised Higgs case (upper-right panel), correlations are absent only for $Y_\star = 3$. As mentioned before, for $Y_\star = 1/2$ $\mu \rightarrow e\gamma$ receives non-negligible contributions from tree-level operators, which manifests itself in a weak correlation.

For the same reasons $\mu \rightarrow 3e$ and $\mu \rightarrow e$ (bottom row) are strongly correlated for small Yukawa couplings in *MII* model, but only feature a lower bound on the branching fraction of $\mu \rightarrow 3e$ for a given $\text{Br}(\mu \rightarrow e)$ in the other scenarios. As noted in the previous subsection, the branching fraction of $\mu \rightarrow e$ decreases with increasing values for Y_\star . This effect can best be seen in the upper left panel of Figure 6.5. The slopes of the three sample trajectories also verify this effect.

6.2.2.2 Custodially protected model

Figure 6.6 shows the combined results for the custodially protected model. The left panels correspond to the bulk Higgs model *CI* and the right panels to the exactly brane-localised model *CII*. The colour coding is the same as above. Here the KK scale T was fixed to 8TeV , since for T around 4TeV it is already non-trivial to find points, which are not in conflict with the muon conversion bound.

The broad picture for model *CI* is almost the same as for *MI*. The shape of the distri-

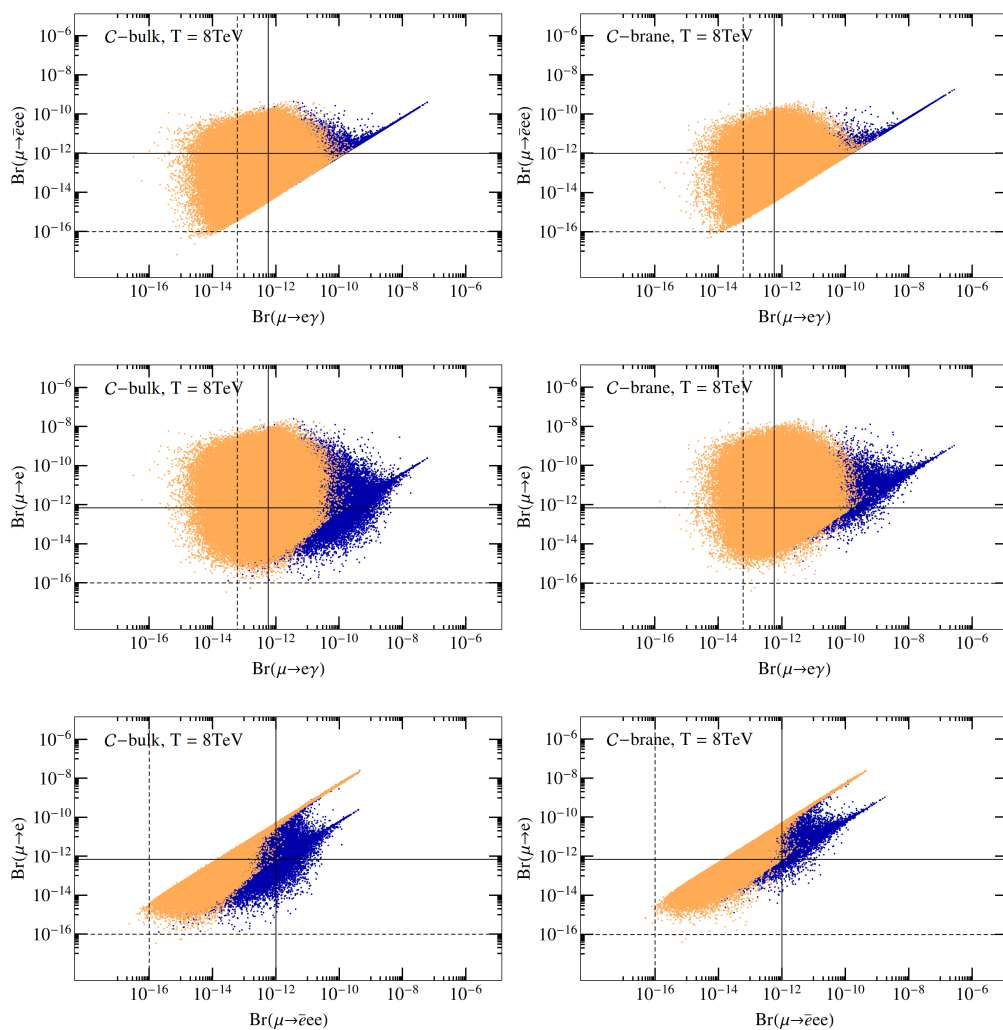


Figure 6.6: Correlation of the branching ratios for $\mu \rightarrow e\gamma$ and $\mu \rightarrow 3e$ (top row), $\mu \rightarrow e\gamma$ and $\mu \rightarrow e$ (middle row), and $\mu \rightarrow 3e$ and $\mu \rightarrow e$ (bottom row) for $T = 8$ TeV in the custodially protected model. Model points with $Y_{\max} = 1/2$ are indicated by orange (light grey) points. For $Y_{\max} = 3$ we use blue (dark grey) points. The *left panels* show the results for the $\mathcal{C}I$, the *right panels* for the $\mathcal{C}II$ model.

butions does not change. Quantitatively, the custodially protected model generates significantly larger branching fractions. In particular, the $\mu \rightarrow e\gamma$ branching fraction, which is most sensitive to the magnitude of the dipole operator coefficient, is typically enhanced by a factor of about five. This was to be expected as the main difference in the custodially protected model is a larger gauge- and Higgs-contribution to the dipole coefficient a_{ij}^A . Again the dipole operator creates a correlation of $\mu \rightarrow e\gamma$ and $\mu \rightarrow 3e$ especially for the larger value of Y_{\max} .

For the *CII* model the distributions are very different from the result in the *MII* model. This is a consequence of the new additional terms (5.47) in a_{ij}^H . This additional contribution to the dipole coefficient is only slightly larger than the corresponding contribution for a bulk Higgs. The phenomenology for bulk and brane Higgs case is therefore quite similar in the custodial RS model. The bounds imposed by the non-observation of LFV are comparable, although more restrictive for the exactly brane-localised Higgs.

The fact that the sign of a_{ij}^H depends on the Higgs localisation does not lead to a noticeable effect. If the dipole operator is dominated by the Higgs contribution, a sign flip of the coefficients a_{ij} only affects terms in (3.16), (3.18) and (3.20) that come from an interference of the dipole with a four-fermion operator. In general, these terms do not provide the dominant contribution to the branching fractions. The situation would be different if the RS contribution could interfere with a sizeable SM contribution to LFV observables. An observed enhanced or reduced rate could then be used to discriminate the brane from the bulk Higgs model.²

6.2.2.3 EDM constraint

The randomly sampled Yukawa matrices also generate electric dipole moments (EDMs) of the leptons through the non-hermitian part of α_{ij}^A , see (3.7). We checked that the present experimental limit on the electron electric dipole moment [120],

$$|d_e| < 8.7 \cdot 10^{-29} e \text{ cm} \quad (\text{at } 90\% \text{ CL}), \quad (6.24)$$

does not affect our conclusions. To this end we first consider the quantify

$$\sqrt{\frac{m_\mu}{m_e}} \frac{\text{Im } \alpha_{11}^A}{\text{Im } \alpha_{12}^A}, \quad (6.25)$$

shown in Figure 6.7 for $T=8$ TeV in the custodial protection model including Higgs KK excitations. The quantity is centred around the value 1 for anarchic Yukawa matrices. There are large deviations from one in both possible directions depending on the particular Yukawa structure. This demonstrates that the EDM and the LFV observables are uncorrelated. In total the EDM bound eliminates 85 % (12 %) for the *CI* model with $Y_{\max} = 3$ ($Y_{\max} = 0.5$) and 90 % (25 %) for the *MI* model with $Y_{\max} = 3$ ($Y_{\max} = 0.5$). Nevertheless the general form of the scatter plots remains untouched by this huge point elimination, due to the EDM and LFV sector not being correlated. We show this in Figure 6.8 for all six scenarios for the correlation of the branching ratios for $\mu \rightarrow e\gamma$ and $\mu \rightarrow 3e$ and $Y_{\max} = 3$. The surviving points still cover almost the whole range for the bulk Higgs models and the custodial protected RS model with a brane localised Higgs. We observe that the EDM bound only removes the edges with large branching fractions. However these points are already excluded by the bounds on the searches of $\mu \rightarrow e\gamma$ and $\mu \rightarrow 3e$. In addition the *MI* model is almost not affected by the EDM bound, due to the missing wrong chirality terms

²This is precisely what is observed in Higgs production, see e.g. [78].

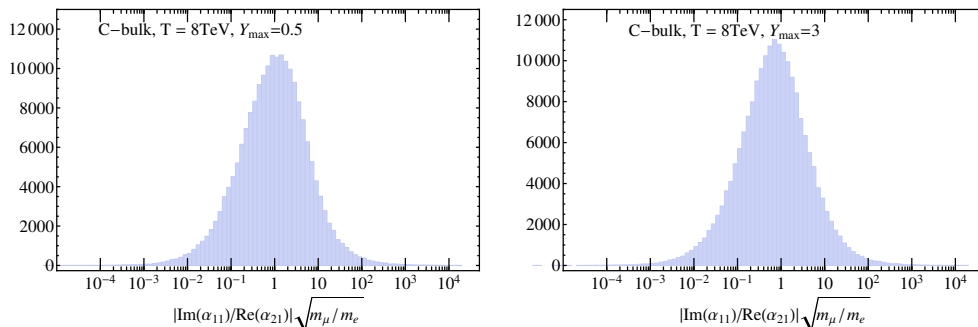


Figure 6.7: *Left panel:* $\sqrt{\frac{m_\mu}{m_e}} \frac{\text{Im} \alpha_{11}^A}{\text{Im} \alpha_{12}^A}$ for the CI model with $Y_{\text{max}} = 0.5$. *Right panel:* Same as left but with $Y_{\text{max}} = 3$

in the Higgs exchange. Note that for $Y_{\text{max}} = 0.5$ the difference between the EDM passed and the complete set of theory points can almost not be seen in scatter plots of the style of Figure 6.8. We observe the same behaviour in all other correlation plots in the LFV. For this reason the main points of our analysis of theory points without the consideration of the EDM bound still, despite the exclusion of the majority of most of the points.

6.2.2.4 A note on LFV τ decays

Tau decays offer another opportunity to study LFV. However, the short lifetime of the τ and its high mass make it unsuited for studies in low-energy facilities. The best bounds on processes like $\tau \rightarrow e\gamma$ or $\tau \rightarrow 3\mu$ come from Babar [125], Belle [126] as well as LHCb [127].

The RS model naturally generates higher rates for $\tau \rightarrow \mu, e$ transitions than for $\mu \rightarrow e$ transitions, since there is a close relation of lepton masses with the corresponding zero-mode profiles, which also control the size of LFV. However, the fantastic sensitivity of past and future experiments searching for muon flavour violation still makes searches in the muon sector the most promising avenue, unless additional flavour structure suppresses muon flavour violation.

Nevertheless, it is instructive to provide the expectations for tau LFV in the RS model. In Figure 6.9 we show the values and correlation of the $\tau \rightarrow \mu\gamma$ and $\tau \rightarrow 3\mu$ branching fractions. The colour coding is the same as in the previous subsection. The solid lines correspond to the current best upper bounds on the branching fractions. Compared to the bounds in the muon sector the current limits from tau decays are not restrictive even for $T = 4 \text{ TeV}$. An improvement of more than five orders of magnitude would be required for constraints as severe as those from muon decays.

Qualitatively, the $\tau \rightarrow \mu\gamma$ vs. $\tau \rightarrow 3\mu$ plot is similar to the corresponding “muonic” plots (first row in Figure 6.4). The main difference is the large effect of the four-fermion and fermion-Higgs operators. For the exactly brane-localised Higgs this generates the strong correlation for small Yukawa couplings $Y_{\text{max}} = 0.5$. In the bulk Higgs case this effect prevents scatter points close to the dipole-dominance line.

6.2.3 Radiative b decays

To see the potential effect of the additional contribution to $C_{7\gamma}^{(f)}$ on the $B \rightarrow X_s \gamma$ decay we need to scan over the parameter space of the RS model. We will, as mentioned before,

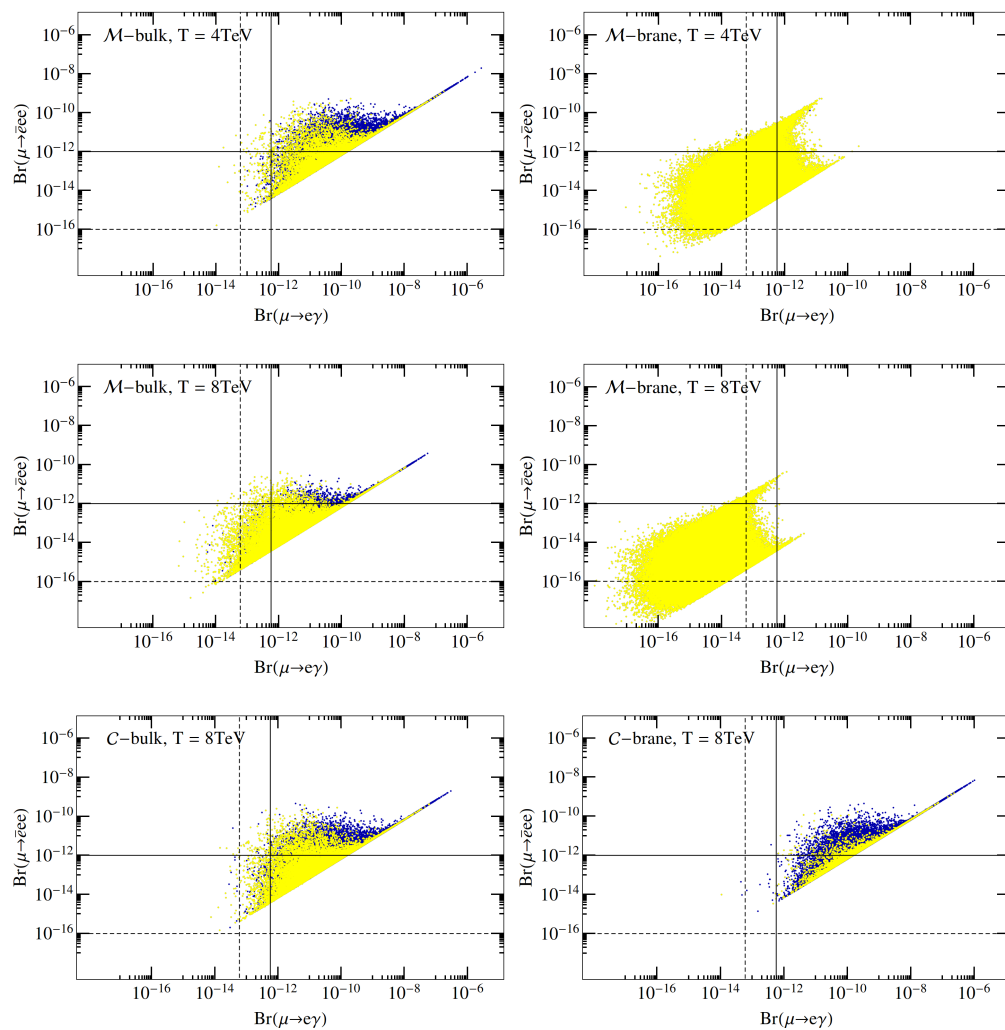


Figure 6.8: Correlation of the branching ratios for $\mu \rightarrow e\gamma$ and $\mu \rightarrow 3e$. For the $Y_{\max} = 3$ set for all six different models the points passing the EDM constraint (yellow) are overlaid over all points (blue). The *left panels* show the result for the bulk Higgs models. The *right panels* show the result for brane Higgs localisation. From top to down: minimal $T = 4$ TeV, minimal $T = 8$ TeV and custodial protected $T = 8$ TeV.

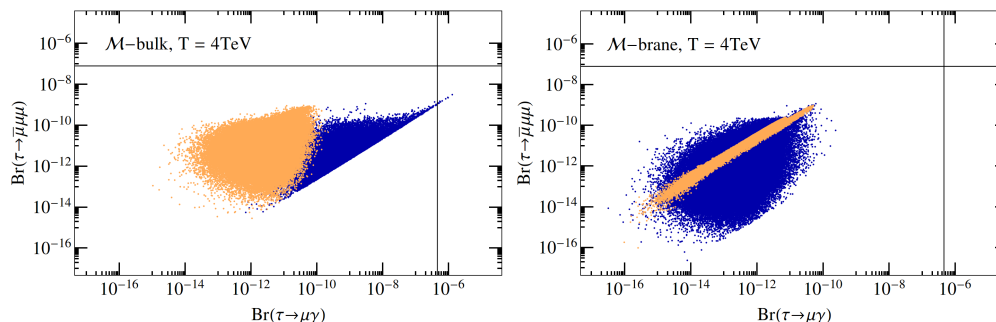


Figure 6.9: Correlation of the branching ratios of $\tau \rightarrow \mu\gamma$ and $\tau \rightarrow 3\mu$ for $T = 4\text{ TeV}$ in the minimal model. The left panel shows the bulk Higgs, the right the exactly brane-localised Higgs case.

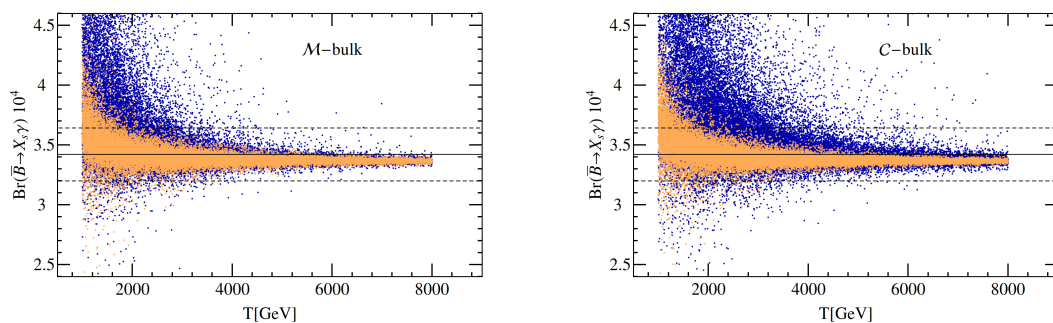


Figure 6.10: $\text{Br}(\bar{B} \rightarrow X_s \gamma)$ as a function of the KK scale T . The blue (dark grey) points correspond to the data set with large Yukawas, $Y_{max} = 3$. The orange (light grey) points correspond to $Y_{max} = 1/2$. The horizontal lines indicate the experimental value of and uncertainty on the branching fraction. The left panel shows the result for the minimal RS model, the right panel for the custodially protected model.

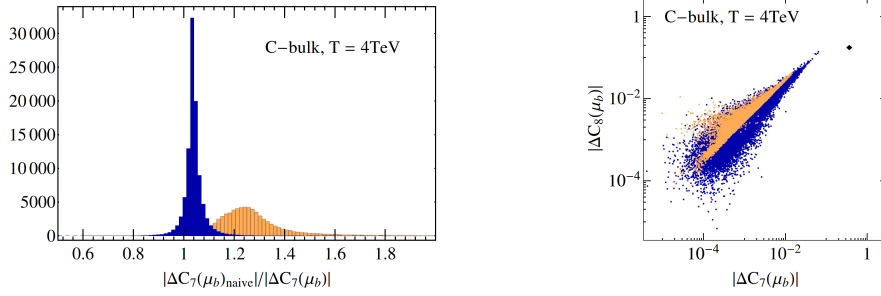


Figure 6.11: *left panel*: Effect of operator mixing on $\Delta C_{7\gamma}$. The histogram shows the distribution of $|\Delta C_{7\gamma}(\mu_b)|$ without operator mixing relative to the full $|\Delta C_{7\gamma}(\mu_b)|$ with mixing (see text for details). The blue (dark grey) and orange (light grey) histogram corresponds to $Y_{max} = 3$ and $Y_{max} = 1/2$. *right panel*: Correlation of ΔC_{8g} and $\Delta C_{7\gamma}$ in the custodially protected RS model for $T = 4$ TeV. The triangle represents the SM values of $C_{7\gamma}$ and C_{8g} ; the dashed diagonal line indicates $|\Delta C_{8g}| = |\Delta C_{7\gamma}|$. Same colour coding as in the left panel.

consider a minimal and a custodially protected RS model with an IR-localised bulk Higgs. The model parameters include the 5D masses of the fermions as well as the two Yukawa couplings Y_d and Y_u .

The main result of our scan through the RS parameter space is shown in figure 6.10. It shows the branching fraction $\bar{B} \rightarrow X_s \gamma$ as a function of the KK scale³ T for the minimal RS model (left panel) and the custodially protected model (right panel). The blue (dark grey) points correspond to $Y_{max} = 3$, the orange (light grey) points to $Y_{max} = 1/2$. The current experimental central value, see equation (1.3), is represented by the solid horizontal line; the dashed lines indicate the uncertainty.

We find that the branching fraction is, especially for small Yukawas, predominantly larger than in the SM. This is due to a sizeable contribution from $C'_{7\gamma}$, that lacks an unsuppressed interference term with the SM contribution—its contribution to the branching fraction is always positive. In addition to that the contribution to $C'_{7\gamma}$ is generally larger than the contribution to the unprimed dipole coefficient. The reason for this, as was observed already in [48], is that the 5D profile of the doublet Q_3 (that very roughly corresponds to the b_L after EWSB) is typically larger than the profiles of the down-type singlets D near the IR brane; consequently the operator $Q'_{7,\gamma} \propto (\bar{s}_R)_\alpha \sigma^{\mu\nu} (b_L)_\alpha F_{\mu\nu}$ receives a larger BSM contribution.

Only for the $Y_{max} = 3$ sample one can observe data points with a significantly reduced branching fraction compared to the SM. This is due to a destructive interference of $C_{7\gamma}^{SM}$ and $\Delta C_{7\gamma}$ that can counteract the contribution due to $C'_{7\gamma}$ if the Higgs contribution to $C_{7,\gamma}(\mu_{KK})$ is large. This effect is more pronounced in the custodially protected model where the additional fermion states enhance the dipole coefficient, cp. (5.74) and (5.70). For small Yukawas the phenomenology of minimal and custodially protected model is quite similar. This is to some extent a consequence of working only with QCD- and Higgs-mediated contributions to the Wilson coefficient; QCD is treated the same in both models while the electroweak sector is extended and features additional bosonic modes. In the $Y_{max} = 1/2$ scenario the main distinction between the two models—the Higgs contribution—is suppressed.

³Note that the mass of the first KK excitation of the gluon is roughly given by $2.5 \times T$ [17]

The smallness of the Higgs contribution for $Y_{max} = 1/2$ and the consequently smaller $\Delta C_{7\gamma}(\mu_{KK})$ also make the inclusion of operator mixing mandatory. To see this we consider two quantities: the full $\Delta C_{7\gamma}(\mu_b)$ as obtained from the RGE (3.49) and $\Delta C_{7\gamma}(\mu_b)|_{naive}$ which is also obtained via (3.49) but we set the Wilson coefficients of all four-fermion operators at the high scale μ_{KK} to zero. We then consider the ratio $\Delta C_{7\gamma}(\mu_b)|_{naive}/\Delta C_{7\gamma}(\mu_b)$. The deviation of the ratio from one indicates the relative importance of the four-fermion operators for the $b \rightarrow s\gamma$ transition. Histograms of $\Delta C_{7\gamma}(\mu_b)|_{naive}/\Delta C_{7\gamma}(\mu_b)$ are shown in the left panel of figure 6.11. For simplicity we only show the plot in the minimal model for $T = 4$ TeV. For large Yukawas, $Y_{max} = 3$ in blue (dark grey), neglecting the contribution of from four-fermion operators leads on average to an increase of $\Delta C_{7\gamma}(\mu_b)$ by 5%. For a few Yukawa data sets the shift can be of the order of $\pm 15\%$. In the case of small 5D Yukawa coupling (shown in orange) ignoring the four-fermion operator mixing basically always increases ΔC_7 . This can lead to an overestimate of the BSM contribution to the $B \rightarrow X_s\gamma$ branching fraction by up to 40%. Hence including the mixing is relevant and should not be neglected. This is of course quite general as FCNCs mediated by new, massive gauge bosons usually create simultaneous contributions to $\Delta C_{7\gamma}$ and to the $\Delta C_{1,2}^q[A, B]$ as is indicated by the need to include the four-fermion operators to obtain a scheme-independent result.

For completeness we also show the correlation of $\Delta C_{7\gamma}(\mu_b)$ and $\Delta C_{8\gamma}(\mu_b)$ in the right panel of figure 6.11. We see that on average the BSM contribution to $C_{7\gamma}$ is smaller than the contribution to $C_{8\gamma}$ as was also noted in [83]. This is more noticeable for the small Yukawa sample shown in orange (light grey). The two Wilson coefficients are then clearly correlated and one observes a "lower bound" on $\Delta C_{7\gamma}$ for a given value of $\Delta C_{8\gamma}$. However, with $Y_{max} = 3$, it is straightforward to find parameter points where $\Delta C_{7\gamma}$ is much larger than the BSM contribution to $C_{8\gamma}$. The reason for this is the following: The zero-mode Higgs contribution to a^g and a^γ are almost proportional to each other, see equations (5.74)–(5.70). However, the sizeable KK Higgs contribution has a more complicated structure; it contributes in a different way to a^g and to a^γ . This blurs the correlation.

6.3 Discussion

In the following we summarize and emphasize the main conclusions from the phenomenological study. We studied first the anomalous magnetic moment of the muon. Here the total correction by the custodial protected model is in line with the minimal RS model result [28]. The contribution is mainly driven by Higgs exchange penguin dipole diagrams. These diagrams depend strongly on the structure and the size of the 5D Yukawa. In contrast to that the other important contribution generated by the gauge boson dipole diagrams is mostly 5D independent. Therefore, it yields a lower bound on the potential magnitude of the effects of the RS model on the muon g-2. Compared to the previous calculation for the minimal RS model [28] this lower bound is about three times as high. It noteworthy that possible explanation the muon g-2 discrepancy by the RS model favours lower RS scales T and larger Yukawa sizes. Ideally it would generate an RS scale T , which is larger than other existing lower bounds on T like for example the bounds created from the electroweak precision test [23]. In such ideal scenario one would be able to constrain the KK scale from both sides. However the numerical scan shows, that the upper bounds on T generated by the muon g-2 computation are too low. That is dominantly because the RS model contribution is either too small for choices of T , which compatible to the electroweak precision parameter bounds, or it is generated by large Higgs exchange dipole transitions, which generate an EDM in conflict with the experimental bounds. This is our main message for the muon g-2 calculation in the custodial protected model.

Considering the topologies of the decays we would naively expect the muon conversion and $\mu \rightarrow 3e$ to be dominantly mediated by the current-current operators $(\bar{\ell}_e \Gamma \ell_\mu)(\bar{\psi} \Gamma \psi)$. These operators are determined by the Wilson coefficients c_{ij}^a and b_{ij} , in the dimension-six SM effective Lagrangian (3.2). On the contrary, the branching ratio for the decay $\mu \rightarrow e\gamma$ should be mainly mediated by the loop-induced dipole operators. This idealised scenario would then open the possibility to extract different informations of the underlying RS model through the different parameter structure of the relevant Wilson coefficients.

In spite of this, our numerical scan shows that this is not the case. That is also our main message #1 for the LFV sector. In particular, the decay $\mu \rightarrow 3e$ receives sizeable contributions from dipole operators for a large range of the parameter space. Our initial expectations can be even reversed for a minimal RS model with an exactly brane-localised Higgs or a minimal bulk Higgs model with small 5D Yukawas. In such case the dominant contributions to $\mu \rightarrow e\gamma$ can be generated by tree-level dimension six operators. Therefore, it becomes clear that the inclusion of all dimension-six operators for every observable is needed to generate a reliable picture of the lepton flavour violation in the RS model.

Our numerical analysis shows that the inclusion of the Higgs and gauge boson exchange contribution to the penguin diagrams that generate the dipole Wilson coefficient α_{ij}^A is important, because their parameter dependence is fundamentally different. Here the most notable difference lies in the dependence of the Yukawa coupling. In fact we cannot give an accurate description of the $\mu \rightarrow e\gamma$ decay over a large range of Yukawa sizes. An omission of the Higgs exchange dipole contributions drops the numerical dominant effects for large Yukawas. On the other hand the gauge boson exchange stops the dipole from irrelevance for small Yukawa couplings. This itself creates a lower bound on $\text{Br}(\mu \rightarrow e\gamma)$, which depends only on the structure of the Yukawa matrix, but not on the overall magnitude of the couplings. Thus our main message #2 is that the Higgs and gauge boson induced flavour violation have the possibility to be both important. Therefore, only a full computation of the dipole operator coefficient yields a reliable overview of the LFV sector.

The numerical analysis indicates that anarchic RS models with minimal particle content typically need KK scales T larger than 4 TeV to be compatible with the current data on charged LFV. Furthermore, the combination of $\mu \rightarrow e\gamma$ and muon conversion yields the bound on T almost insensitive to the size of the Yukawa matrix for models with bulk Higgs. The situation is not so simple for an exactly brane-localised Higgs, although the bound $T \gtrsim 4$ TeV is still valid for small Yukawa. It is mainly generated by the muon conversion analysis. The muon conversion is dominated by tree-level operators, which contain decreasing Wilson coefficients for increasing Y_\star . This implies a weaker bound for larger Yukawas complementary to the behaviour of the Higgs exchange dipole operator Wilson coefficients. For this reason there are still many points for $Y_{\max} = 3$ that are within the experimental bounds for T as low as 2 TeV. The larger particle content of the custodially protected model leads directly to larger Wilson coefficients. For this reason the bound on the KK scale T is higher. It is noteworthy that the appearance of the Y_\star^2 term for an exactly brane localised Higgs yields to a good approximation a Higgs localisation independent bound on T .

We expect significant improvements on the KK scale T in future experiments. Especially the next generation muon conversion searches will provide strong constraints on RS models. Our analysis was performed for a gold target nucleus—DeeMe [128], Mu2E [129] and COMET [130] use silicon and aluminium target nuclei, respectively. Aluminium and silicon have an approximately 20 times smaller muon capture rate compared to gold, which enhances the branching fraction, but the wave-function overlap integrals $(\mathcal{D}, \mathcal{V}, \mathcal{S})$ relevant to muon conversion are also smaller, see Table 6.1. Thus an expected lower bound on the branching fraction of 7×10^{-17} for aluminium is roughly equal to a bound around 10^{-16}

in gold [95] (indicated by the dashed lines in the plots). This combined with the expected improvement on $\text{Br}(\mu \rightarrow e\gamma)$ during the next run of the MEG experiment [131] could exclude the parameter space of anarchic RS models (custodially protected or minimal) up to a lowest KK resonance mass of 20 TeV, which corresponds to $T \gtrsim 8$ TeV. The current $\mu \rightarrow 3e$ constraint is less constraining than the one from muon conversion. However, the proposed Mu3e experiment [132] aims for sensitivity to a branching fraction of about 10^{-16} . At this level $\mu \rightarrow 3e$ alone will be able to exclude anarchic models with $T \lesssim 5$ TeV. Naturally, should LFV be observed in any of the new experiments, the model-dependent correlations among different processes can be used to further constrain the RS parameter space. Hence, our main message #3: LFV violation provides very strong constraints on RS models, and future experiments will further strengthen them.

It is interesting to compare the charged LFV constraints on the RS model and its KK scale to those derived from other processes. The non-observation of direct KK gluon production forces T to be larger than only about 1 TeV. This cannot compete with the bounds from electroweak precision observables, notably the S and T parameter, which are essentially model-independent. They only depend on the particle content of the model and to a lesser degree on the 5D Higgs profile [90]. For the two models discussed in this work the electroweak precision observable bounds are $T > 2.3$ TeV (custodially protected) and $T > 4$ TeV (minimal) [23].

If one allows for a somewhat stronger dependence of the bounds on the model parameters, Higgs production (and subsequent decay) is also an interesting observable. It depends more strongly on the (mainly quark) Yukawa matrices Y_u, Y_d than the oblique parameters, but is still far less sensitive to its detailed structure than processes like $\mu \rightarrow 3e$, because Higgs production depends to leading order only on the traces of $Y_u^\dagger Y_u, Y_d^\dagger Y_d$. The trace of a product of anarchic matrices follows a narrower distribution than an individual matrix element. One finds that T has to be larger than 2 (4) TeV @ 95% CL for $Y_\star \approx 3$ in the minimal (custodially protected) model with a narrow bulk Higgs [78]. For smaller Yukawa couplings the bound becomes weaker as the effect on the production cross section decreases with Y_\star . For the exactly brane-localised Higgs the constraints are stronger, and one finds the same bounds on T as above already for $Y_\star \approx 1$. As we have seen the situation is different for LFV observables. In the minimal model an exactly brane-localised Higgs leads to weaker bounds than a bulk Higgs, and in the custodially protected model the bound from the bulk Higgs (with KK modes) is comparable to the one in the exactly brane-localised scenario. Thus for large quark Yukawa couplings and the exactly brane-localised Higgs, Higgs production provides at least equally strong bounds on the KK scale than the non-observation of charged LFV. The LHC will be able to improve on this further in the future. In all other cases the next generation LFV experiments will be able to set the most stringent limits on the KK scale. Of course, this comparison assumes that the magnitude of anarchic Yukawa couplings is roughly the same in the quark and lepton sectors.

Our findings can be compared to the results of [31], which provided the first detailed analysis of lepton flavour violation in the minimal RS model in the KK mode picture. The branching ratio of $\mu \rightarrow e\gamma$ is determined from the Higgs-exchange contribution to the dipole Wilson coefficient alone, which is computed via one-loop diagrams involving the Higgs zero-mode and first fermion KK excitation. Muon conversion and $\mu \rightarrow 3e$ are computed from the tree-level Wilson coefficients, while the dipole contribution is neglected. Both exactly brane-localised and bulk Higgs scenarios are investigated. We can compare with our full results only for the bulk Higgs case as their exactly brane-localised Higgs result for the dipole operator is cut-off dependent. Despite these caveats the overall size of the bound on the KK scale T for a bulk Higgs is compatible with the one found above. The main difference is the dependence of the

CHAPTER 6. PHENOMENOLOGY

branching fractions on the model parameters. As [31] only includes the Higgs contribution,⁴ the dipole coefficient has a straightforward dependence on the Yukawa coupling size Y_\star . The identification of the dependence on the Yukawa coupling size as a distinguishing feature of tree-level and loop-induced observables, i.e. muon conversion and tri-lepton decay as opposed to $\ell' \rightarrow \ell\gamma$, is however valid only for medium-size Yukawa couplings, since otherwise the neglected gauge-boson contribution with its different dependence on Y_\star becomes relevant for small Y_\star , and for large Y_\star the tri-lepton decay is dominated by the dipole operator and therefore effectively also loop-induced.

We can also compare our results with [32]. Here the Higgs-exchange contribution to the dipole operator is not considered. The dipole coefficient is computed in the 5D framework from a subset of gauge-boson exchange diagrams including a dimension-eight effect with three Yukawa matrices. Comparing orders of magnitudes their results for $\mu \rightarrow e\gamma$ and $\mu \rightarrow 3e$ are similar to our exactly brane-localised Higgs case in the minimal model. In particular, the lower bound on the $\mu \rightarrow e\gamma$ branching fraction for small Yukawa couplings is also present in their estimates.

To conclude this chapter let us turn a final focus on the $\bar{B} \rightarrow X_s\gamma$ decay. Comparing with the experimental value for $\bar{B} \rightarrow X_s\gamma$ we find that for $Y_{max} = 1/2$ the RS model parameter space is generally compatible with experimental data for $T > 2$ TeV. Since electroweak precision observables already put stricter bounds on the KK scale [23,27], $\bar{B} \rightarrow X_s\gamma$ does not give any new constraints on the KK scale. Nonetheless, sizeable corrections of about 5–10% are still possible. For large Yukawas the situation is much more intriguing, especially in the custodially protected model. As the large effects come almost exclusively from the Higgs exchange contribution to the dipole coefficients $a^{g/\gamma}$ they are strongly dependent on the specific form of the anarchic Yukawa matrices. As for the muon g-2 and the LFV it is difficult to deduce any hard bounds on RS parameter space. However, the total BSM correction to the branching fraction can be quite substantial. Even for $T \sim 5$ TeV it is easy to find parameter points outside the current experimental limits. Consequently, the new Belle II searches would have the potential to discover the impact of KK states on $\bar{B} \rightarrow X_s\gamma$ with masses well above 10 TeV.

⁴The absence of the KK modes does affect the qualitative characteristics of the Higgs contribution.

Chapter 7

Summary

The first run of the LHC was a huge success with the discovery of the Higgs boson, the long sought last piece of the standard model. However, this first run can also be considered a disappointment as any significant indication for new physics has not been found yet. In this thesis we considered Randall-Sundrum models, which are potential candidates for a field theory model that describes physics beyond the SM. Based on the old intriguing idea of a spacetime with additional spacial dimensions, this model addresses the long known gauge-gravity hierarchy problem, which is even more pressing now with the discovery of the Higgs. It also contains a mechanism to generate the quark mass flavour hierarchies and mixing angles naturally and therein providing one of best explanations of the SM flavour puzzle. However, the potential lowest mass range of the lightest Kaluza-Klein particles are potentially too heavy for direct production at the maximum design centre of mass energy of 14 TeV at the LHC. We explained this in chapter 2. In such a situation it is time to look for possible indirect signatures of interactions of Kaluza-Klein and SM particles. One possibility to search for such signatures are the experimental measurement of processes, which are mediated by dipole operators and contain energy scales far below the scale of the LHC. For this reason we explored the one-loop-induced dipole transitions in the RS model in this thesis. In particular we concentrated on the muon g-2, the lepton number violating decays, $\mu \rightarrow e\gamma$, $\mu \rightarrow 3e$, $\mu \rightarrow e$ conversion and the inclusive electromagnetic penguin B decay $\bar{B} \rightarrow X_s\gamma$.

To this end we first we introduced the RS model with minimal field content in chapter two. There we saw that the main prediction of a RS model with bulk fermions and gauge bosons is the existence of a large tower of heavy particles for each SM fermion and gauge boson, whose lowest mass is of the order of the KK scale T . We also discussed the careful treatment of the necessary localisation of the Higgs near the IR brane and introduced three different localisations schemes, which have phenomenological consequences. In particular we included the discussion of a bulk Higgs with a β localisation. Such a localisation scheme gives rise to KK excitations of the Higgs, which are important for dipole transition even in the near localisation limit [79]. The mostly 5D parameter independent constraints generated by tree-level contributions on the electroweak precision parameter S and especially the T parameter [23] led to the introduction of the RS model with custodial symmetry, whose extended gauge group gives rise to new gauge boson, lepton and quark fields. It is noteworthy that this model contains heavy quark fields with a charge of $5/3$. These are potential smoking gun signatures for direct production at a particle accelerators with a sufficient high centre of mass energy.

We then integrated the fifth dimension of the RS model out in chapter 3. To this end we in-

CHAPTER 7. SUMMARY

roduced an effective theory containing the SM Lagrangian and a dimension six Lagrangian based on the Buchmüller-Wyler Lagrangian [51] containing a complete set of all operators, which contribute to the relevant processes. We selected operators that can be generated by the RS model. Our selection criteria was that this generation by the RS model is either a tree-level process or in the case of the electromagnetic lepton and quark dipole operators as well as the gluonic dipole operator a one-loop transition. This effective theory allowed us to express all leptonic processes of interest in terms of the Wilson coefficients after the a transition to the broken phase. To compute the branching fraction of $\bar{B} \rightarrow X_s \gamma$ we focussed on the contributions of KK Klein gluons and the Higgs exchange. Here we matched the associated dimension six Lagrangian to an effective weak Hamiltonian and then used the results of [108] to include the effect of operator mixing due to RGE evolution from the KK scale T to μ_b to leading log LL accuracy. This is necessary as already in the SM the QCD corrections are sizeable and the dipole operator coefficient alone is not regularisation scheme independent.

With the formulation of the basic 5D formalism in chapter two and the computation of the processes of interest in terms of an effective theory the next step was to match the 5D theory to the dimension six Lagrangian. This was done in chapter four for the case of tree-level operators and in chapter five for the loop-induced dipole operators. Using the 5D approach the tree-level Wilson coefficient matching can be performed analytically. The dipole are mostly accessible via numerical calculations, the only exception are the Higgs exchange dipole diagrams, which were computed analytically for a nearly or exactly brane localised Higgs. Our calculation is the first complete one of dimension-six effects, which are not suppressed by powers of small fermion masses in the lepton sector. It considerably sharpens previous results from [31, 32, 53]. This concerns in particular the electromagnetic dipole coefficient. This Wilson coefficient depends on the localisation scheme of the Higgs near the IR brane. It also receives contributions, which dependent parametrically different on the the magnitude of the anarchical 5D Yukawa matrices. This leads to distinctive features in the 5d parameter scan we provided in the next chapter.

Equipped with all Wilson coefficients in terms of 5D parameters we then assumed generic anarchic Yukawas matrices and studied the branching ratios $\mu \rightarrow e\gamma$, $\mu \rightarrow 3e$, $\mu N \rightarrow \mu N$ as well as $\tau \rightarrow \mu\gamma$, $\tau \rightarrow 3\mu$ and the quark flavour violating process $\bar{B} \rightarrow X_s \gamma$ in both the minimal and custodial protected RS model in chapter six. Here the combination of $\mu \rightarrow e\gamma$ and $\mu N \rightarrow \mu N$ causes the most stringent constraints on the parameter space of the models. For the minimal RS model this leads to a lower bound on the KK scale T of about 2 TeV . However, for a bulk Higgs the lower bound can be up to 4 TeV, which is about the size of the bounds coming from the electroweak precision parameters. For the custodial protected RS model we deduced bounds up to 4 TeV for T , which corresponds to first Kaluza-Klein masses of about 10 TeV far beyond the limit for direct production at the LHC. We note that the upcoming next generation of LFV experiments with their expected exclusion range could lead to bounds on T of about $T \sim 8\text{TeV}$, which would mean lightest Kaluza-Klein masses of about 20 TeV. Compared to the LFV sector the RS contribution to the branching ratio $\bar{B} \rightarrow X_s \gamma$ yields weaker bounds on the RS scale T . However, for large Yukawas there can be deviations of $Br(\bar{B} \rightarrow X_s \gamma)$ even for KK scales of around 4 TeV. For small Yukawas the impact of the RS model is mild: KK scales that are not in conflict with electroweak precision bounds, the deviations generated by the RS model are generally small.

Appendix A

5D Feynman rules

In this part of the appendix we will provide modified Feynman rules for the custodially protected Randall–Sundrum model compared to the minimal RS model. We use the same notation as in [28].

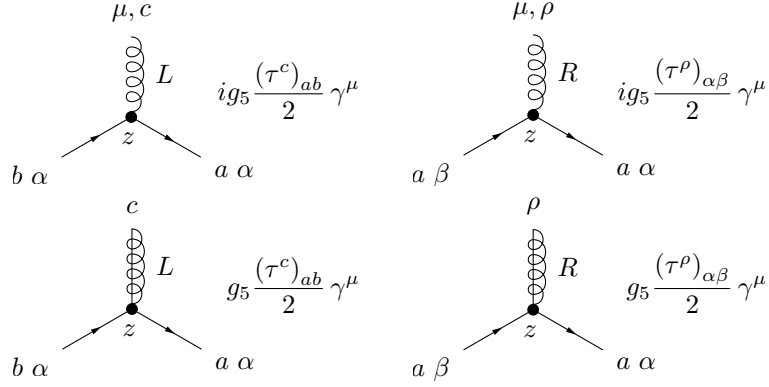
A.1 Vertices

We supply the for the calculation of g-2 needed vertex factor for the custodially protected Randall–Sundrum model. The gauge-boson self interactions are not modified for the $SU(2)_L$ and $SU(2)_R$ compared to the minimal RS model. Therefore we will not write them down explicitly here. Note that for the vertex factors we use the \tilde{T}_4 field basis of the Lagrangian density (2.96). The complete set of all vertex can be found for instance in [26] with slightly different conventions.

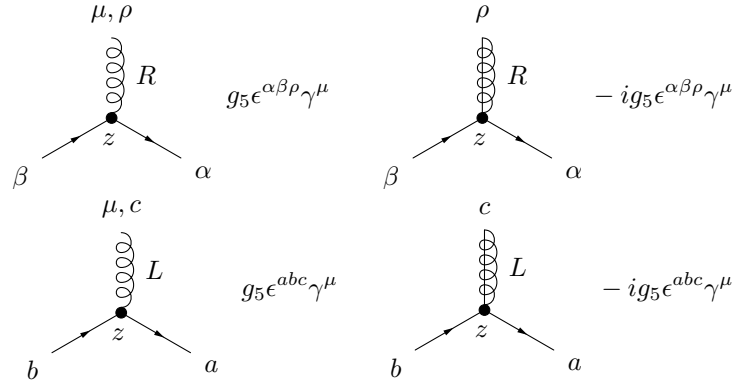
Fermion-gauge field vertices We distinguish here between the $SU(2)_L \times SU(2)_R$ bi-doublet ξ_1 and the two $SU(2)$ triplets \tilde{T}_4 and \tilde{T}_3 . We write an R or L next to the gauge-boson line to denote $SU(2)_R$ or $SU(2)_L$ gauge-bosons. As above introduced a Greek indices labels a $SU(2)_R$ indices, while a Latin indices marks a $SU(2)_L$ indices. Note that the Greek indices μ is only used here for the Lorentz index of the gauge-boson line. We work here in the unbroken theory, which is flavour diagonal, thus we neglect here the flavour indices. For every vertex one hast perform additionally an integral $\int_{1/k}^{1/T} (kz)^{-4} dz$ over the remaining bulk coordinate z

For the $SU(2)$ bi-doublet we read off the following vertex factor of the Lagrangian:

APPENDIX A. 5D FEYNMAN RULES



The vertex factor of the \tilde{T}_4 and \tilde{T}_3 gauge-boson interaction can be determined as:



Higgs Interactions We write down only the Yukawah interaction vertex between the \tilde{T}_4 and the ξ^1 field, since the Yukawah vertex factor of the \tilde{T}_4 and the ξ^1 can be used by replacing the Greek indices by Latin ones for the $\tilde{T}_3 \xi^1$ vertex factor. As usual the Yukawah interaction vertex is the only one in our unbroken theory, which changes the flavour. The flavour indices we use here are i and j . Note that the Higgs-field attains an additional $SU(2)_R$ index being a $SU(2)_L \times SU(2)_R$ bi-doublet. Note that due to the the covariant derivative the kinetic term of the Higgs bi-doublet induces a mixing between the $SU(2)_{L/R}$ field. This mixing generates the photon-Higgs vertices if there is one W_R^3 field and or one W_L^3 gauge-boson included into this vertex.

A.2 Propagators

The notations and conventions of [28] cover only the minimal RS model, therefore we need to adapt them to custodially protected RS model. Because we are working here in the unbroken theory this gives rise to two different kinds of fermion propagators for the new fermion fields of the ξ^1 and T^4 multiplets and one new type gauge-boson propagator for the new gauge-boson fields.

A.2.1 Fermion propagators

For the calculation of the new fermion propagators we distinguish between the ξ^1 and \tilde{T}^4 fermion multiplets. We define the ξ^1 propagator as follows

$$a \alpha \xrightarrow[y]{\vec{p}} x \quad b \beta = \delta^{ab} \delta^{\alpha\beta} \Delta_{\alpha}^{\xi^1}(p, x, y) \quad (\text{A.1})$$

where x, y are 5-coordinates and a, b, α, β $SU(2)$ indices. Observe that we neglect here the generation indices. The object $\Delta_{\alpha}^{\xi^1}(p, x, y)$ can be decomposed in the unbroken theory in the following way:

$$\Delta_{\alpha}^{\xi^1}(p, x, y) = \Delta_{mp}^{\xi^1}(p, x, y) \delta^{\alpha 1} + \Delta_L(p, x, y) \delta^{\alpha 2} \quad (\text{A.2})$$

where $\Delta_L(p, x, y)$ is the already in calculated doublet propagator, while $\Delta_{mp}(p, x, y)$ belongs to the new fermion fields inside the ξ^1 bi-doublet, which have $(-, +)$ boundary conditions for the left-handed mode functions.

For the \tilde{T}^4 $SU(2)$ triplet the fermion propagator can be written as

$$\alpha \xrightarrow[y]{\vec{p}} x \quad \beta = \Delta_{\alpha\beta}^{T^4}(p, x, y). \quad (\text{A.3})$$

APPENDIX A. 5D FEYNMAN RULES

In the \tilde{T}^4 basis the object $\Delta_{\alpha\beta}^{T^4}(p, x, y)$ is not diagonal in the two $SU(2)_R$ indices, because the first two components of \tilde{T}^4 are a linear combination (2.102) of the standard model singlet field L and a new field λ with $(-, +)$ boundary conditions for the right-handed mode functions. The object $\Delta_{\alpha\beta}^{T^4}(p, x, y)$ can be written in the basis (C.17) as

$$\Delta_{\alpha\beta}^{T^4}(p, x, y) = \begin{pmatrix} \Delta_E(p, x, y) + \Delta_{pm}(p, x, y) & i\Delta_E(p, x, y) - i\Delta_{pm}(p, x, y) & 0 \\ -i\Delta_E(p, x, y) + i\Delta_{pm}(p, x, y) & \Delta_E(p, x, y) + \Delta_{pm}(p, x, y) & 0 \\ 0 & 0 & 2\Delta_{pm}(p, x, y) \end{pmatrix}_{\alpha\beta} \times \frac{1}{2}. \quad (\text{A.4})$$

Here $\Delta_E(p, x, y)$ is the standard model singlet propagator and $\Delta_{mp}(p, x, y)$ the propagator for the fields of the T^4 triplet, which have $(-, +)$ ($(+, -)$) boundary conditions for the right (left)-handed mode functions. Note that one finds for T^3 triplet directly the propagator

$$\Delta_{ab}^{T^4}(p, x, y) = \delta_{ab}\Delta_{mp}(p, x, y) \quad (\text{A.5})$$

To compute $\Delta_{pm}(p, x, y)$ and $\Delta_{mp}(p, x, y)$ we use the general form of a fermion propagator in a RS model in conformal coordinates [28].

$$\Delta_X(p, x, y) = -F_X^-(p, x, y)\not{p}P_L - F_X^+(p, x, y)\not{p}P_R + d^+F_X^-(p, x, y)P_L + d^-F_X^+(p, x, y)P_R, \quad (\text{A.6})$$

where X can stand for arbitrary boundary conditions. The operators d^+ and d^- are defined as

$$d^+ = \partial_x - \frac{2}{x} - \frac{c}{x} \quad d^- = -\partial_x + \frac{2}{x} - \frac{c}{x}.$$

The F functions obey the differential equations [28]

$$\left[-p^2 - \partial_x^2 + \frac{c^2 - c - 6}{x} + \frac{4}{x} \right] F_X^-(p, x, y) = i(kx)^4 \delta(x - y) \quad (\text{A.7})$$

$$\left[-p^2 - \partial_x^2 + \frac{c^2 + c - 6}{x} + \frac{4}{x} \right] F_X^+(p, x, y) = i(kx)^4 \delta(x - y) \quad (\text{A.8})$$

and can be decomposed as follows in terms of Kaluza-Klein mode sums [28]:

$$F_X^+(p, x, y) = \sum_n f_X^{(n)}(x) \frac{-i}{p^2 - m_n^2} f_X^{(n)}(y) \quad (\text{A.9})$$

$$F_X^-(p, x, y) = \sum_n g_X^{(n)}(x) \frac{-i}{p^2 - m_n^2} g_X^{(n)}(y) \quad (\text{A.10})$$

$$d^- F_X^+(p, x, y) = \sum_n g_X^{(n)}(x) \frac{im_n}{p^2 - m_n^2} f_X^{(n)}(y) \quad (\text{A.11})$$

$$d^+ F_X^-(p, x, y) = \sum_n f_X^{(n)}(x) \frac{im_n}{p^2 - m_n^2} g_X^{(n)}(y) \quad (\text{A.12})$$

where $f_X(x)$ ($g_X(x)$) is the left (right)-handed mode function. The Kaluza-Klein decomposition is useful to determine the boundary conditions for the $\Delta_{pm}(p, x, y)$ and $\Delta_{mp}(p, x, y)$

A.2. PROPAGATORS

propagators.

The $\Delta_{mp}(p, x, y)$ propagator is the propagator of a ξ^i fermion field with $(-, +)$ $((+, -))$ boundary conditions for the left (right)-handed mode functions, i.e.

$$f_{mp}(x)|_{x=\frac{1}{k}} = 0 \quad g_{mp}(x)|_{x=\frac{1}{T}}. \quad (\text{A.13})$$

Using this we can deduct the boundary conditions of the F functions to be

$$F_{mp}^+(p, x, y)|_{x=\frac{1}{k}} = 0 \quad F_{mp}^-(p, x, y)|_{x=\frac{1}{T}} = 0 \quad (\text{A.14})$$

$$d^- F_{mp}^+(p, x, y)|_{x=\frac{1}{T}} = 0 \quad d^+ F_{mp}^-(p, x, y)|_{x=\frac{1}{k}} = 0. \quad (\text{A.15})$$

For the $\Delta_{pm}(p, x, y)$ propagator we note that boundary conditions of the associated mode functions are flipped compare to the $\Delta_{mp}(p, x, y)$ case, i.e.

$$f_{pm}(x)|_{x=\frac{1}{T}} = 0 \quad g_{pm}(x)|_{x=\frac{1}{k}}. \quad (\text{A.16})$$

This yields the following boundary conditions for the F function

$$F_{pm}^+(p, x, y)|_{x=\frac{1}{T}} = 0 \quad F_{pm}^-(p, x, y)|_{x=\frac{1}{k}} = 0 \quad (\text{A.17})$$

$$d^- F_{pm}^+(p, x, y)|_{x=\frac{1}{k}} = 0 \quad d^+ F_{pm}^-(p, x, y)|_{x=\frac{1}{T}} = 0. \quad (\text{A.18})$$

Note that in the unbroken phase we the propagator The chiral components of the fermion propagator can be written in a shorter way using the following definitions

$$S_+(p, x, y, c) = I_{c+\frac{1}{2}}(px) K_{c+\frac{1}{2}}(py) - K_{c+\frac{1}{2}}(px) I_{c+\frac{1}{2}}(py) \quad (\text{A.19})$$

$$S_-(p, x, y, c) = I_{c-\frac{1}{2}}(px) K_{c-\frac{1}{2}}(py) - K_{c-\frac{1}{2}}(px) I_{c-\frac{1}{2}}(py) \quad (\text{A.20})$$

$$\tilde{S}_+(p, x, y, c) = I_{c+\frac{1}{2}}(px) K_{c-\frac{1}{2}}(py) + K_{c+\frac{1}{2}}(px) I_{c-\frac{1}{2}}(py) \quad (\text{A.21})$$

$$\tilde{S}_-(p, x, y, c) = I_{c-\frac{1}{2}}(px) K_{c+\frac{1}{2}}(py) + K_{c-\frac{1}{2}}(px) I_{c+\frac{1}{2}}(py) \quad (\text{A.22})$$

APPENDIX A. 5D FEYNMAN RULES

which were first introduced by . With this new notation the chiral components of the $\Delta_{mp}^{\xi_1}$ propagator can be written as

$$F_{mp}^- (p, x, y) = \Theta(x-y) \frac{ik^4 x^{\frac{5}{2}} y^{\frac{5}{2}} \tilde{S}_+ (p, x, \frac{1}{T}, c) S_- (p, y, \frac{1}{k}, c)}{\tilde{S}_+ (p, \frac{1}{T}, \frac{1}{k}, c)} + \Theta(y-x) \frac{ik^4 x^{\frac{5}{2}} y^{\frac{5}{2}} \tilde{S}_+ (p, y, \frac{1}{T}, c) S_- (p, x, \frac{1}{k}, c)}{\tilde{S}_+ (p, \frac{1}{T}, \frac{1}{k}, c)} \quad (\text{A.23})$$

$$F_{mp}^+ (p, x, y) = -\Theta(x-y) \frac{ik^4 x^{\frac{5}{2}} y^{\frac{5}{2}} S_+ (p, x, \frac{1}{T}, c) \tilde{S}_+ (p, y, \frac{1}{k}, c)}{\tilde{S}_+ (p, \frac{1}{T}, \frac{1}{k}, c)} - \Theta(y-x) \frac{ik^4 x^{\frac{5}{2}} y^{\frac{5}{2}} S_+ (p, y, \frac{1}{T}, c) \tilde{S}_+ (p, x, \frac{1}{k}, c)}{\tilde{S}_+ (p, \frac{1}{T}, \frac{1}{k}, c)} \quad (\text{A.24})$$

$$d^+ F_{mp}^- (p, x, y) = p\Theta(x-y) \frac{ik^4 x^{\frac{5}{2}} y^{\frac{5}{2}} S_+ (p, x, \frac{1}{T}, c) S_- (p, y, \frac{1}{k}, c)}{\tilde{S}_+ (p, \frac{1}{T}, \frac{1}{k}, c)} + p\Theta(y-x) \frac{ik^4 x^{\frac{5}{2}} y^{\frac{5}{2}} \tilde{S}_+ (p, y, \frac{1}{T}, c) \tilde{S}_+ (p, x, \frac{1}{k}, c)}{\tilde{S}_+ (p, \frac{1}{T}, \frac{1}{k}, c)} \quad (\text{A.25})$$

$$d^- F_{mp}^+ (p, x, y) = p\Theta(x-y) \frac{ik^4 x^{\frac{5}{2}} y^{\frac{5}{2}} \tilde{S}_+ (p, x, \frac{1}{T}, c) \tilde{S}_+ (p, y, \frac{1}{k}, c)}{\tilde{S}_+ (p, \frac{1}{T}, \frac{1}{k}, c)} + p\Theta(y-x) \frac{ik^4 x^{\frac{5}{2}} y^{\frac{5}{2}} S_+ (p, y, \frac{1}{T}, c) S_- (p, x, \frac{1}{k}, c)}{\tilde{S}_+ (p, \frac{1}{T}, \frac{1}{k}, c)}. \quad (\text{A.26})$$

The chiral components of Δ_{pm} propagator can be expressed as

$$F_{pm}^- (p, x, y) = -\Theta(x-y) \frac{ik^4 x^{\frac{5}{2}} y^{\frac{5}{2}} S_- (p, x, \frac{1}{T}, cr) \tilde{S}_- (p, y, \frac{1}{k}, cr)}{\tilde{S}_- (p, \frac{1}{T}, \frac{1}{k}, cr)} - \Theta(y-x) \frac{ik^4 x^{\frac{5}{2}} y^{\frac{5}{2}} S_- (p, y, \frac{1}{T}, cr) \tilde{S}_- (p, x, \frac{1}{k}, cr)}{\tilde{S}_- (p, \frac{1}{T}, \frac{1}{k}, cr)} \quad (\text{A.27})$$

$$F_{pm}^+ (p, x, y) = \Theta(x-y) \frac{ik^4 x^{\frac{5}{2}} y^{\frac{5}{2}} \tilde{S}_+ (p, x, \frac{1}{T}, cr) S_+ (p, y, \frac{1}{k}, cr)}{\tilde{S}_- (p, \frac{1}{T}, \frac{1}{k}, cr)} + \Theta(y-x) \frac{ik^4 x^{\frac{5}{2}} y^{\frac{5}{2}} \tilde{S}_+ (p, y, \frac{1}{T}, cr) S_+ (p, x, \frac{1}{k}, cr)}{\tilde{S}_- (p, \frac{1}{T}, \frac{1}{k}, cr)} \quad (\text{A.28})$$

$$d^+ F_{pm}^- (p, x, y) = -p\Theta(x-y) \frac{ik^4 x^{\frac{5}{2}} y^{\frac{5}{2}} \tilde{S}_+ (p, x, \frac{1}{T}, cr) \tilde{S}_- (p, y, \frac{1}{k}, cr)}{\tilde{S}_- (p, \frac{1}{T}, \frac{1}{k}, cr)} + p\Theta(y-x) \frac{ik^4 x^{\frac{5}{2}} y^{\frac{5}{2}} S_- (p, y, \frac{1}{T}, cr) S_+ (p, x, \frac{1}{k}, cr)}{\tilde{S}_- (p, \frac{1}{T}, \frac{1}{k}, cr)} \quad (\text{A.29})$$

$$d^- F_{pm}^+ (p, x, y) = -p\Theta(x-y) \frac{ik^4 x^{\frac{5}{2}} y^{\frac{5}{2}} S_- (p, x, \frac{1}{T}, cr) S_+ (p, y, \frac{1}{k}, cr)}{\tilde{S}_- (p, \frac{1}{T}, \frac{1}{k}, cr)} + p\Theta(y-x) \frac{ik^4 x^{\frac{5}{2}} y^{\frac{5}{2}} \tilde{S}_+ (p, y, \frac{1}{T}, cr) \tilde{S}_- (p, x, \frac{1}{k}, cr)}{\tilde{S}_- (p, \frac{1}{T}, \frac{1}{k}, cr)} \quad (\text{A.30})$$

Note that these propagators can only be obtained after performing a Wick rotation $p \rightarrow ip_E$. For the off-shell Higgs exchange diagrams we need the zero mode subtracted brane to brane

A.2. PROPAGATORS

$F_{DZMS}^+(0, \frac{1}{T}, \frac{1}{T})$ and $F_{XZMS}^-(0, \frac{1}{T}, \frac{1}{T})$ functions, where X can be E or pm. Using the definition of F_E^+ in [28] one can find

$$F_{EZMS}^+ \left(p, \frac{1}{T}, \frac{1}{T} \right) = i \frac{k^4 \left(K_{cr+\frac{1}{2}} \left(\frac{p}{k} \right) I_{cr-\frac{1}{2}} \left(\frac{p}{T} \right) + I_{cr+\frac{1}{2}} \left(\frac{p}{k} \right) K_{cr-\frac{1}{2}} \left(\frac{p}{T} \right) \right)}{pT^4 \left(K_{cr+\frac{1}{2}} \left(\frac{p}{k} \right) I_{cr+\frac{1}{2}} \left(\frac{p}{T} \right) - I_{cr+\frac{1}{2}} \left(\frac{p}{k} \right) K_{cr+\frac{1}{2}} \left(\frac{p}{T} \right) \right)} \quad (\text{A.31})$$

$$-i \frac{g_E^{(0)} \left(\frac{1}{T} \right) g_E^{(0)} \left(\frac{1}{T} \right)}{p^2}. \quad (\text{A.32})$$

To perform the limit $p \rightarrow 0$ one has to use the series representation of I Bessel function. To do this we apply first

$$K_\mu(x) = \frac{\pi}{2} \frac{I_{-\mu}(x) - I_\mu(x)}{\sin(\pi\mu)} \quad (\text{A.33})$$

to find

$$F_{EZMS}^+ \left(p, \frac{1}{T}, \frac{1}{T} \right) = i \frac{k^4 \left(I_{-cr-\frac{1}{2}} \left(\frac{p}{k} \right) I_{cr-\frac{1}{2}} \left(\frac{p}{T} \right) - I_{cr+\frac{1}{2}} \left(\frac{p}{k} \right) I_{\frac{1}{2}-cr} \left(\frac{p}{T} \right) \right)}{pT^4 \left(I_{-cr-\frac{1}{2}} \left(\frac{p}{k} \right) I_{cr+\frac{1}{2}} \left(\frac{p}{T} \right) - I_{cr+\frac{1}{2}} \left(\frac{p}{k} \right) I_{-cr-\frac{1}{2}} \left(\frac{p}{T} \right) \right)} \quad (\text{A.34})$$

$$-i \frac{g_E^{(0)} \left(\frac{1}{T} \right) g_E^{(0)} \left(\frac{1}{T} \right)}{p^2}.$$

Then using the series representation of the Bessel functions like for example

$$I_\mu(x) = \sum_{n=0}^{\infty} \frac{1}{n! \Gamma(\mu + n + 1)} \left(\frac{x}{2} \right)^{\mu+2n} \quad (\text{A.35})$$

we find

$$F_{EZMS}^+ \left(0, \frac{1}{T}, \frac{1}{T} \right) =$$

$$i \frac{(2cr-1)k^{4cr+6} - (2cr+3)k^4 T^{4cr+2}}{(4cr(cr+1)-3)T^5 (k^{2cr+1} - T^{2cr+1})^2}$$

$$+ i \frac{k^{2cr+3} T^{2cr+1} ((3-4cr(cr+1))k^2 + (2crT+T)^2)}{(4cr(cr+1)-3)T^5 (k^{2cr+1} - T^{2cr+1})^2} \quad (\text{A.36})$$

For the other two needed F functions finds the limit in the same way

$$F_{DZMS}^+ \left(0, \frac{1}{T}, \frac{1}{T} \right) =$$

$$i \frac{(2c-3)T^2 k^{4c+4} - (2c+1)k^6 T^{4c}}{(2c-3)(2c+1)T^5 (Tk^{2c} - kT^{2c})^2}$$

$$+ i \frac{k^{2c+3} T^{2c+1} ((3-4(c-1)c)k^2 + (1-2c)^2 T^2)}{(2c-3)(2c+1)T^5 (Tk^{2c} - kT^{2c})^2} \quad (\text{A.37})$$

$$F_{pm}^- \left(0, \frac{1}{T}, \frac{1}{T} \right) =$$

$$\frac{ik^4}{T^5} - \frac{ik^{2cr+3} T^{-2cr-4}}{1-2cr} \quad (\text{A.38})$$

APPENDIX A. 5D FEYNMAN RULES

A.2.2 Gauge boson propagator

In this section we will derive the gauge propagator for the Z_X and $W_R^{b=1,2}$ fields, which have $(-, +)$ boundary conditions. The derivation stays close to [28]. We use the R_ξ gauge here. The vector part of a general gauge-boson propagator can be written as [28]

$$\Delta_{mp}^{\mu\nu}(p, x, y) = \Delta_{mp}(p, x, y) \eta^{\mu\nu} + \frac{p^\mu p^\nu}{p^2} \left(\Delta_{mp} \left(\frac{p}{\sqrt{\xi}}, x, y \right) - \Delta_{mp}(p, x, y) \right) \quad (\text{A.39})$$

where the transverse part of the gauge-boson propagator $\Delta_{mp}(p, x, y)$ is defined by the differential equation [28]

$$\left(p^2 + x \partial_x \frac{1}{x} \partial_x \right) \Delta_{mp}(p, x, y) = -ikx \delta(x - y). \quad (\text{A.40})$$

A complete solution can be found by demanding the boundary conditions

$$\partial_x \Delta_{mp}(p, x, y)|_{x=\frac{1}{T}} = 0 \quad \Delta_{mp}(p, x, y)|_{x=\frac{1}{k}} = 0. \quad (\text{A.41})$$

The scalar propagator of the fifth coordinate satisfies the the differential equation [28]

$$\left[p^2 + \xi \partial_x x \partial_x \frac{1}{x} \right] \Delta_{5mp}(p, x, y) = ikx \delta(x - y). \quad (\text{A.42})$$

The solution can be easily computed by using the fifth coordinate mode functions, which obey the equation [28]

$$\xi \partial_x \left(x \partial_x \frac{1}{x} f_{W_5 mp}^{(n)}(x) \right) = -\xi m_n^2 f_{W_5 mp}^{(n)}(x). \quad (\text{A.43})$$

Thus the Kaluza-Klein decomposition of $\Delta_{5mp}(p, x, y)$ is after using the completeness relation of the mode functions

$$\Delta_{5mp}(p, x, y) = \sum_n f_{W_5 mp}^{(n)}(x) \frac{i}{p^2 - \xi m_n^2} f_{W_5 mp}^{(n)}(y). \quad (\text{A.44})$$

The fifth coordinate mode function $f_{W_5 mp}^{(n)}(x)$ are not independent of the mode functions of the vector part of the gauge-boson fields. There exists the following relation between this two kinds of mode functions [28]

$$\partial_x f_{W mp}^{(n)}(x) = m_n f_{W_5 mp}^{(n)}(x). \quad (\text{A.45})$$

Here the vector part mode function satisfies the equation [28]

$$x \partial_x \left(\frac{1}{x} \partial_x f_{W mp}^{(n)}(x) \right) = -m_n^2 f_{W mp}^{(n)}(x)$$

with the boundary conditions

$$\partial_x f_{W mp}^{(n)}(x)|_{x=\frac{1}{T}} = 0 \quad f_{W mp}^{(n)}(x)|_{x=\frac{1}{k}} = 0. \quad (\text{A.46})$$

Thus we find with the mode expansion of $\Delta_{5mp}(p, x, y)$ and $\Delta_{mp}(p, x, y)$

$$\Delta_{mp}(p, x, y) = \sum_n f_{W mp}^{(n)}(x) \frac{-i}{p^2 - m_n^2} f_{W mp}^{(n)}(y)$$

the relation

$$\Delta_{5mp}(p, x, y) + \frac{\partial_x \partial_y}{p^2} \Delta_{mp} \left(\frac{p}{\sqrt{\xi}}, x, y \right) = \frac{1}{p^2} \sum_n f_{W_5 mp}^{(n)}(x) f_{W_5 mp}^{(n)}(y) = \frac{ikx}{p^2} \delta(x - y) \quad (\text{A.47})$$

which gives us directly the solution of the scalar fifth propagator in terms of the transverse part of the vector part of the gauge-boson propagator. Note that the delta function on the right-handside of equation (A.47) is being cancelled by the derivatives acting on the heavisidetheta functions of $\Delta_{mp}(p, x, y)$.

Again we only give the full solution of the free gauge propagators after wickrotation

$$\begin{aligned} \Delta_{mp}(p, x, y) &= ikxy \Theta(x - y) \frac{\tilde{S}_+ \left(p, x, \frac{1}{T}, \frac{1}{2} \right) S_+ \left(p, y, \frac{1}{k}, \frac{1}{2} \right)}{\tilde{S}_+ \left(p, \frac{1}{k}, \frac{1}{T}, \frac{1}{2} \right)} \\ &\quad + ikxy \Theta(y - x) \frac{\tilde{S}_+ \left(p, y, \frac{1}{T}, \frac{1}{2} \right) S_+ \left(p, x, \frac{1}{k}, \frac{1}{2} \right)}{\tilde{S}_+ \left(p, \frac{1}{k}, \frac{1}{T}, \frac{1}{2} \right)} \end{aligned} \quad (\text{A.48})$$

$$\begin{aligned} \Delta_{5mp}(p, x, y) &= ikxy \Theta(x - y) \frac{S_- \left(\frac{p}{\sqrt{\xi}}, x, \frac{1}{T}, \frac{1}{2} \right) \tilde{S}_+ \left(\frac{p}{\sqrt{\xi}}, \frac{1}{k}, y, \frac{1}{2} \right)}{\tilde{S}_+ \left(p, \frac{1}{k}, \frac{1}{T}, \frac{1}{2} \right)} \\ &\quad + ikxy \Theta(y - x) \frac{S_- \left(\frac{p}{\sqrt{\xi}}, y, \frac{1}{T}, \frac{1}{2} \right) \tilde{S}_+ \left(\frac{p}{\sqrt{\xi}}, \frac{1}{k}, x, \frac{1}{2} \right)}{\tilde{S}_+ \left(p, \frac{1}{k}, \frac{1}{T}, \frac{1}{2} \right)} \end{aligned} \quad (\text{A.49})$$

APPENDIX A. 5D FEYNMAN RULES

Appendix B

The bulk Higgs

For the bulk Higgs we follow [80, 81]. The 5D Higgs action reads

$$S_\Phi = \int d^4x \int_{\frac{1}{k}}^{\frac{1}{T}} dz \frac{1}{(kz)^5} \left[g^{MN} (D_M \Phi)^\dagger (D_N \Phi) - \frac{\mu^2}{z^2} \Phi^\dagger \Phi \right. \\ \left. - \delta(\sqrt{g_{55}}(z - 1/T)) V_{1/T} - \delta(\sqrt{g_{55}}(z - 1/k)) V_{1/k} \right]. \quad (\text{B.1})$$

The brane potentials are

$$V_{1/k} = m_{1/k} \Phi^\dagger \Phi, \quad V_{1/T} = -m_{1/T} \Phi^\dagger \Phi + \lambda (\Phi^\dagger \Phi)^2 \quad (\text{B.2})$$

with $m_{1/k} = (2 + \beta)k$. We define $\beta = \sqrt{4 + \mu^2}$. Note that in [80] the IR brane potential is, up to normalization, written as

$$V_{1/T} = \frac{\tilde{\lambda}}{2k^2} \left[\Phi^\dagger \Phi - \frac{v_{\text{TeV}}^2}{2} \right]^2 \quad (\text{B.3})$$

where the coupling constant $\tilde{\lambda}$ is dimensionless. For our purposes the form of (B.2) is more convenient. The choice for the UV potential parameter $m_{1/k}$ leads to a Higgs vacuum expectation value (vev) that rises towards the IR brane for positive β .

B.1 Zero mode and vacuum expectation value

The zero-mode equations of motion are given by

$$\left(z^3 \partial_z z^{-3} \partial_z - \frac{\mu^2}{z^2} \right) \Phi^{(0)}(z) = -m_0^2 \Phi^{(0)}(z) \quad (\text{B.4})$$

$$\frac{\partial_z \Phi^{(0)}}{\Phi^{(0)}} \Big|_{z=1/k} = m_{1/k}, \quad \frac{\partial_z \Phi^{(0)}}{\Phi^{(0)}} \Big|_{z=1/T} = m_{1/T} \frac{T}{k} \quad (\text{B.5})$$

The boundary conditions ensure that the boundary terms arising from integration by parts vanish. m_0^2 is the squared mass of the zero mode in the *unbroken* phase. As we will see

APPENDIX B. THE BULK HIGGS

below it is tachyonic and of the order of the physical Higgs mass, i.e. much smaller than the KK scale T .

The general solution of the differential equation is

$$\Phi^{(0)}(z) = \mathcal{N}_0 z^2 (\mathcal{J}_\beta(m_0 z) + C \mathcal{Y}_\beta(m_0 z)). \quad (\text{B.6})$$

The UV-brane boundary condition can be used to determine

$$C = -\frac{\mathcal{J}_{\beta+1}(m_0/k)}{\mathcal{Y}_{\beta+1}(m_0/k)} \approx \frac{2^{-2(1+\beta)}\pi}{\Gamma(1+\beta)\Gamma(2+\beta)} \left(\frac{m_0}{k}\right)^{2+2\beta} \quad \text{for } m_0 \ll k. \quad (\text{B.7})$$

Observing that $\mathcal{J}_\beta(x)/\mathcal{Y}_\beta(x) \propto x^{2\beta}$ for small arguments, we find that

$$\mathcal{J}_\beta(m_0 z) \gg C \mathcal{Y}_\beta(m_0 z) \quad (\text{B.8})$$

for $m_0 \ll T$. We can use this approximation for the zero mode to obtain

$$\Phi^{(0)}(z) = \mathcal{N}_0 z^2 \mathcal{J}_\beta(m_0 z) \approx \mathcal{N}_0 z^{2+\beta} + \mathcal{O}(m_0 z). \quad (\text{B.9})$$

The overall normalization is given by

$$\int_{\frac{1}{k}}^{\frac{1}{T}} \frac{dz}{(kz)^3} \Phi^{(0)}(z)^2 = 1 \quad \Rightarrow \quad \mathcal{N}_0 \approx \sqrt{\frac{2(1+\beta)}{1-\epsilon^{2+2\beta}}} k^{3/2} T^{1+\beta}. \quad (\text{B.10})$$

Up to higher terms in m_0/T the zero-mode mass is determined by the equation

$$\left. \frac{\partial_z \Phi}{\Phi} \right|_{z=1/T} = T(2+\beta) - m_0 \frac{\mathcal{J}_{\beta+1}(m_0/T)}{\mathcal{J}_\beta(m_0/T)} = m_{1/T} \frac{T}{k}. \quad (\text{B.11})$$

Expanding the Bessel function for small argument, we find

$$m_{1/T} \frac{T}{k} - T(2+\beta) = -\frac{m_0^2}{2(1+\beta)T} + \text{higher-order terms}, \quad (\text{B.12})$$

which implies

$$m_0^2 \approx 2(1+\beta) \left(2+\beta - \frac{m_{1/T}}{k}\right) T^2. \quad (\text{B.13})$$

Note that m_0 must be a small compared to T , otherwise the expansions above would not have been allowed. We return to this point below.

The 5D profile of the vev is not needed in our computation, since it is done in the unbroken electroweak phase. The Higgs vev only enters at the 4D level in the effective Lagrangian—as a low-energy parameter determined from experiment. Still it is instructive to see how the vev profile arises. To this end we substitute $\Phi \rightarrow \frac{1}{\sqrt{2}}(v+h)$ into the Lagrangian (B.1) and expand all terms (see [78] for a more detailed derivation). We can use that 4D derivatives on v vanish. This leads to the equations

$$(-\partial_z + \frac{T}{k} m_{1/T} - 3\frac{T}{k} \lambda v^2) h|_{z \rightarrow 1/T} = 0 \quad (\text{B.14})$$

$$(\partial_z - m_{1/k}) h|_{z \rightarrow 1/k} = 0 \quad (\text{B.15})$$

$$(-\partial_z + \frac{T}{k} m_{1/T} - \frac{T}{k} \lambda v^2) v|_{z \rightarrow 1/T} = 0 \quad (\text{B.16})$$

$$(\partial_z - m_{1/k}) v|_{z \rightarrow 1/k} = 0 \quad (\text{B.17})$$

along with the standard equation for Higgs bulk profiles. This gives the solution

$$v(z) = \mathcal{N}_v z^{2+\beta}, \quad (\text{B.18})$$

which is strongly IR localised already for moderately large, positive values of β . The IR boundary condition determines

$$\mathcal{N}_v^2 = (m_{1/T} - (2 + \beta)k) \frac{1}{\lambda} T^{4+2\beta}. \quad (\text{B.19})$$

Equivalently, by requiring that W boson acquires the correct mass

$$\mathcal{N}_v = \sqrt{\frac{2(1 + \beta)}{1 - \epsilon^{2+2\beta}}} T^{\beta+1} k^{3/2} v_{\text{SM}}. \quad (\text{B.20})$$

With this input we can compute the physical Higgs mass

$$\begin{aligned} m_H^2 &= m_0^2 + 6(1 + \beta) \frac{T^2}{k} \lambda v(1/T)^2 \\ &= 2(1 + \beta) \left((2 + \beta)k - m_{1/T} + 3\lambda v(1/T)^2 \right) \frac{T^2}{k}. \end{aligned} \quad (\text{B.21})$$

Using

$$\lambda \frac{v(1/T)^2}{k} = \frac{m_{1/T}}{k} - (2 + \beta) \quad (\text{B.22})$$

this result can be rewritten into

$$m_H^2 = 4(1 + \beta) \lambda \frac{v(1/T)^2}{k} T^2 \stackrel{!}{\approx} (125 \text{ GeV})^2 \quad (\text{B.23})$$

and

$$m_0^2 = -\frac{m_H^2}{2} < 0. \quad (\text{B.24})$$

Thus we find $|m_0^2| \ll T^2$, which was necessary to justify the expansion in the broken phase. We note that the requirement that $m_H \approx 125$ GeV implies a fine-tuning between the parameters $m_{1/T}$ and $(2 + \beta)k$, see (B.13). We further note the relations

$$\lambda v(1/T)^2 = \frac{m_H^2}{4(1 + \beta)T^2} k, \quad (\text{B.25})$$

$$m_{1/T} = (2 + \beta)k + \underbrace{\frac{m_H^2}{4(1 + \beta)T^2}}_{\ll 1} k. \quad (\text{B.26})$$

B.2 Higgs Propagator

The 5D Higgs propagator is determined by the equations

$$\left[p^2 - \frac{\mu^2}{z^2} + z^3 \partial_z z^{-3} \partial_z \right] \Delta_\Phi(p, z, z') = i(kz')^3 \delta(z - z'), \quad (\text{B.27})$$

$$\partial_z \Delta_\Phi(p, z, z')|_{z=1/k} = m_{1/k} \Delta_\Phi(p, 1/k, z'), \quad (\text{B.28})$$

$$\partial_z \Delta_\Phi(p, z, z')|_{z=1/T} = m_{1/T} \frac{T}{k} \Delta_\Phi(p, 1/T, z'), \quad (\text{B.29})$$

APPENDIX B. THE BULK HIGGS

which can be solved in the standard way, see e.g. [28]. After Wick rotation to Euclidean space, the full Higgs propagator is given by

$$\begin{aligned} \Delta_\phi(p, z, z') &= \Theta(z - z') ik^3 z^2 z'^2 \\ &\times \frac{(I_{\beta+1}(\frac{p}{k}) K_\beta(pz') + K_{\beta+1}(\frac{p}{k}) I_\beta(pz')) (I_{\beta+1}(\frac{p}{T}) K_\beta(pz) + K_{\beta+1}(\frac{p}{T}) I_\beta(pz))}{I_{\beta+1}(\frac{p}{k}) K_{\beta+1}(\frac{p}{T}) - K_{\beta+1}(\frac{p}{k}) I_{\beta+1}(\frac{p}{T})} \\ &+ \{z \leftrightarrow z'\}, \end{aligned} \quad (\text{B.30})$$

where K and I are modified Bessel functions. It is useful to not only have the full propagator, but also the zero-mode subtracted propagator. We only work to leading accuracy in v/T , that is we approximate

$$m_{1/T} \frac{T}{k} = (2 + \beta)T. \quad (\text{B.31})$$

The Higgs zero mode is then massless, and its profile is proportional to the vev profile derived previously. The zero mode can readily be removed from Euclidean propagator via

$$\Delta_\phi^{\text{ZMS}}(p, z, z') = \Delta_\phi(p, z, z') - \frac{i}{(-p^2)} \Phi^{(0)}(z) \Phi^{(0)}(z'), \quad (\text{B.32})$$

since removing the zero mode corresponds to removing the pole at $p^2 = 0$ from the full propagator.

B.3 Yukawa matrix scaling

For the bulk Higgs field the Yukawa coupling develops a dependence on the Higgs 5D mass μ or, equivalently, β . To see how this dependence arises let us compare the situation with the delta-regularized narrow bulk Higgs (2.64). In the latter case, we find for the 4D SM lepton Yukawa matrix the standard expression

$$\begin{aligned} y_{ij} &= f_{L_i}^{(0)}(1/T) g_{E_j}^{(0)}(1/T) \frac{T^3}{k^4} Y_{ij} + \text{higher terms} \\ &= \sqrt{\frac{1 - 2c_{L_i}}{1 - \epsilon^{1-2c_{L_i}}}} \sqrt{\frac{1 + 2c_{E_j}}{1 - \epsilon^{1+2c_{E_j}}}} Y_{ij}. \end{aligned} \quad (\text{B.33})$$

For the bulk Higgs the bulk action contains the interaction term

$$S \supset - \int \frac{\frac{1}{T}}{(kz)^5} \int d^4x Y_{ij}^\beta \bar{L}_i(x, z) \Phi(x, z) E_j(x, z) + \text{h.c.}, \quad (\text{B.34})$$

where L, E, Φ are 5D fields, and Y^β is the dimensionful bulk Higgs Yukawa coupling. Inserting zero modes and integrating over z , we obtain (up to terms suppressed by powers of ϵ)

$$y_{ij} = Y^\beta \sqrt{\frac{1 - 2c_{L_i}}{1 - \epsilon^{1-2c_{L_i}}}} \sqrt{\frac{1 + 2c_{E_j}}{1 - \epsilon^{1+2c_{E_j}}}} \frac{\sqrt{2(1 + \beta)} k^{1/2}}{2 - c_{L_i} + c_{E_j} + \beta}. \quad (\text{B.35})$$

B.4. KK HIGGS EXAMPLE: FOUR-FERMION OPERATORS

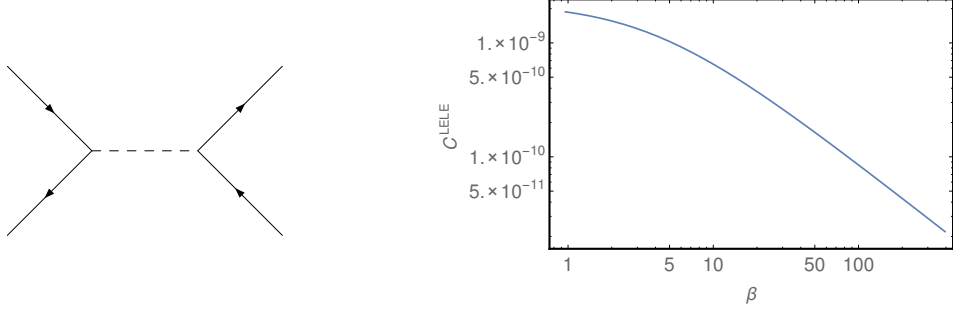


Figure B.1: *Left panel:* Diagram contributing to the matching onto $\bar{L}_i E_j \bar{L}_k E_l$. The intermediate Higgs propagator is zero-mode subtracted to remove long-distance contributions. *Right panel:* Wilson coefficient C_{1111}^{LELE} as a function of β for $T = 1$ TeV, $c_{L_1} = -c_{E_1} = 0.6$ and $Y = 1$.

Since the SM Yukawa coupling should remain finite for large β , the bulk-Higgs Yukawa coupling scales as

$$Y^\beta \propto \frac{2 - c_{L_i} + c_{E_j} + \beta}{\sqrt{2(1 + \beta)}} \xrightarrow{\beta \rightarrow \infty} \frac{\sqrt{\beta}}{\sqrt{2}}. \quad (\text{B.36})$$

Comparing the expressions (B.33) and (B.35) we identify

$$Y^\beta = \frac{Y}{\sqrt{k}} \frac{2 - c_{L_i} + c_{E_j} + \beta}{\sqrt{2(1 + \beta)}}. \quad (\text{B.37})$$

B.4 KK Higgs example: Four-fermion operators

To gain some intuition for the properties of the Higgs KK modes we consider the example of the Feynman diagram in Figure B.1, which might contribute to the matching of four-fermion operators of the form $\bar{L}_i E_j \bar{L}_k E_l$. The corresponding Wilson coefficient is given by

$$\frac{C_{ijkl}^{LELE}}{T^2} = iY_{ij}^\beta Y_{kl}^\beta \int_{\frac{1}{k}}^{\frac{1}{T}} \frac{dx}{(kx)^5} \int_{\frac{1}{k}}^{\frac{1}{T}} \frac{dy}{(ky)^5} f_{L_i}^{(0)}(x) g_{L_j}^{(0)}(x) \Delta_\phi^{\text{ZMS}}(p = 0, x, y) f_{L_k}^{(0)}(y) g_{L_l}^{(0)}(y). \quad (\text{B.38})$$

For vanishing four-momentum exchange the zero-mode subtracted Higgs propagator has the particularly simple form

$$\begin{aligned} \Delta_\phi^{\text{ZMS}}(0, x, y) = & -\frac{ik^3 x^{2-\beta} y^{2-\beta}}{2\beta} \left[T^{2\beta} x^{2\beta} y^{2\beta} \left(\beta (T^2 (x^2 + y^2) - 2) - \frac{2}{2 + \beta} \right) \right. \\ & \left. + x^{2\beta} \theta(y - x) + y^{2\beta} \theta(x - y) \right], \end{aligned} \quad (\text{B.39})$$

where we dropped terms suppressed by powers of T/k . With this expression the integrals over x and y in (B.38) are straightforward, and C_{ijkl}^{LELE} can be determined analytically for all values of β . C_{ijkl}^{LELE} vanishes as $1/\beta$ in the limit $\beta \rightarrow \infty$, as illustrated in the right panel of Figure B.1.

APPENDIX B. THE BULK HIGGS

This result can be understood by looking at the defining expression. The scaling with β is determined by three factors: the Yukawa matrix scaling, the scaling of the Higgs propagator, and the scaling of the integration variables x, y in the relevant integration regions. The two Yukawa couplings each contribute a factor of $\sqrt{\beta}$. The Higgs propagator is slightly more complicated. Let us examine the three terms square brackets in (B.39) separately. The first term (without step-functions) does not feature an immediate suppression for large β , since the $1/\beta$ in the prefactor of the square bracket is cancelled. The suppression arises only after integration over the bulk coordinates. To see this, we write x and y in the overall factor $(T^2xy)^\beta$ as $1/T(1 - x_0/\beta)$ and $1/T(1 - y_0/\beta)$, respectively, such that x_0 and y_0 measure the distance of x, y from the IR brane in units of $1/(\beta T)$, the typical scale for Higgs KK excitations. We then find factors of the form $(1 - x_0/\beta)^\beta$ and $(1 - y_0/\beta)^\beta$, which behave as e^{-x_0} and e^{-y_0} for large β , respectively. Hence the first term counts as $\mathcal{O}(1)$ only for x and y within $1/(\beta T)$ of the IR brane. The 5D coordinate integrals then count as $1/(\beta T)$ each, and the contribution of the first term in (B.39) to the Wilson coefficient is of order $(\sqrt{\beta})^2 \times 1 \times 1/\beta^2$, which vanishes for large β . The remaining two terms in (B.39) have different properties. There is a global factor of $1/\beta$, but there is no requirement that x, y are close to the IR brane. Let us focus on the second term, which is non-zero only for $y > x$. It contains the factor $(x/y)^\beta$, which ensures that the contribution to the Wilson coefficient is exponentially suppressed if $x \ll y(1 - 1/\beta)$. Changing integration variables from x, y to $y, x - y$ shows that the integral over $x - y$ counts as $1/(\beta T)$, while the integral over y is effectively unconstrained. Thus the overall total scaling is $(\sqrt{\beta})^2 \times 1/\beta \times 1/\beta$, which also vanishes for large β . The same argument with $x \leftrightarrow y$ ensures that the third term in (B.39) does not contribute to C_{ijkl}^{LELE} for $\beta \rightarrow \infty$.

B.5 KK Higgs contributions

The contribution of KK Higgs modes to a_{ij}^H is proportional to the corresponding contribution for the Higgs zero-mode for each diagram topology. It is therefore convenient to study the ratio of the two contributions,

$$R = \frac{a_{\text{KK}}^H}{a_{\text{ZM}}^H}. \quad (\text{B.40})$$

Up to small corrections this ratio is also independent of the flavour of the propagating states. The Higgs KK contribution can then be obtained by multiplying the zero-mode result by the corresponding R . It should be noted that not all topologies shown below actually contribute to a_{ij}^H in a specific RS model, either because the combination of SU(2) and U(1) group factors vanishes or because the model does not have Feynman rules that allow for the particular diagram to exist. Note that we do not separate contributions from wrong- and correct-chirality Higgs couplings. The numbers refer to the sum of both type of contributions, and are given by:

B.5. KK HIGGS CONTRIBUTIONS

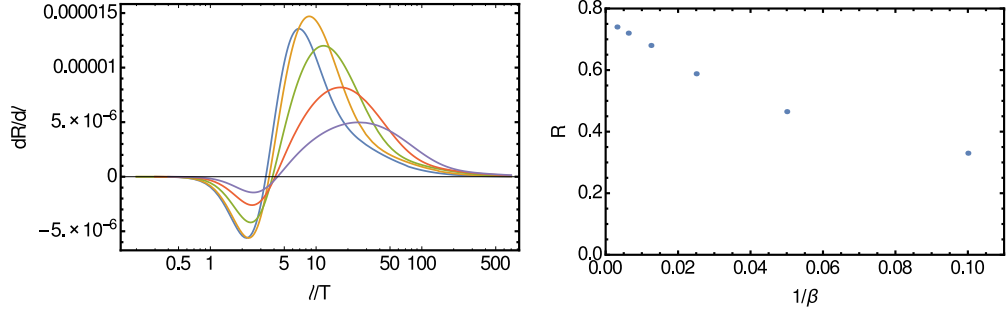


Figure B.2: *Left panel:* dR/dl as a function of the loop momentum for $\beta = 10, 20, 40, 80, 160$ (curves from left to right) for the diagrams in the last line of (B.41). *Right panel:* Corresponding ratio R as a function of $1/\beta$ (no uncertainties shown).

The figure shows four Feynman diagrams, each with a corresponding R value and error estimate in parentheses:

- Diagram 1: $R \approx 0.27(0.01)$
- Diagram 2: $R \approx 0.27(0.01)$
- Diagram 3: $R \approx 0.08(0.01)$
- Diagram 4: $R \approx 0.08(0.01)$
- Diagram 5: $R \approx 0.15(0.05)$
- Diagram 6: $R \approx 0.77(0.08)$

(B.41)

Our error estimates are shown in parenthesis. It arises from the numerical integration error and an estimate for the extrapolation error to $\beta = \infty$, since a numerically stable evaluation is possible only up to $\beta \approx 200 - 300$. The numerically most challenging diagrams are the ones where the photon is emitted from the Higgs, since they contain products of KK Higgs propagators. We also note that the KK Higgs contribution converges relatively slowly as $\beta \rightarrow \infty$, if the diagrams involve an external Higgs attachment to a fermion line in the loop, as illustrated in Figure B.2. The typical scaling with powers of β in the different momentum regions discussed in the main text does not set in until $\beta \sim 40$. This behaviour agrees with observations made in [79].

APPENDIX B. THE BULK HIGGS

Appendix C

Explicit diagram expressions

This part of the appendix is dedicated to write down the explicit analytic expressions of the Wilson coefficients for the leptonic dipole operator. We only include the genuine custodial protected RS model diagrams. [28]. The abelian diagrams with Z_x field inside the loop can be directly build the gauge-boson propagator $\Delta_{ZMS} \rightarrow \Delta_{mp}$, $\Delta_5 \rightarrow \Delta_{5mp}$ and the coupling $(g'_5)^2 \rightarrow g_5^2 - (g'_5)^2$ in the explicit expressions. Thus in the gauge exchange sector we will write down only the new non-abelian diagrams appearing in the custodially protected Randall-Sundrum model.

In all diagrams we assume that an external photon is emitted and that the external Higgs field denoted by the grey square can be replaced by its vacuum expectation value. To generate the incoming SM singlet it is insightful first to look at the \tilde{T}_4 triplet after setting all other fields except the SM singlet to zero.

$$\tilde{T}_{4|\lambda=N=0}^\alpha = \frac{E}{\sqrt{2}} (\delta^{\alpha 1} - i\delta^{\alpha 2}) \quad (\text{C.1})$$

Thus if we define $SU(2)_R$ factor

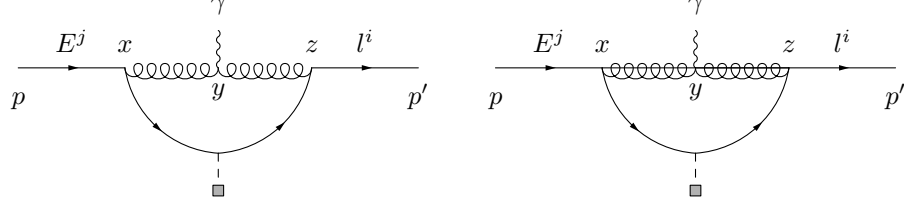
$$C^\alpha = \frac{1}{\sqrt{2}} (\delta^{\alpha 1} - i\delta^{\alpha 2}) \quad (\text{C.2})$$

we are able to take the appearance of the SM singlet as the initial state into account. To shorten the notation in some diagrams it is useful to write the Higgs vev as follows

$$\tilde{H}_{ab} = \begin{pmatrix} 0 & -1 \\ 1 & 0 \end{pmatrix}_{ab}. \quad (\text{C.3})$$

We use the notation $\hat{p} = p - l$ and $\hat{p}' = p' - l$ for the momenta appearing in the loops. Similar to [28] the first expression of the diagrams contains almost any simplification. The second expression of each diagram contains some simplifications. In particular the fermion propagators are decomposed into their non-vanishing chiral components and the $SU(2)$ group factors have been calculated. We only write down the analytic form of the on-shell contribution. To differentiate better between Lorentz indices and the $SU(2)_R$ indices we give up the Greek notation for the $SU(2)_R$ indices and use only Latin digits for those. Our convention is to sum over multiple $SU(2)$ indices of the same kind. There are usually more than two $SU(2)$ indices of the same kind appearing in each diagram expression. For the analytic expressions of each diagram we have also included the generation indices of the charged leptons.

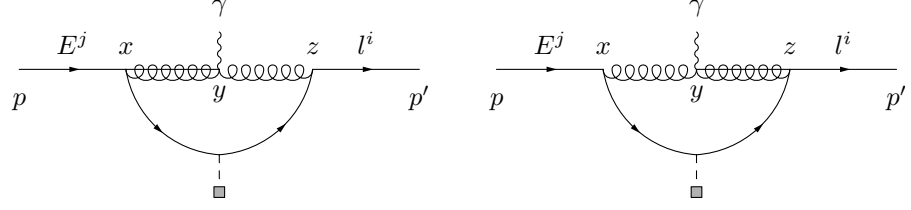
C.1 Gauge boson exchange diagrams



$$\begin{aligned}
 W1c &= ig_5^2 (-e_5) \left(-i \frac{\sqrt{2} T^3}{k^3} y_{ij}^{5D} \right) \frac{\nu}{\sqrt{2}} \frac{(\tau^a)_{2c}}{2} \frac{(\tau^b)_{c1}}{2} \epsilon^{dek} C^e \epsilon^{ak3} \int_{\frac{1}{k}}^{\frac{1}{T}} \frac{dx}{(kx)^4} \\
 &\int_{\frac{1}{k}}^{\frac{1}{T}} \frac{dy}{(ky)} \int_{\frac{1}{k}}^{\frac{1}{T}} \frac{dz}{(kz)^4} \int \frac{d^4 l}{(2\pi)^4} f_{l_i}^{(0)}(z) f_{\gamma}^{(0)} g_{E_j}(x) \epsilon^{*\mu} \Delta_{mp}^{\lambda\kappa}(\hat{p}, x, y) \Delta_{mp}^{\nu\theta}(\hat{p}', y, z) \\
 &\times \left[(p' - 2p + l)_{\nu} \eta_{\mu\lambda} + (p' + p - 2l)_{\mu} \eta_{\nu\lambda} + (p - 2p' + l)_{\lambda} \eta_{\mu\nu} \right] \\
 &\times \bar{L}^i(p') P_R \gamma_{\theta} \Delta_c^{\xi_i}(l, z, 1/T) \Delta_{bd}^{T_j^4}(l, 1/T, x) \gamma_{\kappa} P_R E^j(p) \\
 &= -\frac{g_5^2 e_5 T^3 y_{ij}^{5D}}{2k^3} \frac{\nu}{\sqrt{2}} \int_{\frac{1}{k}}^{\frac{1}{T}} \frac{dx}{(kx)^4} \int_{\frac{1}{k}}^{\frac{1}{T}} \frac{dy}{(ky)} \int_{\frac{1}{k}}^{\frac{1}{T}} \frac{dz}{(kz)^4} \int \frac{d^4 l}{(2\pi)^4} \\
 &f_{l_i}^{(0)}(z) f_{\gamma}^{(0)} g_{E_j}(x) \epsilon^{*\mu} \Delta_{mp}^{\lambda\kappa}(\hat{p}, x, y) \Delta_{mp}^{\nu\theta}(\hat{p}', y, z) \\
 &\times \left[(p' - 2p + l)_{\nu} \eta_{\mu\lambda} + (p' + p - 2l)_{\mu} \eta_{\nu\lambda} + (p - 2p' + l)_{\lambda} \eta_{\mu\nu} \right] \\
 &\times \bar{L}^i(p') l^2 F_{mp_i}^+(l, z, 1/T) F_{pm_j}^-(l, 1/T, x) [\gamma_{\theta} \gamma_{\kappa}] P_R E^j(p) \tag{C.4}
 \end{aligned}$$

$$\begin{aligned}
 W2c &= -ig_5^2 e_5 \left(-i \frac{\sqrt{2} T^3}{k^3} y_{ij}^{5D} \right) \frac{\nu}{\sqrt{2}} \frac{(\tau^a)_{2c}}{2} \frac{(\tau^b)_{c1}}{2} \epsilon^{dek} C^e \epsilon^{ak3} \int_{\frac{1}{k}}^{\frac{1}{T}} \frac{dx}{(kx)^4} \\
 &\int_{\frac{1}{k}}^{\frac{1}{T}} \frac{dy}{(ky)} \int_{\frac{1}{k}}^{\frac{1}{T}} \frac{dz}{(kz)^4} \int \frac{d^4 l}{(2\pi)^4} f_{l_i}^{(0)}(z) f_{\gamma}^{(0)} g_{E_j}(x) \epsilon^{*\mu} \Delta_{5mp}(\hat{p}, x, y) \Delta_{5mp}(\hat{p}', y, z) \\
 &\times [(p - l) - (l - p')]_{\mu} \\
 &\times \bar{L}^i(p') P_R \gamma_5 \Delta_c^{\xi_i}(l, z, 1/T) \Delta_{bd}^{T_j^4}(l, 1/T, x) \gamma_5 P_R E^j(p) \\
 &= -\frac{g_5^2 e_5 T^3 y_{ij}^{5D}}{2k^3} \frac{\nu}{\sqrt{2}} \int_{\frac{1}{k}}^{\frac{1}{T}} \frac{dx}{(kx)^4} \int_{\frac{1}{k}}^{\frac{1}{T}} \frac{dy}{(ky)} \int_{\frac{1}{k}}^{\frac{1}{T}} \frac{dz}{(kz)^4} \int \frac{d^4 l}{(2\pi)^4} \\
 &f_{l_i}^{(0)}(z) f_{\gamma}^{(0)} g_{E_j}(x) \epsilon^{*\mu} \Delta_{5mp}(\hat{p}, x, y) \Delta_{5mp}(\hat{p}', y, z) \\
 &\times \bar{L}^i(p') d^- F_{mp_i}^+(l, z, 1/T) d^- F_{pm_j}^+(l, 1/T, x) (p' + p - 2l)_{\mu} P_R E^j(p) \tag{C.5}
 \end{aligned}$$

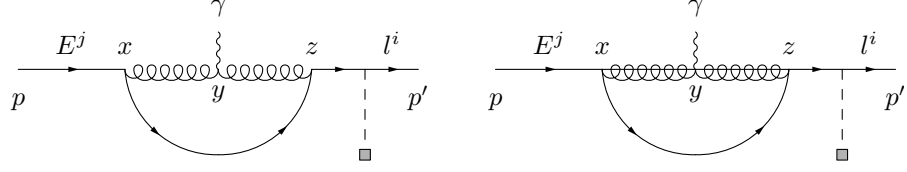
C.1. GAUGE BOSON EXCHANGE DIAGRAMS



$$\begin{aligned}
\text{W3ac} &= g_5^2 e_5 \left(-i \frac{\sqrt{2} T^3}{k^3} y_{ij}^{5D} \right) \frac{\nu}{\sqrt{2}} \frac{(\tau^a)_{2c}}{2} \frac{(\tau^b)_{c1}}{2} \epsilon^{dek} C^e \epsilon^{k3a} \int_{\frac{1}{k}}^{\frac{1}{T}} \frac{dx}{(kx)^4} \\
&\int_{\frac{1}{k}}^{\frac{1}{T}} \frac{dy}{(ky)} \int_{\frac{1}{k}}^{\frac{1}{T}} \frac{dz}{(kz)^4} \int \frac{d^4 l}{(2\pi)^4} f_{l_i}^{(0)}(z) f_{\gamma}^{(0)} g_{E_j}(x) \epsilon^{*\mu} \Delta_{5mp}(\hat{p}, x, y) (-\partial_y \Delta_{mp}^{\lambda\nu}(\hat{p}', y, z)) \eta_{\nu\mu} \\
&\times \bar{L}^i(p') P_R \gamma_{\lambda} \Delta_c^{\xi^1}(l, z, 1/T) \Delta_{bd}^{T^4}(l, 1/T, x) \gamma_5 P_R E^j(p) \\
&= -\frac{g_5^2 e_5 T^3 y_{ij}^{5D}}{2k^3} \frac{\nu}{\sqrt{2}} \int_{\frac{1}{k}}^{\frac{1}{T}} \frac{dx}{(kx)^4} \int_{\frac{1}{k}}^{\frac{1}{T}} \frac{dy}{(ky)} \int_{\frac{1}{k}}^{\frac{1}{T}} \frac{dz}{(kz)^4} \int \frac{d^4 l}{(2\pi)^4} \\
&f_{l_i}^{(0)}(z) f_{\gamma}^{(0)} g_{E_j}(x) \epsilon^{*\mu} \Delta_{5mp}(\hat{p}, x, y) (\partial_y \Delta_{mp}^{\lambda\nu}(\hat{p}', y, z)) \eta_{\nu\mu} \\
&\times \bar{L}^i(p') F_{mp_i}^+(l, z, 1/T) d^- F_{pm_j}^+(l, 1/T, x) \gamma_{\lambda} P_R E^j(p) \tag{C.6}
\end{aligned}$$

$$\begin{aligned}
\text{W3bc} &= -i g_5^2 e_5 \left(-i \frac{\sqrt{2} T^3}{k^3} y_{ij}^{5D} \right) \frac{\nu}{\sqrt{2}} \frac{(\tau^a)_{2c}}{2} \frac{(\tau^b)_{c1}}{2} \epsilon^{dek} C^e \epsilon^{a3k} \int_{\frac{1}{k}}^{\frac{1}{T}} \frac{dx}{(kx)^4} \\
&\int_{\frac{1}{k}}^{\frac{1}{T}} \frac{dy}{(ky)} \int_{\frac{1}{k}}^{\frac{1}{T}} \frac{dz}{(kz)^4} \int \frac{d^4 l}{(2\pi)^4} f_{l_i}^{(0)}(z) f_{\gamma}^{(0)} g_{E_j}(x) \epsilon^{*\mu} (-\partial_y \Delta_{mp}^{\lambda\nu}(\hat{p}, y, z)) \eta_{\nu\mu} \Delta_{5mp}(\hat{p}', y, z) \\
&\times \bar{L}^i(p') P_R \gamma_5 \Delta_c^{\xi^1}(l, z, 1/T) \Delta_{bd}^{T^4}(l, 1/T, x) \gamma_{\lambda} P_R E^j(p) \\
&= +\frac{g_5^2 e_5 T^3 y_{ij}^{5D}}{2k^3} \frac{\nu}{\sqrt{2}} \int_{\frac{1}{k}}^{\frac{1}{T}} \frac{dx}{(kx)^4} \int_{\frac{1}{k}}^{\frac{1}{T}} \frac{dy}{(ky)} \int_{\frac{1}{k}}^{\frac{1}{T}} \frac{dz}{(kz)^4} \int \frac{d^4 l}{(2\pi)^4} \\
&f_{l_i}^{(0)}(z) f_{\gamma}^{(0)} g_{E_j}(x) \epsilon^{*\mu} (\partial_y \Delta_{mp}^{\lambda\nu}(\hat{p}, y, z)) \Delta_{5mp}(\hat{p}', y, z) \eta_{\nu\mu} \\
&\times \bar{L}^i(p') d^- F_{mp_i}^+(l, z, 1/T) F_{pm_j}^-(l, 1/T, x) \gamma_{\lambda} P_R E^j(p) \tag{C.7}
\end{aligned}$$

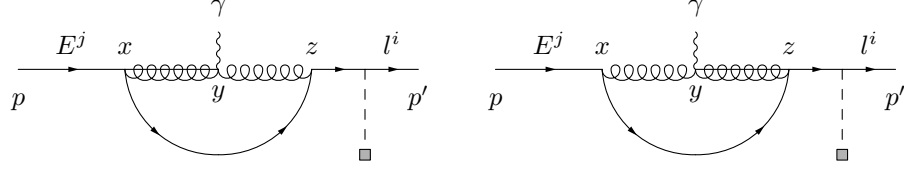
APPENDIX C. EXPLICIT DIAGRAM EXPRESSIONS



$$\begin{aligned}
\text{W4c} &= g_5^2 (-e_5) \left(-i \frac{\sqrt{2} T^3}{k^3} y_{ij}^{5D} \right) \frac{\nu}{\sqrt{2}} \frac{(\tau^a)_{21}}{2} \epsilon^{bcd} \epsilon^{efg} C^f \epsilon^{dg3} \int_{\frac{1}{k}}^{\frac{1}{T}} \frac{dx}{(kx)^4} \\
&\int_{\frac{1}{k}}^{\frac{1}{T}} \frac{dy}{(ky)} \int_{\frac{1}{k}}^{\frac{1}{T}} \frac{dz}{(kz)^4} \int \frac{d^4 l}{(2\pi)^4} f_{li}^{(0)} (1/T) f_\gamma^{(0)} g_{E_j} (x) \epsilon^{*\mu} \Delta_{mp}^{\lambda\kappa} (\hat{p}, x, y) \Delta_{mp}^{\nu\theta} (\hat{p}', y, z) \\
&\times \left[(p' - 2p + l)_\nu \eta_{\mu\lambda} + (p' + p - 2l)_\mu \eta_{\nu\lambda} + (p - 2p' + l)_\lambda \eta_{\mu\nu} \right] \\
&\times \bar{L}^i (p') P_R \Delta_{ab}^{T_j^4} (p, 1/T, z) \gamma_\theta \Delta_{ce}^{T_j^4} (l, z, x) \gamma_\kappa P_R E^j (p) \\
&= -\frac{g_5^2 e_5 T^3 y_{ij}^{5D}}{k^3} \frac{\nu}{\sqrt{2}} \int_{\frac{1}{k}}^{\frac{1}{T}} \frac{dx}{(kx)^4} \int_{\frac{1}{k}}^{\frac{1}{T}} \frac{dy}{(ky)} \int_{\frac{1}{k}}^{\frac{1}{T}} \frac{dz}{(kz)^4} \int \frac{d^4 l}{(2\pi)^4} \\
&f_{li}^{(0)} (1/T) f_\gamma^{(0)} g_{E_j} (x) \epsilon^{*\mu} \Delta_{mp}^{\lambda\kappa} (\hat{p}, x, y) \Delta_{mp}^{\nu\theta} (\hat{p}', y, z) \\
&\times \left[(p' - 2p + l)_\nu \eta_{\mu\lambda} + (p' + p - 2l)_\mu \eta_{\nu\lambda} + (p - 2p' + l)_\lambda \eta_{\mu\nu} \right] \\
&\times \bar{L}^i (p') d^- F_{S_j}^+ (l, 1/T, z) d^+ F_{pm_j}^- (l, z, x) [\gamma_\theta \gamma_\kappa] P_R E^j (p) \tag{C.8}
\end{aligned}$$

$$\begin{aligned}
\text{W5c} &= (-ig_5)^2 e_5 \left(-i \frac{\sqrt{2} T^3}{k^3} y_{ij}^{5D} \right) \frac{\nu}{\sqrt{2}} \frac{(\tau^a)_{21}}{2} \epsilon^{bcd} \epsilon^{efg} C^f \epsilon^{dg3} \int_{\frac{1}{k}}^{\frac{1}{T}} \frac{dx}{(kx)^4} \\
&\int_{\frac{1}{k}}^{\frac{1}{T}} \frac{dy}{(ky)} \int_{\frac{1}{k}}^{\frac{1}{T}} \frac{dz}{(kz)^4} \int \frac{d^4 l}{(2\pi)^4} f_{li}^{(0)} (1/T) f_\gamma^{(0)} g_{E_j} (x) \epsilon^{*\mu} \Delta_{5mp} (\hat{p}, x, y) \Delta_{5mp} (\hat{p}', y, z) \\
&\times [(p - l) - (l - p')]_\mu \\
&\times \bar{L}^i (p') P_R P_R \Delta_{ab}^{T_j^4} (p, 1/T, z) \gamma_5 \Delta_{ce}^{T_j^4} (l, z, x) \gamma_5 P_R E^j (p) \\
&= -\frac{g_5^2 e_5 T^3 y_{ij}^{5D}}{k^3} \frac{\nu}{\sqrt{2}} \int_{\frac{1}{k}}^{\frac{1}{T}} \frac{dx}{(kx)^4} \int_{\frac{1}{k}}^{\frac{1}{T}} \frac{dy}{(ky)} \int_{\frac{1}{k}}^{\frac{1}{T}} \frac{dz}{(kz)^4} \int \frac{d^4 l}{(2\pi)^4} \\
&f_{li}^{(0)} (1/T) f_\gamma^{(0)} g_{E_j} (x) \epsilon^{*\mu} \Delta_{5mp} (\hat{p}, x, y) \Delta_{5mp} (\hat{p}', y, z) \\
&\times \bar{L}^i d^- F_{S_j}^+ (l, 1/T, z) d^- F_{pm_j}^+ (l, z, x) (p' + p - 2l)_\mu P_R E^j (p) \tag{C.9}
\end{aligned}$$

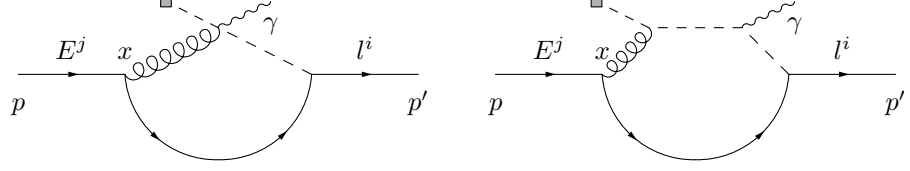
C.1. GAUGE BOSON EXCHANGE DIAGRAMS



$$\begin{aligned}
\text{W6ac} &= -ig_5^2 e_5 \left(-i \frac{\sqrt{2} T^3}{k^3} y_{ij}^{5D} \right) \frac{\nu}{\sqrt{2}} \frac{(\tau^a)_{21}}{2} \epsilon^{bcd} \epsilon^{efg} C^f \epsilon^{g3d} \int_{\frac{1}{k}}^{\frac{1}{T}} \frac{dx}{(kx)^4} \\
&\int_{\frac{1}{k}}^{\frac{1}{T}} \frac{dy}{(ky)} \int_{\frac{1}{k}}^{\frac{1}{T}} \frac{dz}{(kz)^4} \int \frac{d^4 l}{(2\pi)^4} f_{l_i}^{(0)}(1/T) f_\gamma^{(0)} g_{E_j}(x) \epsilon^{*\mu} \Delta_{5mp}(-\partial_y \Delta_{mp}^{\lambda\nu}(\hat{p}', y, z)) \eta_{\nu\mu} \\
&\times \bar{L}^i(p') P_R \Delta_{ab}^{T_j^4}(p, 1/T, z) \gamma_\lambda \Delta_{ce}^{T_j^4}(l, z, x) \gamma_5 P_R E^j(p) \\
&= -\frac{g_5^2 e_5 T^3 y_{ij}^{5D}}{k^3} \frac{\nu}{\sqrt{2}} \int_{\frac{1}{k}}^{\frac{1}{T}} \frac{dx}{(kx)^4} \int_{\frac{1}{k}}^{\frac{1}{T}} \frac{dy}{(ky)} \int_{\frac{1}{k}}^{\frac{1}{T}} \frac{dz}{(kz)^4} \int \frac{d^4 l}{(2\pi)^4} \\
&f_{l_i}^{(0)}(1/T) f_\gamma^{(0)} g_{E_j}(x) \epsilon^{*\mu} \Delta_{5mp}(\hat{p}, x, y) (\partial_x \Delta_{mp}^{\lambda\nu}(\hat{p}', y, z)) \eta_{\nu\mu} \\
&\times \bar{L}^i(p') d^- F_{S_j^+}^+(l, 1/T, z) F_{pm_j}^+(l, z, x) \gamma_\lambda \not{l} P_R E^j(p) \tag{C.10}
\end{aligned}$$

$$\begin{aligned}
\text{W6bc} &= -ig_5^2 e_5 \left(-i \frac{\sqrt{2} T^3}{k^3} y_{ij}^{5D} \right) \frac{\nu}{\sqrt{2}} \frac{(\tau^a)_{21}}{2} \epsilon^{bcd} \epsilon^{efg} C^f \epsilon^{d3g} \int_{\frac{1}{k}}^{\frac{1}{T}} \frac{dx}{(kx)^4} \\
&\int_{\frac{1}{k}}^{\frac{1}{T}} \frac{dy}{(ky)} \int_{\frac{1}{k}}^{\frac{1}{T}} \frac{dz}{(kz)^4} \int \frac{d^4 l}{(2\pi)^4} f_{l_i}^{(0)}(1/T) f_\gamma^{(0)} g_{E_j}(x) \epsilon^{*\mu} (-\partial_y \Delta_{mp}^{\lambda\nu}(\hat{p}', y, z)) \eta_{\nu\mu} \Delta_{5mp}(\hat{p}, y, z) \\
&\times \bar{L}^i(p') P_R \Delta_{ab}^{T_j^4}(p, 1/T, z) \gamma_5 \Delta_{ce}^{T_j^4}(l, z, x) \gamma_\lambda P_R E^j(p) \\
&= +\frac{g_5^2 e_5 T^3 y_{ij}^{5D}}{k^3} \frac{\nu}{\sqrt{2}} \int_{\frac{1}{k}}^{\frac{1}{T}} \frac{dx}{(kx)^4} \int_{\frac{1}{k}}^{\frac{1}{T}} \frac{dy}{(ky)} \int_{\frac{1}{k}}^{\frac{1}{T}} \frac{dz}{(kz)^4} \int \frac{d^4 l}{(2\pi)^4} \\
&f_{l_i}^{(0)}(1/T) f_\gamma^{(0)} g_{E_j}(x) \epsilon^{*\mu} (\partial_y \Delta_{mp}^{\lambda\nu}(\hat{p}, y, z)) \eta_{\nu\mu} \Delta_{5mp}(\hat{p}', y, z) \\
&\times \bar{L}^i(p') d^- F_{mp_j}^+(l, z, 1/T) F_{pm_j}^-(l, 1/T, x) \not{l} \gamma_\lambda P_R E^j(p) \tag{C.11}
\end{aligned}$$

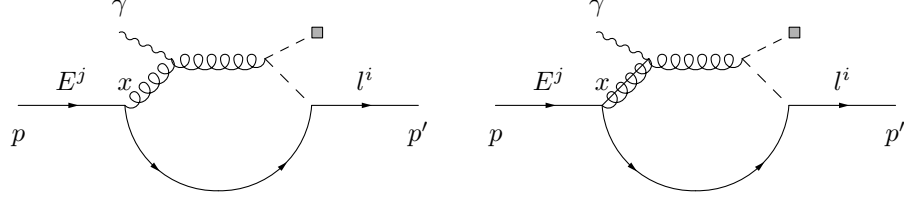
APPENDIX C. EXPLICIT DIAGRAM EXPRESSIONS



$$\begin{aligned}
 \text{W7c} &= ig_5^2 e_5 \left(-i \frac{\sqrt{2} T^3}{k^3} y_{ij}^{5D} \right) \frac{\nu}{\sqrt{2}} \frac{(\tau^a)_{2b}}{2} \epsilon^{cde} C^{d-} \frac{(\tau^e)_{b1} + \delta^{e3} \delta_{b1}}{2} \int_{\frac{1}{k}}^{\frac{1}{T}} \frac{dx}{(kx)^4} \int \frac{d^4 l}{(2\pi)^4} \\
 &\quad f_{l_i}^{(0)} (1/T) f_\gamma^{(0)} g_{E_j} (x) \epsilon_\mu^* (\Delta_{mp}^{\mu\nu} (\hat{p}, x, 1/T)) \Delta_H (\hat{p}') \\
 &\quad \times \bar{L}^i (p') P_R \Delta_{ac}^{T^4} (l, 1/T, x) \gamma_\lambda P_R E^j (p) \\
 &= -\frac{ig_5^2 e_5 T^3 y_{ij}^{5D}}{2k^3} \frac{\nu}{\sqrt{2}} \int_{\frac{1}{k}}^{\frac{1}{T}} \frac{dx}{(kx)^4} \int \frac{d^4 l}{(2\pi)^4} \\
 &\quad f_{l_i}^{(0)} (1/T) f_\gamma^{(0)} g_{E_j} (x) \epsilon_\mu^* (\Delta_{mp}^{\mu\nu} (\hat{p}, x, 1/T)) \Delta_H (\hat{p}') \\
 &\quad \times \bar{L}^i (p') F_{pm_j}^- (l, z, x) l \gamma_\nu P_R E^j (p) \tag{C.12}
 \end{aligned}$$

$$\begin{aligned}
 \text{W8c} &= ig_5^2 e_5 \left(-i \frac{\sqrt{2} T^3}{k^3} y_{ij}^{5D} \right) \frac{\nu}{\sqrt{2}} \frac{(\tau^a)_{2b}}{2} \epsilon^{cde} C^{d-} \frac{(\tau^3)_{2f} \delta_{gb} + (\tau^3)_{bg} \delta_{f2}}{2} \frac{(\tau^e)_{gh}}{2} \tilde{H}_{fa} \int_{\frac{1}{k}}^{\frac{1}{T}} \frac{dx}{(kx)^4} \\
 &\quad \int \frac{d^4 l}{(2\pi)^4} f_{l_i}^{(0)} (1/T) f_\gamma^{(0)} g_{E_j} (x) \epsilon^{*\mu} (\Delta_{mp}^{\lambda\nu} (\hat{p}, x, 1/T)) \Delta_H (\hat{p}) \Delta_H (\hat{p}') \\
 &\quad \times \bar{L}^i (p') P_R \Delta_{ab}^{T^4} (p, 1/T, z) \gamma_\lambda (p-l)_\nu (p+p'-2l)_\mu P_R E^j (p) \\
 &= +\frac{g_5^2 e_5 T^3 y_{ij}^{5D}}{2k^3} \frac{\nu}{\sqrt{2}} \int_{\frac{1}{k}}^{\frac{1}{T}} \frac{dx}{(kx)^4} \int \frac{d^4 l}{(2\pi)^4} \\
 &\quad f_{l_i}^{(0)} (1/T) f_\gamma^{(0)} g_{E_j} (x) \epsilon^{*\mu} (\Delta_{mp}^{\lambda\nu} (\hat{p}, x, 1/T)) \Delta_H (\hat{p}) \Delta_H (\hat{p}') \\
 &\quad \times \bar{L}^i (p') F_{pm_j}^- (l, 1/T, x) l \gamma_\lambda (p-l)_\nu (p+p'-2l)_\mu P_R E^j (p) \tag{C.13}
 \end{aligned}$$

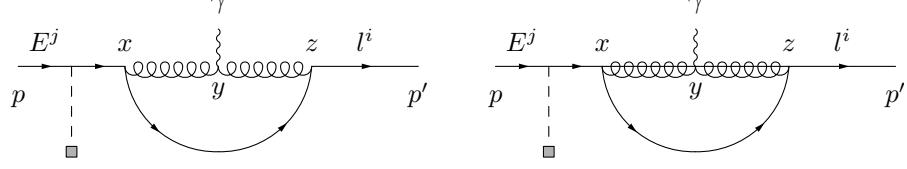
C.1. GAUGE BOSON EXCHANGE DIAGRAMS



$$\begin{aligned}
\text{W9c} &= ig_5^2 (-e_5) \left(-i \frac{\sqrt{2} T^3}{k^3} y_{ij}^{5D} \right) \frac{\nu}{\sqrt{2}} \frac{(\tau^a)_{2c}}{2} \frac{(\tau^b)_{c1}}{2} \epsilon^{def} C^e \epsilon^{3kf} \int_{\frac{1}{k}}^{\frac{1}{T}} \frac{dx}{(kx)^4} \\
&\int_{\frac{1}{k}}^{\frac{1}{T}} \frac{dy}{(ky)} \int_{\frac{1}{k}}^{\frac{1}{T}} \frac{dz}{(kz)^4} \int \frac{d^4 l}{(2\pi)^4} f_{l_i}^{(0)} (1/T) f_{\gamma}^{(0)} g_{E_j} (x) \epsilon^{*\mu} \Delta_{mp}^{\lambda\alpha} (\hat{p}, x, y) \Delta_{mp}^{\nu\rho} (\hat{p}', y, z) \\
&\times \left[(p' - 2p + l)_{\nu} \eta_{\mu\lambda} + (p' + p - 2l)_{\mu} \eta_{\nu\lambda} + (p - 2p' + l)_{\lambda} \eta_{\mu\nu} \right] (p' - l)_{\rho} \\
&\times \bar{L}^i (p') P_R \Delta_{ad}^{T^4} (l, 1/T, x) \gamma_{\alpha} P_R E^j (p) \Delta_H (\hat{p}') \\
&= \frac{g_5^2 e_5 T^3 y_{ij}^{5D}}{2k^3} \frac{\nu}{\sqrt{2}} \int_{\frac{1}{k}}^{\frac{1}{T}} \frac{dx}{(kx)^4} \int_{\frac{1}{k}}^{\frac{1}{T}} \frac{dy}{(ky)} \int_{\frac{1}{k}}^{\frac{1}{T}} \frac{dz}{(kz)^4} \int \frac{d^4 l}{(2\pi)^4} \\
&f_{l_i}^{(0)} (1/T) f_{\gamma}^{(0)} g_{E_j} (x) \epsilon^{*\mu} \Delta_{mp}^{\lambda\alpha} (\hat{p}, x, y) \Delta_{mp}^{\nu\rho} (\hat{p}', y, z) \\
&\times \left[(p' - 2p + l)_{\nu} \eta_{\mu\lambda} + (p' + p - 2l)_{\mu} \eta_{\nu\lambda} + (p - 2p' + l)_{\lambda} \eta_{\mu\nu} \right] (l - p')_{\rho} \\
&\times \bar{L}^i (p') F_{pm_j}^{-} (l, 1/T, x) \gamma_{\alpha} P_R E^j (p) \Delta_H (\hat{p}') \tag{C.14}
\end{aligned}$$

$$\begin{aligned}
\text{W10c} &= g_5^2 (-ie_5) \left(-i \frac{\sqrt{2} T^3}{k^3} y_{ij}^{5D} \right) \frac{\nu}{\sqrt{2}} \frac{(\tau^a)_{2b}}{2} \epsilon^{cde} C^d \frac{(\tau^f)_{b1}}{2} \epsilon^{ef3} \int_{\frac{1}{k}}^{\frac{1}{T}} \frac{dx}{(kx)^4} \\
&\int_{\frac{1}{k}}^{\frac{1}{T}} \frac{dy}{(ky)} \int_{\frac{1}{k}}^{\frac{1}{T}} \frac{dz}{(kz)^4} \int \frac{d^4 l}{(2\pi)^4} f_{l_i}^{(0)} (1/T) f_{\gamma}^{(0)} g_{E_j} (x) \epsilon^{*\mu} \Delta_{5mp} (\hat{p}, x, y) \eta_{\mu\nu} (-\partial_y \Delta_{mp}^{\nu\rho} (\hat{p}', y, z)) \\
&\times \bar{L}^i (p') P_R \Delta_{ad}^{T^4} (l, 1/T, x) \gamma_5 P_R E^j (p) \Delta_H (\hat{p}') (p' - l)_{\rho} \\
&= -\frac{g_5^2 e_5 T^3 y_{ij}^{5D}}{2k^3} \frac{\nu}{\sqrt{2}} \int_{\frac{1}{k}}^{\frac{1}{T}} \frac{dx}{(kx)^4} \int_{\frac{1}{k}}^{\frac{1}{T}} \frac{dy}{(ky)} \int_{\frac{1}{k}}^{\frac{1}{T}} \frac{dz}{(kz)^4} \int \frac{d^4 l}{(2\pi)^4} \\
&f_{l_i}^{(0)} (1/T) f_{\gamma}^{(0)} g_{E_j} (x) \epsilon^{*\mu} \Delta_{5mp} (\hat{p}, x, y) \eta_{\mu\nu} (\partial_y \Delta_{mp}^{\nu\rho} (\hat{p}', y, z)) \\
&\bar{L}^i (p') d^- F_{pm_j}^+ (l, 1/T, x) P_R E^j (p) \Delta_H (\hat{p}') (l - p')_{\rho} \tag{C.15}
\end{aligned}$$

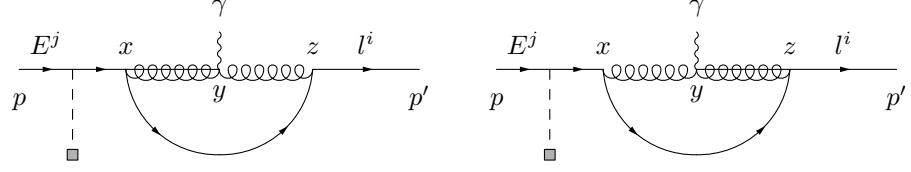
APPENDIX C. EXPLICIT DIAGRAM EXPRESSIONS



$$\begin{aligned}
W11c &= (ig_5)^2 (-e_5) \left(-i \frac{\sqrt{2}T^3}{k^3} y_{ij}^{5D} \right) \frac{\nu}{\sqrt{2}} \frac{(\tau^a)_{2b}}{2} \frac{(\tau^c)_{bc}}{2} \frac{(\tau^d)_{c1}}{2} C^d \epsilon^{ac3} \int_{\frac{1}{k}}^{\frac{1}{T}} \frac{dx}{(kx)^4} \\
&\int_{\frac{1}{k}}^{\frac{1}{T}} \frac{dy}{(ky)} \int_{\frac{1}{k}}^{\frac{1}{T}} \frac{dz}{(kz)^4} \int \frac{d^4l}{(2\pi)^4} f_{l_i}^{(0)}(z) f_{\gamma}^{(0)} g_{E_j} (1/T) \epsilon^{*\mu} \Delta_{mp}^{\lambda\kappa}(\hat{p}, x, y) \Delta_{mp}^{\nu\theta}(\hat{p}', y, z) \\
&\times \left[(p' - 2p + l)_{\nu} \eta_{\mu\lambda} + (p' + p - 2l)_{\mu} \eta_{\nu\lambda} + (p - 2p' + l)_{\lambda} \eta_{\mu\nu} \right] \\
&\times \bar{L}^i(p') P_R \gamma_{\theta} \Delta_b^{\xi_i^1}(l, x, z) \gamma_{\kappa} \Delta_c^{\xi_i^1}(p, x, 1/T) P_R E^j(p) \\
&= -\frac{g_5^2 e_5 T^3 y_{ij}^{5D}}{2k^3} \frac{\nu}{\sqrt{2}} \int_{\frac{1}{k}}^{\frac{1}{T}} \frac{dx}{(kx)^4} \int_{\frac{1}{k}}^{\frac{1}{T}} \frac{dy}{(ky)} \int_{\frac{1}{k}}^{\frac{1}{T}} \frac{dz}{(kz)^4} \int \frac{d^4l}{(2\pi)^4} \\
&f_{l_i}^{(0)}(x) f_{\gamma}^{(0)} g_{E_j} (1/T) \epsilon^{*\mu} \Delta_{mp}^{\lambda\kappa}(\hat{p}, x, y) \Delta_{mp}^{\nu\theta}(\hat{p}', y, z) \\
&\times \left[(p' - 2p + l)_{\nu} \eta_{\mu\lambda} + (p' + p - 2l)_{\mu} \eta_{\nu\lambda} + (p - 2p' + l)_{\lambda} \eta_{\mu\nu} \right] \\
&\times \bar{L}^i(p') d^+ F_{mp_i}^- (l, x, z) d^- F_{D_i}^+ (p, x, 1/T) [\gamma_{\theta} \gamma_{\kappa}] P_R E^j(p) \tag{C.16}
\end{aligned}$$

$$\begin{aligned}
W12c &= (g)^2 (e_5) \left(-i \frac{\sqrt{2}T^3}{k^3} y_{ij}^{5D} \right) \frac{\nu}{\sqrt{2}} \frac{(\tau^a)_{2b}}{2} \frac{(\tau^c)_{bc}}{2} \frac{(\tau^d)_{c1}}{2} C^d \epsilon^{ac3} \int_{\frac{1}{k}}^{\frac{1}{T}} \frac{dx}{(kx)^4} \\
&\int_{\frac{1}{k}}^{\frac{1}{T}} \frac{dy}{(ky)} \int_{\frac{1}{k}}^{\frac{1}{T}} \frac{dz}{(kz)^4} \int \frac{d^4l}{(2\pi)^4} f_{l_i}^{(0)}(x) f_{\gamma}^{(0)} g_{E_j} (1/T) \epsilon^{*\mu} \Delta_{5mp}(\hat{p}, x, y) \Delta_{5mp}(\hat{p}', y, z) \\
&\times [(p - l) - (l - p')]_{\mu} \\
&\times \bar{L}^i(p') P_R \gamma_5 \Delta_b^{\xi_i^1}(l, x, z) \gamma_5 \Delta_c^{\xi_i^1}(p, x, 1/T) P_R E^j(p) \\
&= -\frac{g_5^2 e_5 T^3 y_{ij}^{5D}}{k^3} \frac{\nu}{\sqrt{2}} \int_{\frac{1}{k}}^{\frac{1}{T}} \frac{dx}{(kx)^4} \int_{\frac{1}{k}}^{\frac{1}{T}} \frac{dy}{(ky)} \int_{\frac{1}{k}}^{\frac{1}{T}} \frac{dz}{(kz)^4} \int \frac{d^4l}{(2\pi)^4} \\
&f_{l_i}^{(0)}(x) f_{\gamma}^{(0)} g_{E_j} (1/T) \epsilon^{*\mu} \Delta_{5mp}(\hat{p}, x, y) \Delta_{5mp}(\hat{p}', y, z) \\
&\times \bar{L}^i(p') d^- F_{mp_i}^+ (l, x, z) d^- F_{D_i}^+ (p, x, 1/T) [\gamma_{\theta} \gamma_{\kappa}] P_R E^j(p) \tag{C.17}
\end{aligned}$$

C.1. GAUGE BOSON EXCHANGE DIAGRAMS



$$\begin{aligned}
\text{W13ac} &= ig_5^2 (-ie_5) \left(-i \frac{\sqrt{2} T^3}{k^3} y_{ij}^{5D} \right) \frac{\nu}{\sqrt{2}} \frac{(\tau^a)_{2b}}{2} \frac{(\tau^c)_{bc}}{2} \frac{(\tau^d)_{c1}}{2} C^d \epsilon^{c3a} \int_{\frac{1}{k}}^{\frac{1}{T}} \frac{dx}{(kx)^4} \\
&\int_{\frac{1}{k}}^{\frac{1}{T}} \frac{dy}{(ky)} \int_{\frac{1}{k}}^{\frac{1}{T}} \frac{dz}{(kz)^4} \int \frac{d^4 l}{(2\pi)^4} f_{l_i}^{(0)}(x) f_{\gamma}^{(0)} g_{E_j} (1/T) \epsilon^{*\mu} \Delta_{5mp}(\hat{p}, x, y) \\
&\times (-\partial_y \Delta_{mp}^{\lambda\nu}(\hat{p}', y, z)) \eta_{\nu\mu} \bar{L}^i(p') P_R \gamma_{\lambda} \Delta_b^{\xi_i^1}(l, x, z) \gamma_5 \Delta_c^{\xi_i^1}(p, x, 1/T) P_R E^j(p) \\
&= -\frac{g_5^2 e_5 T^3 y_{ij}^{5D}}{k^3} \frac{\nu}{\sqrt{2}} \int_{\frac{1}{k}}^{\frac{1}{T}} \frac{dx}{(kx)^4} \int_{\frac{1}{k}}^{\frac{1}{T}} \frac{dy}{(ky)} \int_{\frac{1}{k}}^{\frac{1}{T}} \frac{dz}{(kz)^4} \int \frac{d^4 l}{(2\pi)^4} \\
&f_{l_i}^{(0)}(1/T) f_{\gamma}^{(0)} g_{E_j}(x) \epsilon^{*\mu} \Delta_{5mp}(\hat{p}, x, y) (\partial_y \Delta_{mp}^{\lambda\nu}(\hat{p}', y, z)) \eta_{\nu\mu} \\
&\times \bar{L}^i(p') F_{mp_i}^+(l, z, x) d^- F_{D_i}^+(l, z, x) \gamma_{\lambda} \not{l} P_R E^j(p) \tag{C.18}
\end{aligned}$$

$$\begin{aligned}
\text{W13bc} &= ig_5^2 (-ie_5) \left(-i \frac{\sqrt{2} T^3}{k^3} y_{ij}^{5D} \right) \frac{\nu}{\sqrt{2}} \frac{(\tau^a)_{2b}}{2} \frac{(\tau^c)_{bc}}{2} \frac{(\tau^d)_{c1}}{2} C^d \epsilon^{c3a} \int_{\frac{1}{k}}^{\frac{1}{T}} \frac{dx}{(kx)^4} \\
&\int_{\frac{1}{k}}^{\frac{1}{T}} \frac{dy}{(ky)} \int_{\frac{1}{k}}^{\frac{1}{T}} \frac{dz}{(kz)^4} \int \frac{d^4 l}{(2\pi)^4} f_{l_i}^{(0)}(x) f_{\gamma}^{(0)} g_{E_j} (1/T) \epsilon^{*\mu} \Delta_{5mp}(\hat{p}', y, z) \\
&\times (-\partial_y \Delta_{mp}^{\lambda\nu}(\hat{p}, x, y)) \eta_{\nu\mu} \bar{L}^i(p') P_R \gamma_{\lambda} \Delta_b^{\xi_i^1}(l, x, z) \gamma_{\lambda} \Delta_c^{\xi_i^1}(p, x, 1/T) P_R E^j(p) \\
&= -\frac{g_5^2 e_5 T^3 y_{ij}^{5D}}{k^3} \frac{\nu}{\sqrt{2}} \int_{\frac{1}{k}}^{\frac{1}{T}} \frac{dx}{(kx)^4} \int_{\frac{1}{k}}^{\frac{1}{T}} \frac{dy}{(ky)} \int_{\frac{1}{k}}^{\frac{1}{T}} \frac{dz}{(kz)^4} \int \frac{d^4 l}{(2\pi)^4} \\
&f_{l_i}^{(0)}(1/T) f_{\gamma}^{(0)} g_{E_j}(x) \epsilon^{*\mu} (\partial_y \Delta_{mp}^{\lambda\nu}(\hat{p}, x, y)) \Delta_{5mp}(\hat{p}', y, z) \eta_{\nu\mu} \\
&\times \bar{L}^i(p') F_{mp_i}^-(l, z, x) d^- F_{D_i}^+(l, z, x) \gamma_{\lambda} \not{l} P_R E^j(p) \tag{C.19}
\end{aligned}$$

APPENDIX C. EXPLICIT DIAGRAM EXPRESSIONS

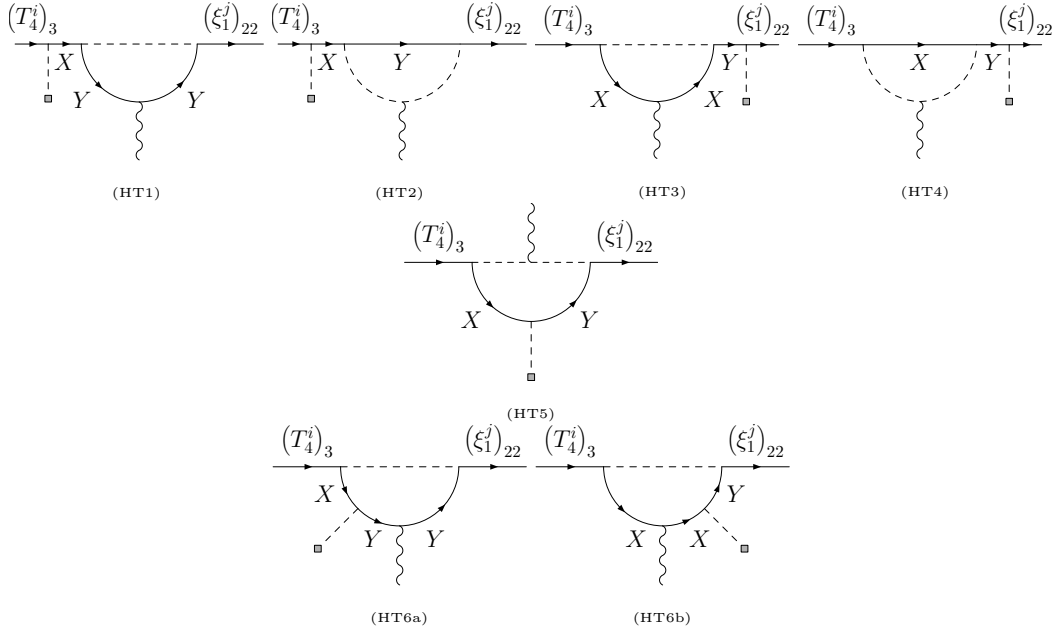


Figure C.1: All Higgs exchange dipole topologies.

C.2 Higgs exchange diagrams

At there are only four different diagram topologies with a Higgs exchange inside the loop possible that give rise to a $\mathcal{O}(\nu)$ contribution to the dipole operator. All possible diagrams generated by these diagrams are listed in the tables below. The first column of each table contains the name of the diagrams we will use from now on. The second and third column defines the fermion multiplet in the associated part of the diagram. There is no need to define individual particle, since this information is automatically generated after performing the calculation of the SU(2) colour factors. We suppress in this table the generation index for simplicity's sake. We write down the expressions using the narrow width regularisation of the delta function

$$\phi(z) = \theta\left(z - \frac{1-\delta}{T}\right) \left(\frac{T}{\delta}\right) \cdot \phi^{4d} \frac{T^3}{k^3}. \quad (\text{C.20})$$

As discussed above the limit $\delta \rightarrow 0$ has to be taken carefully, as the limit is not commutable with the momentum integration. For all expressions the four dimensional momentum integration is written down in d dimensions for dimensional regularisation.

We can write the analytic expression off the on-shell terms in the same way as we did for the gauge-boson propagators. The factor c_{Diag} contains the colour factor, that has to be

C.2. HIGGS EXCHANGE DIAGRAMS

HT1	X	Y	HT3	X	Y
H1	ξ_1	T_4	H3	ξ_1	T_4
H5	ξ_1	T_3	H7	ξ_1	T_3
			H9	ξ_1	ξ_2
HT2	X	Y	HT4	X	Y
H2	ξ_1	T_4	H4	ξ_1	T_4
H6	ξ_1	T_3	H8	ξ_1	T_3
HT5	X	Y	HT6	X	Y
H10	ξ_1	T_4	H11	ξ_1	T_4
H12	ξ_1	T_3	H13	ξ_1	T_3
H14	ξ_1	ξ_2			

Table C.1: All possible combination of leptonic Higgs exchange diagrams contributing to the dipole operators

calculated for each diagram independently.

$$\begin{aligned}
 HT1 = & -c_{Diag} \int_{\frac{1-T}{\delta}}^{\frac{1}{T}} dx \int_{\frac{1}{k}}^{\frac{1}{T}} \frac{dy}{(kz)^4} \int_{\frac{1-T}{\delta}}^{\frac{1}{T}} dz \int_{\frac{1-T}{\delta}}^{\frac{1}{T}} dw \left(\frac{T}{\delta}\right)^3 \mu^{d-4} \int \frac{d^d l}{(2\pi)^d} \epsilon^{*\mu} \frac{i}{l^2} \\
 & \times (Y)_{ia} (Y^\dagger)_{ab} (Y)_{bj} f_{l_i}^{(0)}(z) f_\gamma^{(0)} g_{E_j}(w) \bar{L}^i(p') [d^- F_{Y_a}^+(\hat{p}', z, y) F_{Y_a}^+(\hat{p}, y, x) \gamma_\mu \hat{p} \\
 & + F_{Y_a}^-(\hat{p}', z, y) d^- F_{Y_a}^+(\hat{p}, y, x) \hat{p}' \gamma_\mu] d^- F_{X_b}^+(p, x, w) P_R E^j(p) \quad (C.21)
 \end{aligned}$$

$$\begin{aligned}
 HT2 = & -c_{Diag} \int_{\frac{1-T}{\delta}}^{\frac{1}{T}} dx \int_{\frac{1}{k}}^{\frac{1}{T}} \frac{dy}{(kz)^4} \int_{\frac{1-T}{\delta}}^{\frac{1}{T}} dz \int_{\frac{1-T}{\delta}}^{\frac{1}{T}} dw \left(\frac{T}{\delta}\right)^3 \mu^{d-4} \int \frac{d^d l}{(2\pi)^d} \epsilon^{*\mu} \frac{i}{l^2} \\
 & \times (Y)_{ia} (Y^\dagger)_{ab} (Y)_{bj} \bar{L}^i(p') d^- F_{Y_a}^+(p', w, x) [d^- F_{X_b}^+(\hat{p}', z, y) F_{X_b}^+(\hat{p}, y, x) \gamma_\mu \hat{p} \\
 & + F_{X_b}^-(\hat{p}', z, y) d^- F_{X_b}^+(\hat{p}, y, x) \hat{p}' \gamma_\mu] P_R E^j(p) f_{l_i}^{(0)}(w) f_\gamma^{(0)} g_{E_j}(x) \quad (C.22)
 \end{aligned}$$

$$\begin{aligned}
 HT3 = & c_{Diag} \int_{\frac{1-T}{\delta}}^{\frac{1}{T}} dx \int_{\frac{1-T}{\delta}}^{\frac{1}{T}} dy \int_{\frac{1-T}{\delta}}^{\frac{1}{T}} dz \int_{\frac{1-T}{\delta}}^{\frac{1}{T}} dw \left(\frac{T}{\delta}\right)^4 \mu^{d-4} \int \frac{d^d l}{(2\pi)^d} \epsilon^{*\mu} (p + p' - 2l)_\mu \\
 & \times (Y')_{ia} (Y'^\dagger)_{ab} (Y)_{bj} f_{l_i}^{(0)}(w) f_\gamma^{(0)} g_{E_j}(x) \frac{i}{(p' - l)^2} \frac{i}{(p - l)^2} \\
 & \times \bar{L}^i(p') d^- F_{Y_a}^+(l, z, x) d^- F_{X_b}^+(p, x, w) P_R E^j(p) \quad (C.23)
 \end{aligned}$$

$$\begin{aligned}
 HT4 = & c_{Diag} \int_{\frac{1-T}{\delta}}^{\frac{1}{T}} dx \int_{\frac{1-T}{\delta}}^{\frac{1}{T}} dy \int_{\frac{1-T}{\delta}}^{\frac{1}{T}} dz \int_{\frac{1-T}{\delta}}^{\frac{1}{T}} dw \left(\frac{T}{\delta}\right)^4 \mu^{d-4} \int \frac{d^d l}{(2\pi)^d} \epsilon^{*\mu} (p + p' - 2l)_\mu \\
 & \times (Y)_{ia} (Y^\dagger)_{ab} (Y)_{bj} f_{l_i}^{(0)}(z) f_\gamma^{(0)} g_{E_j}(w) \frac{i}{(p' - l)^2} \frac{i}{(p - l)^2} \\
 & \times \bar{L}^i(p') d^- F_{Y_a}^+(p', w, z) d^- F_{X_b}^+(l, z, x) P_R E^j(p) \quad (C.24)
 \end{aligned}$$

APPENDIX C. EXPLICIT DIAGRAM EXPRESSIONS

$$\begin{aligned}
HT5 &= c_{Diag} \int_{\frac{1-\delta}{T}}^{\frac{1}{T}} dx \int_{\frac{1-\delta}{T}}^{\frac{1}{T}} dy \int_{\frac{1-\delta}{T}}^{\frac{1}{T}} dz \int_{\frac{1-\delta}{T}}^{\frac{1}{T}} dw \left(\frac{T}{\delta}\right)^4 \mu^{d-4} \int \frac{d^d l}{(2\pi)^d} \epsilon^{*\mu} (p+p'-2l)_\mu \\
&\quad \times (Y')_{ia} (Y'^{\dagger})_{ab} (Y)_{bj} f_{l_i}^{(0)}(z) f_\gamma^{(0)} g_{E_j}(x) \frac{i}{(p'-l)^2} \frac{i}{(p-l)^2} \\
&\quad \times \bar{L}^i(p') d^- F_{Y_a^+}^+(l, z, x) d^- F_{X_b^+}^+(l, x, w) P_R E^j(p). \tag{C.25}
\end{aligned}$$

$$\begin{aligned}
HT6 &= c_{Diag} \int_{\frac{1-\delta}{T}}^{\frac{1}{T}} dx \int_{\frac{1-\delta}{T}}^{\frac{1}{T}} dy \int_{\frac{1-\delta}{T}}^{\frac{1}{T}} dz \int_{\frac{1-\delta}{T}}^{\frac{1}{T}} dw \left(\frac{T}{\delta}\right)^4 \mu^{d-4} \int \frac{d^d l}{(2\pi)^d} \epsilon^{*\mu} (p+p'-2l)_\mu \\
&\quad \times (Y')_{ia} (Y'^{\dagger})_{ab} (Y)_{bj} f_{l_i}^{(0)}(z) f_\gamma^{(0)} g_{E_j}(x) \frac{i}{(p'-l)^2} \frac{i}{(p-l)^2} \\
&\quad \times \bar{L}^i(p') d^- F_{Y_a^+}^+(l, z, x) d^- F_{X_b^+}^+(l, x, w) P_R E^j(p) \tag{C.26}
\end{aligned}$$

The 5D Yukawah coupling Y' equals λ_{5D}^u for the diagram H9. For all other diagrams we have $Y' = \lambda_{5D}$. In order to compute the correct sign for the general diagram topologies HT3 and HT4 the SU(2) flow has to be considered carefully here. Splitting the Higgs bi-doublet fields for these diagram topologies leads to the obvious conclusion, that the photon-Higgs vertex is always a $\phi^- \partial_\nu A^\nu \phi^+$ for both topologies. Thus the SU(2) and therefore the sign remains the same for HT3 and HT4. The off-shell expressions for the four topologies is obtained by the following replacement rules

$$\Delta_D^i(p, x, y) \rightarrow -\frac{\not{p}}{p^2} f_{l_i}^{(0)}(x) f_{l_i}^{(0)}(y) \quad \Delta_E^j(p, x, y) \rightarrow -\frac{\not{p}}{p^2} g_{E_j}(x) g_{E_j}(y) \tag{C.27}$$

C.2. HIGGS EXCHANGE DIAGRAMS

for the external propagators. Then the off-shell expression for the Higgs exchange topologies can be written as

$$\begin{aligned}
HT1 &= -c_{Diag} \int_{\frac{1-\delta}{T}}^{\frac{1}{T}} dx \int_{\frac{1}{k}}^{\frac{1}{T}} \frac{dy}{(kz)^4} \int_{\frac{1-\delta}{T}}^{\frac{1}{T}} dz \int_{\frac{1-\delta}{T}}^{\frac{1}{T}} dw \left(\frac{T}{\delta}\right)^3 \mu^{d-4} \int \frac{d^d l}{(2\pi)^d} \epsilon^{*\mu} \frac{i}{l^2} \\
&\times (Y)_{ia} (Y^\dagger)_{ab} (Y)_{bj} f_{l_i}^{(0)}(z) f_\gamma^{(0)} g_{E_j}(w) \bar{L}^i(p') [d^- F_{Y_a}^+(\hat{p}', z, y) d^+ F_{Y_a}^-(\hat{p}, y, x) \gamma_\mu \\
&+ F_{Y_a}^-(\hat{p}', z, y) F_{Y_a}^-(\hat{p}, y, x) \not{p}' \gamma_\mu \not{p}] \frac{i \not{p}}{p^2} f_{l_b}^{(0)}(x) f_{l_b}^{(0)}(w) P_R E^j(p) \quad (C.28)
\end{aligned}$$

$$\begin{aligned}
HT2 &= -c_{Diag} \int_{\frac{1-\delta}{T}}^{\frac{1}{T}} dx \int_{\frac{1}{k}}^{\frac{1}{T}} \frac{dy}{(kz)^4} \int_{\frac{1-\delta}{T}}^{\frac{1}{T}} dz \int_{\frac{1-\delta}{T}}^{\frac{1}{T}} dw \left(\frac{T}{\delta}\right)^3 \mu^{d-4} \int \frac{d^d l}{(2\pi)^d} \epsilon^{*\mu} \frac{i}{l^2} \\
&\times (Y)_{ia} (Y^\dagger)_{ab} (Y)_{bj} \bar{L}^i(p') \frac{i \not{p}'}{p'^2} g_{E_a}(w) g_{E_a}(z) [d^+ F_{X_b}^-(\hat{p}', z, y) d^+ F_{X_b}^-(\hat{p}, y, x) \gamma_\mu \\
&+ F_{X_b}^+(\hat{p}', z, y) F_{X_b}^+(\hat{p}, y, x) \not{p}' \gamma_\mu \not{p}] P_R E^j(p) f_{l_i}^{(0)}(w) f_\gamma^{(0)} g_{E_j}(x) \quad (C.29)
\end{aligned}$$

$$\begin{aligned}
HT3 &= c_{Diag} \int_{\frac{1-\delta}{T}}^{\frac{1}{T}} dx \int_{\frac{1-\delta}{T}}^{\frac{1}{T}} dy \int_{\frac{1-\delta}{T}}^{\frac{1}{T}} dz \int_{\frac{1-\delta}{T}}^{\frac{1}{T}} dw \left(\frac{T}{\delta}\right)^4 \mu^{d-4} \int \frac{d^d l}{(2\pi)^d} \epsilon^{*\mu} (p+p'-2l)_\mu \\
&\times (Y')_{ia} (Y'^\dagger)_{ab} (Y)_{bj} f_{l_i}^{(0)}(w) f_\gamma^{(0)} g_{E_j}(x) \frac{i}{(p'-l)^2} \frac{i}{(p-l)^2} \\
&\times \bar{L}^i(p') F_{Y_a}^-(l, z, x) \frac{i \not{p}'}{p'^2} f_{l_b}^{(0)}(x) f_{l_b}^{(0)}(w) P_R E^j(p) \quad (C.30)
\end{aligned}$$

$$\begin{aligned}
HT4 &= c_{Diag} \int_{\frac{1-\delta}{T}}^{\frac{1}{T}} dx \int_{\frac{1-\delta}{T}}^{\frac{1}{T}} dy \int_{\frac{1-\delta}{T}}^{\frac{1}{T}} dz \int_{\frac{1-\delta}{T}}^{\frac{1}{T}} dw \left(\frac{T}{\delta}\right)^4 \mu^{d-4} \int \frac{d^d l}{(2\pi)^d} \epsilon^{*\mu} (p+p'-2l)_\mu \\
&\times (Y)_{ia} (Y^\dagger)_{ab} (Y)_{bj} f_{l_i}^{(0)}(z) f_\gamma^{(0)} g_{E_j}(w) \frac{i}{(p'-l)^2} \frac{i}{(p-l)^2} \\
&\times \bar{L}^i(p') \frac{i \not{p}'}{p'^2} g_{E_a}(w) g_{E_a}(z) F_{x_b}^+(l, z, x) P_R E^j(p) \quad (C.31)
\end{aligned}$$

Note that one has to include the initial fermion propagator before chiral decomposition for the determination of the c_{Diag} factors of the diagrams H1-H9, because these propagators (A.2, A.4) depend on the $SU(2)_L \times SU(2)_R$ indices. To calculate the c_{Diag} factors we write down the $SU(2)_L \times SU(2)_R$ dependent part of the diagram expression. In the first step the $SU(2)_L \times SU(2)_R$ dependent expression is written out based on the Feynman rules of the RS model with custodial protection, In the second step the final results of the evaluation of the $SU(2)_L \times SU(2)_R$ factors is presented. Then the c_{Diag} equal the part of the final answer, which comes before the part containing the Dirac spinors. The part with the Dirac spinors determines, which F functions have to be inserted into the explicit form of the associated

APPENDIX C. EXPLICIT DIAGRAM EXPRESSIONS

topology. In the expressions below we suppress the generation indices.

$$\begin{aligned}
H1 & : \left(-i\frac{T^3}{k^4}\right) \frac{(\tau^\alpha)_{2\beta}}{\sqrt{2}} \left(-i\frac{T^3}{k^4}\right) \frac{(\tau^\sigma)_{\beta\eta}}{\sqrt{2}} \left(-i\frac{T^3}{k^4}\right) \frac{(\tau^\nu)_{\eta 1}}{\sqrt{2}} C^\eta \cdot e_5 \\
& \times \frac{\nu}{\sqrt{2}} \bar{L}^i(p') P_R \Delta_{\alpha\delta}^{T^4}(\hat{p}', z, y) \epsilon^{\delta\rho 3} \gamma_\mu \Delta_{\rho\sigma}^{T^4}(\hat{p}, y, x) \Delta_\eta^{\xi_1}(p, x, w) P_R E^j(p) \\
& = \frac{T^9}{k^{12}} e_5 \frac{\nu}{\sqrt{2}} \bar{L}^i(p') P_R \Delta_E(\hat{p}', z, y) \\
& \times \gamma_\mu \Delta_E(\hat{p}, y, x) \Delta_D(p, x, w) P_R E^j(p) \tag{C.32}
\end{aligned}$$

$$\begin{aligned}
H2 & : \left(-i\frac{T^3}{k^4}\right) \frac{(\tau^\alpha)_{21}}{\sqrt{2}} \left(-i\frac{T^3}{k^4}\right) \frac{(\tau^\beta)_{\eta\delta}}{\sqrt{2}} i e_5 (\tau^3)_{\nu\eta} \\
& \times \left(-i\frac{T^3}{k^4}\right) \frac{(\tau^\sigma)_{\delta\nu}}{\sqrt{2}} C^\sigma \cdot \frac{\nu}{\sqrt{2}} \\
& \bar{L}^i(p') P_R \Delta_{\alpha\beta}^{T^4}(p', w, z) \Delta_\eta^{\xi_1}(\hat{p}', z, y) \gamma_\mu \Delta_\nu^{\xi_1}(\hat{p}, y, x) P_R E^j(p) \\
& = \frac{T^9}{k^{12}} e_5 \frac{\nu}{\sqrt{2}} \bar{L}^i(p') P_R \Delta_E(\hat{p}', w, z) \\
& \times \Delta_D(\hat{p}', z, y) \gamma_\mu \Delta_D(p, y, x) P_R E^j(p)
\end{aligned}$$

$$\begin{aligned}
H3 & : \left(-i\frac{T^3}{k^4}\right) \frac{(\tau^\alpha)_{2\beta}}{\sqrt{2}} \frac{e_5}{2} \left((\tau^3)_{2a} \delta_{\beta\rho} + \delta_{2a} (\tau^3)_{\beta\rho} \right) \frac{\nu}{\sqrt{2}} \\
& \left(-i\frac{T^3}{k^4}\right) \frac{(\tau^\sigma)_{\rho\gamma}}{\sqrt{2}} \left(-i\frac{T^3}{k^4}\right) \frac{(\tau^\nu)_{\gamma\eta}}{\sqrt{2}} H_{a\eta} C^\nu \\
& \times \bar{L}^i(p') P_R \Delta_{\alpha\sigma}^{T^4}(l, z, x) \Delta_\gamma^{\xi_1}(p, x, w) P_R E^j(p) \\
& = -\frac{1}{2} \frac{T^9}{k^{12}} e_5 \frac{\nu}{\sqrt{2}} \bar{L}^i(p') P_R \Delta_{pm}(l, z, x) \\
& \times \Delta_D(p, x, w) P_R E^j(p) \tag{C.33}
\end{aligned}$$

$$\begin{aligned}
H4 & : \left(-i\frac{T^3}{k^4}\right) \frac{(\tau^\alpha)_{21}}{\sqrt{2}} \left(-i\frac{T^3}{k^4}\right) \frac{(\tau^\gamma)_{\sigma\rho}}{\sqrt{2}} \frac{e_5}{2} \left((\tau^3)_{ab} \delta_{\sigma\eta} + \delta_{ab} (\tau^3)_{\sigma\eta} \right) \\
& \delta_{ab} \left(-i\frac{T^3}{k^4}\right) \frac{(\tau^\nu)_{\rho\eta}}{\sqrt{2}} C^\nu \frac{\nu}{\sqrt{2}} \\
& \times \bar{L}^i(p') P_R \Delta_{\alpha\sigma}^{T^4}(p', w, z) \Delta_\rho^{\xi_1}(l, z, x) P_R E^j(p) \\
& = -\frac{1}{2} \frac{T^9}{k^{12}} e_5 \frac{\nu}{\sqrt{2}} \bar{L}^i(p') P_R \Delta_E(p', w, z) \\
& \times \Delta_D(l, z, x) P_R E^j(p) \tag{C.34}
\end{aligned}$$

The computation of the group factor is straightforward for the other diagrams. We only list the final results in table C.2 for the coefficient c_{diag}

C.3. WILSON COEFFICIENTS OF THE EXTENDED ELECTROWEAK HAMILTONIAN AT THE SCALE μ_{KK}

	c_{diag}		c_{diag}
H1	$\frac{T^9}{k^{12}} \frac{\nu}{\sqrt{2}} e_5$	H5	$\frac{T^9}{k^{12}} \frac{\nu}{\sqrt{2}} e_5$
H2	$\frac{T^9}{k^{12}} \frac{\nu}{\sqrt{2}} e_5$	H6	0
H3	$-\frac{1}{2} \frac{T^9}{k^{12}} \frac{\nu}{\sqrt{2}} e_5$	H7	$-\frac{1}{2} \frac{T^9}{k^{12}} \frac{\nu}{\sqrt{2}} e_5$
H4	$-\frac{T^9}{k^{12}} \frac{\nu}{\sqrt{2}} e_5$	H8	0
H9	$\frac{T^9}{k^{12}} \frac{\nu}{\sqrt{2}} e_5$	H10	$\frac{T^9}{k^{12}} \frac{\nu}{\sqrt{2}} e_5$
H11	0	H12	$-\frac{T^9}{k^{12}} \frac{\nu}{\sqrt{2}} e_5$
H13	$-\frac{T^9}{k^{12}} \frac{\nu}{\sqrt{2}} e_5$	H14	$\frac{T^9}{k^{12}} \frac{\nu}{\sqrt{2}} e_5$

Table C.2: Table of c_{Diag} for the Higgs-exchange diagrams in the lepton sector.

C.3 Wilson coefficients of the extended electroweak Hamiltonian at the scale μ_{KK}

In the following we collect the coefficients of the various four-fermion operators in (3.44). To this end we first map each operator in the dimension-six Lagrangian unto operators in the broken electroweak theory and extract the Wilson coefficients by comparing with (3.44). For brevity, let us first introduce the abbreviation $\mathcal{V} = \frac{4G_F V_{ts}^* V_{tb}}{\sqrt{2}}$.

$$\begin{aligned}
b_{ij}^{QU} \bar{Q}_i \gamma^\mu T^A Q_i \bar{U}_j \gamma_\mu T^A U_j &\longrightarrow \beta_{sbq_u q_u}^{QU} \bar{s} \gamma^\mu T^A P_R b \bar{q}_u \gamma_\mu T^A P_R q_u = \\
&= -\frac{1}{2N_c} \beta_{sbq_u q_u} \bar{s} \gamma^\mu P_L b \bar{q}_u \gamma^\mu P_R q_u + \frac{1}{2} \beta_{sbuu} \bar{s}_\alpha \gamma^\mu P_L b_\beta (\bar{q}_u)_\beta \gamma^\mu P_R (q_u)_\alpha \\
&= -\frac{1}{2N_c} \beta_{sbq_u q_u} O_2^{q_u}[L, R] + \frac{1}{2} \beta_{sbq_u q_u} O_1^{q_u}[L, R]
\end{aligned} \tag{C.35}$$

gives

$$\mathcal{V} \Delta C_1^{q_u}[L, R](\mu_{KK}) = \frac{1}{2T^2} \beta_{sbq_u q_u}^{QU} \quad \mathcal{V} \Delta C_2^{q_u}[L, R](\mu_{KK}) = -\frac{1}{2N_c T^2} \beta_{sbq_u q_u}^{QU}. \tag{C.36}$$

$$\begin{aligned}
b_{ij}^{DD} \bar{D}_i \gamma^\mu T^A D_i \bar{D}_j \gamma_\mu T^A D_j &\longrightarrow \\
&= -\frac{1}{N_c} \beta_{sbdd}^{DD} O_2^d[R, R] + \beta_{sbdd}^{DD} O_1^d[R, R] - \frac{1}{N_c} \beta_{sddb}^{DD} \hat{O}_2^d[R, R] + \beta_{sddb}^{DD} \hat{O}_1^d[R, R]
\end{aligned} \tag{C.37}$$

$$-\frac{1}{N_c} \beta_{sbbb}^{DD} O_2^b[R, R] + \beta_{sbbb}^{DD} O_1^b[R, R] - \frac{1}{N_c} \beta_{sbss}^{DD} O_2^s[R, R] + \beta_{sbss}^{DD} O_1^s[R, R] \tag{C.38}$$

APPENDIX C. EXPLICIT DIAGRAM EXPRESSIONS

gives

$$\begin{aligned}
\mathcal{V}\Delta C_1^s[R, R](\mu_{KK}) &= \frac{1}{T^2} \beta_{sbs s}^{DD} & \mathcal{V}\Delta C_2^s[R, R](\mu_{KK}) &= -\frac{1}{N_c T^2} \beta_{sbs s}^{DD} \\
\mathcal{V}\Delta C_1^b[R, R](\mu_{KK}) &= \frac{1}{T^2} \beta_{sbbb}^{DD} & \mathcal{V}\Delta C_2^b[R, R](\mu_{KK}) &= -\frac{1}{N_c T^2} \beta_{sbbb}^{DD} \\
\mathcal{V}\Delta C_1^d[R, R](\mu_{KK}) &= \frac{1}{T^2} \beta_{sbdd}^{DD} & \mathcal{V}\Delta C_2^d[R, R](\mu_{KK}) &= -\frac{1}{N_c T^2} \beta_{sbdd}^{DD} \\
\mathcal{V}\Delta \widehat{C}_1^d[R, R](\mu_{KK}) &= \frac{1}{T^2} \beta_{sddb}^{DD} & \mathcal{V}\Delta \widehat{C}_2^d[R, R](\mu_{KK}) &= -\frac{1}{N_c T^2} \beta_{sddb}^{DD} \quad (C.39)
\end{aligned}$$

$$\begin{aligned}
& b_{ij}^{QQ} \bar{Q}_i \gamma^\mu T^A Q_i \bar{Q}_j \gamma_\mu T^A Q_j \longrightarrow \\
& = -\frac{1}{N_c} \beta_{sbuu}^{QQ} O_2^u[L, L] + \beta_{sbuu}^{QQ} O_1^u[L, L] \\
& \quad - \frac{1}{N_c} \beta_{sbdd}^{QQ} O_2^d[L, L] + \beta_{sbbb}^{QQ} O_1^d[L, L] - \frac{1}{N_c} \beta_{sddb}^{QQ} \widehat{O}_2^s[L, L] + \beta_{sddb}^{QQ} \widehat{O}_1^s[L, L] \\
& \quad - \frac{1}{N_c} \beta_{sbs s}^{QQ} O_2^d[L, L] + \beta_{sbs s}^{QQ} O_1^s[L, L] - \frac{1}{N_c} \beta_{sbbb}^{QQ} O_2^b[L, L] + \beta_{sbbb}^{QQ} O_1^b[L, L] \quad (C.40)
\end{aligned}$$

gives

$$\begin{aligned}
\mathcal{V}\Delta C_1^s[L, L](\mu_{KK}) &= \frac{1}{T^2} \beta_{sbs s}^{QQ} & \mathcal{V}\Delta C_2^s[L, L](\mu_{KK}) &= -\frac{1}{N_c T^2} \beta_{sbs s}^{QQ} \\
\mathcal{V}\Delta C_1^b[L, L](\mu_{KK}) &= \frac{1}{T^2} \beta_{sbbb}^{QQ} & \mathcal{V}\Delta C_2^b[L, L](\mu_{KK}) &= -\frac{1}{N_c T^2} \beta_{sbbb}^{QQ} \\
\mathcal{V}\Delta C_1^d[L, L](\mu_{KK}) &= \frac{1}{T^2} \beta_{sbdd}^{QQ} & \mathcal{V}\Delta C_2^d[L, L](\mu_{KK}) &= -\frac{1}{N_c T^2} \beta_{sbdd}^{QQ} \\
\mathcal{V}\Delta \widehat{C}_1^d[L, L](\mu_{KK}) &= \frac{1}{T^2} \beta_{sddb}^{QQ} & \mathcal{V}\Delta \widehat{C}_2^d[L, L](\mu_{KK}) &= -\frac{1}{N_c T^2} \beta_{sddb}^{QQ} \\
\mathcal{V}\Delta C_1^{qu}[L, L](\mu_{KK}) &= \frac{1}{T^2} \beta_{sdququ}^{QQ} & \mathcal{V}\Delta C_2^{qu}[L, L](\mu_{KK}) &= -\frac{1}{N_c T^2} \beta_{sdququ}^{QQ} \quad (C.41)
\end{aligned}$$

Finally

$$\begin{aligned}
& b_{ij}^{QD} \bar{Q}_i \gamma^\mu T^A Q_i \bar{D}_j \gamma_\mu T^A D_j \longrightarrow \\
& = -\frac{1}{2N_c} \beta_{uus b}^{QD} O_2^u[R, L] + \frac{1}{2} \beta_{uus b}^{QD} O_1^u[R, L] \\
& \quad - \frac{1}{2N_c} \beta_{sbdd}^{QD} O_2^d[L, R] + \frac{1}{2} \beta_{sbdd}^{QD} O_1^d[L, R] - \frac{1}{2N_c} \beta_{dds b}^{QD} O_2^d[R, L] + \frac{1}{2} \beta_{dds b}^{QD} O_1^d[R, L] \\
& \quad - \frac{1}{2N_c} \beta_{sddb}^{QD} \widehat{O}_2^d[L, R] + \frac{1}{2} \beta_{sddb}^{QD} \widehat{O}_1^d[L, R] - \frac{1}{2N_c} \beta_{dbs d}^{QD} \widehat{O}_2^d[R, L] + \frac{1}{2} \beta_{dbs d}^{QD} \widehat{O}_1^d[R, L] \\
& \quad - \frac{1}{2N_c} \beta_{sbs s}^{QD} O_2^s[L, R] + \frac{1}{2} \beta_{sbs s}^{QD} O_1^s[L, R] - \frac{1}{2N_c} \beta_{sss b}^{QD} O_2^s[R, L] + \frac{1}{2} \beta_{sss b}^{QD} O_1^s[R, L] \\
& \quad - \frac{1}{2N_c} \beta_{sbbb}^{QD} O_2^b[L, R] + \frac{1}{2} \beta_{sbbb}^{QD} O_1^b[L, R] - \frac{1}{2N_c} \beta_{bbs b}^{QD} O_2^b[R, L] + \frac{1}{2} \beta_{bbs b}^{QD} O_1^b[R, L] \quad (C.42)
\end{aligned}$$

C.3. WILSON COEFFICIENTS OF THE EXTENDED ELECTROWEAK HAMILTONIAN AT THE SCALE μ_{KK}

gives

$$\begin{aligned}
\mathcal{V}\Delta C_1^{qu}[R, L](\mu_{KK}) &= \frac{1}{2T^2}\beta_{ququsb}^{QD} & \mathcal{V}\Delta C_2^{qu}[R, L](\mu_{KK}) &= -\frac{1}{2N_c T^2}\beta_{ququsb}^{QD} \\
\mathcal{V}\Delta C_1^d[R, L](\mu_{KK}) &= \frac{1}{2T^2}\beta_{ddsb}^{QD} & \mathcal{V}\Delta C_2^d[R, L](\mu_{KK}) &= -\frac{1}{2N_c T^2}\beta_{ddsb}^{QD} \\
\mathcal{V}\Delta C_1^d[L, R](\mu_{KK}) &= \frac{1}{2T^2}\beta_{sbdd}^{QD} & \mathcal{V}\Delta C_2^d[L, R](\mu_{KK}) &= -\frac{1}{2N_c T^2}\beta_{sbdd}^{QD} \\
\mathcal{V}\Delta \widehat{C}_1^d[R, L](\mu_{KK}) &= \frac{1}{2T^2}\beta_{dbsd}^{QD} & \mathcal{V}\Delta \widehat{C}_2^d[R, L](\mu_{KK}) &= -\frac{1}{2N_c T^2}\beta_{dbsd}^{QD} \\
\mathcal{V}\Delta \widehat{C}_1^d[L, R](\mu_{KK}) &= \frac{1}{2T^2}\beta_{sddb}^{QD} & \mathcal{V}\Delta \widehat{C}_2^d[L, R](\mu_{KK}) &= -\frac{1}{2N_c T^2}\beta_{sddb}^{QD} \\
\mathcal{V}\Delta C_1^s[L, R](\mu_{KK}) &= \frac{1}{2T^2}\beta_{sbss}^{QD} & \mathcal{V}\Delta C_2^s[L, R](\mu_{KK}) &= -\frac{1}{2N_c T^2}\beta_{sbss}^{QD} \\
\mathcal{V}\Delta C_1^b[L, R](\mu_{KK}) &= \frac{1}{2T^2}\beta_{sbbb}^{QD} & \mathcal{V}\Delta C_2^b[L, R](\mu_{KK}) &= -\frac{1}{2N_c T^2}\beta_{sbbb}^{QD} \\
\mathcal{V}\Delta C_1^s[R, L](\mu_{KK}) &= \frac{1}{2T^2}\beta_{sssb}^{QD} & \mathcal{V}\Delta C_2^s[R, L](\mu_{KK}) &= -\frac{1}{2N_c T^2}\beta_{sssb}^{QD} \\
\mathcal{V}\Delta C_1^b[R, L](\mu_{KK}) &= \frac{1}{2T^2}\beta_{bbbs}^{QD} & \mathcal{V}\Delta C_2^b[R, L](\mu_{KK}) &= -\frac{1}{2N_c T^2}\beta_{bbbs}^{QD}
\end{aligned} \tag{C.43}$$

APPENDIX C. EXPLICIT DIAGRAM EXPRESSIONS

Bibliography

- [1] G. Aad *et al.* [ATLAS Collaboration], Phys. Lett. B **716** (2012) 1 [arXiv:1207.7214 [hep-ex]].
- [2] S. Chatrchyan *et al.* [CMS Collaboration], Phys. Lett. B **716** (2012) 30 [arXiv:1207.7235 [hep-ex]].
- [3] E. Gildener, Phys. Rev. D **14** (1976) 1667.
- [4] E. Gildener and S. Weinberg, Phys. Rev. D **13** (1976) 3333.
- [5] J. Charles *et al.*, Phys. Rev. D **91** (2015) 7, 073007 [arXiv:1501.05013 [hep-ph]].
- [6] S. Weinberg, Phys. Rev. Lett. **19** (1967) 1264.
- [7] S. P. Martin, Adv. Ser. Direct. High Energy Phys. **21** (2010) 1 [Adv. Ser. Direct. High Energy Phys. **18** (1998) 1] [hep-ph/9709356].
- [8] M. E. Peskin, arXiv:0801.1928 [hep-ph].
- [9] M. M. Nojiri *et al.*, arXiv:0802.3672 [hep-ph].
- [10] E. Dudas, S. Pokorski and C. A. Savoy, Phys. Lett. B **369** (1996) 255 [hep-ph/9509410].
- [11] L. J. Hall and H. Murayama, Phys. Rev. Lett. **75** (1995) 3985 [hep-ph/9508296].
- [12] R. Barbieri, L. J. Hall, S. Raby and A. Romanino, Nucl. Phys. B **493** (1997) 3 [hep-ph/9610449].
- [13] G. Jungman, M. Kamionkowski and K. Griest, Phys. Rept. **267** (1996) 195 [hep-ph/9506380].
- [14] L. Randall, R. Sundrum, Phys. Rev. Lett. **83** (1999) 3370 [hep-ph/9905221].
- [15] L. Randall and R. Sundrum, Phys. Rev. Lett. **83** (1999) 4690 [hep-th/9906064].
- [16] H. Davoudiasl, J. L. Hewett and T. G. Rizzo, Phys. Lett. B **473** (2000) 43 [hep-ph/9911262].
- [17] A. Pomarol, Phys. Lett. B **486** (2000) 153 [hep-ph/9911294].
- [18] S. Chang, J. Hisano, H. Nakano, N. Okada and M. Yamaguchi, Phys. Rev. D **62** (2000) 084025 [hep-ph/9912498].
- [19] T. Gherghetta and A. Pomarol, Nucl. Phys. B **586** (2000) 141 [hep-ph/0003129].

BIBLIOGRAPHY

- [20] Y. Grossman, M. Neubert, Phys. Lett. **B474** (2000) 361 [hep-ph/9912408].
- [21] S. J. Huber and Q. Shafi, Phys. Lett. B **498** (2001) 256 [hep-ph/0010195].
- [22] S. J. Huber, Nucl. Phys. B **666** (2003) 269 [hep-ph/0303183].
- [23] S. Casagrande, F. Goertz, U. Haisch, M. Neubert and T. Pfoh, JHEP **0810** (2008) 094, arXiv:0807.4937 [hep-ph].
- [24] K. Agashe, A. Delgado, M. J. May and R. Sundrum, JHEP **0308** (2003) 050 [hep-ph/0308036].
- [25] K. Agashe, R. Contino, L. Da Rold and A. Pomarol, Phys. Lett. B **641** (2006) 62 [hep-ph/0605341].
- [26] M. E. Albrecht, M. Blanke, A. J. Buras, B. Duling and K. Gemmler, JHEP **0909** (2009) 064 [arXiv:0903.2415 [hep-ph]].
- [27] S. Casagrande, F. Goertz, U. Haisch, M. Neubert and T. Pfoh, JHEP **1009** (2010) 014 [arXiv:1005.4315 [hep-ph]].
- [28] M. Beneke, P. Dey and J. Rohrwild, JHEP **1308** (2013) 010, arXiv:1209.5897 [hep-ph].
- [29] R. Kitano, Phys. Lett. B **481** (2000) 39 [hep-ph/0002279].
- [30] G. Moreau and J. I. Silva-Marcos, JHEP **0603** (2006) 090 [hep-ph/0602155].
- [31] K. Agashe, A. E. Blechman and F. Petriello, Phys. Rev. D **74** (2006) 053011 [hep-ph/0606021].
- [32] C. Csaki, Y. Grossman, P. Tanedo and Y. Tsai, Phys. Rev. D **83** (2011) 073002, arXiv:1004.2037 [hep-ph].
- [33] M. Misiak *et al.*, Phys. Rev. Lett. **98** (2007) 022002 [hep-ph/0609232].
- [34] M. Misiak and M. Steinhauser, Nucl. Phys. B **764** (2007) 62 [hep-ph/0609241].
- [35] M. Czakon, U. Haisch and M. Misiak, JHEP **0703** (2007) 008 [hep-ph/0612329].
- [36] M. Czakon, P. Fiedler, T. Huber, M. Misiak, T. Schutzmeier and M. Steinhauser, JHEP **1504** (2015) 168 [arXiv:1503.01791 [hep-ph]].
- [37] M. Misiak *et al.*, Phys. Rev. Lett. **114** (2015) 22, 221801 [arXiv:1503.01789 [hep-ph]].
- [38] Y. Amhis *et al.* [Heavy Flavor Averaging Group (HFAG) Collaboration], arXiv:1412.7515 [hep-ex].
- [39] T. Saito *et al.* [Belle Collaboration], Phys. Rev. D **91** (2015) 5, 052004 [arXiv:1411.7198 [hep-ex]].
- [40] J. P. Lees *et al.* [BaBar Collaboration], Phys. Rev. Lett. **109** (2012) 191801 [arXiv:1207.2690 [hep-ex]].
- [41] J. P. Lees *et al.* [BaBar Collaboration], Phys. Rev. D **86** (2012) 112008 [arXiv:1207.5772 [hep-ex]].
- [42] J. P. Lees *et al.* [BaBar Collaboration], Phys. Rev. D **86** (2012) 052012 [arXiv:1207.2520 [hep-ex]].

-
- [43] A. Limosani *et al.* [Belle Collaboration], Phys. Rev. Lett. **103** (2009) 241801 [arXiv:0907.1384 [hep-ex]].
- [44] B. Aubert *et al.* [BaBar Collaboration], Phys. Rev. D **77** (2008) 051103 [arXiv:0711.4889 [hep-ex]].
- [45] S. Chen *et al.* [CLEO Collaboration], Phys. Rev. Lett. **87** (2001) 251807 [hep-ex/0108032].
- [46] K. Abe *et al.* [Belle Collaboration], Phys. Lett. B **511** (2001) 151 [hep-ex/0103042].
- [47] T. Aushev *et al.*, arXiv:1002.5012 [hep-ex].
- [48] M. Blanke, B. Shakya, P. Tanedo and Y. Tsai, JHEP **1208** (2012) 038 [arXiv:1203.6650 [hep-ph]].
- [49] A. Azatov, M. Toharia and L. Zhu, Phys. Rev. D **80** (2009) 035016, arXiv:0906.1990 [hep-ph].
- [50] R. Malm, M. Neubert and C. Schmell, arXiv:1509.02539 [hep-ph].
- [51] W. Buchmüller and D. Wyler, Nucl. Phys. B **268** (1986) 621.
- [52] B. Grzadkowski, M. Iskrzynski, M. Misiak and J. Rosiek, JHEP **1010** (2010) 085, arXiv:1008.4884 [hep-ph].
- [53] M. Beneke, P. Moch and J. Rohrwild, Int. J. Mod. Phys. A **29** (2014) 1444011, arXiv:1404.7157 [hep-ph].
- [54] P. Moch and J. Rohrwild, J. Phys. G **41** (2014) 105005, arXiv:1405.5385 [hep-ph].
- [55] M. Beneke, P. Moch and J. Rohrwild, arXiv:1508.01705 [hep-ph].
- [56] P. Moch and J. Rohrwild, arXiv:1509.04643 [hep-ph].
- [57] G. Nordstrom, Phys. Z. **15** (1914) 504 [physics/0702221 [physics.gen-ph]].
- [58] T. Kaluza, Sitzungsber. Preuss. Akad. Wiss. Berlin (Math. Phys.) **1921** (1921) 966.
- [59] O. Klein, Z. Phys. **37** (1926) 895 [Surveys High Energ. Phys. **5** (1986) 241].
- [60] J. Polchinski,
- [61] J. Polchinski,
- [62] C. D. Hoyle, D. J. Kapner, B. R. Heckel, E. G. Adelberger, J. H. Gundlach, U. Schmidt and H. E. Swanson, Phys. Rev. D **70** (2004) 042004 [hep-ph/0405262].
- [63] D. J. Kapner, T. S. Cook, E. G. Adelberger, J. H. Gundlach, B. R. Heckel, C. D. Hoyle and H. E. Swanson, Phys. Rev. Lett. **98** (2007) 021101 [hep-ph/0611184].
- [64] N. Arkani-Hamed, S. Dimopoulos and G. R. Dvali, Phys. Lett. B **429** (1998) 263 [hep-ph/9803315].
- [65] H. Davoudiasl and T. G. Rizzo, Phys. Lett. B **512** (2001) 100 [hep-ph/0104199].
- [66] W. D. Goldberger and M. B. Wise, Phys. Rev. Lett. **83** (1999) 4922 [hep-ph/9907447].

BIBLIOGRAPHY

- [67] A. Lukas, B. A. Ovrut, K. S. Stelle and D. Waldram, *Phys. Rev. D* **59** (1999) 086001 [hep-th/9803235].
- [68] I. R. Klebanov and M. J. Strassler, *JHEP* **0008** (2000) 052 [hep-th/0007191].
- [69] K. Agashe, G. Perez and A. Soni, *Phys. Rev. D* **71** (2005) 016002 [hep-ph/0408134].
- [70] K. Agashe, G. Perez and A. Soni, *Phys. Rev. Lett.* **93** (2004) 201804 [hep-ph/0406101].
- [71] S. J. Huber and Q. Shafi, *Phys. Rev. D* **63** (2001) 045010 [hep-ph/0005286].
- [72] H. Davoudiasl, J. L. Hewett and T. G. Rizzo, *Phys. Rev. D* **63** (2001) 075004 [hep-ph/0006041].
- [73] T. G. Rizzo, *Phys. Rev. D* **64** (2001) 095010 [hep-ph/0106336].
- [74] C. D. Froggatt and H. B. Nielsen, *Nucl. Phys. B* **147** (1979) 277.
- [75] L. Randall and M. D. Schwartz, *JHEP* **0111** (2001) 003 [hep-th/0108114].
- [76] A. Azatov, M. Toharia and L. Zhu, *Phys. Rev. D* **82**, 056004 (2010), arXiv:1006.5939 [hep-ph].
- [77] M. Carena, S. Casagrande, F. Goertz, U. Haisch and M. Neubert, *JHEP* **1208** (2012) 156, arXiv:1204.0008 [hep-ph].
- [78] R. Malm, M. Neubert, K. Novotny and C. Schmell, *JHEP* **1401** (2014) 173, arXiv:1303.5702 [hep-ph].
- [79] K. Agashe, A. Azatov, Y. Cui, L. Randall and M. Son, *JHEP* **1506** (2015) 196, arXiv:1412.6468 [hep-ph].
- [80] G. Cacciapaglia, C. Csaki, G. Marandella and J. Terning, *JHEP* **0702** (2007) 036 [hep-ph/0611358].
- [81] H. Davoudiasl, B. Lillie and T. G. Rizzo, *JHEP* **0608** (2006) 042 [hep-ph/0508279].
- [82] C. Csaki, A. Falkowski and A. Weiler, *JHEP* **0809** (2008) 008, arXiv:0804.1954 [hep-ph].
- [83] M. Blanke, A. J. Buras, B. Duling, S. Gori and A. Weiler, *JHEP* **0903** (2009) 001 [arXiv:0809.1073 [hep-ph]].
- [84] M. Bauer, R. Malm and M. Neubert, *Phys. Rev. Lett.* **108** (2012) 081603, arXiv:1110.0471 [hep-ph].
- [85] M. E. Peskin and T. Takeuchi, *Phys. Rev. Lett.* **65** (1990) 964.
- [86] M. Carena, A. Delgado, E. Ponton, T. M. P. Tait and C. E. M. Wagner, *Phys. Rev. D* **68** (2003) 035010 [hep-ph/0305188].
- [87] H. Davoudiasl, J. L. Hewett and T. G. Rizzo, *Phys. Rev. D* **68** (2003) 045002 [hep-ph/0212279].
- [88] J. A. Cabrer, G. von Gersdorff and M. Quiros, *Phys. Lett. B* **697** (2011) 208 [arXiv:1011.2205 [hep-ph]].

-
- [89] J. A. Cabrer, G. von Gersdorff and M. Quiros, *JHEP* **1105** (2011) 083 [arXiv:1103.1388 [hep-ph]].
- [90] J. A. Cabrer, G. von Gersdorff and M. Quiros, *Phys. Rev. D* **84** (2011) 035024, arXiv:1104.3149 [hep-ph].
- [91] A. Carmona, E. Ponton and J. Santiago, *JHEP* **1110** (2011) 137 [arXiv:1107.1500 [hep-ph]].
- [92] R. Alonso, E. E. Jenkins, A. V. Manohar and M. Trott, *JHEP* **1404** (2014) 159, arXiv:1312.2014 [hep-ph].
- [93] M. Bauer, S. Casagrande, U. Haisch and M. Neubert, *JHEP* **1009** (2010) 017 [arXiv:0912.1625 [hep-ph]].
- [94] W. -F. Chang and J. N. Ng, *Phys. Rev. D* **71** (2005) 053003 [hep-ph/0501161].
- [95] R. Kitano, M. Koike and Y. Okada, *Phys. Rev. D* **66** (2002) 096002 Erratum-ibid. *D* **76** (2007) 059902], [hep-ph/0203110].
- [96] Y. Kuno and Y. Okada, *Rev. Mod. Phys.* **73** (2001) 151 [hep-ph/9909265].
- [97] A. Crivellin, M. Hoferichter and M. Procura, *Phys. Rev. D* **89** (2014) 054021, arXiv:1312.4951 [hep-ph].
- [98] M. A. Shifman, A. I. Vainshtein and V. I. Zakharov, *Phys. Lett. B* **78** (1978) 443.
- [99] A. Crivellin, M. Hoferichter and M. Procura, *Phys. Rev. D* **89** (2014) 093024, arXiv:1404.7134 [hep-ph].
- [100] S. M. Barr and A. Zee, *Phys. Rev. Lett.* **65** (1990) 21 [Erratum-ibid. **65** (1990) 2920].
- [101] D. Chang, W. S. Hou and W. Y. Keung, *Phys. Rev. D* **48** (1993) 217 [hep-ph/9302267].
- [102] R. G. Leigh, S. Paban and R. M. Xu, *Nucl. Phys. B* **352** (1991) 45.
- [103] E. E. Jenkins, A. V. Manohar and M. Trott, *JHEP* **1310** (2013) 087, arXiv:1308.2627 [hep-ph].
- [104] E. E. Jenkins, A. V. Manohar and M. Trott, *JHEP* **1401** (2014) 035, arXiv:1310.4838 [hep-ph].
- [105] A. J. Buras, hep-ph/9806471.
- [106] S. Bertolini, F. Borzumati and A. Masiero, *Phys. Lett. B* **192** (1987) 437.
- [107] N. G. Deshpande, P. Lo, J. Trampetic, G. Eilam and P. Singer, *Phys. Rev. Lett.* **59** (1987) 183.
- [108] A. J. Buras, L. Merlo and E. Stamou, *JHEP* **1108**, 124 (2011) [arXiv:1105.5146 [hep-ph]].
- [109] M. Ciuchini, E. Franco, G. Martinelli, L. Reina and L. Silvestrini, *Phys. Lett. B* **316**, 127 (1993) [hep-ph/9307364].
- [110] M. Ciuchini, E. Franco, L. Reina and L. Silvestrini, *Nucl. Phys. B* **421** (1994) 41 [hep-ph/9311357].

BIBLIOGRAPHY

- [111] C. Niehoff, P. Stangl and D. M. Straub, arXiv:1508.00569 [hep-ph].
- [112] A. F. Falk, M. E. Luke and M. J. Savage, Phys. Rev. D **49** (1994) 3367 [hep-ph/9308288].
- [113] P. Gambino and M. Misiak, Nucl. Phys. B **611** (2001) 338 [hep-ph/0104034].
- [114] C. W. Bauer, Phys. Rev. D **57**, 5611 (1998) [Phys. Rev. D **60**, 099907 (1999)] [hep-ph/9710513].
- [115] M. Neubert, Eur. Phys. J. C **40** (2005) 165 [hep-ph/0408179].
- [116] T. Hahn, Comput. Phys. Commun. **168** (2005) 78 [hep-ph/0404043].
- [117] M. E. Peskin and D. V. Schroeder, Reading, USA: Addison-Wesley (1995) 842 p
- [118] DLMF NIST Digital Library of Mathematical Functions. <http://dlmf.nist.gov/>, Release 1.0.9 of 2014-08-29.
- [119] F. W. J. Olver and D. W. Lozier and R. F. Boisvert and C. W. Clark, editors. NIST Handbook of Mathematical Functions. Cambridge University Press, New York, NY, 2010.
- [120] J. Baron *et al.* [ACME Collaboration], Science **343** (2014) 269, arXiv:1310.7534 [physics.atom-ph].
- [121] K. A. Olive *et al.* [Particle Data Group Collaboration], Chin. Phys. C **38** (2014) 090001.
- [122] T. A. Filippas, P. Pabit, R. T. Siegel, and R. E. Welsh, Phys. Lett. **6**, 118 (1963)
- [123] T. Suzuki, D. F. Measday and J. P. Roalsvig, Phys. Rev. C **35** (1987) 2212.
- [124] J. Beringer *et al.* [Particle Data Group Collaboration], Phys. Rev. D **86** (2012) 010001.
- [125] B. Aubert *et al.* [BaBar Collaboration], Phys. Rev. Lett. **104** (2010) 021802, arXiv:0908.2381 [hep-ex].
- [126] K. Hayasaka *et al.* [Belle Collaboration], Phys. Lett. B **666**, 16 (2008), arXiv:0705.0650 [hep-ex].
- [127] R. Aaij *et al.* [LHCb Collaboration], Phys. Lett. B **724** (2013) 36, arXiv:1304.4518 [hep-ex].
- [128] M. Aoki [DeeMe Collaboration], AIP Conf. Proc. **1441** (2012) 599.
- [129]
- [129] R. M. Carey *et al.* [Mu2e Collaboration], FERMILAB-PROPOSAL-0973.
- [130] Y. G. Cui *et al.* [COMET Collaboration], KEK-2009-10.
- [131] A. M. Baldini, F. Cei, C. Cerri, S. Dussoni, L. Galli, M. Grassi, D. Nicolo and F. Raffaelli *et al.*, arXiv:1301.7225 [physics.ins-det].
- [132] N. Berger [Mu3e Collaboration], Nucl. Phys. Proc. Suppl. **248-250** (2014) 35.

Acknowledgements

I would like to thank Martin Beneke and especially Jürgen Rohrwild for the fruitful collaboration on the warped extra dimension project. I thank Jürgen Rohrwild for the great discussions we had and of course for his careful reading of parts of my thesis. I thank Yuming Wang for the pleasant and encouraging working atmosphere. In addition I would also like to thank Stefan Recksiegel for the great computer setup in the physic department and his advices on the proper usage of this system.